

ULTRASONIC AND THERMODYNAMIC EFFECTS OF SELF-ASSOCIATION OF ALIPHATIC ALCOHOLS IN $\text{c-C}_6\text{H}_{12}$. I. PRIMARY BUTANOLS

K. BEBEK, S. ERNST

Institute of Chemistry, Silesian University
(40-006 Katowice, ul. Szkolna 9)

The ultrasound velocities in and densities of mixtures of n-butanol and iso-butanol with cyclohexane as a common component have been measured at 293.15 K. The adiabatic compressibility coefficients, $\beta_s = -1/V(\partial V/\partial p)_s$, compressibilities, $\kappa_s = \beta_s V$, and the free intermolecular lengths, L , of those mixtures were estimated and their dependence on the alcohol concentration reproduced by simple polynomials. The excess values of the above quantities, V^E , β_s^E and κ_s^E were calculated and discussed. The dependence of those excess functions on the mixture composition, expressed in mole fractions of alcohol, x_1 , can be successfully reproduced by the Redlich-Kister equation.

1. Introduction

Although the dependence of thermodynamic properties of binary liquid mixtures on their composition has been usually attributed to structural variations accompanying the mixing of the component, there is still lacking a theoretical foundation of that dependence in terms of microscopic characteristics determining the structure of the two-components liquid, i.e. on the size and shape of the molecules and intermolecular interactions affecting the liquid structure. However, significant progress in understanding the link between macroscopic properties and structure has been made by studying liquid mixtures in that relatively strong interactions by hydrogen bonding are expected to be the main structure determining factor, particularly by studying alcohols in dipolar and non-polar solvents.

The general problem which we address in this paper is the effect of variations in the self-association of n-butanol and iso-butanol caused by mixing with cyclohexane on the ultrasound velocity in and the volume and compressibility of those binary mixtures.

It is customary to analyze the effect of composition on a molar property Z in terms of deviations ΔZ from an arbitrary chosen ideal reference state $Z^{id} = \sum x_i Z_i^0$, where Z_i^0 are the corresponding molar properties of the pure components and x_i the molar fractions of the latters. We believe that, although the choice of the ideal reference state is merely a matter of convention, in order to achieve a compatibility of the deviations of different quantities, it is necessary to choose a common reference state for all those quantities. In this study we have therefore chosen the thermodynamically ideal two-component system defined by the equation

$G = \sum_{i=1}^2 x_i (\mu_i^0 + RT \ln x_i)$ (where G — molar free enthalpy, μ_i^0 — standard chemical potential of the i -th component) for determining both volume and compressibility deviations.

2. Experimental

For dehydration and purification, the pure components (n-butanol, iso-butanol and cyclohexane, POCh Gliwice, Poland, all of analytical grade) were shaken for a longer time with molecular sieves A3 and A4 of granulation 1/16" (POCh Gliwice) and distilled under reduced pressure. After purification the refractive indices and boiling points were controled (n-butanol: 1.3992, 117.7 K; iso-butanol: 1.3959, 107.9 K; c-C₆H₁₂: 1.4464, 82.6 K).

The mixtures were prepared by weighing immediately before the measurements.

The densities of the pure components and mixtures were determined pycnometrically and by the Kohlrausch method, i.e. by using a quartz float that has been weighed at 293.15 \pm 0.01 K in air and after immersing it in the liquid under test. In both cases the weights were reduced to vacuum. The accuracy was \pm 0.1 kg/m³.

The ultrasound velocities were measured by a sing-around equipment designed and constructed in our laboratory (the frequency was measured with a frequency-meter KZ-2026A-2, ZOPAN Warsaw, Poland). The temperature deviations did not exceed \pm 0.002 K and \pm 0.005 K in n-butanol-cyclohexane and iso-butanol-cyclohexane, respectively. The repeatability of the ultrasound velocity measurements was better than \pm 0.05 m/s.

3. Measurement results

The measured sound velocities and densities are given in Table 1.

The molar volumes, V , isentropic compressibility coefficients, β_s , and isentropic compressibilities, κ_s , were calculated from the following equations

$$\begin{aligned} V &= (x_1 M_1 + x_2 M_2) / \rho \\ \beta_s &= 1 / \rho c^2 \\ \kappa_s &= \beta_s V \end{aligned} \quad (1)$$

Table 1. Speeds of sound and densities at 293.15 K

x_1	$c/(m/s)$	$\rho/(kg/m^3)$	x_1	$c/(m/s)$	$\rho/(kg/m^3)$
{ $x_1 n-C_4H_9OH + (1-x_1)C_6H_{12}$ }			{ $x_1 iso-C_4H_9OH + (1-x_1)C_6H_{12}$ }		
0	1277.4	778.4	0	1276.7	778.1
0.0499	1266.5	779.0	0.1356	1250.1	779.3
0.0972	1259.9	779.7	0.2212	1239.7	780.4
0.1246	1255.3	780.7	0.3394	1229.5	783.1
0.2426	1249.8	781.8	0.4442	1222.8	785.6
0.3179	1246.5	784.3	0.5358	1218.0	787.9
0.3901	1244.4	786.6	0.6649	1212.3	791.3
0.4636	1243.2	788.7	0.7845	1208.0	794.7
0.5409	1242.7	791.5	0.8612	1205.6	797.2
0.6178	1243.2	794.2	1	1204.1	801.9
0.6730	1243.8	796.3			
0.7728	1246.1	800.2			
0.8741	1249.6	804.5			
0.9415	1253.4	807.7			
1	1256.6	810.5			

where M_1 and M_2 are the molar masses of the mixed components, c is the ultrasound velocity and ρ is the density of the mixture.

Using the isobaric coefficients of thermal expansion, α_i^0 , calculated from the measured densities and density data available in literature [1] and the isobaric molar heat capacities, $C_{p,i}^0$, taken as well from literature [1-3], the corresponding isothermic quantities for the pure components, $\beta_{T,i}^0$ and $\kappa_{T,i}^0$, as well as their isochoric molar heat capacities, $C_{V,i}^0$, were calculated from the following equations

$$\begin{aligned}\beta_{T,i}^0 &= \beta_{s,i}^0 + (\alpha_i^0)^2 VT/C_{p,i}^0 \\ \kappa_{T,i}^0 &= \beta_{T,i}^0 V_i^0 \\ C_{V,i}^0 &= C_{p,i}^0 \beta_{s,i}^0 / \beta_{T,i}^0\end{aligned}\quad (2)$$

(where V_i^0 are the molar volumes of the pure components and T is temperature) and collected in Table 2.

Table 2. Isothermic compressibility coefficients, isothermic compressibilities and isochoric molar heat capacities for pure components at 293.15 K

Property	n-butanol	iso-butanol	cyclohexane
$\beta_T^0/(1/TPa)$	889.93	995.18	1088.53
$\kappa_T^0/(m^3/Pa \cdot mol) \cdot 10^{14}$	8.1354	9.1990	11.7725
$C_V^0/(J/mol K)$	188.91	158.58	112.97

The excess quantities V^E , β_s^E and κ_s^E were obtained from the equations

$$\begin{aligned} V^E &= V - V^{id} \\ \beta_s^E &= \beta_s - \beta_s^{id} \\ \kappa_s^E &= \kappa_s - \beta_s^{id} V^{id} \end{aligned} \quad (3)$$

where $V^{id} = x_1 V_1^0 + (1 - x_1) V_2^0$ (x_1 is the mole fraction of alcohol, V_1^0 and V_2^0 are the molar volumes of alcohol and cyclohexane, respectively) β_s^{id} is the isentropic compressibility coefficient of the corresponding ideal mixture calculated as suggested by BENSON et al. [4, 5]:

$$\begin{aligned} \beta_s^{id} &= \beta_T^{id} - (\alpha^{id})^2 V^{id} T / C_p^{id} \\ \beta_T^{id} &= x_{v,1} \beta_{T,1}^0 + (1 - x_{v,1}) \beta_{T,2}^0 \\ x_{v,1} &= x_1 V_1^0 / V^{id} \\ \alpha^{id} &= x_{v,1} \alpha_1^0 + (1 - x_{v,1}) \alpha_2^0 \\ C_p^{id} &= x_1 C_{p,1}^0 + (1 - x_1) C_{p,2}^0 \end{aligned} \quad (4)$$

where the lower indices "1" and "2" refer to alcohol and cyclohexane, respectively, and the upper one "id" indicates quantities related to ideal mixtures. Thus, the excess functions have been calculated using the states of the pure components under the measurement conditions as their standard states: $\mu_i^0 = \mu_i^0$ (where μ_i^0 and μ_i^0 are the standard chemical potential and the chemical potential of the pure components, respectively).

The free intermolecular lengths, L , were obtained, according to JACOBSON [6], from the following relationship

$$\beta_s = k_\beta L^{2.4} \quad (5)$$

where k_β is an empirical constant given in [3, 6].

It was found that the dependences of V , β_s , κ_s and L on the mole fraction of alcohol, x_1 , can be satisfactorily represented by simple polynomials

$$F = \sum_{j=1}^n A_j x_1^{j-1} \quad (6)$$

and those of V^E , β_s^E and κ_s^E by the Redlich-Kister equations:

$$F^E = x_1 (1 - x_1) \sum_{j=1}^n A_j (1 - 2x_1)^{j-1} \quad (7)$$

The A_j parameter values together with the mean standard deviations, s , are given in Table 3.

Table 3. Parameters of equations (6) and (7) and standard deviations *s*.

<i>F</i> or <i>F^E</i>	<i>A</i> ₁	<i>A</i> ₂	<i>A</i> ₃	<i>A</i> ₄	<i>A</i> ₅	<i>s</i>
$\{x_1 \text{n-C}_4\text{H}_9\text{OH} + (1-x_1)\text{C}_6\text{H}_{12}\}$						
<i>V</i> /(m ³ /mol) × 10 ⁷	1081.4	−149.23	−18.73	1.22	—	0.91
<i>β</i> _s /(1/TPa)	788.21	256.68	−665.34	698.08	−297.57	0.99
<i>κ</i> _s /(m ³ /Pa · mol) × 10 ¹⁶	852.05	167.37	−795.55	848.25	−359.11	0.09
<i>L</i> /(m) × 10 ¹⁴	5415.1	728.53	−1898.0	2005.4	−859.46	0.07
<i>V^E</i> /(m ³ /mol) × 10 ⁸	160.77	9.6228	97.499	—	—	0.78
<i>β</i> _s ^{<i>E</i>} /(1/TPa)	30.194	38.016	63.437	—	—	0.27
<i>κ</i> _s ^{<i>E</i>} /(m ³ /Pa · mol) × 10 ¹⁶	43.326	43.334	43.926	—	—	0.27
$\{x_1 \text{iso-C}_4\text{H}_9\text{OH} + (1-x_1)\text{C}_6\text{H}_{12}\}$						
<i>V</i> /(m ³ /mol) × 10 ⁷	1081.7	−139.99	−29.879	12.716	—	0.27
<i>β</i> _s /(1/TPa)	789.72	297.47	−559.51	554.34	−221.81	0.18
<i>κ</i> _s /(m ³ /Pa · mol) × 10 ¹⁶	854.10	214.77	−679.97	670.27	−264.07	0.05
<i>L</i> /(m) × 10 ¹⁴	5419.3	842.81	−1606.5	1597.4	−637.15	0.10
<i>V^E</i> /(m ³ /mol) × 10 ⁹	1063.8	647.11	762.33	—	—	0.03
<i>β</i> _s ^{<i>E</i>} /(1/TPa) × 10 ¹⁴	6299.5	5450.7	5534.6	—	—	0.43
<i>κ</i> _s ^{<i>E</i>} /(m ³ /Pa · mol) × 10 ¹⁶	72.253	66.184	65.860	—	—	0.06

4. Discussion of measurement results

The ultrasonic velocity does not vary linearly with the concentration of alcohols which is obviously related to the complex variations of the thermodynamic parameters. The excessive values of those parameters are positive in the whole concentration range (Figs. 1–3, Table 3) and, except that of the excess volume, are

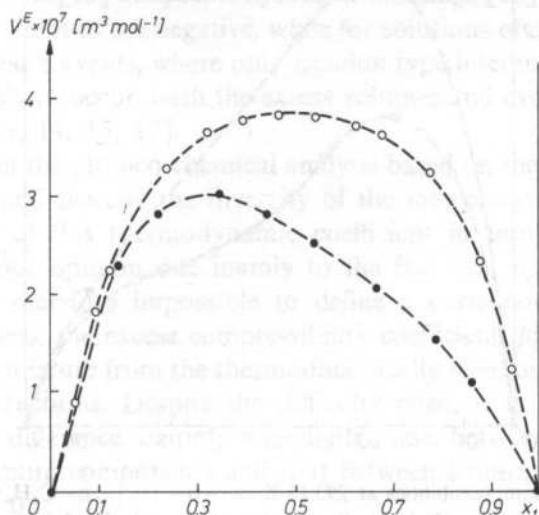


FIG. 1. Excess molar volumes at 293.15 K. —○—, $\{x_1 \text{n-C}_4\text{H}_9\text{OH} + (1-x_1)\text{C}_6\text{H}_{12}\}$; —●—, $\{x_1 \text{iso-C}_4\text{H}_9\text{OH} + (1-x_1)\text{C}_6\text{H}_{12}\}$. Broken lines were calculated from eq. (7) by the best-fit procedure

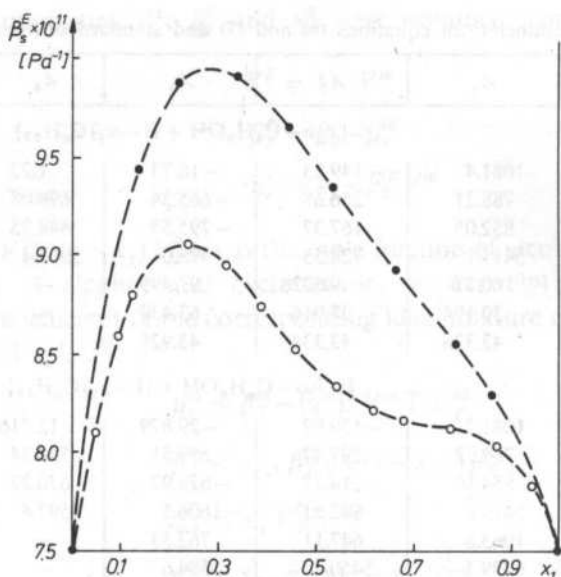


FIG. 2. Excess isentropic compressibility coefficients at 293.15 K —○—, $\{x_1 n\text{-C}_4\text{H}_9\text{OH} + (1-x_1)\text{C}_6\text{H}_{12}\}$; —●—, $\{x_1 \text{iso-C}_4\text{H}_9\text{OH} + (1-x_1)\text{C}_6\text{H}_{12}\}$. Broken lines were calculated from eq. (7) by the best-fit procedure

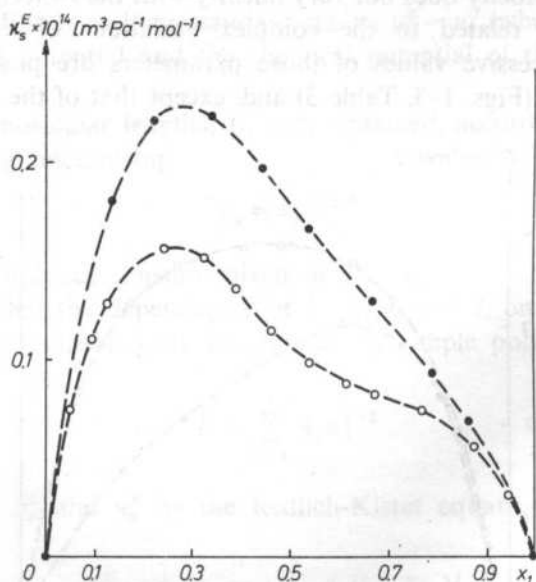


FIG. 3. Excess isentropic compressibilities at 293.15 K. —○—, $\{x_1 n\text{-C}_4\text{H}_9\text{OH} + (1-x_1)\text{C}_6\text{H}_{12}\}$; —●—, $\{x_1 \text{iso-C}_4\text{H}_9\text{OH} + (1-x_1)\text{C}_6\text{H}_{12}\}$. Broken lines were calculated from eq. (7) by the best-fit procedure

larger for the iso-butanol solutions than for the n-butanol ones of corresponding composition. Furthermore, the concentration dependences of the excess parameters show a clear-cut dissymmetry, except that of the excess volume of n-butanol which is almost symmetrical. From inspection of the figures in Table 2 one learns also that the values of all the parameters of pure iso-butanol collected in this table (molar volumes, isothermic and isentropic compressibilities and compressibility coefficients, expansion coefficients and free path lengths) are larger than the corresponding values of pure n-butanol and the difference in the molar volumes of the pure alcohols is almost negligible if compared to those in the compressibility and free path length.

Basing on the Jacobson's model [3], according to which molecular association should result in an increase of the free path length, i.e. in an increase in the intermolecular distance and thereby in a corresponding increase in compressibility, positive deviations of the compressibility of binary mixtures from additivity have been sometimes interpreted as a result of the formation of complexes between the components (for instance [7] and [8]). However it can be easily shown that the reasoning based on this model would be completely justifiable if the volume effect of mixing were zero [9]. As indicated by the above and other data [10–12], mixing of polar liquids with non-polar solvents (e.g. ketones with alicyclic and aliphatic hydrocarbons [14]) is accompanied, as a rule, by positive volume effects (positive excess volumes), i.e. the increase in self-association of the polar component with the increase of its concentrations does not proceed isochorically but results in an decrease of the mean molar volume, while the break-up of multimers of the associating component when, diluted by the non-polar solvent, leads to an increase in volume. There is also convincing evidence that, in spite of the expectations arising from Jacobson's model, if interactions between the components are likely to occur (e.g. interactions of dipole – dipole induced type in mixtures of ketones with aromatic hydrocarbons [15] or specific hydrogen-bondings [16]), the excess volumes and excess compressibilities are negative, while for solutions of alcohols and ketones in aliphatic non-polar solvents, where only London type interactions between solute and solvent are likely to occur, both the excess volumes and excess compressibilities are positive [10, 11, 14, 15, 17].

The difficulties in the physico-chemical analysis based on the isentropic compressibility coefficient, and thereby the diversity of the interpretations of the concentration dependence of this thermodynamic coefficient in terms of intermolecular interactions, is in our opinion due mainly to the fact that β_s is not an extensive quantity and it is therefore impossible to define a corresponding partial molar quantity. Nevertheless, the excess compressibility coefficient, β_s^E , characterizing the deviations of a real mixture from the thermodynamically ideal one must be related to intermolecular interactions. Despite the difficulty cited, it is believed [32] that

i. if there is no difference, or only a negligible one, between the intermolecular interactions in the pure components and that between heterogeneous molecules in the mixtures, $\beta_s^E = 0$,

ii. if the interactions between the heterogeneous molecules are weaker than those

between the molecules in the pure components or, at least, between the molecules in one of them (for instance, because of molecular self-association), $\beta_s^E > 0$,

iii. if, on the contrary, there are only weak intermolecular interactions in the pure components but the components are able to interact effectively with one another (for instance by forming complexes), $\beta_s^E < 0$,

iv. if the effects of self-association and complexation are overlapping, the concentration dependence of β_s^E may be very complex, sometimes β_s^E even changes sign at particular concentrations.

Pure butanols, like other alcohols, are remarkably associated [18, 19], being composed most probably of "open" entities with free OH groups (simple or branched multimetric chains), as well as of "closed" ones. Also in solutions in non-polar solvents, butanols are self-associated [20-27] and form various structures (oligomers): rings or chains with oxygen atoms engaged in one or two hydrogen bonds [19, 20] or, as indicated by the relatively large dipole moments, rings with chains when the "closing" occurs between a terminal OH group and the residual lone-pair of electrons of the oxygen atom of an intermediate mer of the chain [21]. Dielectric studies indicate that the different entities resulting from self-association exist in the solution in different proportions depending on the alcohol concentration.

Some authors suggested that rings are typical rather of multimers of lower order existing in dilute solutions [28], while others believe that those structures exist only in concentrated solutions and are rather typical of higher order multimers [21, 25, 29].

Whatever the particular multimetric structures, it seems to be beyond all question that the observed excessive volumes and compressibilities observed for solutions of alcohols in inert non-polar solvents should be attributed to the weakened hydrogen bonds between the alcohol molecules resulting in an increase in volume and compressibility. This conclusion is corroborated by the positive zeotropy observed for those solutions. Though measurements of dielectric saturation in solutions of n-butanol, iso-butanol and some other alcohols in benzene [22] indicate relatively strong interactions between the molecules of the alcohol and those of benzene leading to the formation of alcohol-solvent assemblies that may compete successfully with the self-association of the alcohols, this effect seems to be due mainly to the easiness of the deformation of the delocalized π -electron orbitals of benzene and distinguish the benzenic solutions from those in cyclohexane. Also, the values of the partition coefficient of n-butanol between water and various organic solvents [21], as well as the data of STEURER and WOLF [30], referring to the self-association of ethanol in cyclohexane, benzene and dioxane, showed the interactions of alcohols with cyclohexane to be markedly weaker than those with other solvents. Thus, it can be assumed that the interactions of the alcohol molecules with most non-polar solvents, and particularly with the low-polarizable cyclohexane, are only weak interactions of Van der Waals type.

Assuming, according to [32] that the maximum compressibility coefficient appears at the concentration at which the main contribution to the total compressibility coefficient arises from intermolecular interactions between heterogeneous

molecules, i.e. from alcohol – cyclohexane Van der Waals interactions, the more pronounced asymmetry of the excess compressibility of n-butanol solutions indicate that the self-association of n-butanol is stronger than that of iso-butanol, while the shape of this concentration dependence, showing, except the maximum, two distinct inflexion points (Table 4), suggests that, at least two kinds of multimers differing in composition and/or structure predominate depending on the composition of the mixtures, while in the iso-butanol solutions the shift of the equilibrium between the different possible multimers is rather a “smooth” one.

Table 4. Maxima and inflexion points of the values determined from measurements

$\{x_1 n - C_4H_9OH + (1 - x_1) C_6H_{12}\} \{x_1 iso - C_4H_9OH + (1 - x_1) C_6H_{12}\}$					
$\beta_{s,max}/(1/TPa)$	822.03	for $x = 0.339$	862.98	for $x = 0.864$	
$\kappa_{s,max}/(m^3/Pa \cdot mol) \times 10^{16}$	862.12	$x = 0.130$	874.96	$x = 0.223$	
$L_{max}/(m) \times 10^{13}$	551.07	$x = 0.340$	562.35	$x = 0.865$	
$V_{max}^E/(m^3/mol) \times 10^9$	402.82	$x = 0.463$	303.72	$x = 0.314$	
$\beta_{s,max}^E/(1/Pa) \times 10^{13}$	122.59	$x = 0.229$	196.98	$x = 0.285$	
$\beta_{s,inf}^E/(1/Pa) \times 10^{13}$	94.743	$x = 0.409$	150.31	$x = 0.526$	
	51.083	$x = 0.741$	100.25	$x = 0.720$	
$\kappa_{s,max}^E/(m^3/Pa \cdot mol) \times 10^{17}$	156.60	$x = 0.243$	230.08	$x = 0.280$	
$\kappa_{s,inf}^E/(m^3/Pa \cdot mol) \times 10^{17}$	126.34	$x = 0.423$	174.90	$x = 0.517$	
	77.456	$x = 0.724$	108.79	$x = 0.734$	

This corresponds well with IR spectra of alcohol- CCl_4 solutions from which it is evident that most solutions of monohydroxy alcohols, except certain sterically hindered ones, contain at moderate concentrations at least two associated species having different numbers of monomer units [31].

The difference in the association potential of both the isomeric alcohols studied arises most probably from the presence of the methyl group at the second carbon atom of the iso-butanol molecule which prevents to a certain degree the self-association since it may act as a small steric obstacle [25] and may also decrease the polarization of the OH group exerting an inductive effect on the latter. Also other physico-chemical constants collected in Table 5 furnish evidence of the difference in the self-association potential of n- and iso-butanol.

Table 5. Physico-chemical properties for the pure alcohols at 293.15 K

	Boiling point [K]	Freezing point [K]	Saturated vapour pressure [kPa]	Density [kg/m ³]	Viscosity [Pa · s] $\times 10^3$	Refractive index (n_D)
n-butanol	390.88	183.55	0.60	809.8	2.948	1.3922
iso-butanol	381.04	165.15	1.17	801.9	3.9068	1.3959

Because of the branched carbon chain, the size of the iso-butanol is smaller than that of n-butanol [7]. Thus, in spite of what is observed (Figs. 4, 5 and 6), the molar volume, compressibility and the free path length of pure iso-butanol are expected to be smaller than the corresponding parameters of n-butanol. This discrepancy may be

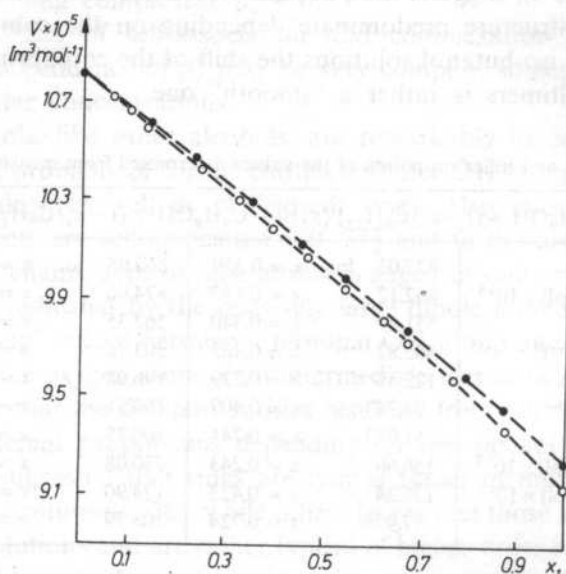


FIG. 4. Molar volumes at 293.15 K. —○—, $\{x_1 n\text{-C}_4\text{H}_9\text{OH} + (1-x_1)\text{C}_6\text{H}_{12}\}$; —●—, $\{x_1 \text{iso-C}_4\text{H}_9\text{OH} + (1-x_1)\text{C}_6\text{H}_{12}\}$. Broken lines were calculated from eq. (6) by the best-fit procedure

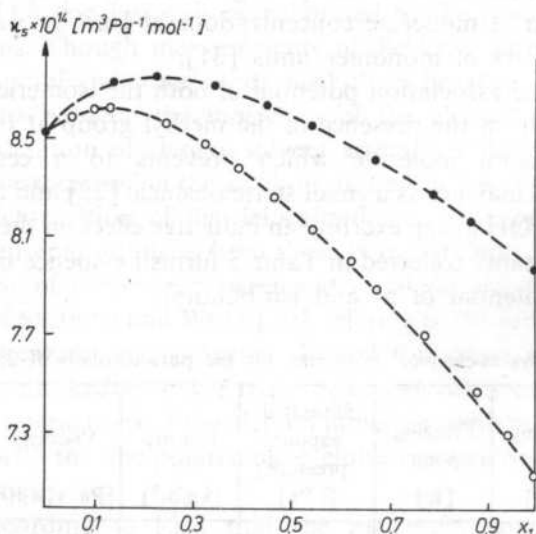


FIG. 5. Isentropic compressibilities at 293.15 K. —○—, $\{x_1 n\text{-C}_4\text{H}_9\text{OH} + (1-x_1)\text{C}_6\text{H}_{12}\}$; —●—, $\{x_1 \text{iso-C}_4\text{H}_9\text{OH} + (1-x_1)\text{C}_6\text{H}_{12}\}$. Broken lines were calculated from eq. (6) by the best-fit procedure

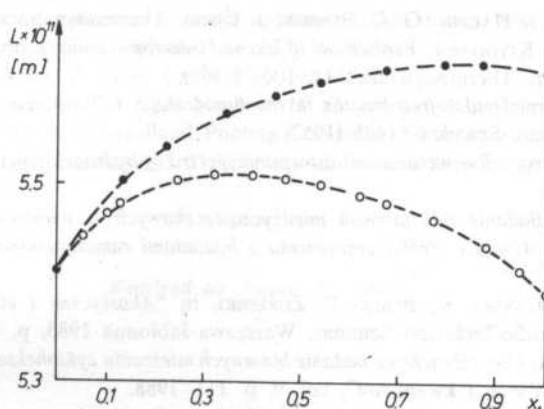


FIG. 6. The free intermolecular lengths at 293.15 K. —o—, $\{x_1 n\text{-C}_4\text{H}_9\text{OH} + (1-x_1)\text{C}_6\text{H}_{12}\}$; —●—, $\{x_1 \text{iso-C}_4\text{H}_9\text{OH} + (1-x_1)\text{C}_6\text{H}_{12}\}$. Broken lines were calculated from eq. (6) by the best-fit procedure

easily explained if, in accordance with the above discussion, a smaller degree of self-association in iso-butanol is assumed. That difference in the self-association potential also makes of the iso-butanol solution the excessive volume increase more slowly when the associates gradually break-down with increasing dilution (Fig. 1).

The results of our measurements, in connection with the literature information, lead to the conclusion that the acoustic and thermodynamic properties of the liquid systems studied are determined mainly by the extent of hydrogen bondings occurring between the molecules of the associating component, i.e. by the "chemical nature" of the alcohols, while the "physical" properties, i.e. the Van der Waals interactions and the space-filling ability, seem to be of lower significance. The results also constitute strong evidence that, despite the anticipation arising from the Jacobson's model, the increase in self-association does not increase the compressibility, but, on the contrary, makes it become smaller than in a corresponding hypothetical non-associated liquid in accordance with the considerations given in [17].

This work was financially supported by the Polish Academy of Sciences, Project CPBP 02.03.

References

- [1] A. WEISSBERGER, *Technique of organic chemistry*, Volume VII., Interscience Publishers, London 1955.
- [2] K. TAMURA, K. OHMURO, S. MURAKAMI, *Speed of sound, isentropic and isothermal compressibilities, and isochoric heat capacities of...*, *J. Chem. Thermodynamics* **15**, 859 (1983).
- [3] B. JACOBSON, *Association numbers in liquid systems from intermolecular free length relationships*, *Acta Chem. Scand.* **9**, 997 (1955).

- [4] O. KIOHARA, C. J. HALPIN, G. C. BENSON, *J. Chem. Thermodynamics* **10**, 721 (1978).
- [5] G. C. BENSON, O. KIOHARA, *Evaluation of excess isentropic compressibilities and isochoric heat capacities*, *J. Chem. Thermodynamics* **11**, 1061 (1979).
- [6] B. JACOBSON, *Intermolecular free lengths in the liquid state. I. Adiabatic and isothermal compressibilities*, *Acta Chem. Scand.* **6**, 1485 (1952).
- [7] W. KAYE, R. POULSON, *Far ultra-violet absorption spectra of hydrogen-bonded methanol*, *Nature* **193**, 675 (1962).
- [8] A. PIOTROWSKA, *Badanie oddziaływań międzycząsteczkowych w mieszaninach cieczy za pomocą pomiaru prędkości dźwięku. Próba zestawienia z badaniami ramanowskimi*, *Roczn. Chem.* **39**, 437 (1965).
- [9] S. ERNST, M. WACIŃSKI, K. BEBEK, E. ZORĘBSKI, in "Akustyczne i elektryczne metody badań materiałowych", Scientific-Technical Seminar, Warszawa-Jabłonna 1983, p. 427.
- [10] K. BEBEK, S. ERNST, *Ultradźwiękowe badanie binarnych mieszanin cykloheksan — alkohole alifatyczne, "Akustyka molekularna i kwantowa"*, vol. 9, p. 111, 1988.
- [11] K. BEBEK, S. ERNST, *Ultrasonic investigation of binary liquid mixtures of aliphatic alcohols with cyclohexane*, (to be published in *Acta Phys. Slov.*).
- [12] S. S. BHATTI, D. P. SINGH, *Molecular association in some n-butanol systems*, *Ind. J. Pure Appl. Phys.* **21**, 506 (1983).
- [13] K. TAMURA, S. MURAKAMI, R. FUJISHIRO, *J. Chem. Thermodynamics* **7**, 1089 (1975).
- [14] K. OHOMURO, K. TAMURA, S. MURAKAMI, *Speed of sound, excess molar volumes, and isentropic compressibilities of $\{x\text{CH}_3\text{COC}_2\text{H}_5 + (1-x)\text{C}_7\text{H}_{16}\}$, $\{x\text{CH}_3\text{COC}_2\text{H}_5 + (1-x)\text{C}_6\text{H}_{12}\}$, $\{x\text{CH}_3\text{COC}_2\text{H}_5 + (1-x)\text{C}_6\text{H}_{11}\text{CH}_3\}$, $\{x\text{C}_2\text{H}_5\text{COC}_2\text{H}_5 + (1-x)\text{C}_7\text{H}_{16}\}$, and $\{x\text{C}_2\text{H}_5\text{COC}_2\text{H}_5 + (1-x)\text{C}_6\text{H}_{12}\}$ at 298.15 K*, *ibid.* **19**, 163 (1987).
- [15] K. OHOMURO, K. TAMURA, S. MURAKAMI, *Speed of sound, excess molar volumes, and isentropic compressibilities of $\{x\text{CH}_3\text{COC}_2\text{H}_5 + (1-x)\text{C}_6\text{H}_6\}$, $\{x\text{CH}_3\text{COC}_2\text{H}_5 + (1-x)\text{C}_6\text{H}_5\text{CH}_3\}$, $\{x\text{CH}_3\text{COC}_2\text{H}_5 + (1-x)\text{C}_6\text{H}_5\text{Cl}\}$, and $\{x\text{C}_2\text{H}_5\text{COC}_2\text{H}_5 + (1-x)\text{C}_6\text{H}_6\}$ at 298.15 K*, *ibid.* **19**, 171 (1987).
- [16] C. SCHUMANN, N. MELCHER, H. KEHLEN, P. HAUPTMANN, *Schallgeschwindigkeiten, Exzeßvolumina, Exzeßwärmekapazitäten und Exzeßkompressibilitäten in Systemen aus Pyridin oder Anilin und Carbonsäuren*, *Z. Phys. Chem., Leipzig* **268**, 401 (1987).
- [17] S. ERNST, J. GLIŃSKI, B. JEŻOWSKA-TRZEBIATOWSKA, *Dependence of the ultrasound velocity on association of liquids*, *Acta Phys. Polonica* **A55**, 501 (1971).
- [18] W. H. ZACHARIASEN, *J. Chem. Phys.* **3**, 158 (1935).
- [19] W. C. PIERCE, D. P. McMILLAN, *X-ray Studies on Liquids: the Inner Peak for Alcohols and Acids*, *J. Am. Chem. Soc.* **60**, 779 (1938).
- [20] P. HUYSKENS, T. ZEEGERS-HUYSKENS, A. M. DIERCKX, *Étude par R.M.N. et spectrométrie I.R. de l'influence du solvant sur les liaisons hydrogène des butanols*, *Ann. Soc. Sci. Bruxelles* **78**, 175 (1964).
- [21] E. MEEUSSEN, P. HUYSKENS, *Étude de la structure du butanol-n en solution par les coefficients de partage*, *J. Chim. Physique* **6**, 845 (1966).
- [22] J. MAŁECKI, *Dielectric polarization of aliphatic alcohols in strong electric fields*, *Acta Phys. Polon.* **21**, 13 (1962).
- [23] J. MAŁECKI, J. NOWAK, *Dielectric study of the effect of deuteration on self-association in t-butanol*, *Acta Phys. Polon.* **A55**, 55 (1979).
- [24] J. MAŁECKI, S. BALANICKA, J. NOWAK, *Study of self-association of t-butyl alcohol by linear and non-linear dielectric effects*, *J.C.S. Faraday II*, **76**, 42 (1980).
- [25] B. B. SWAIN, G. S. RAY, *Studies of dielectric properties of binary liquid mixtures of butanols in nonpolar solvents — linear correlation factor, Excess Molar Polarization and Excess Free Energy*, *Jpn. J. Appl. Phys.* **25**, 2 (1986).
- [26] K. SESHARDI, N. PRABHAKARA RAO, *Ultrasonic behaviour of binary liquid mixtures containing cyclohexane*, *Z. Phys. Chem.* **89**, 108 (1974).
- [27] K. GOPAL, B. RAJESWARA REDDY, N. PRABHAKARA RAO, *Ultrasonic behaviour of binary liquid mixtures containing n-octanol as a common component*, *Arch. Acoust.* **11**, 191 (1986).

- [28] G. OSTER, *The dielectric properties of liquid mixtures*, J. Am. Chem. Soc. **68**, 2036 (1946).
- [29] L. J. BELLAMY, W. PACE, *Spectrochim. Acta* **22**, 535 (1966).
- [30] E. STEURER, K. L. WOLF, *Z. Phys. Chem* **B39**, 101 (1938).
- [31] E. E. TUCKER, E. LIPPERT, "The Hydrogen bond/II. Structure and spectroscopy, eds. P. Schuster, G. Zundel, C. Sandorfy, North-Holland Publing Company, Amsterdam-New York-Oxford, 1976.
- [32] И. Г. МИХАЙЛОВ, Н. Н. СОЛОВЕВ, И. П. СЫРНИКОВ, *Основы молекулярной акустики*, Наука, Москва 1964, с. 129.

Received on August 17, 1989

ON A POSSIBILITY OF REALIZATION OF SAW RESONATOR WITH SURFACE MODES CONVERSION

E. DANICKI

Institute of Fundamental Technological Research of the Polish Academy of Sciences
(00-049 Warszawa, ul. Świętokrzyska 21)

It is shown that surface mode conversion can take place in the reflecting grating on some piezoelectric crystals. When one of the modes is piezoelectrically coupled, while the other is not, the resonator performance will not be sensitive to the IDT position in the resonator cavity region.

1. Introduction

It is known that the Q -factor of surface acoustic wave (SAW) resonator is highly sensitive to the interdigital transducer (IDT) position in the resonator cavity region which can be a problem in resonator design. A layered structure [1] with Rayleigh to Sezawa mode conversion can overcome the above-mentioned difficulty, but another problem arises, namely that concerning the quality of the layered structure.

It is shown below that, at least for some cases of piezoelectric crystals, a similar concept for a SAW resonator can be implemented by operating with a pair of surface modes propagating on a piezoelectric halfspace, namely the generalized Rayleigh, and the generalized Bleustein-Gulayev (B-G) modes.

2. A pair of surface modes

A pair of piezoelectrically coupled and uncoupled modes exists in many crystals. Usually, the first one is a B-G mode, and the second one is a Rayleigh mode, the particle displacement vectors of which on the substrate surface are perpendicular to each other. This makes the coupling between them impossible in grooved, or metal strip grating reflector [2, 3].

But consider the case of GaAs, or LiNbO₃ substrates with cut, and wave propagation direction given by the Euler's angles as shown in Table 1. We see that

Table1. Data for SAW on Metallized Substrate Surface (field amplitudes concern the harmonic wave having an angular frequency $1s^{-1}$ and having power flux density equal to 1 W/m , their values are given for the substrate surface, TCD means the temperature coefficient of delay)

Material Euler's angles Mode	LiNbO ₃ (90°, 90°, 51.9°)		GaAs (45°, 35.7°, 0°)	
	Rayleigh	B-G	Rayleigh	B-G
Displacement vector components [nm]:				
– in propag. direct.	2.347	0.082	1.145	–.012+j2.410
– norm. to surface	j3.137	j0.390	j2.137	–2.644–j.017
– transv. horizont.	–1.401	1.256	j1.928	2.953
el. flux dens. [nC/m ²]	0	0.707	0	–0.136
TCD [ppm/°C]	80	71	38	44
$\Delta v/v$	0	.00242	0	.00035
Velocity	3.5645	3.9489	2.4452	3.0379
Beam steering [°]	–6.4	–6.1	0	0

both modes, one of which is piezoelectrically uncoupled ($\Delta v/v = 0$), have all three components of displacement vector on the substrate surface different from zero. Both are surface modes for a metallized substrate surface (the coupled mode, having $\Delta v/v \neq 0$ is of the SSBW [4] type for the case of a free substrate surface).

Following [3], the coupling between these two modes in a metal strip grating can be evaluated as having about 1/3 of the value for SAW-to-SAW coupling in a similar grating on ST-cut quartz. This weak coupling is still acceptable for SAW resonator operation. (It should be noted however, that the theory [3] concerns SAW to SAW coupling, where the wavenumber of a SAW is well above the cut-off wavenumber of bulk waves. This is not the case for the B-G mode, so that the theory [3] can give only an approximation for the coupling coefficient in the case considered [5]).

3. The resonator frequency response

Let us consider a resonator with a single IDT placed in the cavity region between two reflecting metal strip grating. The grating period Λ is chosen to fulfill the Bragg's condition concerning both modes which are to be coupled and propagating in opposite directions, that is

$$1/\lambda^{(1)} + 1/\lambda^{(2)} = 1/\Lambda, \quad (1)$$

where $\lambda^{(i)}$ is the wavelength of the i -th mode. This ensures the "reflection" of the incident mode with simultaneous conversion to the second mode.

The interdigital transducer radiates the piezoelectrically coupled mode only, which propagates to the grating reflector where mode conversion occurs. The "reflected" mode is piezoelectrically uncoupled so that it reaches the second grating reflector without being "noticed" by the IDT, when the wave is passing by. The second reflector converts this mode to the coupled one propagating back to the cavity region and the IDT in it, generating electric charge on the IDT fingers.

Let the reflecting grating performance be characterized by Γ , where Γ^2 describes the power of the reflected and converted mode as compared to the incident mode power. The above consideration and the theory of IDT [6] leads to the formula for the resonator input admittance as follows

$$Y = j\omega C + \frac{G}{1 + \Gamma^2 \exp(\tau)}, \quad (2)$$

where τ is the phase shift of the harmonic wave on the way from the IDT, through double reflection and conversion, back to the IDT, C is the IDT capacitance and G is the transducer radiation conductance (on a free substrate, without reflectors).

As we see, the transducer position in the cavity region is not a parameter in the above formula, so it has no influence on the resonator performance.

Reference

- [1] R. M. Melloch, R. L. Gunshor, R. F. Pierret, *Sezawa to Rayleigh mode conversion in ZnO-on-Si surface acoustic wave device configuration*, Appl. Phys. Lett., **39**, p. 476 (1981).
- [2] E. DANICKI, *Reflection of SAW from periodic shallow grooves*, Wave motion, **9**, pp. 445-453 (1987).
- [3] E. DANICKI, *Perturbation theory of surface acoustic wave reflection from a periodic structure with arbitrary angle of incidence*, Arch. Mech., **36**, pp. 623-638 (1984).
- [4] M. F. LEWIS, *Surface skimming bulk waves*, SSBW, IEEE Ultras. Symp. Proc. p. 744 (1977).
- [5] E. DANICKI, *Propagation of transverse surface acoustic waves in rotated Y-cut quartz under heavy periodic metal electrodes*, IEEE Trans., SU-30, pp. 304-312 (1983).
- [6] E. DANICKI, *Analysis of nearly periodic IDTs by means of scattering matrix for periodic metal strips*, Int. Sch. Phys. Acoust., Erice, Italy 1988, World Sci. Singapore 1989, pp. 425-440.

Received on January 21, 1990

SCATTERING OF ELASTIC SURFACE WAVES ON A LOCALIZED MECHANICAL LOAD OF THE SURFACE

A. DUKATA, J. KAPELEWSKI

Institute of Technical Physics
(00-908 Warszawa, ul. S. Kaliskiego 2/9)

This paper presents a model of scattering of elastic surface waves (ESW) on a single reflective elements of dot structures loading the surface of a hexagonal structure with a sixfold rotation axis, normal to the plane of propagation. Qualitative results obtained with the use of TIERSTEN type boundary conditions [7] and reduced Green's functions presented by MARADUDIN and DOBRZYŃSKI [14] are given for a rectangular dot. Resultant components of the scattering amplitude were achieved with the utilization of an approximation of the stationary phase and approximation of far distances.

Przedstawiono model rozpraszania sprężystych fal powierzchniowych SFP na pojedynczych elementach odbiciowych struktur kropkowych, obciążających powierzchnię ośrodka heksagonalnego z sześciokrotną osią obrotu w kierunku normalnym do płaszczyzny propagacji. Podano jakościowe rezultaty dla kropki prostokątnej wykorzystując warunki brzegowe typu TIERSTENA [7] oraz zredukowane funkcje Greena podane przez MARADUDINĄ i DOBRZYŃSKIEGO [14]. Wynikowe składowe amplitudy rozpraszania uzyskano wykorzystując przybliżenie stacjonarnej fazy oraz przybliżenie dalekich odległości.

1. Introduction

This paper is aimed at the study of the effect of scattering of an elastic surface wave (ESW) on small mutually insulated loading centres considered as elements of reflection lines (so-called dots). Here small means that the greatest linear dimension of the centre is comparable to the length of incident wave. Such a dot is physically made by applying a thin metallic film with required shape, by picking a shallow groove, or by diffusion of another metal into the substrate, etc.

First devices applying the reflection of surface waves from dot arrays were constructed in 1976-1977 in the USA [1-4]. In the first approximation these arrays can be considered as discontinuous stripe structures, where the number of dots in each line determines the reflecting power, i.e. causes amplitude weighting.

In order to increase the efficiency of devices applying structures mentioned above, theoreticians now investigate the influence of the shape of a single reflector (dot) on the system's response. Besides the classical paper [5] which applies the method of partial waves to describe scattering on dots with circular symmetry profiles paper [6] applies Born's approximation for constructing a theory of scattering on dots with arbitrary profile, on anisotropic substrate. Paper [6] also contains a list of publications concerning mentioned above structures.

This paper contains a model of the scattering. It was built with the use of the Green's function method, familiar from the mechanics of continuous media. It can be applied to dots of arbitrary profile, located on the surface of a medium with hexagonal structure or (after algebraic modifications) an isotropic medium (see [14, 15]).

2. Formulation of the problem

Let us consider an elastic half-space loaded with a thin layer of material with constant thickness h and a given shape. "Loaded" means that the velocity of an acoustic transverse wave in the layer of material is lower than that of a transverse wave in the substrate [7, 8]. Figure 1 shows the geometry of the problem.

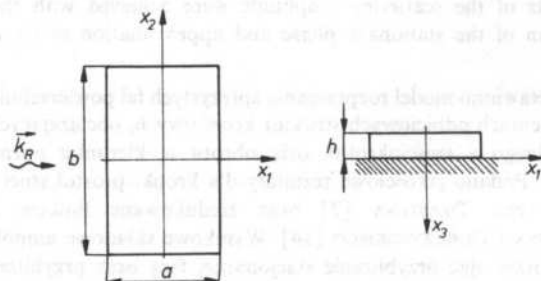


FIG. 1. A rectangular dot located on the surface of an elastic half-space on which a plane surface wave with wave vector k_R is scattered: a , b , h — dimensions of the dot

In further considerations we apply the summation convention. Differentiation with respect to time is denoted with a dot above the symbol, and differentiation with respect to the coordinates is denoted with a comma preceding the index. The equation of motion for an elastic half space can be written as follows

$$\rho \ddot{u}_i = T_{ij,j} + f_i, \quad (2.1)$$

where

$$T_{ij} = C_{ijkl}(\mathbf{x}) \eta_{kl}(\mathbf{x}), \quad (2.2)$$

$$C_{ijkl}(\mathbf{x}) = \theta(x_3) C_{ijkl}, \quad (2.3)$$

$$\eta_{kl}(\mathbf{x}) = \frac{1}{2} (u_{k,l} + u_{l,k}), \quad (2.4)$$

and

$$\theta(x_3) = \begin{cases} 1, & x_3 \geq 0 \\ 0, & x_3 < 0 \end{cases}$$

Denotation T_{ij} — stress tensor; η_{kl} — strain tensor; u_i — displacement vector, ρ — density of the material of the half space, $C_{ijkl}(\mathbf{X})$ — elasticity tensor, dependent on coordinates, C_{ijkl} — classical elasticity tensor, independent of coordinates, f_i — density of external forces acting on the half-space. Inserting (2.2)–(2.4) into (2.1) and taking advantage of the symmetry of C_{ijkl} with respect to k, l , we have

$$\rho \ddot{u}_i = \delta(x_3) C_{i3kl} u_{k,l} + \theta(x_3) C_{ijkl} u_{k,lj} + f_i. \quad (2.5)$$

3. Equation of the scattering

In order to determine the equation governing the scattering of elastic waves on the described before type of disturbance, we will apply the method given in [9]. Let us consider two fields, u_i and v_i in an undisturbed medium, which satisfy the following equations of motion in the region R (elastic half-space, in our case)

$$\rho \ddot{u}_i = \delta(x_3) C_{i3kl} u_{k,l} + \theta(x_3) C_{ijkl} u_{k,lj} + f_i. \quad (3.1)$$

$$\rho \ddot{v}_i = \delta(x_3) C_{i3kl} v_{k,l} + \theta(x_3) C_{ijkl} v_{k,lj} + g_i. \quad (3.2)$$

where f_i and g_i as before are non-homogeneities in these differential equations.

If

$$\begin{aligned} u_i(\mathbf{x}, t) &= u_i(\mathbf{x}) \exp(-i\omega t), \\ f_i(\mathbf{x}, t) &= f_i(\mathbf{x}) \exp(-i\omega t), \\ v_i(\mathbf{x}, t) &= v_i(\mathbf{x}) \exp(-i\omega t), \\ g_i(\mathbf{x}, t) &= g_i(\mathbf{x}) \exp(-i\omega t), \end{aligned} \quad (3.3)$$

then equations (3.1) and (3.2) are reduced to the following form

$$\delta(x_3) C_{i3kl} u_{k,l} + \theta(x_3) C_{ijkl} u_{k,lj} + \rho \omega^2 u_i + f_i = 0, \quad (3.4)$$

$$\delta(x_3) C_{i3kl} v_{k,l} + \theta(x_3) C_{ijkl} v_{k,lj} + \rho \omega^2 v_i + g_i = 0. \quad (3.5)$$

From a combination of these equations we have

$$v_i f_i - u_i g_i + \delta(x_3) C_{i3kl} (v_i u_{k,l} - u_i v_{k,l}) + \theta(x_3) C_{ijkl} (v_i u_{k,lj} - u_i v_{k,lj}) = 0. \quad (3.6)$$

and further

$$\begin{aligned} v_i f_i - u_i g_i + \delta(x_3) C_{i3kl} (v_i u_{k,l} - u_i v_{k,l}) + \theta(x_3) C_{ijkl} (v_i u_{k,l} - u_i v_{k,l})_j + \\ - \theta(x_3) C_{ijkl} (v_{i,j} u_{k,l} - u_{i,j} v_{k,l}) = 0. \end{aligned} \quad (3.7)$$

The last term in this equation is equal to zero, because of the symmetry of C_{ijkl} with respect to pairs of indices ij , kl .

Substituting now

$$\begin{aligned} g_i &= \delta_{im} \delta(\mathbf{x} - \mathbf{x}'), \\ v_i &= G'_{im}(\mathbf{x}, \mathbf{x}'), \end{aligned} \quad (3.8)$$

where G'_{im} is a Green's function of equation (3.2) with the condition (3.8)₁, we reach

$$\begin{aligned} f_i G'_{im} - u_i \delta_{im} \delta(\mathbf{x} - \mathbf{x}') + \delta(x_3) C_{i3kl} (G'_{im} u_{k,l} - u_i G'_{km,l}) + \\ + \theta(x_3) C_{ijkl} (G'_{im} u_{k,l} - u_i G'_{km,l})_{,j} = 0. \end{aligned} \quad (3.9)$$

After integrating the above expression in terms of volume and taking advantage of the Gauss theorem in region R we have:

$$u_m(\mathbf{x}') = \int_R \delta(x_3) C_{i3kl} (G'_{im} u_{k,l} - u_i G'_{km,l}) dV + C_{ijkl} \int_S (G'_{im} u_{k,l} - u_i G'_{km,l}) n_j dS + \int_R dV f_i G'_{im}, \quad (3.10)$$

where n_j is the external normal to the region R limited by the surface S (Fig. 2). In

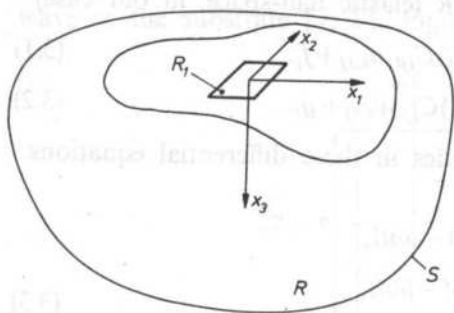


FIG. 2. Coordinates system with the region R , of interest to us, limited by surface S partially contained in the plane of the surface

accordance with reasoning in paper [9], the first two integrals depend on boundary conditions only and can be substituted with a field of displacements $u_m^0(\mathbf{x}')$. This field satisfies the following homogeneous equation:

$$\delta(x'_3) C_{i3kl} u_{k,l}^0 + \theta(x'_3) C_{ijkl} u_{k,l,j}^0 + \varrho \omega^2 u_i^0 = 0. \quad (3.11)$$

The boundary condition for S usually has the following form in the problem of scattering

$$u_i^0(\mathbf{x}, t) = u_i^0 \exp [i(\mathbf{k}\mathbf{x}) - \omega t], \quad (3.12)$$

i.e. $u_i^0(\mathbf{x}, t)$ is an incident wave with frequency ω and wave vector \mathbf{k} . In general the amplitude u_i^0 can be a function of coordinate x_3 . Finally, we can write:

$$u_m = u_m^0 + \int_R dV f_i G'_{im} \quad \text{for } \mathbf{x}' \text{ in } R, \quad (3.13)$$

where Green's function G'_{im} satisfies the equation

$$\left(\delta_{ji} \rho \omega^2 + \delta(x_3) C_{j3ik} \frac{\partial}{\partial x_k} + \theta(x_3) C_{jlik} \frac{\partial^2}{\partial x_k \partial x_l} \right) G'_{im}(\mathbf{x}, \mathbf{x}'; \omega) = \delta_{jm} \delta(\mathbf{x} - \mathbf{x}'). \quad (3.14)$$

4. Thin layer deposited on the surface of an elastic half-space as a disturbance

In a case of thin isotropic films ($h \ll \lambda$) loading a substrate, the film can be substituted with an equivalent stress pattern [10]:

$$T_{31}(x_3 = 0) = \left\{ -h \left(k^2 \frac{c'_{11} - c'_{12}}{c'_{11}} - \rho' \omega^2 \right) u_1^{(0)} \right\} \exp(ikx_1), \quad (4.1)$$

$$T_{32}(x_3 = 0) = \left\{ -h \left(k^2 \frac{c'_{11} - c'_{12}}{2} - \rho' \omega^2 \right) u_2^{(0)} \right\} \exp(ikx_1), \quad (4.2)$$

$$T_{33}(x_3 = 0) = \{ h \rho' \omega^2 u_3^{(0)} \} \exp(ikx_1), \quad (4.3)$$

In general $T_{3i}(x_3 = 0) = T_i \exp(ikx_1)$. In above expressions, h is the film's thickness, k denotes the wavevector length, ω — frequency of wave propagating in the direction of x_1 in the elastic half-space, ρ' — mass density of the film, c'_{11} and c'_{12} reduced components of the elasticity tensor in Voigt's notation [11] of the thin isotropic layer.

In the case of a thin film, the disturbing force in equation (3.13) is equal to

$$f_i = T_{ik} n_k, \quad (4.4)$$

where n_k is the external normal $n_k = [0, 0, -1]$ with the dimension of the surface. As the disturbance occurs in plane $x'_3 = 0$, so

$$f_i(\mathbf{x}') = \delta(x'_3) T_{ik}(\mathbf{x}') n_k \theta(R_1), \quad (4.5)$$

where

$$\theta(R_1) = \begin{cases} 1 & (x'_1, x'_2) \in R_1, \\ 0 & (x'_1, x'_2) \notin R_1 \end{cases}$$

and R_1 — disturbance region in plane x'_1, x'_2 . Including (4.5) in equation (3.13), we get

$$\begin{aligned} u_m(\mathbf{x}) &= u_m^{(0)}(\mathbf{x}) + \int_R f_i(\mathbf{x}') G_{im}(\mathbf{x}, \mathbf{x}') d\mathbf{x}' = \\ &= u_m^{(0)}(\mathbf{x}) + \int_R \delta(x'_3) T_{ik}(\mathbf{x}') n_k \theta(R_1) G_{im}(\mathbf{x}, \mathbf{x}') d\mathbf{x}'. \end{aligned}$$

And finally

$$u_m(\mathbf{x}) = u_m^{(0)}(\mathbf{x}) + \int_{R_1} -T_{i3}(x'_1, x'_2, x'_3 = 0) G_{im}(\mathbf{x}'_{\parallel} - \mathbf{x}_{\parallel}, x'_3 = 0) dx'_1 dx'_2.$$

The minus sign in the above expression is the result of the convention accepted in equation (4.4), that the so-called "compressive" stress has a negative sign. In order to shorten the notation, index \parallel was introduced in expression (4.6). This sign denotes the projection of a corresponding vector (e.g. \mathbf{x}) on the plane of the half-space's surface.

5. Amplitude of ESW scattering on a single dot

The method of determining the Green's function G_{im} , satisfying equation (S. 0), in quadratures is presented in the Supplement. Comparing (3.14) and (S. 0) we see that the sought function G'_{im} is equal to

$$G'_{im} = G_{im} \frac{1}{Q}. \quad (5.0)$$

Let us rewrite the equation (S. 1) in the following form

$$G_{im}(\mathbf{x}, \mathbf{x}'; \omega) = \int_0^{\infty} \int_0^{2\pi} \exp(ikr \cos \gamma) d_{im}(k, \theta, \omega | x_3 x'_3) d\gamma k dk, \quad (5.1)$$

where $\mathbf{r} = \mathbf{x}_{\parallel} - \mathbf{x}'_{\parallel}$, $v = \theta - \Phi$ — angle between vectors \mathbf{k} and \mathbf{r} , $r = r \cos \Phi$, $r_2 = r \sin \Phi$, $k_1 = k \cos \theta$, $k_2 = k \sin \theta$.

We will take advantage of the approximation of the stationary phase (see e.g. [12], page 46) in order to integrate with respect to angle v . This result in

$$G_{im}(\mathbf{x}, \mathbf{x}'; \omega) = \frac{1}{(2\pi)^2} (2\pi)^{1/2} \int \frac{\exp[i(kr + \pi/4)]}{(2kr)^{1/2}} d_{im}(k, \Phi, \omega | x_3 x'_3) k dk. \quad (5.2)$$

Tensor d_{im} can be easily found if we write equation (S. 7) in the matrix form

$$\tilde{d} = \tilde{S}^{-1} \tilde{q} \tilde{S}$$

hence

$$\tilde{d} = \begin{pmatrix} \cos^2 \Phi g_{11} + \sin^2 \Phi g_{22}; & \cos \Phi \sin \Phi (g_{11} - g_{22}); & \cos \Phi g_{13} \\ \cos \Phi \sin \Phi (g_{11} - g_{22}); & \sin^2 \Phi g_{11} + \cos^2 \Phi g_{22}; & \sin \Phi g_{13} \\ \cos \Phi g_{31}; & \sin \Phi g_{31}; & g_{33} \end{pmatrix}. \quad (5.3)$$

Including (5.0) and (5.2) in (4.6), and applying the theory of residua (for an analogic approach — see [13]) we obtain resulting components of displacement vector for the scattering wave

$$u_m(\mathbf{x}) = \frac{\exp(i\pi/4)}{i2(2\pi)^{1/2}} \sum_s \text{Res} \left\{ \int T_{i3}(x'_1, x'_2, x'_3 = 0) \frac{\exp(ik_s |\mathbf{x}_{\parallel} - \mathbf{x}'_{\parallel}|)}{(k_s |\mathbf{x}_{\parallel} - \mathbf{x}'_{\parallel}|)^{1/2}} \times \right. \\ \left. \times \frac{1}{Q} d_{im}(k_s, \Phi, \omega | x_3 x'_3 = 0) k_s d\bar{x}'_{\parallel} \right\}, \quad (5.4)$$

where k_s denotes a pole associated with every possible type of wave occurring in the crystal and it is a solution to equation $D(k_s) = 0$ for surface waves or $\alpha_i(k_s) = 0$ for bulk waves (see "Supplement" expressions (S. 12) and (S. 13)).

Coefficients accompanying $\exp(ik_s x_{\parallel})/(x_{\parallel})^{1/2}$ are the amplitudes of scattering for individual modes.

In order to isolate them we will proceed as in the quantum mechanics theory of scattering and apply the following approximation in the expression in the exponent

$$k_s |\mathbf{x}_{\parallel} - \mathbf{x}'_{\parallel}| \approx k_s x_{\parallel} - \mathbf{k}_s \mathbf{x}'_{\parallel} \quad (5.5)$$

($\mathbf{k}_s \parallel \mathbf{x}_{\parallel}$) when at the same time \mathbf{x}'_{\parallel} neglected in the denominator in expression (5.4). Angle Φ will now be the angle between vector \mathbf{x}_{\parallel} and the Ox_1 axis. Our considerations result in an expression for scattering of ESW on a localized stress pattern

$$u_m(\mathbf{x}) = \sum_s A_m^s(\Phi, \omega) \frac{\exp(ik_s x_{\parallel})}{(x_{\parallel})^{1/2}} \quad (5.6)$$

with amplitudes of scattering

$$A_m^s(\Phi, \omega) = \frac{\exp(i\pi/4)}{i2(2\pi)^{1/2}} \text{Res}_{k_s} \{d_{im}(k_s, \Phi, \omega | x_3 x'_3 = 0) k_s \times \\ \times \int T_{i3}(\mathbf{x}'_{\parallel}, x'_3 = 0) \exp(ik_s x'_{\parallel}) d^2 \bar{x}'_{\parallel}\}. \quad (5.7)$$

The asymptotic expression (5.6)–(5.7) is a solution to the problem of scattering of ESW on localized thin films loading a crystalline half-space of one of the types listed at the beginning of the "Supplement". The complicated form of relation $D(k_s) = 0$ requires numerical calculations. For particular case of isotropic substrate only (see [15]), an analytical solution can be found [16]. Qualitative relationships can be relatively easily obtained for a case when an elastic surface wave with vector k_R incides onto a rectangular dot (Fig. 1) with dimensions a and b . In such a case the components of the amplitude of scattering for a surface wave associated with vector k_R can be determined. The integral in expression (5.7) assumes the following value:

$$ab Sa[(1 + \cos \Phi) k_R a/2] Sa[\sin \Phi k_R b/2], \quad (5.8)$$

where $Sa(x) = \sin(x)/x$.

Components of the amplitude of scattering are expressed by

$$A_1^R(\Phi, k_R) = A(\Phi, k_R) \{\cos^2 \Phi G_{11} T_1 + \cos \Phi \sin \Phi G_{11} T_2 + \cos \Phi G_{31} T_3\},$$

$$A_2^R(\Phi, k_R) = A(\Phi, k_R) \{\cos \Phi \sin \Phi G_{11} T_1 + \sin^2 \Phi G_{11} T_2 + \sin \Phi G_{31} T_3\},$$

$$A_3^R(\Phi, k_R) = A(\Phi, k_R) \{\cos \Phi G_{13} T_1 + \sin \Phi G_{13} T_2 + G_{33} T_3\},$$

where

$$A(\Phi, k_R) = \frac{ab \exp(i\Pi/4)}{i2(2\Pi)^{1/2}} k_R Sa[(1 + \cos \Phi) k_R a/2] Sa[\sin \Phi k_R b/2],$$

$$G_{im}(k_R) = \frac{1}{Q} \operatorname{Res}_{k=k_R} [g_{im}(k) - g_{im}^p(k)].$$

Quantities g_{im} and G_{im}^p are explained in the "Supplement"

Supplement

The Green's function for a half-infinite hexagonal crystal

In order to understand given above considerations it is necessary to present in short at least, results of DOBRZYŃSKI'S and MARADUDIN'S paper [14]. It presents a method of finding Green's function $G_{im}(\mathbf{x}, \mathbf{x}'; \omega)$ for a half-infinite hexagonal crystal in quadratures.

This function satisfies the following equation

$$\sum_i \left(\delta_{ji} \omega^2 + \frac{1}{\varrho} \delta(x_3) \sum_k C_{j3ik} \frac{\partial}{\partial x_k} + \frac{1}{\varrho} \sum_{mk} C_{jlik} \frac{\partial^2}{\partial x_l \partial x_k} \right) G_{im}(\mathbf{x}, \mathbf{x}', \omega) = \delta_{jm}(\mathbf{x} - \mathbf{x}'). \quad (\text{S.0})$$

As previously, latin indices accept values from the set (1, 2, 3), which denote directions in the cartesian coordinates system.

a) Bivariate Fourier distribution $G_{im}(\mathbf{x}, \mathbf{x}'; \omega)$. Green's function $G_{im}(\mathbf{x}, \mathbf{x}'; \omega)$ for an elastic medium with arbitrary symmetry which occupies half-space $x_3 > 0$ can be distributed according to the Fourier distribution as follows:

$$G_{im}(\mathbf{x}, \mathbf{x}'; \omega) = \int \frac{d^2 k}{(2\Pi)^2} \exp[i\mathbf{k}(\mathbf{x}_{\parallel} - \mathbf{x}'_{\parallel})] d_{im}(\mathbf{k}\omega; x_3 x'_3), \quad (\text{S.1})$$

where \mathbf{x}_{\parallel} and \mathbf{k} are vectors with components $(x_1, x_2, 0)$ and $(k_1, k_2, 0)$, respectively. If equation (5.1) together with representation

$$\delta(\mathbf{x} - \mathbf{x}') = \delta(x_3 - x'_3) \int \frac{d^2 k}{(2\Pi)^2} \exp[i\mathbf{k}(\mathbf{x}_{\parallel} - \mathbf{x}'_{\parallel})] \quad (\text{S.2})$$

are included in equation (S.0) and the resulting equation is specified for a case of a hexagonal crystal structure with a sixfold rotation axis in direction x_3 , i.e. structure included in one of crystal classes 6, $\bar{6}$, 6/m, 6 mm, $\bar{6}m2$, 62,6/mm in the Herman-Maugin's notation, then the equation fulfilled by Fourier's coefficients $d_{im}(\mathbf{k}\omega; x_3 x'_3)$ assumes the following form

$$\sum_j L_{ij}(\mathbf{k}\omega; x_3) d_{jm}(\mathbf{k}\omega; x_3 x'_3) = \delta_{im}(x_3 - x'_3). \quad (\text{S.3})$$

b) Transformation of the set of equations (S.3) Elements of the matrix of the differential operator $L_{ij}(\mathbf{k}\omega: x_3)$ have very complicated form [14]. It can be simplified, if we take advantage of the isotropy of the hexagonal structure in the plane perpendicular to the sextuple axis of rotation (plane $x_3 = 0$, in this case). We will transform the set of equations (S.3) with respect to matrix $\tilde{S}(\mathbf{k})$, noted as:

$$\tilde{S}(\mathbf{k}) = \begin{pmatrix} \hat{k}_1 & \hat{k}_2 & 0 \\ -\hat{k}_2 & \hat{k}_1 & 0 \\ 0 & 0 & 1 \end{pmatrix}, \quad (\text{S.4})$$

$$\tilde{S}^{-1}(\mathbf{k}) = \begin{pmatrix} \hat{k}_1 & -\hat{k}_2 & 0 \\ \hat{k}_2 & \hat{k}_1 & 0 \\ 0 & 0 & 1 \end{pmatrix},$$

where $\hat{k}_1 = k_1/k$ and $\hat{k}_2 = k_2/k$. This real, orthogonal matrix is a matrix which rotates vector \mathbf{k} into vector $(k, 0, 0)$. Equation (S.3) has the following form after the transformation:

$$\sum_j \mathcal{L}_{ij}(\mathbf{k}\omega: x_3) g_{jm}(\mathbf{k}\omega: x_3 x'_3) = \delta_{im} \delta(x_3 - x'_3), \quad (\text{S.5})$$

where

$$\tilde{\mathcal{L}}(\mathbf{k}\omega: x_3) = \tilde{S}(\mathbf{k}) \tilde{L}(\mathbf{k}\omega: x_3) \tilde{S}^{-1}(\mathbf{k}) \quad (\text{S.6})$$

and

$$d_{im}(\mathbf{k}\omega: x_3 x'_3) = \sum_{jk} S_{ji}(\mathbf{k}) S_{km}(\mathbf{k}) g_{jk}(\mathbf{k}\omega: x_3 x'_3). \quad (\text{S.7})$$

The above transformation eliminates certain elements of the matrix of the differential operator, and makes other elements dependent on the modulus of vector \mathbf{k} , only.

c) Solution of the set of equations (S.5) The solution of the set of equations (S.5) is reduced to a solution of the following set of equations noted in matrix form

$$\begin{pmatrix} \omega^2 - \frac{c_{11}}{\varrho} k^2 + \frac{c_{44}}{\varrho} \frac{d^2}{dx_3^2} & 0 & \frac{i}{\varrho} (c_{13} + c_{44}) k \frac{d}{dx_3} \\ 0 & \omega^2 - \frac{c_{11} - c_{12}}{2\varrho} k^2 + \frac{c_{44}}{\varrho} \frac{d^2}{dx_3^2} & 0 \\ \frac{i}{\varrho} (c_{13} + c_{44}) k \frac{d}{dx_3} & 0 & \omega^2 - \frac{c_{44}}{\varrho} k^2 + \frac{c_{33}}{\varrho} \frac{d^2}{dx_3^2} \end{pmatrix} \times$$

$$\times \begin{pmatrix} g_{11} & g_{12} & g_{13} \\ g_{21} & g_{22} & g_{23} \\ g_{31} & g_{32} & g_{33} \end{pmatrix} = \delta(x - x') \begin{pmatrix} 1 & 0 & 0 \\ 0 & 1 & 0 \\ 0 & 0 & 1 \end{pmatrix}. \quad (\text{S.8})$$

Elements of matrix \tilde{g} have to satisfy noted below boundary conditions on plane $x_3 = 0$.

$$\begin{aligned} \frac{c_{44}}{\varrho} \frac{d}{dx_3} g_{1i} + i \frac{c_{44}}{\varrho} k g_{3i} &= 0, \\ \frac{c_{44}}{\varrho} \frac{d}{dx_3} g_{2i} &= 0, \\ i \frac{c_{13}}{\varrho} k g_{1i} + \frac{c_{33}}{\varrho} \frac{d}{dx_3} g_{3i} &= 0, \end{aligned} \quad (\text{S.9})$$

where $i = 1, 2, 3$. We will omit rather complicated calculations and write the final form of the matrix of reduced Green's functions $g_{jk}(k\omega: x_3 x'_3)$ for a hexagonal system described above [14]

$$\tilde{g} = \begin{bmatrix} g_{11} & 0 & g_{13} \\ 0 & g_{22} & 0 \\ g_{31} & 0 & g_{33} \end{bmatrix}. \quad (\text{S.10})$$

Elements not equal to zero assume values given below. Quantities g_{11} and g_{31}

$$\begin{aligned} g_{11}(k\omega: x_3 x'_3) &= [D(k\omega)]^{-1} [A_{11}(k\omega) \exp \{-\alpha_1(x_3 + x'_3)\} + \\ &+ A_{12}(k\omega) \exp \{-\alpha_1 x_3 - \alpha_2 x'_3\} + A_{21}(k\omega) \exp \{-\alpha_2 x_3 - \alpha_1 x'_3\} + \\ &+ A_{22}(k\omega) \exp \{-\alpha_2(x_3 + x'_3)\} + g_{11}^p(k\omega: x_3 x'_3)], \end{aligned} \quad (\text{S.11 a})$$

$$\begin{aligned} g_{31}(k\omega: x_3 x'_3) &= -i \frac{c_{44}}{(c_{13} + c_{44})\alpha_1 k} \left(\alpha_1^2 - \frac{c_{11}}{c_{44}} k^2 + \frac{\varrho \omega^2}{c_{44}} \right) [D(k\omega)]^{-1} \times \\ &\times (A_{11}(k\omega) \exp \{-\alpha_1(x_3 + x'_3)\} + A_{12}(k\omega) \exp \{-\alpha_1 x_3 - \alpha_2 x'_3\}) - \\ &- i \frac{c_{44}}{(c_{13} + c_{44})\alpha_2 k} \left(\alpha_2^2 - \frac{c_{11}}{c_{44}} k^2 + \frac{\varrho \omega^2}{c_{44}} \right) [D(k\omega)]^{-1} \times \\ &\times (A_{21}(k\omega) \exp \{-\alpha_2 x_3 - \alpha_1 x'_3\} + A_{22}(k\omega) \exp \{-\alpha_2(x_3 + x'_3)\}) + \\ &+ g_{31}^p(k\omega: x_3 x'_3). \end{aligned} \quad (\text{S.11 b})$$

In these expressions

$$\begin{aligned} A_{11} &= M_{22} C_{11} - M_{12} C_{21}, \\ A_{12} &= M_{22} C_{12} - M_{12} C_{22}, \\ A_{21} &= -M_{21} C_{11} + M_{11} C_{21}, \\ A_{22} &= -M_{21} C_{12} + M_{11} C_{22} \end{aligned}$$

all quantities are functions of k and ω , where

$$M_{1(1,2)}(k\omega) = [(c_{13} + c_{44})\alpha_{1,2}]^{-1} \left[-(c_{13} + c_{44})\alpha_{1,2}^2 + c_{44} \left(\alpha_{1,2}^2 - \frac{c_{11}}{c_{44}}k^2 + \frac{q\omega^2}{c_{44}} \right) \right],$$

$$M_{2(1,2)}(k\omega) = [(c_{13} + c_{44})k]^{-1} \left[(c_{13} + c_{44})k^2 + \frac{c_{33}c_{44}}{c_{13}} \left(\alpha_{1,2}^2 - \frac{c_{11}}{c_{44}}k^2 + \frac{q\omega^2}{c_{44}} \right) \right],$$

$$C_{1(1,2)}(k\omega) = \frac{q}{2c_{44}} \frac{1}{\alpha_{1,2}^2 - \alpha_{2,1}^2} \left(\alpha_{1,2}^2 + \frac{c_{13} + c_{44}}{c_{33}}k^2 - \frac{c_{44}}{c_{33}}k^2 + \frac{q\omega^2}{c_{33}} \right),$$

$$C_{2(1,2)}(k\omega) = \frac{qk}{2c_{44}c_{13}} \frac{1}{\alpha_{1,2}(\alpha_{1,2}^2 - \alpha_{2,1}^2)} \times \left[c_{13} \left(\alpha_{1,2}^2 - \frac{c_{44}}{c_{33}}k^2 + \frac{q\omega^2}{c_{33}} \right) - (c_{13} + c_{44})\alpha_{1,2}^2 \right].$$

Quantities g_{13} and g_{33}

$$\begin{aligned} g_{13}(k\omega; x_3, x'_3) = & [D(k\omega)]^{-1} [B_{11}(k\omega) \exp \{-\alpha_1(x_3 + x'_3)\} + \\ & + B_{12}(k\omega) \exp \{-\alpha_1 x_3 - \alpha_2 x'_3\} + B_{21}(k\omega) \exp \{-\alpha_2 x_3 - \alpha_1 x'_3\} + \\ & + B_{22}(k\omega) \exp \{-\alpha_2(x_3 + x'_3)\}] + g_{13}^p(k\omega; x_3, x'_3), \quad (\text{S.11 c}) \end{aligned}$$

$$\begin{aligned} g_{33}(k\omega; x_3, x'_3) = & -i \frac{c_{44}}{(c_{13} + c_{44})k\alpha_1} \left(\alpha_1^2 - \frac{c_{11}}{c_{44}}k^2 + \frac{q\omega^2}{c_{44}} \right) [D(k\omega)]^{-1} \times \\ & \times [B_{11}(k\omega) \exp \{-\alpha_1(x_3 + x'_3)\} + B_{12}(k\omega) \exp \{-\alpha_1 x_3 - \alpha_2 x'_3\}] - \\ & - i \frac{c_{44}}{(c_{13} + c_{44})k\alpha_2} \left(\alpha_2^2 - \frac{c_{11}}{c_{44}}k^2 + \frac{q\omega^2}{c_{44}} \right) [D(k\omega)]^{-1} + \\ & + [B_{21}(k\omega) \exp \{-\alpha_2 x_3 - \alpha_1 x'_3\} + B_{22}(k\omega) \exp \{-\alpha_2(x_3 + x'_3)\}] + \\ & + g_{33}^p(k\omega; x_3, x'_3). \quad (\text{S.11 d}) \end{aligned}$$

In these expressions

$$B_{11} = M_{22} C'_{11} - M_{12} C'_{21},$$

$$B_{12} = M_{22} C'_{12} - M_{12} C'_{22},$$

$$B_{21} = -M_{21} C'_{11} + M_{11} C'_{21},$$

$$B_{22} = -M_{21} C'_{12} + M_{11} C'_{22},$$

$$C'_{1(1,2)}(k\omega) = \frac{iqk}{2c_{44}c_{33}} \frac{1}{\alpha_{1,2}(\alpha_{1,2}^2 - \alpha_{2,1}^2)} \times \left[c_{44} \left(\alpha_{1,2}^2 - \frac{c_{11}}{c_{44}}k^2 + \frac{q\omega^2}{c_{44}} \right) - (c_{13} + c_{44})\alpha_{1,2}^2 \right].$$

$$C'_{2(1,2)}(k\omega) = \frac{iq}{2c_{13}} \frac{1}{\alpha_{1,2}^2 - \alpha_{2,1}^2} \left(\alpha_{1,2}^2 + c_{13} \frac{c_{13} + c_{44}}{c_{33}c_{44}}k^2 - \frac{c_{11}}{c_{44}}k^2 + \frac{q\omega^2}{c_{44}} \right).$$

While quantities g_{11}^P , g_{31}^P , g_{13}^P , g_{33}^P

$$\begin{aligned}
 g_{31}^P &= g_{13}^P = -\frac{i\rho(c_{13}+c_{44})k}{2c_{33}c_{44}} \frac{1}{\alpha_1^2-\alpha_2^2} [\exp\{-\alpha_1|x_3-x'_3|\} - \\
 &\quad - \exp\{-\alpha_2|x_3-x'_3|\}] \operatorname{sgn}(x_3-x'_3) \\
 g_{11}^P &= -\frac{\rho}{2\alpha_1c_{44}} \frac{1}{\alpha_1^2-\alpha_2^2} \left(\alpha_1^2 - \frac{c_{44}}{c_{33}}k + \frac{\rho\omega^2}{c_{33}} \right) \exp\{-\alpha_1|x_3-x'_3|\} + \\
 &\quad + \frac{\rho}{2\alpha_2c_{44}} \frac{1}{\alpha_1^2-\alpha_2^2} \left(\alpha_2^2 - \frac{c_{44}}{c_{33}}k + \frac{\rho\omega^2}{c_{33}} \right) \exp\{-\alpha_2|x_3-x'_3|\} \\
 g_{33}^P &= -\frac{\rho}{2\alpha_1c_{33}} \frac{1}{\alpha_1^2-\alpha_2^2} \left(\alpha_1^2 - \frac{c_{11}}{c_{44}}k^2 + \frac{\rho\omega^2}{c_{44}} \right) \exp\{-\alpha_1|x_3-x'_3|\} + \\
 &\quad + \frac{\rho}{2\alpha_2c_{33}} \frac{1}{\alpha_1^2-\alpha_2^2} \left(\alpha_2^2 - \frac{c_{11}}{c_{44}}k^2 + \frac{\rho\omega^2}{c_{44}} \right) \exp\{-\alpha_2|x_3-x'_3|\},
 \end{aligned} \tag{S.12 a}$$

where

$$\alpha_1^2 = \frac{1}{2}[x + (x^2 - 4y^2)^{1/2}] \quad \alpha_2^2 = \frac{1}{2}[x - (x^2 - 4y^2)^{1/2}] \tag{S.12 b}$$

with

$$\begin{aligned}
 x &= (c_{33}c_{44})^{-1} [(c_{44} + c_{11}c_{33})k^2 - (c_{13} + c_{44})^2k^2 - (c_{33} + c_{44})\rho\omega^2], \\
 y^2 &= (c_{33}c_{44})^{-1} (c_{44}k^2 - \rho\omega^2)(c_{11}k^2 - \rho\omega^2).
 \end{aligned}$$

Functions α_1 , α_2 are defined by equations (S.12) with the following limitations resulting from boundary conditions for $x_3 = +\infty$

$$\operatorname{Re}\alpha_{1,2} > 0 \quad \operatorname{Im}\alpha_{1,2} < 0.$$

Quantity g_{22}

$$g_{22}(k\omega; x_3x'_3) = -\frac{\rho}{2c_{44}\alpha_t} \exp\{-\alpha_t(x_3+x'_3)\} + g_{22}^P(k\omega; x_3x'_3) \tag{S.12 c}$$

$$g_{22}^P = -\frac{\rho}{2c_{44}\alpha_t} \exp\{-\alpha_t|x_3+x'_3|\},$$

where

$$\alpha_t = \begin{cases} \left(\frac{c_{11}-c_{12}}{2c_{44}}k^2 - \frac{\rho\omega^2}{c_{44}} \right)^{1/2} & \text{for } -\frac{1}{2}(c_{11}-c_{12})k^2 > \rho\omega^2, \\ -i \left(\frac{\rho\omega^2}{c_{44}} - \frac{c_{11}-c_{12}}{2c_{44}}k^2 \right)^{1/2} & \text{for } \rho\omega^2 > \frac{1}{2}(c_{11}-c_{12})k^2. \end{cases}$$

In the above equations

$$D(k\omega) = M_{11}(k\omega) M_{22}(k\omega) - M_{12}(k\omega) M_{21}(k\omega). \quad (\text{S.13})$$

Conclusion

The presented model can be used for detailed analysis of scattering of elastic surface waves on a single centre of a dot array, i.e. evaluation of energy radiated in the form of ESW, as well as losses in the form of bulk waves, in hexagonal crystals with a sixfold rotation axis in the direction normal to the surface.

The results can be applied for piezoelectric crystals with good approximation although the electric component of interactions is neglected. Detailed considerations can be found in [6].

This work was supported by the Problem CPBP 01.08.

References

- [1] L. P. SOLIE, *Surface acoustic wave reflection dot array*, Appl. Phys. Lett., **28**, 420-422 (1976).
- [2] L. P. SOLIE, *A SAW filter using a reflective dot array*, Proc. IEEE Ultr. Symp. Cat. No. 76Ch1120-SSU, 309-312 (1976).
- [3] L. P. SOLIE, *Reflective dot array devices*, Proc. IEEE Ultr. Symp. Cat. No. 77CH1264-ISU, pp. 579-584 1977.
- [4] H. VAN DE VAART, L. P. SOLIE, *A SAW pulse compression filter using the reflective dot array*, Appl. Phys. Lett. **31**, 1-3 (1977).
- [5] E. AKCAKAYA, G. W. FARNELL, *Reflection acoustic surface waves from a row of dots*, Wave Electronics, **4**, 49-55 (1979).
- [6] J. KAPELEWSKI, B. KAMIŃSKI, *Scattering of surface elastic waves on dot structures — theoretical model*, Bulletin of the Polish Academy of Sciences — Technical Sciences **35**, 473-487 (1987).
- [7] *Surface wave filters*, [Ed.] H. Matthews, John Wiley, New York 1977 p. 35.
- [8] E. DANICKI, *Reflection of a SAW from periodic shallow grooves*, Wave Motion, **9**, 445-453 (1987).
- [9] J. E. GUBERNATIS, E. DOMANY, J. A. KRUMHANS, *Formal aspects of the theory of scattering of ultrasound by flaws in elastic materials*, J. Appl. Phys., **48**, 7, 2804-2811 (1977).
- [10] See [7] p. 41 Eq. (1.53).
- [11] E. DIEULESANT, D. ROYER, *Ondes elastiques dans les solides*, [in Russian] Nauka, Moskva p. 125.
- [12] U. A. COOK, M. BERNFELD, *Radar signals* [in Russian], Sovetskoje radio, Moskva 1971.
- [13] *Dynamika układów sprężystych*, [Ed.] G. Eason. Ossolineum, Wrocław 1976 p. 83.
- [14] L. DOBRZYŃSKI, A. A. MARADUDIN, *Surface contribution to the low-temperature specific heat of a hexagonal crystal*, Phys. Rev. B, **14**, 2200-2210 (1976).
- [15] Matrix of elasticity tensor in reduced notation Voigt's for a hexagonal structure changes into a matrix of isotropic structure, when the substitution: $c_{33} = c_{11}$, $c_{13} = c_{12}$, $c_{44} = c_{11} - c_{12}/2$ is carried out; see e.g. [11], p. 132.
- [16] A. DUKATA, J. KAPELEWSKI, *A scattering of elastic surface waves by local irregularities*, 2 nd Conference on Surface Physics Proceedings, vol. IV pp. 77-80, Wyd. Uniwersytetu Łódzkiego, Łódź 1988.

Received on August 18, 1988, revised version January 1, 1989.

THE ACOUSTIC EMISSION TRANSDUCER CALIBRATION USING SPARK METHOD

F. DUŠEK*, C. SEIDL**, J. SIEDLACZEK***, S. PILECKI****

* Institute of Physical Metallurgy, Czechoslovak Academy of Sciences
(616-62 Brno, Zizkova 22)

** Institute of Physical Metallurgy, Czechoslovak Academy of Sciences
(616-62 Brno, Zizkova 22)

*** High Pressure Centre, Polish Academy of Sciences
(01-142 Warszawa, ul. Sokołowska 29)

**** Institute of Fundamental Technological Research Polish Academy of Sciences
(00-049 Warszawa, ul. Świętokrzyska 21)

The present paper deals with the problem of frequency characteristics and of the sensitivity of acoustic emission (AE) transducers. Basing on a theoretical analysis of possible calibration methods of AE transducers, the method of random noise was chosen using the spark impact as the exciting signal source. The theoretical fundamentals of the spark calibration method given in the present work were verified experimentally. On these results, the experimental device was designed and built in the Institute of Physical Metallurgy, Czechoslovak Academy of Sciences in Brno. It is presented in this paper. Estimated by this device characteristics of AE transducers made by META, Prague, Czechoslovakia and by UNIPAN, Warsaw, Poland, are presented.

W pracy omówiono problematykę częstotliwościowych charakterystyk czułości przetworników emisji akustycznej (EA). Opierając się na teoretycznej analizie możliwych metod kalibracji przetworników EA, zastosowano metodę szumu przypadkowego, w której używane jest wyładowanie iskrowe jako źródło sygnału wzbudzającego. Naświetlone teoretyczne zasady iskrowej metody kalibrowania przetworników zostały następnie zweryfikowane eksperymentalnie i na tej podstawie w Instytucie Fizycznej Metalurgii Czechosłowackiej Akademii Nauk w Brnie zaprojektowano i zbudowano urządzenie pomiarowe. W pracy opisano to urządzenie oraz ustalone przy jego pomocy charakterystyki niektórych przetworników EA produkowanych przez META w Pradze i przez UNIPAN w Warszawie.

1. Introduction

In the acoustic emission (AE) instrument technology, a serious problem is connected with the detection of AE signals. The acoustic emission (stress wave) rises due to sudden energy release inside of a material (Fig. 1) by the effect of an external

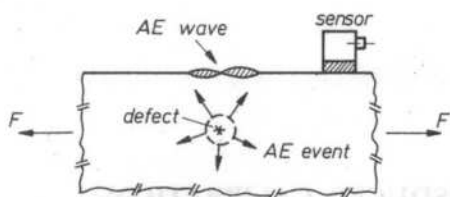


FIG. 1. Acoustic emission rising and propagation

stimulus (mechanical stress, temperature, corrosion etc.). Microphysical conceptions of possible AE sources in metals and metallic systems are demonstrated in Fig. 2. The AE source is here the movement of lattice defects and/or cracking of hard particles as well; the same mechanisms cause the crack nucleation [1,2]. During the

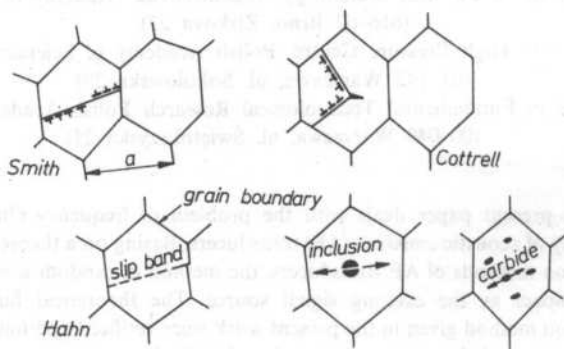


FIG. 2. AE sources in metals

proper crack propagation, the plastic zone is forming ahead the crack front (not the crack itself), thus, the dislocation mechanism again is the source of AE signals.

From this reasoning it is evident that primary signals of the given dynamic effects of moving defects will have the form of very short impulses, the direct registration of which is, under contemporary conditions of measuring technique, impossible. E.g., at the failure propagation over grain of size $a = 10^{-4}$ m, the impulse time

$\tau = \frac{a}{c} \approx 2 \cdot 10^{-8}$ s (c is the dislocation velocity). By means of real AE transducers the

secondary Rayleigh waves on the free surface of the object are read.

Typical representants of AE transducers are the transducers using the piezoelectric effects. The fundamental dependence between the applied stress and the output signal is linear. At dynamic loading, a strong frequency dependence of the sensitivity of transducers manifests itself. These transducers represent a relatively complicate electromechanical system definable only with difficulties. The analytical solution methods do not give a full characteristic of the transducer (its dependence of

sensitivity versus frequency) and it is necessary to complete them by an individual calibration process. Without solving the reliable calibration of transducers, both the objective estimation of the measurement results (e.g., localization of defects) and their physical interpretation, and the comparison of results obtained from various apparatus in particular laboratories, as well, are practically impossible.

The calibration of transducers and the possibility of comparison and transfer of results are then the main problems of AE technology. The development aims to the worldwide standardization by means of unifying standards and recommendations [3].

2. The choice of calibration method

The calibration method was chosen based on the theoretical analysis of possible calibration methods of AE transducers making use of various physical principles.

2.1. The vibration method

It performs the service of calibrating accelerometers. The vibrator excited by means of an electronic oscillator can cover the frequency range $1 \dots 10^5$ Hz, practical upper limit being, due to mechanical resonances of the vibrator, ca $2 \cdot 10^4$ Hz. The output signal of the calibrated transducer is compared to the output of an identically loaded standard. The sensitivity is given directly in pC/g, and mV/g, respectively.

2.2. The impact method

This method makes use of the stress wave excited by a little ball falling from a definable height on an anvil on which the transducer is placed. Taking into account that the wave course can be mathematically well described, see, e.g. [4], even standard transducers can be placed on the anvil. This method enables even the absolute sensitivity calibration.

2.3. The hydrophone method

In this case, the calibration is being carried out in a big water reservoir in which on the one side a standard transmitter, and on the other — a standard transducer are placed. After taking measurements of the transmission, the tested transducer is placed in the whole frequency range instead of the standard one. The calibration curve is obtained by comparison of both test. For the given method, it is necessary the identical geometry to be constant. A normal frequency range is from 1 kHz to 1 MHz.

2.4. The ultrasound method

This method represents a modification of the foregoing one, the transmitter being connected acoustically directly with the transducer by means of viscous medium. The transmitter is excited by a sinusoidal wave generator, over-tuned in the test frequency range. This method is relatively quick and thus is often used.

2.5. The method of random noise

This method tries to model an AE signal, and real conditions for its propagation and scanning. The transducer is placed on the surface of a large block of material on which a flux of fine, hard particles impinges. Their impingement causes the rise of stress waves propagating through the material and reaching the transducer. The signal has the character of noise with a wide frequency spectrum. A frequency analyser is connected to the transducer output. The amplitude dependence on frequency is then registered by an appropriate method. The way of obtaining impulses is in good agreement with the real situation at AE. The individual particle character imitates the point source of a narrow transit impulse quite well. The general continual process has then a wholly random character. This method is being often used for the selection of AE signals from the signals arising due to external sources [5].

When estimating the suitability of mentioned in Sections 2.1...2.5 particular methods for calibrating the transducers, considering their use for scanning the AE signals it is evident that their application is specialized. The acceleration measuring instruments and the conventional ultrasound exciters are, at the present time, calibrated by the verified methods. As mentioned above, these methods do not, however, correlate with the real AE.

In discussions of theoretical and practical results, with regard to the utilizability, the following requirements of calibration process have been respected.

- a) The input calibration signal must have the form of stress impulses with a small amplitude and short time.
- b) The propagation of impulses in the calibration device must be similar to real propagation conditions of AE signals.
- c) The surface contact conditions of the transducer in the apparatus must be near to those in the case of practical application.
- d) Tests (calibration) must be reproducible and exact, having adequate permanent tolerance.

With regard to these requirements, it is evident that for the calibration of AE transducers the method of random noise will be the most convenient. The newest spark calibration method is also based on this principle, using as a source the exciting signal of spark discharge [6,7].

3. Theoretical basis for the spark calibration method

The application of the spark calibration method is conditioned by the validity of the presumption that the sequences of impulses with a certain length can be adjoined the frequency range in which all components have the congruent amplitude. To estimate this presumption, let us consider the sequence of rectangular impulses $u(t)$ with length δ , amplitude E_0 and period T , according to Fig. 3

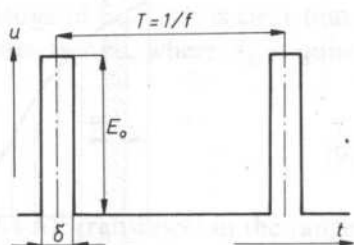


FIG. 3. A rectangular impulse

$$u(t) = 0 \quad t < -\frac{\delta}{2};$$

$$u(t) = E_0 \quad -\frac{\delta}{2} < t < \frac{\delta}{2}, \quad (1)$$

$$u(t) = 0 \quad \frac{\delta}{2} < t < T - \frac{\delta}{2},$$

For the Fourier development of this sequence it is valid, see, e.g., [8]

$$u(t) = \frac{A_0}{2} + \sum_{k=1}^{\infty} A_k \cos \omega_k t, \quad (2)$$

where A_0 and A_k are the amplitudes of harmonic components, respectively, $\omega_k = 2\pi k f_1$, and $f_1 = \frac{1}{T}$ is the repeating frequency. For A_0 and A_k we get

$$A_0 = \frac{2\delta}{T} E_0, \quad (3)$$

$$A_k = \frac{2\delta}{T} E_0 \frac{\sin \frac{\omega_k \delta}{2}}{\frac{\omega_k \delta}{2}}. \quad (4)$$

From Eq. (4) it follows that A_k changes periodically with increasing k , proportionally to $\sin \frac{\omega_k \delta}{2}$ and their courses are damped being hyperbolically proportional to the coefficient $\frac{1}{k}$ (Fig. 4). The dependence $A_k(\omega)$ contains the zero points $\left(\omega_{ok} = \frac{2k\pi}{\delta}\right)$,

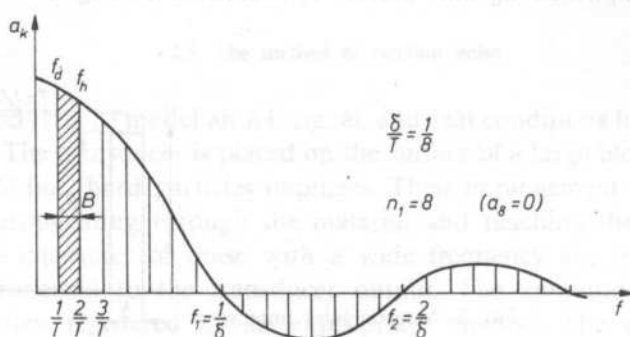


FIG. 4. The spectrum of an unrepeat impulse

separating individual spectrum loops. The number of spectrum components in one loop can be expressed by the relation

$$n = \frac{T}{\delta}. \quad (5)$$

To get the maximum number of components, it is necessary that the impulse is substantially shorter than the period of the given sequence. For $T \rightarrow \infty$, we get a solitary impulse $u(t)$, the spectrum of which is continuous. For the amplitude of spectral function $S(\omega)$, it holds then

$$S(\omega) = E_0 \delta \frac{\sin \frac{\omega_k \delta}{2}}{\frac{\omega_k \delta}{2}}. \quad (6)$$

Comparing Eqs. (4) and (6) we see that it holds

$$A_k = \frac{2}{T} S(\omega). \quad (7)$$

As T is constant, the frequency dependence A_k has the same course as $S(\omega)$.

When considering a general impulse $u(t)$, it is suitable, for the estimation of the

$S(\omega)$ course, to introduce the effective impulse time t_m

$$t_m = \frac{1}{E_0} \int_{-\infty}^{\infty} u(t) dt. \quad (8)$$

For the rectangular impulse, $t_m = \delta$.

When applying now the non-dimensional frequency $\Omega = \frac{\omega}{2\pi} t_m$ it can be demonstrated, see, e.g. [9], that for $\Omega < \frac{1}{2}$ a value of $S(\omega)$ is approximately constant for the majority of impulses. With regard to the knowledge of Eq. (7) it is clear that, for the sequence (1), the interval of frequencies Δf exists as well, where A_k is quite constant, if it holds

$$\Delta f \ll \frac{1}{\delta}. \quad (9)$$

When we want to find the frequency characteristic of the AE transducer in the range 0...2 MHz, the condition

$$\delta < \frac{1}{f_h} = 5 \cdot 10^{-7} \text{ s}$$

must be fulfilled.

From the information obtained it follows that the presumption necessary to apply the spark calibration method can be fulfilled by means of the condition (9), taking into account the relation (5) being necessary to obtain sufficient number of data measured.

4. The experimental verification of validity of theoretical considerations of the spark calibration method

The model connection according to Fig. 5 was used to verify theoretical considerations and clarification of some technical problems. As the source of narrow impulses with very steep fronts ($\delta = 3 \cdot 10^{-8}$ s) the impulse generator TR 0361 was applied. The position of the first spectral function nodal point (as the case may be, of

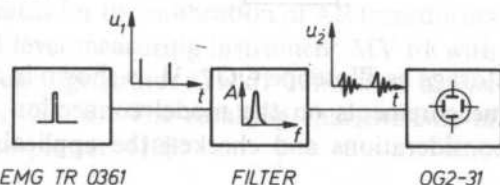


FIG. 5. The model connection

the first spectrum loop) was

$$f_1 = \frac{1}{\delta} = 33 \text{ MHz},$$

When we have chosen the repeating frequency $f_r = 1 \text{ kHz}$, the first spectrum loop contains then

$$n_1 = f_1/f_2 = 3.3 \cdot 10^4$$

of components distant 1 kHz from each other. By the choice of the repeated frequency, it is possible to change the separation of components arbitrarily, i.e. to reduce or magnify it. For finding the characteristics, only frequencies lower than the limit of the zone considered ($f_{\max} = 2 \text{ MHz} \ll 33 \text{ MHz}$, which represents the course of our spectral function — see Fig. 6) are needed. From Fig. 6 it is evident that in the

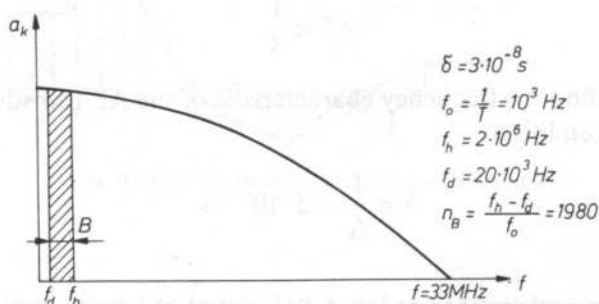


FIG. 6. The spectral curve of impulse $\delta = 3 \cdot 10^{-8} \text{ s}$

zone $B = 0 \dots 2 \text{ MHz}$ the amplitude of all the components of spectrum can be considered to be practically identical.

The frequency selection was carried out by an active filter having the double T-network in the feedback branch (Fig. 7). The registration was performed by the

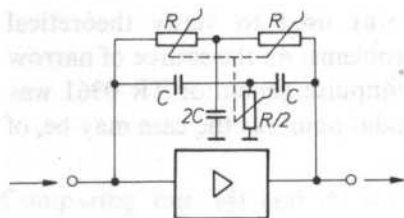


FIG. 7. Block diagram of an active filter

storage oscilloscope OG2-31 as shown in the block diagram on Fig. 5. The results of measurements on the model connection corroborated the rightness of theoretical considerations and checked the applicability of the testing apparatus.

5. The construction proposal and description of the spark calibration apparatus

Basing on a theoretical analysis and obtained practical information and experiences, a calibration device was proposed and built in its final form.

The block diagram of the device is demonstrated in Fig. 8. The AE signal

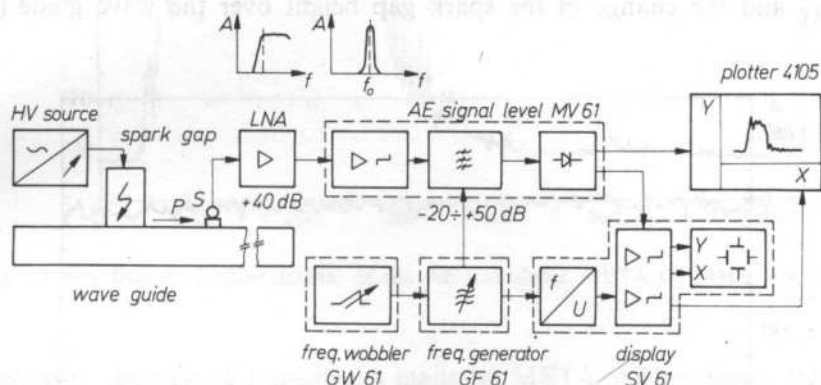


FIG. 8. The block diagram of apparatus for the calibration of AE transducer; S — the probe, LNA — low-noise amplifier: $A = 40$ dB, frequency range 30 kHz...2 MHz

simulator consists of a regulated high voltage HV source, and a spark gap with double electrostatic screening. As the milieu enabling the signal transfer from the source to the transducer a large ARMO block (wave guide) with dimensions $80 \times 45 \times 800$ [mm³] was used. The dimensions of that block were chosen so big to eliminate uncheckable reflections in longitudinal direction: on behalf of big thickness of the bar, the propagation of stress waves from their source in form of the dispersion Rayleigh waves was reached.

The spark source for exciting the impact waves has the discharge capacity $c_n = 250$ pF and its charging constant is $t_n = 5 \cdot 10^{-4}$ s. From the approached calculations, and from the practical measurements it follows that the excited impulse time is $\delta = n \cdot 10^{-8}$ s which satisfies all the requirements very well. The regulated HV source supplies the voltage 0...5 kV with current $I_{\max} = 30$ mA.

In Fig. 8 the block diagram of the apparatus for the calibration of AE transducers is shown. The apparatus has the AE signal level measuring instrument MV 61 with automatically retuning filters by the frequency generator GF 61 controlled by the frequency wobbler GW 61, and the display SV 61. The resulting characteristic of transducer is presented graphically on the plotter 4105.

6. Experimental results of estimation of particular AE transducers

When practically estimating the frequency characteristics and sensitivity of the transducers, the influences of setting the high voltage value (U_{HV}) and of the spark gap axis distance from the block (wave guide) surface were studied. When searching for the character of response to the parameter changes of the generator of impact waves it was found that the jump distance change (and/or change of U_{HV}), current change I_{HV} and the change of the spark gap height over the wave guide (block)

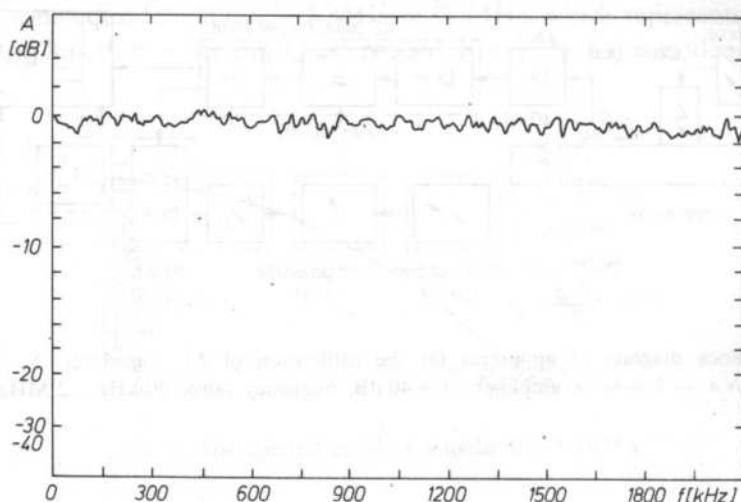


FIG. 9. The frequency course of spark gap in the range of 0...2.1 MHz

surface do not influence the received signal substantially. Only the amplitude was estimated, the frequency course did not practically change. The setting is thus not critical. The frequency course of spark gap in the range of 0...2.1 MHz is given in Fig. 9.

In Figs. 10 and 11 the estimated characteristics of the AE transducers META – 0.5 MHz made in Czechoslovakia are presented (the axis x shows the frequency, y – the amplitude of signal generated by transducer). From the figure it is evident that the tested transducers can work well in the range of 100...300 kHz, where their frequency characteristics and sensitivity are very good.

In the Figs. 12...16, frequency characteristics of transducers UNIPAN made in Poland are shown. It is true that the transducers UNIPAN give larger desired signals but, except for the transducers 0.5 MHz, the frequency characteristics are not so

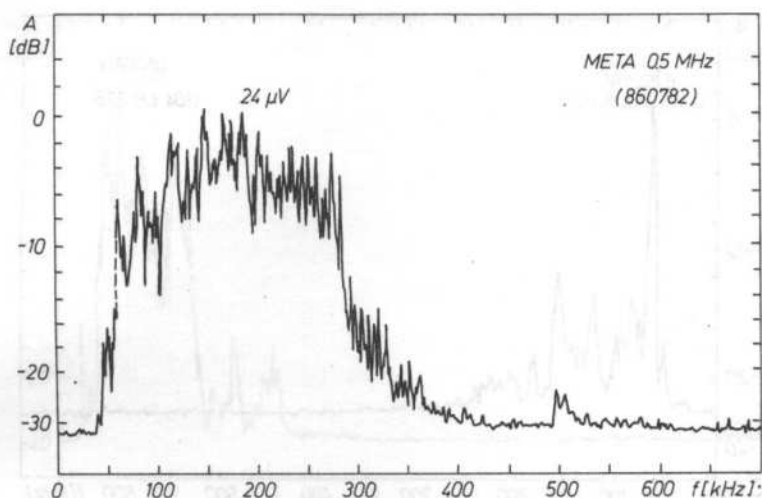


FIG. 10. The frequency characteristic of the AE transducer META 0.5 MHz, No. 860782

balanced as in the case of transducers made by META. All the tested transducers, however, are suitable for measuring the AE signals and they can be recommended; for particular measurements, namely in the frames of basic research, we recommend the transducers META 0.5 MHz, and the transducers UNIPAN 0.5 MHz.

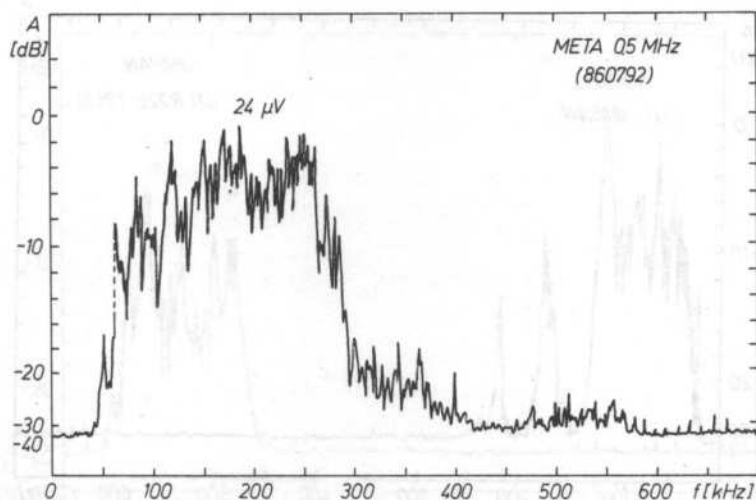


FIG. 11. The frequency characteristic of the AE transducer META 0.5 MHz, No. 860792

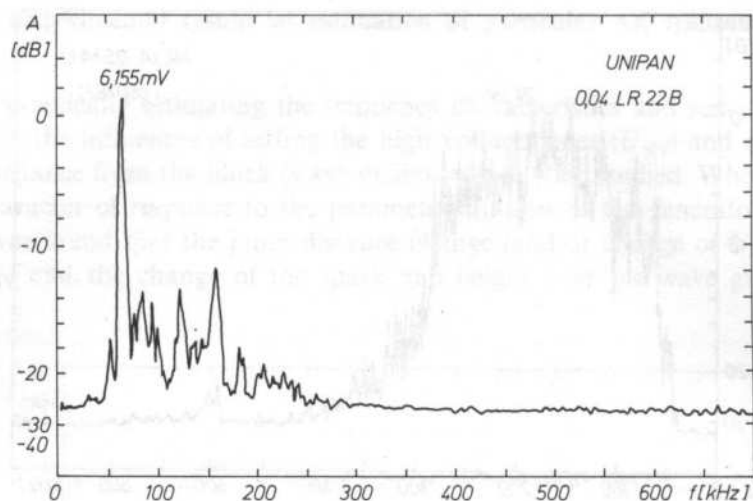


FIG. 12. The frequency characteristic of the AE transducer UNIPAN 0.04LR22B

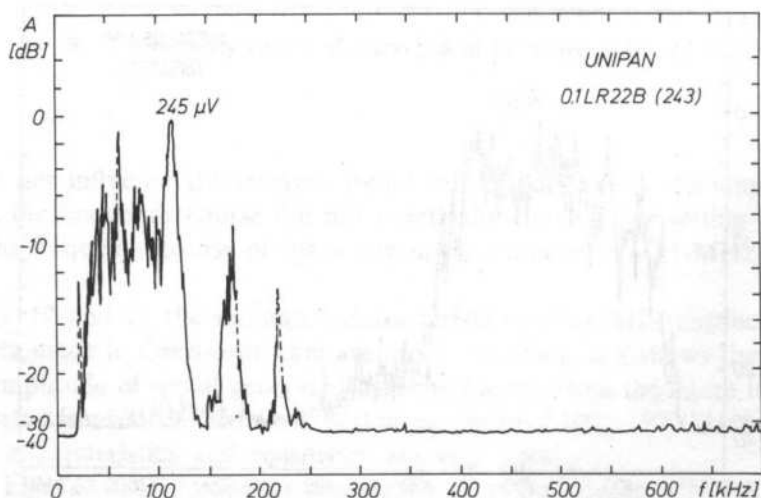


FIG. 13. The frequency characteristic of the AE transducer UNIPAN 0.1LR22B No. 243

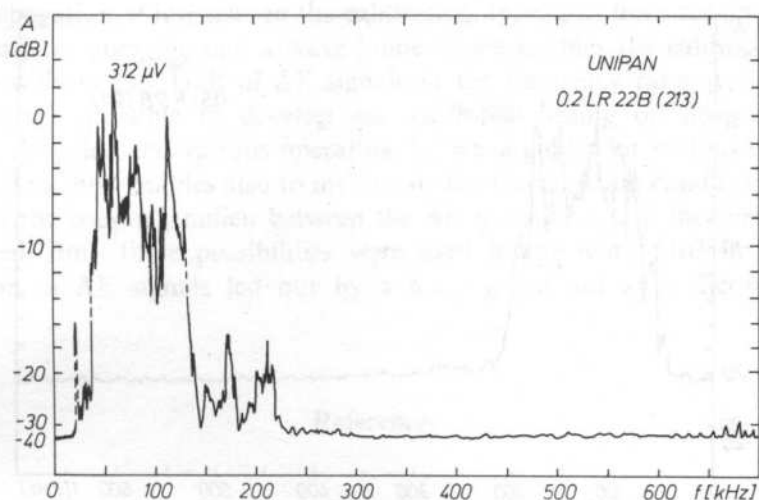


FIG. 14. The frequency characteristic of the AE transducer UNIPAN 0.2LR22B No. 213

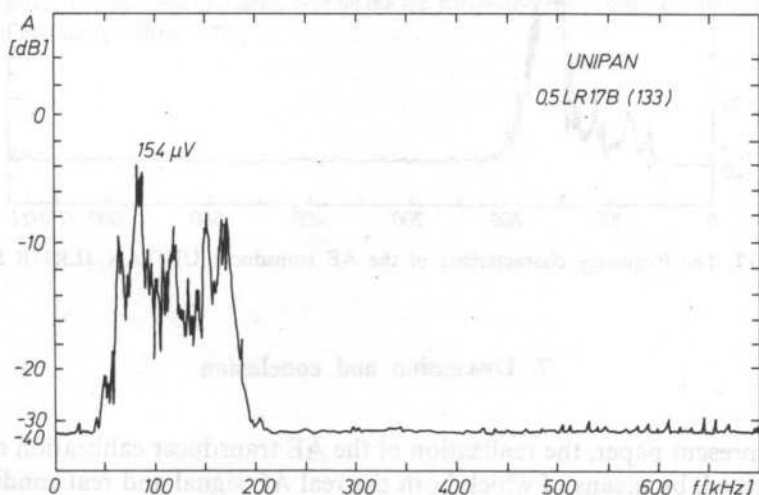


FIG. 15. The frequency characteristic of the AE transducer UNIPAN 0.5LR17B No. 133

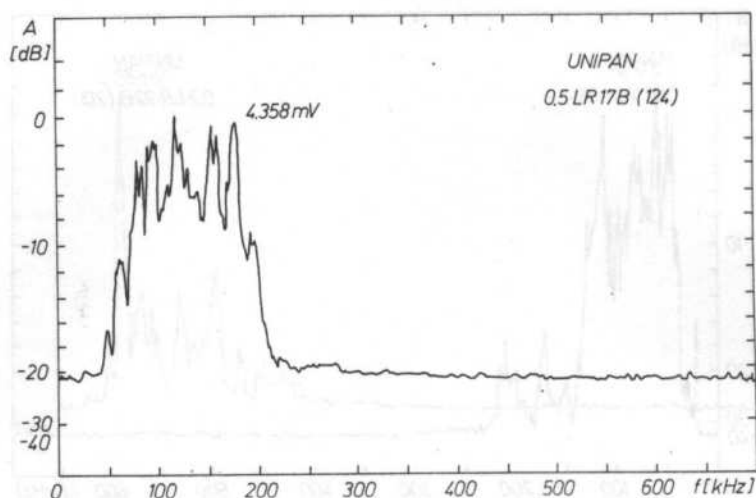


FIG. 16. The frequency characteristic of the AE transducer UNIPAN 0.5LR17B No. 124

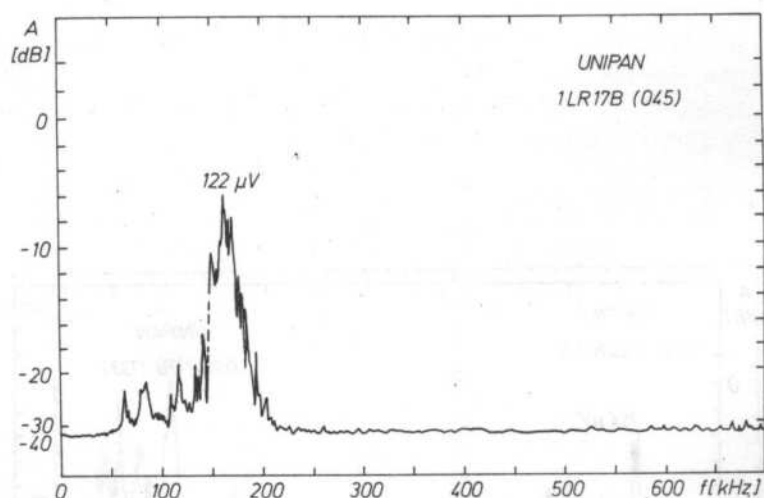


FIG. 17. The frequency characteristic of the AE transducer UNIPAN 1LR17B No. 045

7. Discussion and conclusion

In the present paper, the realization of the AE transducer calibration method has been described, by means of which both the real AE signal and real conditions of its propagation and scanning are shaped. The signal has the character of a noise with a broad frequency spectrum, see Fig. 9. The way of transitive surface wave generated by a spark point source, is in good agreement with the real situation at AE.

The propagation of impulses in the calibration apparatus from the source to the tested transducer goes through a wave guide which enables the calibration of the transducer without any fault of AE signals in the frequency range required. The device makes it possible to develop and calibrate, basing on observations on standard wave guide and various operating AE wave guides for various conditions.

The used method enables also to investigate the transmission conditions, and the influence of the coupling milieu between the AE transducer and the surface of the object tested. Both these possibilities were used in the work [10] in which the transmission of AE signals led out by a wave guide out of a thermostat was concerned.

References

- [1] F. DUŠEK, C. SEIDL, *The calibration of AE transducers* [in Czech] Proceedings of the Letní škola defektoskopie, Stary Smokovec 1987.
- [2] M. HOLZMANN, *Brittle fracture of low-alloyed steels* [in Czech] Research Report of the Institute of Physical Metallurgy 1985.
- [3] The ASTM standard E 569-76. *The recommended method investigated for checking the structures by acoustic emission during the controlled stimulation.*
- [4] R. L. BELL, *AE transducer calibration — transient pulse method.* Proc. of 32 th Nat. Conf. Am. Soc. Nond. Test., Cleveland 1972.
- [5] L. J. GRAHAM, G. A. ALESS, ASTM STP 571, Philadelphia 1975.
- [6] C. C. FENG, *AE transducer calibration*, Res. Rep. No. 74-7-C, Endeveco, California 1974.
- [7] L. GRAHAM, *Acoustic emission transducer characterization*, North-Am. Rocwell Report No. SCTR 19.
- [8] J. D. ACHENBACH, *Wave propagation in elastic solids*, North Holland Publ. Co. 1975.
- [9] E. SKUDRZYK, *The foundations of acoustics*, Springer Verlag, New York 1971.
- [10] E. MÁLIKOVÁ, *The influence of loading rate on the AE parameters* [in Czech]. PhD Thesis Institute of Physical Metallurgy Brno 1988.

SIMPLIFIED SYSTEM FOR ISOLATED WORD RECOGNITION

R. GUBRYNOWICZ, K. MARASEK, W. MIKIEL, W. WIĘZŁAK

Institute of Fundamental Technological Research, Polish Academy of Sciences
(00-049 Warszawa, ul. Świętokrzyska 21)

This paper presents a general-purpose system for recognition of a limited set of words uttered in isolation. Such a system is intended for voice control of robot's movements. In order to minimize the number of operations performed during the recognition process and to limit the memory requirements frequency analysis of the signal was performed in adequately selected bands. Output signals from filters undergo detection and through an A/D converter are introduced into a computer where they undergo further processing logarithmic conversion and linear time standarization, among others. This leads to a reduction of the number range in further calculations. The DTW algorithm was used in the recognition process, while templates of individual words are introduced once, in principle separately for individual operators. The developed system speaker-dependent, in principle was verified experimentally for various vocabularies (containing 20 to 60 words) uttered by 11 voices (including 1 female voice). The average recognition accuracy for a 60 word vocabulary exceeded 98% for individual voices, while in a case of recognition without system accomodation to given voice the average error of recognition increased by about 10%.

W pracy przedstawiono uniwersalny system rozpoznawania ograniczonego zbioru wyrazów wymawianych w izolacji. System ten jest docelowo przeznaczony do sterowania ruchem robota za pomocą głosu. W celu zminimalizowania liczby operacji wykonywanych podczas procesu rozpoznawania oraz zmniejszania zajętości pamięci zastosowano analizę częstotliwościową sygnału w odpowiednio dobranych pasmach. Sygnały wyjściowe filtrów są poddawane detekcji i wprowadzone poprzez przetwornik A/C do komputera, gdzie następuje ich dalsza obróbka, m.in. konwersja logarytmiczna danych oraz liniowa normalizacja czasowa. Uzyskano dzięki temu znaczną redukcję zakresu liczb, którymi operuje się przy dalszych obliczeniach. W procesie rozpoznawania zastosowano algorytm DTW, przy czym wzorce poszczególnych wyrazów są w zasadzie wprowadzane jednokrotnie, oddzielnie dla poszczególnych operatorów. Opracowany system, który w zasadzie jest typu speaker-dependent został zweryfikowany doświadczalnie dla różnych słowników zawierających od 20 do 60 wyrazów wypowiedzianych przez 11 głosów (w tym 1 żeński). Średnia dokładność rozpoznawania dla słownika 60-wyrazowego dla poszczególnych głosów wyniosła ponad 98%, zaś w przypadku rozpoznawania bez dostosowywania systemu na zadany głos, średni błąd rozpoznawania wzrósł o ok. 10%.

1. Introduction

The problem of man-machine communication with the use of speech is at present an issue of great interest in many scientific research centres all over the world. Until the mid 70-ies researches were performed in university centres and, were out of interest of the industry in general. However, the practical application of the results of these researches has been taken into consideration more and more in the second half of this decade. It could be expected that the progress in the realization of automatic speech recognition systems will make their effective operation, also in industry, possible (PELTIN [10]).

The advantages of the use of the so-called acoustic input for data input and control by speech are indisputable. Speech is the most natural and quickest, at the same time, form of communication between people. Table 1 presents the rate of information transmission from a man using different means of communication:

Table 1. Average information transmission rate from man

Speech (10 sounds/s)	— 50 bit/s
Keyboard (60 words/min)	— 30 bit/s
Morse code (12 words/min)	— 6 bit/s
Buttons, keys	— < 6 bit/s

It is worth noticing that the values given for non speaking communication are rather maximal. For example, a lower transmission rate, of about 15–20 bit/s can be expected for an average user of a keyboard.

The freedom of movement of the operator who can perform additional manual operations on his work-stand, as well as the possibility of keeping eye contact with the examined elements, surfaces etc. even when registering control information, are further advantages of an acoustic input. The application of an acoustic input for information feeding greatly increases productivity, especially on stands of visual control of product quality (PELTIN [10]).

Two fundamental kinds of approaches can be distinguished in the problem of automatic speech recognition. The first one is realized on the basis of formalized knowledge concerning phonetic-acoustic, phonological, lexical, syntactic structures and semantics of given language. Speech recognition in such a system is based on sets of rules used for speech signal transformation into sequences of symbols representing definite notions of linguistic units with given structure. This approach is used mainly in systems for continuous speech recognition — very complex and generally constructed for the investigation of foundations of unlimited recognition of continuous speech.

The other approach consists in the recognition of a speech signal with methods of pattern recognition, with the application of numerical classification procedures of measurement results or vectors of features, created on their basis. In this case, in

general, classification process is realized on the basis of the division of the space of features into subspace ranges — individually for every class. Boundaries of these ranges and classification rules are defined on the grounds of geometric, topologic or probabilistic criteria.

Recognition models of the first type are very complicated and require the entire linguistic and phonetic knowledge of a given language to be presented in formalized form. In this case the optimization of recognition algorithms is an extremely difficult task, while for models based on the analysis of similarity between the recognised and reference pattern it can be relatively easily formulated formally, since the fact that individual models can be derived automatically from data observation during training is applied. This makes it possible to construct relatively easily a practical recognition system, but with limited effectiveness. It is a result of an assumption that ideal patterns, generated by a fairly simple model, exist. Only in such a case the problem of parameter estimation can be given in analytic and optimized form. Such limitations and simplifications of the description form are possible to accept in definite situations, e.g. when a relatively small number of words spoken in isolation is applied, as it was assumed in this paper.

2. Background of the recognition system of isolated words

Considering the application of the designed system it was accepted that the vocabulary for operator-robot communication, except for 10 digits, has to contain words for the control of its motion, that is such words as "forwards", "backwards", "right", "left", etc. At the same time the replacement, full or partial, of the communication vocabulary was assumed and the limitation resulting from fine tuning of the system to the voice of a given operator was permitted.

It is also essential for the system to work in a laboratory without additional acoustic adaptations of the room and attenuation of outer noise sources. Because of the condition of vocabulary replacement for operator-robot communication, it was necessary to accept a system with an isolated training stage, which would be repeated every time the operator used a new collection of words. The condition of resistance to noise disturbances imposed the necessity of applying a mouth microphone and developing a specific procedure for endpoints detection. The recognition time of one word, which should not exceed 1 s for a computer with a clock of 4.7 MHz, significantly influenced the applied solution. It radically influenced the elaborated method of speech signal processing and the form of the recognition algorithm.

3. Speech signal processing

While elaborating the isolated word recognition system it was accepted that the speech signal corresponding to individual words is sufficiently defined in the frequency domain in the form of time-dependent power spectra. It is furthermore

assumed that changes of the spectrum within a spoken word are sufficient for its identification and more detailed acousto-phonetic analysis, which makes possible, the detection and recognition of smaller linguistic units such as speech sounds, syllables, etc. is not necessary. Such an approach has a certain advantage — it is not necessary to know the phonetical and phonological structure of a given language, and errors of speech signal segmentation are avoided.

The requirement for operation rate and low cost of the recognition system, made it practically impossible to apply more refined spectrum analysis methods, such as FFT or LPC. Thus, a hybrid solution, with a considerable part of processed signal realized by an analogue system was decided upon. To this end a set of 7 band filters with detection circuits on the output was applied. Filters has bands with different widths (from 1/3 to 2 octaves), while their mid-band frequencies were so chosen, that it was possible to differentiate 6 Polish vowels and to divide (unvoiced fricatives) into two classes. The applied preliminary universal for most voices in principle filtration and detection led to a considerable data reduction, with a drastic decrease of their transmission rate to the computer (about 8.4 kb/s), at the same time.

Yet the application of spectrum analysis makes necessary to apply effective amplitude normalization, either on the analogue side, or after digital conversion. In the first case an amplitude compression system is required. But it increases the system's sensitivity to external noises. Whereas for normalization on the digital side, attenuation of components in higher frequency bands occurs frequently. Moreover, this type of normalization causes an increase of processing time. For these reasons an analogue solution was chosen.

Systems with band filtration are still popular (e.g. CROCHIERE, FLANAGAN [4]), especially in systems with practical application, for which the requirement of simplicity and operational reliability is as important as the low price of the recognition system. However it should be noted that, in general, signal filtration is not oriented as in the described system and, in general basis, frequencies are distributed as in vocoder systems, in linear or mel scale. The selection of filter bands adequately to the structure of chosen Polish language speech sounds made considerable reduction of the number of filters possible, and what follows — further reduction of the data size with an increase of reliability at the same time.

4. Description of system's operation

4.1. Speech signal parametrization

Figure 1 presents a general block diagram of the system. After compression, filtration and detection the speech signal is fed into a computer through a multi-channel, standard, 12-bit A/D converter. Used ranges of numbers are reduced by logarithmic matrix conversion of output signals. Figure 2 a presents examples of the

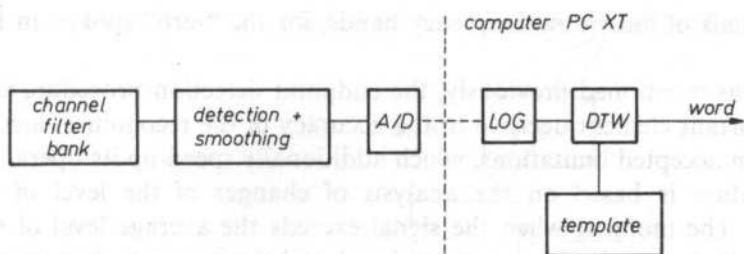


FIG. 1. Block diagram of isolated word recognition system

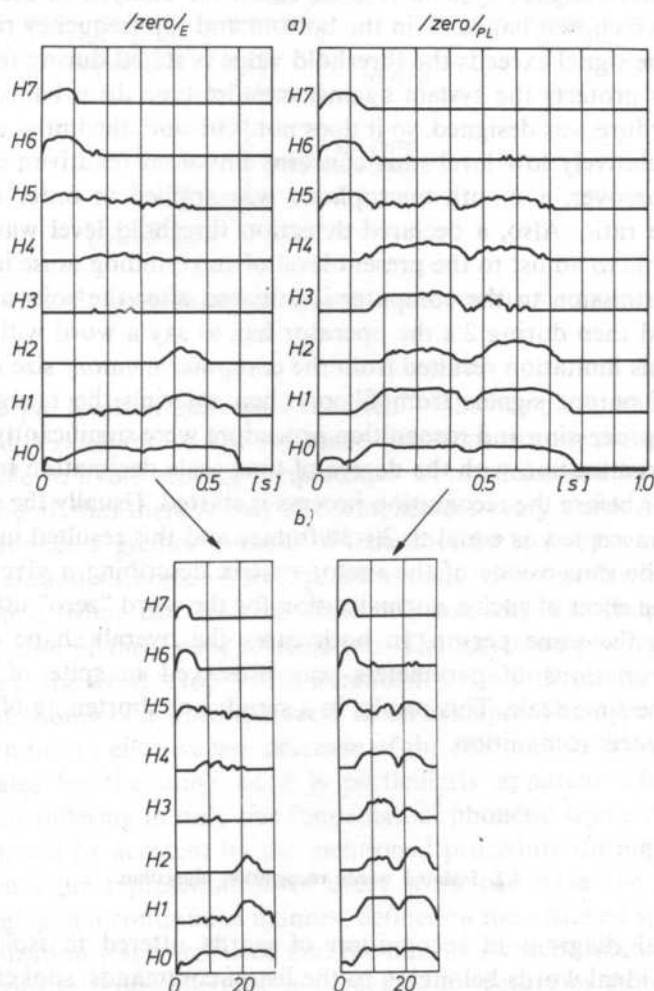


FIG. 2. Examples of output signals from filters before (2a) and after linear time normalization (2b), obtained for the word "zero" said in English and in Polish

output signals of individual frequency bands, for the "zero" spoken in English and Polish.

As it was mentioned previously, the endpoint detection procedure is one of the more important element decisive to the accuracy of the recognition algorithm. This results from accepted limitations, which additionally speed-up its operation. Usually this procedure is based on the analysis of changes of the level of the signal's amplitude. The moment when the signal exceeds the average level of surrounding noise is treated as the beginning of the signal, and the moment when the signal's level becomes lower than the noise level and after which the silence segment of not less than 0.3–0.4 s occurs is accepted as the end of the signal.

A somewhat more complex criterion for the beginning of the signal was elaborated in the designed system. It is based on the analysis of the sum of output signals from two chosen bands — in the bottom and top frequency range. While the fact whether the signal exceeds the threshold value is stated during the first 50 ms of the signal, this protects the system against impulse type disturbances. At the same time this procedure was designed, so it does not "cut-out" the initial and final speech sounds with relatively low level (this concerns unvoiced fricatives, especially) from the signal. Moreover, a mouth microphone was applied in order to improve the signal to noise ratio. Also, a declared detection threshold level was applied, what makes it possible to adjust to the present level of surrounding noise in a given room.

Data transmission to the computer is initiated after the software or hardware interruption and then during 2 s the operator has to say a word with duration time under 1.2 s. This limitation resulted from the computer memory size assigned for the registration of output signals from filters when uttering the recognized word.

The signal processing and recognition procedure were significantly speeded up by linear time normalization with the degree of time scale decimation initially declared by the operator before the recognition process is started. Usually the standard length of a word was accepted as equal to 20–30 frames and this resulted in a reduction by 2–4 times of the dimensions of the vector matrix describing a given word. Figure 2 b presents the effect of such a normalization for the word "zero" uttered in English and Polish by the same person. In both cases the overall shape of the function representing variations of parameters was preserved in spite of an over twice reduction of the time scale. This results in a significant shortening of the calculation time during word recognition.

4.2. Isolated words recognition algorithm

The general diagram of recognition of words uttered in isolation is shown in Fig. 3. Individual words belonging to the list of commands, spoken to control the robot's motions, are uttered — once, in general — in turn by the operator during the training stage. After the word is uttered, the monitor automatically displays

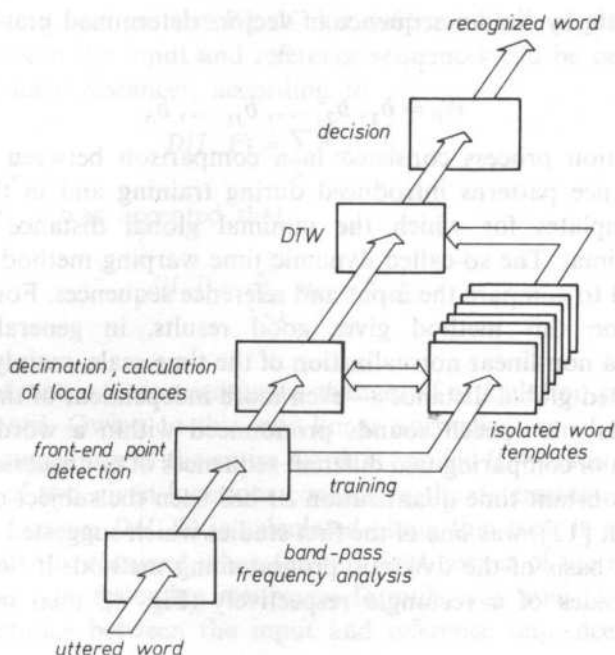


FIG. 3. Block diagram of isolated word recognition algorithm

variations of output levels in individual channels — the beginning and end of spoken word is marked. Visual analysis of registered functions during the training process makes it possible to avoid storing templates of words deformed by chance. It was accepted, in general, that there is only one template for every word. All the same it is possible to introduce a greater number of templates for a word which has various correct pronunciation variants, or has speech sounds with variable level in the final or initial position what can lead to their "cut-out" by the endpoint detection procedure in a case of their poor articulation. The unvoiced plosive /p/ spoken as a final sound (e.g. the word "stop") with a frequently too little intensity of plosion to form an explicit ending of a word can serve as an example. This type of error can be the main reason for an effectiveness decrease of the recognition system. The need of various templates for the same word is particularly apparent when words with similar structure, differing in only one fundamental phonetic segment which may be sometimes removed by accident by the mentioned procedure during learning stage. In a general case the representation of every word can have the form of vector functions changing in a continuous manner, defined in the assigned space of features. Because discretization was introduced and the time axis was normalized to N points, hence every word is represented by a sequence of vectors in the following form

$$W_T = a_1, a_2, \dots, a_j, \dots, a_N.$$

while it's template by similar sequence of vectors determined previously during the learning process

$$W_p = b_1, b_2, \dots, b_j, \dots, b_N.$$

The recognition process consisted in a comparison between input word and succeeding reference patterns introduced during training and in the choice of this word from templates for which the minimal global distance from the input sequence is minimal. The so-called dynamic time warping method DTW (Levinson [7]) was applied to compare the input and reference sequences. For cases of isolated word recognition this method gives good results, in general, owing to the introduction of a non-linear normalization of the time-scale, mainly. This makes the value of calculated global distance — even more independent of the variable rate of uttering syllables and speech sounds pronounced within a word.

The problem of comparing two different sequences of not necessarily equal length at maintained constant time quantization Δt has been the subject of much research. Paper (VINTSYUK [12]) was one of the first studies which suggested a solution to this problem on the basis of the dynamic programming method. If both sequences are drawn on the sides of a rectangle respectively (Fig. 4), then minimal distances

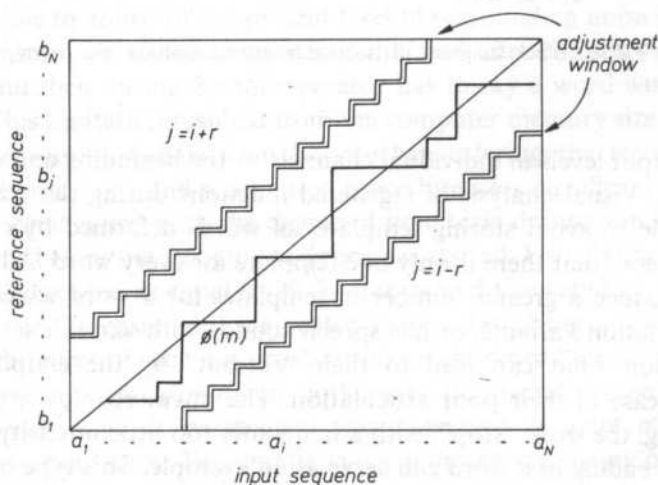


FIG. 4. Determination of cumulative distance between input word and reference sequence with the DTW method

between succeeding segments lie near the rectangle's diagonal when the input sequence and reference sequence are very similar. In a case of perfect compatibility, the line joining minimal local distances $d(i, k)$ coincides exactly with the diagonal. A different rate of uttering the input word and the reference word leads to a deformation of this line to form $\phi(m)$ which is the function of deformation of

pattern W_I adequately into pattern W_p . If this deformation is neglected, then the global distance between the input and reference sequences can be presented in the form of a sum of local distances, according to

$$D(I, P) = \sum_m d_m(i, j)$$

while in this paper it was accepted that

$$d(i, j) = \sum_{k=1}^7 |a_{i,k} - b_{j,k}|,$$

for $1 \leq i, j \leq N$.

Still this type of metric (1) is sensitive to changes of articulation rate of syllables uttered within a word. Owing to this, non-linear normalization of the time scale, including the pronunciation of the entire word, is applied (LEVINSON [7]). Then the similarity analysis of two given functions consists in the determination of the path $\phi(m)$. Cumulative distance $D(I, P)$ is calculated along this path in such a manner that its minimal value is obtained when the top right corner of the matrix of local distances is reached. The following recurrence formula was used to determine the minimal global distance between the input and reference sequence

$$D(i, j) = d(i, j) + \min \{D(i-1, j), D(i-1, j-1), D(i, j-1)\}. \quad (3)$$

When calculating the minimal distance a "corridor" is put along the diagonal $i = j$ in order to prevent too large deviations of function $\phi(m)$ (Fig. 4), according to formula

$$|i - j| \leq r. \quad (4)$$

Because the minimal global distance for a given input word can be calculated for various templates along different optimal paths, an additional normalization is introduced with respect to the number of steps k

$$D_n(W_I, W_p) = \frac{1}{k} \times D(s, u), \quad (5)$$

where $N \leftarrow k \leftarrow 2 \times N$ and $N - r \leftarrow \delta, u \leftarrow N$.

The acceleration of the template search is an important problem, as well as the problem of avoiding the inspection of the entire collection of reference patterns every time a template closest to the spoken word is chosen. At the present moment the searching time can be considerably shortened by including two additional factors when comparing the input word with succeeding templates. These factors are: word length and maximal acceptable cumulative distance value for taking a decision whether the input word belongs to the same class as the given template. The elimination of distance calculation in cases when lengths of the input word and template were positively different, was possible owing to durations analysis. The critical difference of 50% was accepted. When it was exceeded the distance was not calculated and the given template was rejected. A more accurate comparison of

lengths of words expressed in the number of syllables, is planned in the future. At that time the entire vocabulary will be preliminary divided into subsets assembling words with the same number of syllables.

The introduction of the maximal critical cumulative distance for taking a positive decision not only shortens the time necessary to review the template collection, but also reduces the number of incorrect recognitions, especially in a case of a word not belonging to the vocabulary.

Methods of speeding up the lexical retrieval and choice of the template subcollection close to the input word are the object of special interest of designers of recognition systems, because the recognition accuracy and size of the word vocabulary depend on the efficiency of developed searching algorithms. The vocabulary size is decisive to the recognition time. An interesting method of searching the so-called "Geometrical Search" was presented recently (FARAGO, GORDOS, LUGOSI [5]). The elaborated algorithm, taking advantage of preliminary calculated distances between individual templates, makes it possible to shorten the search time by one order of magnitude for a vocabulary of 200–300 words at almost unchanged recognition accuracy.

5. Experimental material

The developed system was practically evaluated on the basis of various vocabularies uttered by 10 persons. Experiments were performed at various time intervals, reaching 3–4 months. The largest vocabulary, containing 60 words, was uttered 15 times by 8 persons. A total of 5000 statements constituted the testing material. The 60-word vocabulary was chosen to make it possible to control by speech data transmission and processing in a computer. At the same time research included another vocabulary consisting of 24 words and containing instructions for a computer system for robot's motion control.

6. Results of recognition

It is worth mentioning at the very beginning that in systems applying the DTW method, recognition accuracy depends on several factors which change the spectrum pattern of an analysed word in an irregular manner. In the first place we should mention: instability of individual characteristics of the operator's voice, considerable information reduction of the signal parametric representation frequently making the discrimination of certain classes of speech sounds impossible and variable phonetic-acoustic structure of individual words included in the accepted vocabulary for communication.

Fluctuations of the level of the input signal are one of the significant elements of

the signal's instability. In this case the application of a logarithmic scale of voltage conversion is insufficient. Therefore, when band-pass frequency analysis is applied an amplitude compressor has to be used. In the case under consideration the compressor converts fluctuations of the input level from about 20 dB to the range of 3 dB.

The stability of individual characteristics and phonetic-acoustic structure greatly depends on the operator's training and knowledge of microphone technique. An operator with big enough practice achieved recognition accuracy of 98–99%, while less trained persons reached about 92% on the average. A recognition accuracy decrease is due to the fact that results of signal parametrization and its acoustic pattern can also depend on the instability of individual characteristics.

The reduction of the parametric description of a speech signal considerably speeds-up the distance calculation. Yet, acoustic patterns of phonetic-acoustic classes with similar physical structure differ only slightly. This leads to difficulties with recognition of words with similar pronunciation. Table 2 contains analysis results of

Table 2. Influence of decimation degree (description reduction) on average distances from input word to correct template and closest incorrect template, and on recognition accuracy

Average distances \ <i>N</i>	10	15	20	25	30
From correct template (a)	97.8	93.3	86.67	80.72	78.38
From nearest incorrect (b)	142.77	145.38	144.26	140.92	138.5
Distance between templates (a) i (b)	44.97	52.08	57.59	60.2	60.12
Recognition score	0.93	0.928	0.98	0.983	0.995

the influence of the number of points *N* for one voice, with duration of uttered word subjected to linear normalization. The table presents average distance changes between the input word and correct template and between the input word and nearest incorrect one. The data given above for a 60-word vocabulary proves that 20–25 is the sufficient number of points. This means that decimation of the signal occurs every 15–20 ms for one-syllable words, while every 40–50 ms on the average for 3 and 4 syllable words. It is characteristic that an increase of the number of points is accompanied not only by an increase of recognition accuracy, but also, what is

logical, by an increase of average distances between the correct and closest incorrect template. This indicator makes possible to closely observe the influence of the reduction of the parametric discription. The value of $N = 20$ was accepted as optimal on the basis of recognition results. This number is two times smaller from the one given usually in literature (Myers et al. [9]), while the optimal width of the window does not differ from the one generally applied in isolated word recognition systems ($r = 5$).

Table 3 presents experimental results of recognition in the speaker — indepen-

Table 3. Average distances from input word to correct template and closest incorrect template, and recognition accuracy obtained for different operator's voice in a speaker-independent mode $N = 20$

Voice	Average distances	From correct template	From closest incorrect template	Between templates	Recognition score
		(a)	(b)	(a) i (b)	
M1		122.17	166.47	44.3	0.9
M2		124.25	161.67	37.42	0.88
M3		137.28	167.75	30.47	0.85
M4		131.35	170.73	39.38	0.92
M5		117.8	157.17	39.37	0.93
M6		109.93	154.78	44.85	0.95
M7		136.66	166.7	30.04	0.84
M8		124.0	155.82	31.82	0.88
M9		150.33	181.05	30.7	0.84
M10		136.05	176.48	40.43	0.9
F1		133.45	165.23	31.82	0.92

dent system, i.e. when reference words are entered by one operator, while recognized words were uttered by other persons. This research included 10 male voices and 1 female voice. A drop of recognition accuracy by about 10–12% on the average occurred in accordance with data given in literature. It can be avoided by creating a greater number of templates for individual words. On the basis of experimental data it was stated (Atal, Rabiner [3]) that in order to obtain a speaker — independent system, 12 templates for one word have to be formed.

Also the structure of the vocabulary itself, or to be precise the similarity of the phonetic-acoustic structure of words included in it, have a significant influence on the recognition accuracy. The relatively low recognition accuracy of about 75% on the average for the words input "wejście" (vejeće) and output "wyjście" (vijeće), extremely dependent on the operators voice, can be an example. Globally the number of recognition errors for 6 words (10% of words included in the vocabulary) with similar structure was equal to 50% of the total number of errors. Therefore, the

communication vocabulary in the presented system should not contain words with too similar or too variable acoustic structure.

To conclude it should be emphasized that reference vocabularies were entered only once by the operator and on this account recognition errors were caused by various, although permissible, pronunciations of the same word. Of course it is advisable to increase the number of reference sequences for a given word in such cases.

7. Conclusions

Achieved results confirmed the practical usefulness of the presented system, in spite of the application of a simplified spectrum analysis. The introduction of amplitude normalization before and logarithmic conversion after A/D conversion increased the system's resistance to random level fluctuations of a speech signal and made it possible to apply a 8-bit converter with relatively low sampling frequency (100 Hz). Logarithmic values were taken from tables, not calculated currently, to avoid further extension of calculation. It was possible to shorten the recognition time without a significant decrease of recognition accuracy by considerable reduction of the parametric description. Yet, in the present form the system is speaker-dependent, although a recognition accuracy reduction in a speaker-independent version can be avoided by an adequate choice of vocabulary.

This work was supported by the Problem CPBP 02.13.

References

- [1] J. ACKENHAUSEN, S. S. ALI, D. BISHOP, L. F. ROSA, R. THORKILDSEN, *Single board general — purpose speech recognition system*, AT and T Technical Journal, **65**, 5, 48–59 (1986).
- [2] J. ALLEN, *A perspective on man — machine communication by speech*, Proc. IEEE, **73**, 11, 1541–1500 (1985).
- [3] B. S. ATAL, R. R. RABINER, *Speech research directions*, AT and T Technical Journal, **65**, 5, 75–85 (1986).
- [4] R. E. CROCHIERE, J. L. FLANAGAN, *Speech processing: An evolving technology*, AT and T Technical Journal, **65**, 5, 2–11 (1986).
- [5] A. FARAGO, S. GORDOS, G. LUGOSI, *Methods for decreasing the response time in isolated word speech recognition*, Proc. Speech Research, 89, Budapest, 255–258 (1989).
- [6] L. L. LAMEL, L. R. RABINER, A. E. ROSENBERG, J. G. WILPON, *An improved endpoint detector for isolated word recognition*, IEEE Trans. on ASSP-29, **4**, 777–785 (1981).
- [7] S. E. LEVINSON, *A unified theory of composite pattern analysis for automatic speech recognition in: Computer Speech Processing* [ed.] F. Fallaido, W. A. Woods, Prentice-Hall, Englewood Cliffs 1985, 243–275.

- [8] T. MARTIN, *Application of limited vocabulary recognition systems*, 1974 Symposium Speech Recognition (Invited papers), Academic Press, New York 1975, 55-71.
- [9] C. MEYERS, L. R. RABINER, A. E. ROSENBERG, *Performance trade offs in dynamic time warping algorithms for isolated word recognition*, IEEE Trans. on ASSP, v. ASSP-28, 12, 1622-1633 (1980).
- [10] M. PELTIN, *Time to have words with your computer*, Int. Management, Nov., 23-25 (1979).
- [11] G. M. WHITE, R. B. NEELY, *Speech recognition experiments with linear prediction, bandpass filtering and dynamic programming*, IEEE Trans. on Acoust. Speech and Signal Processing, ASSP-24, 2, April, 183-188 (1976).
- [12] T. K. VINTSYUK, *Recognition of words of oral speech by dynamic programming methods*, (in Russian), Kibernetika, 1, 81-88 (1968).

Received on June 26, 1989

VELOCITY DISPERSION AND ATTENUATION OF ACOUSTIC WAVES IN CRITICAL MIXTURES

T. HORNOWSKI, M. ŁABOWSKI

Institute of Acoustics Adam Mickiewicz University
(00-769 Poznań, ul. Matejki 48/49)

Theoretical considerations on critical ultrasonic dispersion and attenuation in binary liquid mixtures based on the mode-coupling approach and frequency-dependent heat capacity are presented. A general expression for the critical amplitude $A(T)$ in terms of the parameter $d = (\rho c_{v,x}^0 / T \alpha_p) \cdot (dT_c / dP)$ is derived. It is shown that for specific values of d one obtains expressions for $A(T)$ equivalent to those of Fixman, Kawasaki, Mistura and Chaban. Moreover, an experimental test has been carried out on the system methanol-n-hexane showing good agreement between our general expression for $A(T)$ and experimental data.

W pracy zaprezentowano teoretyczne rozważania odnośnie do dyspersji i absorpcji fal ultradźwiękowych w mieszaninach krytycznych na gruncie teorii modów sprzężonych. Wyprowadzono ogólne wyrażenie na amplitudę pochłaniania $A(T)$ w postaci funkcji parametru d zdefiniowanego jako $d = (\rho c_{v,x}^0 / T \alpha_p) \cdot (dT_c / dP)$ i wykazano, że dla określonych wartości d uzyskuje się wyrażenia na $A(T)$ zgodne z teoriami Fixmana, Kawasaki, Mistury i Czabana. Przeprowadzono również weryfikację uzyskanych wyrażeń otrzymując dobrą zgodność z danymi eksperymentalnymi.

1. Introduction

In the theory of critical phenomena, an important role is played by the mode-coupling method, first formulated by KADANOFF and SWIFT [1] and thereupon applied to the solving of various problems of the physics of phase transitions, i.e., that of the acoustic wave propagation in critical mixtures. The most important theories in this field applying the mode-coupling approach are those of KAWASAKI, [2, 3], MISTURA [4] and CHABAN [5, 6] and, to a lesser degree, that of FIXMAN [7]. These theories lead to expressions for the attenuation α_λ of the acoustic wave (per wave length λ) that can be written in the form $\alpha_\lambda / c^2 = \pi \cdot A(T) \cdot I(\omega^*)$. The scaling function $I(\omega^*)$ is in all cases the same, whereas the amplitudes $A(T)$ differ essentially. Our paper is aimed, i.e., at the elucidation of the source of these differences.

2. Velocity dispersion and attenuation of the ultrasonic waves

Within the framework of mode-coupling theory [4], it can be shown that the excess specific heat at constant pressure related with relaxation of fluctuations in concentration is given by the following expression

$$\langle \delta c_p(\omega^*) \rangle = \frac{k_B T^2}{\pi^2 \varrho} \left(1 - \frac{\eta}{2}\right)^2 \kappa \left(\frac{\partial \kappa}{\partial T}\right)^2 \int_0^\infty \frac{y^2 dy}{(1+y^2)^2} \cdot \frac{\omega^*}{K(y) - i\omega^*}, \quad (1)$$

with k_B — Boltzmann's constant, $\kappa = 1/\xi$ — the inverse correlation of fluctuations in concentration, ϱ — the density of mixture, η — the critical exponent characterizing the deviation of the radial correlation function from the Ornstein-Zernike approximation and $y = k \cdot \xi$. The quantity ω^* is the reduced frequency defined as [8]

$$\omega^* = \omega/\omega_D = 2\pi f/(\omega_0 \varepsilon^{-z\nu}), \quad (2)$$

where ω_D is a temperature-dependent characteristic frequency, related with the concentration-fluctuation lifetime in the critical point of the mixture and given by Stokes-Einstein formula

$$\omega_D = k_B T/3\pi\eta\xi^3 = (k_B T/3\pi\eta\xi_0^3)\varepsilon^{-z\nu}, \quad (3)$$

with $\xi = \xi_0 \varepsilon^{-\nu}$ for the correlation length and $\eta = \eta_0 \varepsilon^{-(z-3)\nu}$ for the shear viscosity. The function $K(y)$ is related with the concentration-fluctuation lifetime $\tau_{\bar{K}}$ by way of the following expression, resulting from dynamical scaling hypothesis:

$$1/\tau_{\bar{K}} = 1/2 \omega_D K(y). \quad (4)$$

The expression (1) enables us to write the total complex specific heat $\tilde{c}_{p,x}$ at constant pressure in the form

$$\tilde{c}_{p,x} = c_{p,x}^0 + i \langle \delta c_p(\omega^*) \rangle = c_{p,x}^0 + \Delta(i\omega^*). \quad (5)$$

In addition to the excess specific heat at constant pressure, we have to determine that at constant volume. To this purpose, one can make use of the formula [9]

$$c_{V,x} = c_{p,x} + \frac{[(\partial V/\partial T)_{p,x}]^2}{(\partial V/\partial P)_{T,x}^0}. \quad (6)$$

By the scaling hypothesis [10], the Gibbs thermodynamical potential in the neighbourhood of the critical point is a homogeneous function and thus can be written in the form [11]

$$G(T, x, P) = G_0(T, x, P) + |\varepsilon(P)|^{2-\alpha} f(\Phi/|\varepsilon(P)|^{-\beta}), \quad (7)$$

where α, β are the critical exponents; $\varepsilon(P) = [T - T_c(P)]/T_c$ the so-called reduced distance from the critical point on the temperature-axis; and $\Phi = (x - x_c(P))/x_c$ the ordering parameter. The Gibbs thermodynamical potential thus defined enables us to determine various thermodynamical parameters, among which are $(\partial V/\partial P)_{T,x}$,

$(\partial V/\partial T)_{P,x}$ and $c_{P,x}$. At $x = x_c$ we have $f(\Phi/|\varepsilon(P)|^{-\beta}) = \text{const}$, whence

$$c_{P,x} = -T(\partial^2 G/\partial T^2)_{P,x} = A_1 |\varepsilon(P)|^{-\alpha} + c_{P,x}^0, \quad (8)$$

$$(\partial V/\partial P)_{T,x} = (\partial^2 G/\partial P^2)_{T,x} = A_1 (\partial T_c/\partial P)^2 |\varepsilon(P)|^{-\alpha} + (\partial V/\partial P)_{T,x}^0, \quad (9)$$

$$(\partial V/\partial T)_{P,x} = (\partial^2 G/\partial T \partial P)_{P,x} = -A_1 (\partial T_c/\partial P) |\varepsilon(P)|^{-\alpha} + (\partial V/\partial T)_{P,x}^0, \quad (10)$$

On insertion of (8), (9), and (10), into Eq. (6) we obtain the specific heat at constant volume in the following form:

$$c_{V,x} = A_1 |\varepsilon(P)|^{-\alpha} + c_{P,x}^0 + \frac{[A_1 (\partial T_c/\partial P) |\varepsilon(P)|^{-\alpha} + (\partial V/\partial T)_{P,x}^0]^2}{-A_1 (\partial T_c/\partial P)^2 |\varepsilon(P)|^{-\alpha} + (\partial V/\partial P)_{T,x}^0}, \quad (11)$$

The expression (11) can be expanded in a series in $(\partial T_c/\partial P)$, restricting the expansion to quadratic terms and omitting the term proportional to $|\varepsilon(P)|^{-2\alpha}$ which is much smaller than the others. We thus obtain

$$c_{V,x} \approx A_1 |\varepsilon(P)|^{-\alpha} \left\{ 1 + 2 \frac{(\partial V/\partial T)_{P,x}^0}{(\partial V/\partial P)_{T,x}^0} \cdot \frac{dT_c}{dP} + \left[\frac{(\partial V/\partial T)_{P,x}^0}{(\partial V/\partial P)_{T,x}^0} \cdot \frac{dT_c}{dP} \right]^2 \right\} + c_{P,x}^0 + \frac{[(\partial V/\partial T)_{P,x}^0]^2}{(\partial V/\partial P)_{T,x}^0}. \quad (12)$$

On introducing the notation

$$c_{V,x}^0 = c_{P,x}^0 + \frac{[(\partial V/\partial T)_{P,x}^0]^2}{(\partial V/\partial P)_{T,x}^0}, \quad (13)$$

$$d = \frac{c_{V,x}^0}{T \alpha_p} \cdot \frac{dT_c}{dP} \quad (14)$$

and applying the thermodynamical identity [12]

$$\frac{(\partial V/\partial T)_{P,x}^0}{(\partial V/\partial P)_{T,x}^0} = -\frac{q}{T \alpha_p} (c_{P,x}^0 - c_{V,x}^0) = -\frac{c_{V,x}^0 q}{T \alpha_p} (\gamma - 1), \quad (15)$$

we obtain

$$c_{V,x} \approx A_1 [1 - d(\gamma - 1)]^2 |\varepsilon(P)|^{-\alpha} + c_{V,x}^0 = A_2 |\varepsilon(P)|^{-\alpha} + c_{V,x}^0. \quad (16)$$

Comparing Eqs. (8) and (16) we get the ratio of the excess specific heats at constant pressure and constant volume, two quantities related with concentration-fluctuation relaxation:

$$\langle \delta c_{V,x}(\omega^*) \rangle = (A_1/A_2) \langle \delta c_{P,x}(\omega^*) \rangle = (A_1/A_2) \Delta(i\omega^*), \quad (17)$$

where

$$A_1/A_2 = [1 - d(\gamma - 1)]^2. \quad (18)$$

Thus, the total complex specific heat at constant volume takes the form

$$\tilde{c}_{V,x} = c_{V,x}^0 + (A_1/A_2)\Delta(i\omega^*). \quad (19)$$

With the complex specific heats available — Eqs. (4) and (18) — we are in a position to determine the complex propagation velocity \tilde{c} of ultrasonic waves from the formula

$$\tilde{c}^2 = \frac{T}{\varrho^2} \left(\frac{\partial P}{\partial T} \right)_{\varrho,x}^2 \frac{\tilde{c}_{P,x}}{\tilde{c}_{V,x}(\tilde{c}_{P,x} - \tilde{c}_{V,x})}. \quad (20)$$

We are now able to determine \tilde{c}^{-1} , inserting the expressions (5) and (19) into (20) and expanding the expression thus obtained in a Taylor series in $\Delta(i\omega^*)$. On restricting ourselves to the first-order terms, we get

$$\tilde{c}^{-1} \approx c_0^{-1} \left[1 + \frac{(A_1/A_2)\gamma^2 - 2(A_1/A_2)\gamma + 1}{2c_{P,x}^0(\gamma - 1)} \Delta(i\omega^*) \right], \quad (21)$$

where

$$c_0^{-1} = \left[\frac{T}{\varrho^2} \left(\frac{\partial P}{\partial T} \right)_{\varrho,x}^2 \frac{c_{P,x}^0}{c_{V,x}^0(c_{P,x}^0 - c_{V,x}^0)} \right]^{-1/2}. \quad (22)$$

With regard to (18), the numerator of Eq. (22) takes the form

$$(A_1/A_2)\gamma^2 - 2(A_1/A_2)\gamma + 1 = (\gamma - 1)^2 f(d), \quad (23)$$

where the function $f(d)$ is defined as the sum of the following two polynomials

$$F_1(d) = \gamma^2(d - 1/\gamma)^2 \quad (24)$$

$$F_2(d) = -2d\gamma[d - 1/(\gamma - 1)]. \quad (25)$$

With $f(d)$ defined as above, we can express the complex velocity of propagation of ultrasonic waves in critical mixtures as follows:

$$\tilde{c}^{-1} = c_0^{-1} \left[1 + \frac{f(d)(\gamma - 1)}{2c_{P,x}^0} \Delta(i\omega^*) \right]. \quad (26)$$

On the other hand, the complex velocity is

$$\tilde{c}^{-1} = c^{-1} + i\omega^{-1}\alpha, \quad (27)$$

whence, with the real and imaginary parts, we finally obtain the following expressions for the velocity dispersion $\Delta c/c_0$ and attenuation coefficient α of acoustic waves in critical mixtures:

$$\alpha\lambda/c_0^2 = \pi A(T) I(\omega^*), \quad (28)$$

$$\Delta c/c_0 = -\frac{1}{2} A(T) J(\omega^*), \quad (29)$$

with the coefficient $A(T)$ and the functions $I(\omega^*)$ and $J(\omega^*)$ given by

$$A(T) = \frac{k_B T^2 (\gamma - 1)}{\pi^2 \rho c_0^2 c_{p,x}^0} \left(1 - \frac{\eta}{2}\right)^2 \kappa \left(\frac{\partial \kappa}{\partial T}\right)^2 f(d), \quad (30)$$

$$I(\omega^*) = \text{Im} \left[\frac{(\gamma - 1) f(d) \Delta(i\omega^*)}{c_{p,x}^0 c_0^2 A(T)} \right] = \int_0^\infty \frac{y^2 dy}{(1 + y^2)^2} \cdot \frac{\omega^* K(y)}{K^2(y) + (\omega^*)^2}, \quad (31)$$

$$J(\omega^*) = \text{Re} \left[\frac{(\gamma - 1) f(d) \Delta(i\omega^*)}{c_{p,x}^0 c_0^2 A(T)} \right] = \int_0^\infty \frac{y^2 dy}{(1 + y^2)^2} \cdot \frac{(\omega^*)^2}{K^2(y) + (\omega^*)^2}. \quad (32)$$

The coefficient $A(T)$ determining the amplitude of the fluctuations in concentration in the critical point, can be expressed in a different way making use of the scaling relation

$$\kappa = \xi^{-1} = \xi_0^{-1} \varepsilon^\nu. \quad (33)$$

for the correlation length of fluctuations in concentration [9]. This leads to the following expression:

$$A(T) = \frac{k_B (\gamma - 1) \nu^2}{\pi^2 \rho c_0^2 c_{p,x}^0 \xi_0^3} \left(1 - \frac{\eta}{2}\right)^2 f(d) \varepsilon^{-\alpha}. \quad (34)$$

3. Analysis and discussion

The formulae (31), (32) and (33) derived by us are general expressions for the propagation velocity and attenuation coefficient of acoustic waves in critical mixtures. The expressions for the attenuation of acoustic waves derived within the framework of the theories of Fixman, Mistura, Kawasaki and Chaban can be shown to represent particular cases of our expressions. To this aim, we have to investigate the properties of the function $f(d)$. As already stated, $f(d)$ is the sum of polynomials of the second degree $F_1(d)$ and $F_2(d)$. Their graphs have the form of the parabol as shown in Fig. 1, the analysis of the latter enables us to distinguish three cases:

i) $d = 0$, implying $(\partial T_c / \partial P) = 0$. In this particular case we have $F_1(d) = 1$, $F_2(d) = 0$ and $f(d) = 1$ thus obtaining an expression for $A(T)$ in accordance with the theories of Fixman and Kawasaki;

ii) $d = 1/(\gamma - 1)$, implying $(\partial T_c / \partial P) = T \alpha_P / [\rho(c_{p,x}^0 - c_{v,x}^0)]$. We thus have $F_1(d) = 1/[(\gamma - 1)^2]$, $F_2(d) = 0$ and $f(d) = 1/(\gamma - 1)^2$. The expression for $A(T)$ is in this case in accordance with the theory of Mistura.

iii) $0 < d < d|_{F_1(d) \gg F_2(d)}$, giving $f(d) \approx F_1(d) = (1 - d\gamma)^2$. The expression for $A(T)$ now takes a form in agreement with the theory of Chaban.

The relations thus obtained are assembled in Table 1.

For the theories of Kawasaki, Mistura and Chaban the form of $K(y)$ is given by

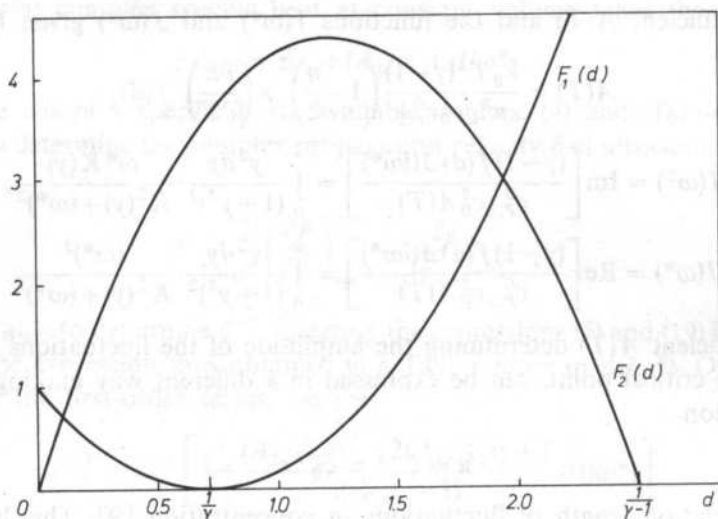
FIG. 1. Shape of the functions $F_1(d)$ and $F_2(d)$ for $\gamma = 1.4$

Table 1

Theory	d	$K(y)$	$A(T)$
FIXMAN [7]	0	$y^2(1+y^2)$	$\frac{k_B(\gamma-1)v^2}{\pi^2 \varrho c_0^2 c_{P,x} \xi_0^3} e^{-\alpha}$
KAWASAKI [2]	0	$K_w(y)$	$\frac{k_B(\gamma-1)v^2}{\pi^2 \varrho c_0^2 c_{P,x} \xi_0^3} e^{-\alpha}$
MISTURA [5]	$\frac{1}{\gamma-1}$	$K_w(y)$	$\frac{k_B v^2}{\pi^2 \varrho c_0^2 c_{P,x} \xi_0^3 (\gamma-1)} \left(1 - \frac{\eta}{2}\right)^2 e^{-\alpha}$
CHABAN [6]	$0 < d < 0.01$	$K_w(y)$	$\frac{k_B(\gamma-1)v^2}{\pi^2 \varrho c_0^2 c_{P,x} \xi_0^3} \left(1 - \frac{\varrho c_{P,x}^0}{\alpha_p T} \frac{\partial T_c}{\partial P}\right)^2 e^{-\alpha}$

the Kawasaki function [4]

$$K_w(y) = \frac{3}{4} [1 + y^2 + (y^3 - 1/y) \arctan y]. \quad (35)$$

In order to check the relationships derived by us, we made use of the experimental results for acoustic wave attenuation in the methanol-cyclohexane critical mixture published in Ref. [13]. The literature [9, 13–15] moreover contains experimental data for $c_{P,x}^0$, $c_{V,x}^0$, α_p , $(\partial T_c / \partial P)$, ξ_0 and ϱ for the above mixture. The parameter d determined with these data amounts to 1.11. For ω_0 we assumed 1.64×10^{12} Hz after the authors of Ref. [13]. Figs. 2–5 show the experimental data in

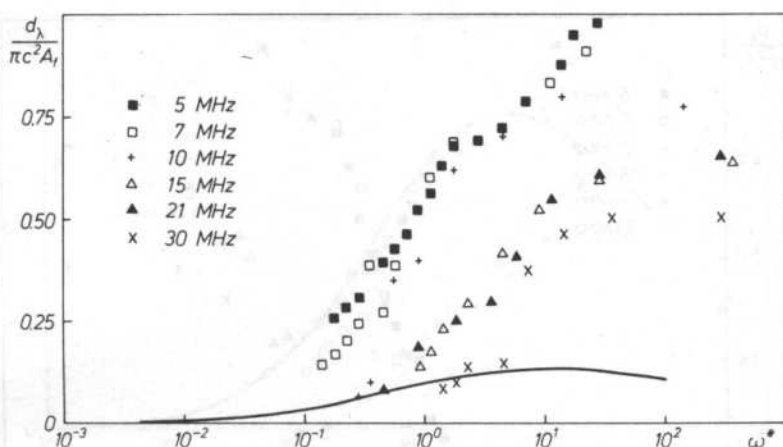


FIG. 2. $\alpha_\lambda/(\pi c^2 A)$ vs. ω^* for the critical methanol-cyclohexane mixture, for $A(T)$ calculated according to the theory of Fixman. The experimental data are taken from Ref. [13]

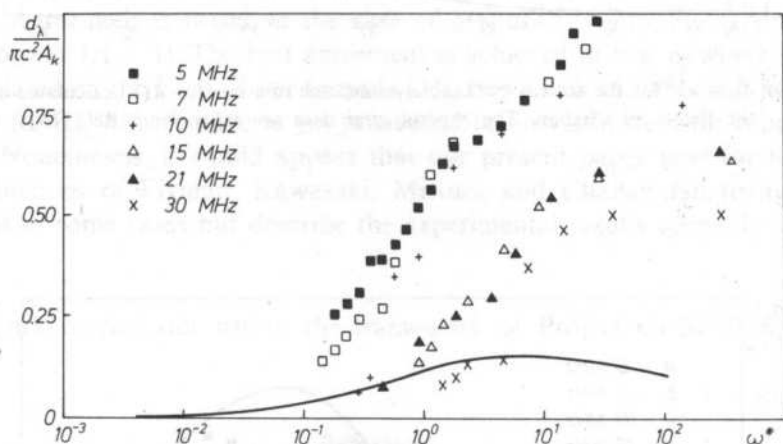


FIG. 3. $\alpha_\lambda/(\pi c^2 A_k)$ vs. ω^* for the critical methanol-cyclohexane mixture, for $A(T)$ calculated according to the theory of Kawasaki. The experimental data are taken from Ref. [13]

the form of $\alpha_\lambda (\pi c_0^2 A)$ versus ω^* , with values of A corresponding to the theories of Fixman, Kawasaki, Mistura and Chaban, respectively. The results shown in Fig. 6 are those obtained with our formula (34). Everywhere, the continuous curves show the scaling function given by Eq. (31). Obviously, agreement between the theories of Fixman (Fig. 2), Kawasaki (Fig. 3) and Chaban (Fig. 4) on the one hand and the experimental results on the other is very weak, this is by no means surprising in the

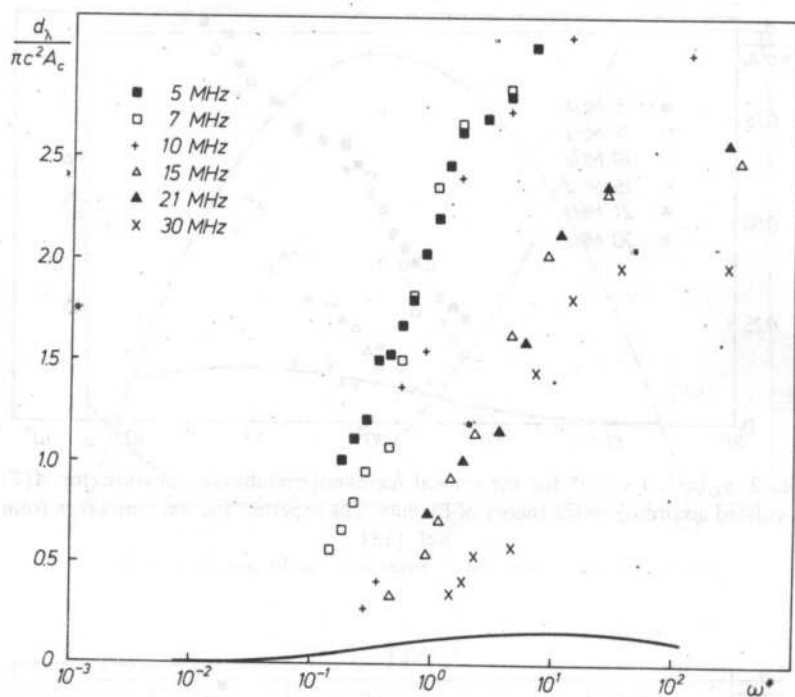


FIG. 4. $\alpha_\lambda/(\pi c^2 A)$ vs. ω^* for the critical methanol-cyclohexane mixture, for $A(T)$ calculated according to the theory of Chaban. The experimental data are taken from Ref. [13]

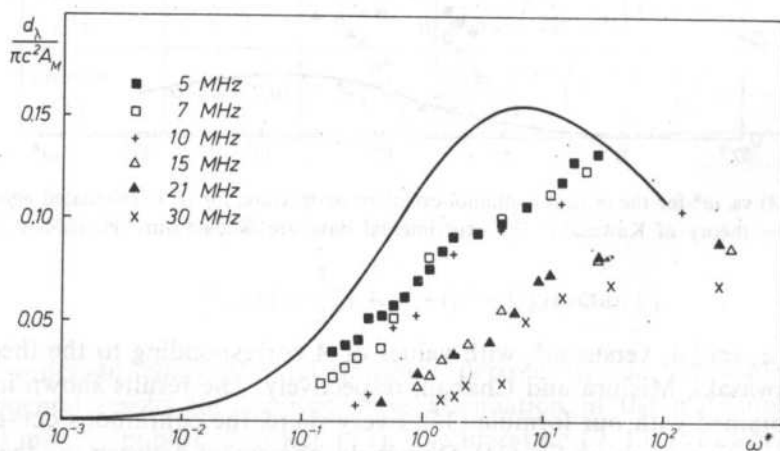


FIG. 5. $\alpha_\lambda/(\pi c^2 A)$ vs. ω^* for the critical methanol-cyclohexane mixture, for $A(T)$ calculated according to the theory of Mistura. The experimental data are taken from Ref. [13]

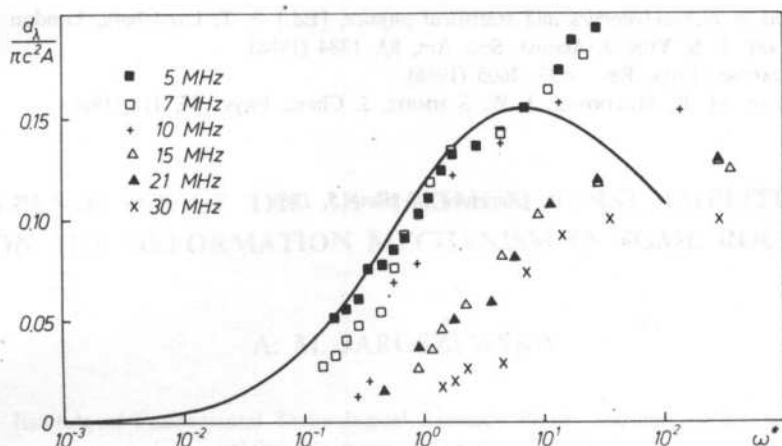


FIG. 6. $\alpha_\lambda/(\pi c^2 A)$ vs. ω^* for the critical methanol-cyclohexane mixture, for $A(T)$ calculated with our formula (34). The experimental results are taken from Ref. [13]

light of our preceding considerations, since the parameter d differs from zero markedly. Agreement is better in the case of Mistura's theory Fig. 5 since d has a value close to $1/(\gamma - 1)$. The best agreement is achieved in Fig. 6, where $A(T)$ has been calculated on the basis of our formula (34). For a lack of sufficiently exact data (especially for $\partial T_c/\partial P$) we have as yet proceeded to no verification for other critical mixtures. Nonetheless, it would appear that our present paper goes for to explain why the theories of Fixman, Kawasaki, Mistura and Chaban fail to agree with experiment in some cases but describe the experimental results correctly in others.

Work carried out within the framework of Project CPBP 02.03

References

- [1] L. P. KADANOFF, J. SWIFT, Phys. Rev., **166**, 89 (1968).
- [2] K. KAWASAKI, Phys. Rev., **A1**, 1750 (1970).
- [3] Y. SHIWA, K. KAWASAKI, Progr. Theor. Phys., **66**, 406 (1981).
- [4] L. MISTURA, J. Chem. Phys., **57**, 2311 (1972).
- [5] I. A. CHABAN, Akust. Zh., **21**, 104 (1975).
- [6] I. A. CHABAN, Akust. Zh., **21**, 286 (1975).
- [7] M. FIXMAN, J. Chem. Phys., **36**, 1961 (1962).
- [8] C. W. GARLAND, G. SANCHEZ, J. Chem. Phys., **75**, 3090 (1983).
- [9] M. A. АНИСИМОВ, Критические явления в жидкостях и жидких кристаллах, Наука 1987.
- [10] L. P. KADANOFF, Physics, **2**, 263 (1966).
- [11] B. WIDOM, J. Chem. Phys., **63**, 3892 (1965).

- [12] *Problems in thermodynamics and statistical physics*, [Ed.] P. T. Landsberg, London 1971.
- [13] S. J. FAST, S. S. YUN, *J. Acoust. Soc. Am.*, **83**, 1384 (1988).
- [14] D. T. JACOBS, *Phys. Rev.*, **A33**, 2605 (1986).
- [15] H. CHAAR, M. R. MOLDOVER, J. W. SCHMIDT, *J. Chem. Phys.*, **85**, 418 (1986).

Received on June 5, 1989

DEPENDENCE OF THE AE MAXIMUM BURST AMPLITUDE ON THE DEFORMATION MECHANISM IN SOME ROCKS

A. M. JAROSZEWSKA

Institute of Fundamental Technological Research Polish Academy of Sciences
(00-049 Warszawa, Świętokrzyska 21)

Maximum amplitude of acoustic emission events in 10 second intervals were measured in the samples of dolomite and sandstone under uniaxial compressive load.

The observed sudden increase of the maximum amplitude, in a function of load, indicates the beginning of the unstable propagation of microfractures, leading to uncontrolled failure of a sample. The maximum amplitude dependence on load, as directly related to the AE source mechanism, can be used in prediction of the rock damage in situ.

Przedstawiono wyniki badań maksymalnej amplitudy emisji akustycznej w interwałach 10-sekundowych, próbek dolomitu i piaskowca, poddawanych jednoosiowym naprężeniom ściskającym. Obserwowany znaczny wzrost maksymalnych amplitud, w funkcji czasu obciążania, wskazuje na rozpoczęcie się propagacji niestabilnej mikropęknięć, które prowadzą do niekontrolowanego zniszczenia próbki. Przebieg maksymalnej amplitudy sygnałów w funkcji obciążeń, jako zależny bezpośrednio od mechanizmu źródła EA, może być wykorzystywany do przewidywania rozpadu skał in situ.

Acoustic emission (AE) used in non-destructive testing of objects and constructions as well as materials, e.g. metals and composite materials, or in testing of leak-proof objects as well as in the localization of leakages, has been almost generally accepted and is recommended by the corresponding standards. It is also used in the industry. However, the use of the AE methods in assessment of stability of rocks in situ, on account of their heterogeneous structure, requires still further studies.

The reported results of investigation in this respect [1-8] indicate that the AE maximum burst amplitude is one of the most representative parameters of acoustic emission observed in brittle rocks under load, since its value depends directly on the AE source mechanism. A sudden increase of maximum amplitudes indicates the beginning of the unstable or semistable fracture propagation which leads to an uncontrolled rupture. Also, the results of measurements of the AE maximum burst amplitude are relatively the less dependent on the technical data of the equipment used and on the dimensions of samples tested. A theoretical pulse signal of the AE event, and its maximum amplitude A_m as a function of time is shown in Fig. 1.

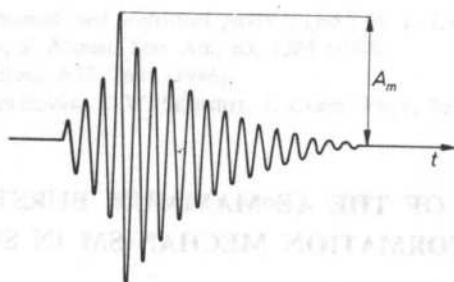


FIG. 1. Theoretical plot of pulse signal — AE event

Most works pertaining to the maximum amplitude of the AE signal in rocks were aimed at a characteristic maximum amplitude/event number statistical distribution, [8–10]. The results obtained show that this distribution obeyed in many cases, for some loading range, Ischimoto-Iida distribution well known in seismology:

$$n(a)da = ka^{-m}da, \quad (1)$$

where: $n(a)$ — number of signals with amplitudes in the range between: $a + da$ and $a - da$, a — maximum signal amplitude, k and m — constants.

Investigation of the exponent m as a function of load has shown, that the rock burst prediction on the grounds of its (i.e. m exponent) changes is possible for brittle rocks characterized by unexplosive rupture and also for quasi-brittle rocks. However, such a prediction is impossible for ductile rocks [8].

In the present work, investigation of the AE maximum burst amplitude under uniaxial compression, in samples of some rocks from Legnica-Glogow Copper District was carried out. The results of the AE maximum burst amplitude measurements presented in this paper were obtained with the use of a modified measurement procedure. In this procedure, the measurement of the maximum burst amplitude as a function of compressive load was taken in 10s time intervals. Both, the procedure as well as the equipment used in its execution were simplified in a substantial degree. The results obtained are quite easy to interpret and, as it seems, could be recognized as good grounds for positive prognosis with regards to the utility of the method.

1. Measurements of samples

For the measurements of the AE maximum burst amplitude, 21 cylindrical samples of dolomite (dolomitic-limestone) and sandstone from the Legnica-Glogow Copper District were used. The diameter to length ratio in this samples was 0.5.

Prior to the measurements of AE, some physical and mechanical properties of the samples were determined. In Table 1 sample dimensions, travel times for elastic longitudinal t_p and transversal t_s waves, longitudinal c_p and transversal c_s wave velocities and their compressive strengths σ_c , obtained in the next part of experimental work, for dolomite samples are given. In Table 2 the same properties for the

Table 1. Results of ultrasonic measurements of cylindrical dolomite samples from Legnica-Glogow Copper District

No. of sample	Dimensions		t_p [μ s]	c_p [m/s]	t_s [μ s]	c_s [m/s]	σ_r [MPa]	Remarks
	l [mm]	\varnothing [mm]						
1	60.0	30.0	12.9	4651	22.6	2655	56.6	
2	61.0	30.0	10.5	5810	18.7	3262	84.9	
5	69.0	30.0	21.7	3180	36.4	1896		
6	68.7	30.0	17.8	3860	30.3	2267		
7	62.0	30.0	15.3	4052	25.9	2394	70.7	
8	60.0	30.0	15.7	3822	27.3	2198	77.8 92.0	sample divided in two parts
10	60.0	30.0	13.7	4380	23.9	2510	70.7	
12	62.0	30.0	10.0	6200	18.1	3425	53.8	
13	63.0	30.0	12.8	4922	22.6	2788	84.9	
15	63.5	30.0	15.7	4045	27.4	2318	42.4	fractured
17	60.0	30.0	9.9	6061	17.8	3370	56.6	
19	60.0	30.0	11.0	5455	19.5	3077	103.3	
20	85.5	42.0	13.6	6287	24.5	3490	65.0	
21	85.5	42.0	13.6	6477	24.2	3533	115.5	
22	85.8	43.0	13.6	6173	25.5	3365	117.1	

Table 2. Results of ultrasonic measurements of cylindrical sandstone samples from Legnica-Glogow Copper District

No. of sample	Dimensions		t_p [μ s]	c_p [m/s]	t_s [μ s]	c_s [m/s]	σ_r [MPa]	Remarks
	l [mm]	\varnothing [mm]						
3p	64.0	30.0	19.0	3368	31.0	2065	14.2	
5p	46.0	30.0	17.9	2570	28.8	1597	18.4	fractured
7p	60.0	30.0	38.5	1558	59.7	1005	21.2	fractured
9p	63.0	30.0	26.2	2405	41.9	1504	22.6	
10p	96.0	47.0	53.1	1808	83.4	1151	64.9	
11p	96.0	48.0	47.5	2021	76.0	1263	78.8	

sandstone samples are given. The measurements of elastic wave velocities were carried out at frequency 200 kHz.

The results of measurements of mass density, bulk density, porosity and absorbability of all the samples and information concerning their lithology are given in Table 3. The observed dispersion of presented data indicates substantial heterogeneity of the rocks tested.

The samples were divided into groups characterized by similarity of the physical and mechanical data given in Tables 1,2 and 3.

Table 3. Results of measurements of mass density ρ_m , bulk density ρ_v , porosity p and absorbability n of samples tested

No of sample	Rock type	ρ_m [Tm ⁻³]	ρ_v [Tm ⁻³]	p [%]	n [%]	Remarks
1	2	3	4	5	6	7
1	fine grained dolomitic limestone	2.77	2.69	2.9	0.7	
2	fine grained dolomitic limestone	2.79	2.69	3.6	0.1	
3 p	fine grained sandstone	2.65	2.22	16.2	—	
5	fine grained limestone	2.82	2.65	6.0	1.7	
5 p	fine grained sandstone	2.77	2.46	11.2	4.0	
6	fine grained limestone	2.75	2.54	7.6	1.0	
7	fine grained limestone	2.84	2.68	5.6	0.9	
7 p	fine grained sandstone	2.65	3.39	9.8	5.4	
8	fine grained dolomitic limestone	2.87	2.72	5.2	0.9	
9 p	fine grained sandstone	2.65	2.50	5.7	1.6	
10	fine grained dolomitic limestone	2.88	2.70	6.2	1.0	
10 p	fine grained powdery sandstone	2.70	2.28	15.5	—	
11 p	fine grained powdery sandstone	2.70	2.28	15.5	—	
12	fine grained dolomitic limestone	2.86	2.74	4.2	0.1	

1	2	3	4	5	6	7
13	fine grained dense dolomitic limenstone	2.87	2,65	7.7	1.3	
15	fine grained dolomitic limestone	2.75	2,61	5.1	0.8	
17	fine grained dolomitic limestone	2.84	2,74	3.5	0.1	
19	coarse grained dense dolomitic limenstone	2.86	2,76	3.5	0.1	
20	fine grained dense dolomitic limenstone	2.93	2,81	4.1	—	
21	fine and average grained dolomite	2.90	2,76	4.8	—	
22	fine grained dolomitic limestone	2.88	2,62	9.0	—	

2. Measurement of the AE maximum burst amplitude and even rate

The described rock samples were tested under uniaxial compressive load exerted by hand operated hydraulic press. The AE maximum burst amplitude was measured in 10s time intervals and registered by x-y plotter and digitally. The results of measurements of the AE event rates were registered in 1s intervals using x-y plotter and digitally in 10s.

Acoustic emission measurements were carried out at/for

1. various loading rates,
2. various frequency ranges,
3. various sample dimensions.

As a receiver of AE signals, a piezoelectric transducer with flat (within ± 3 dB) frequency response in the range 1.5–150 KHz, was used. This transducer was cemented to the side wall of cylindrical samples used.

3. Results of measurements

For the majority of samples a plot of the AE maximum burst amplitude, with increasing load, was in agreement with a plot of event rate which is well manifested in the sample No 19. In Fig. 2 a plot of its AE maximum burst amplitude A_m in 10s

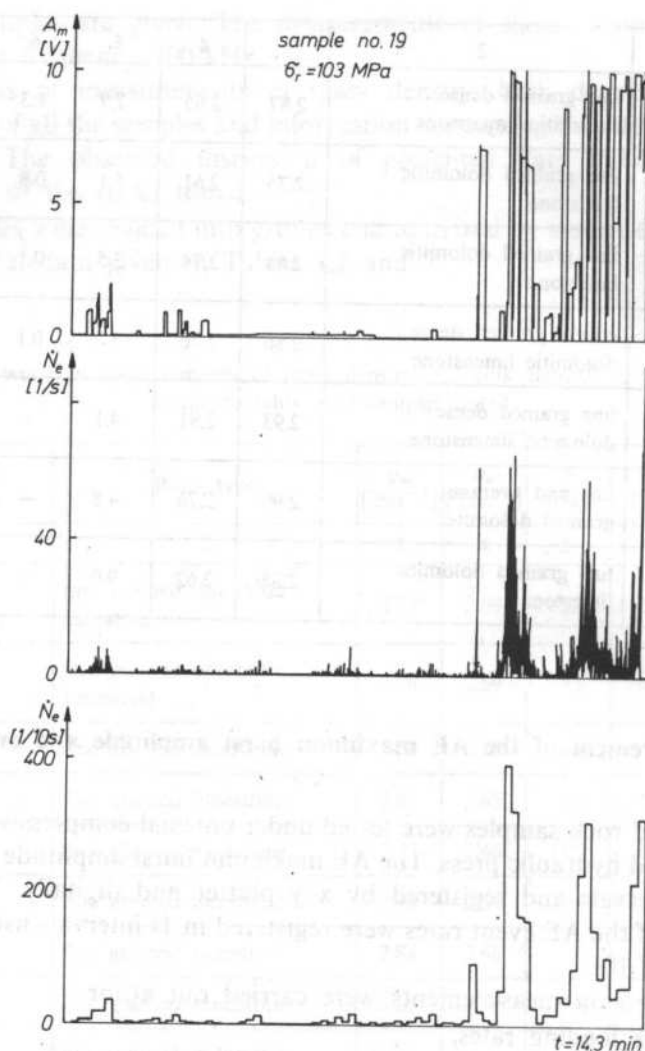


FIG. 2. AE maximum burst amplitude A_m in 10s (upper) and event rate N_e in 1s and 10s (lower) for sample No 19 as a function of loading time t

intervals (upper plot) and the event rate in 1s intervals and 10s intervals (lower plot) is given as a function of loading time t .

However, in some samples a sudden increase of the maximum amplitudes was observed, while the level of event rates was quite small and remained almost unchanged e.g. in samples No 2 and No 7 (Fig. 3 and Fig. 7). Since, it must be observed that the increase of event rate not always is a sufficient indicator to signal a beginning of sample failure and therefore cannot be used explicitly in the prediction of rock burst.

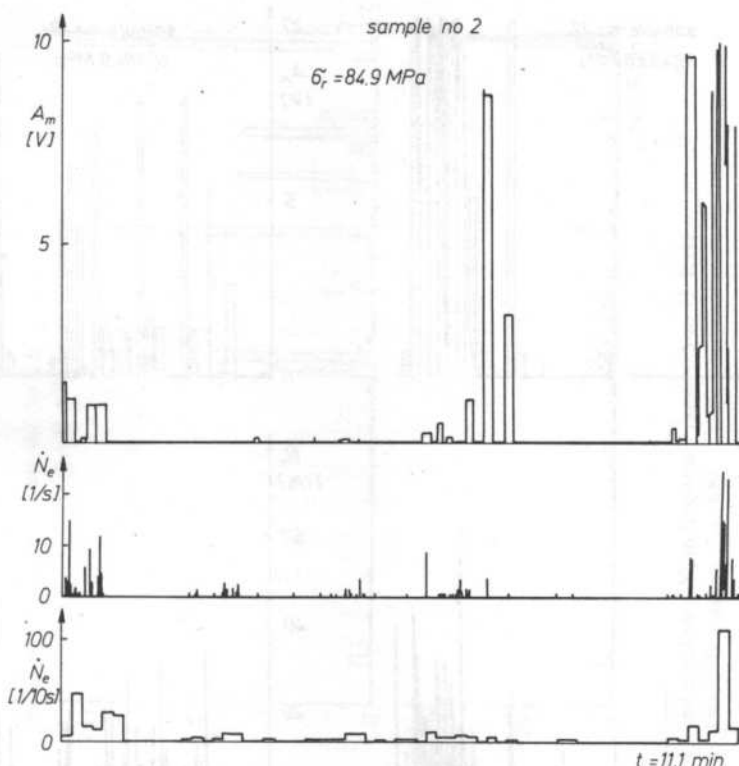


FIG. 3. AE maximum burst amplitude A_m plot in 10s (upper) and event rate N_e in 1s and 10s (lower) for sample No 2

In investigation of the influence of load rate on the acoustic emission in rock, two different sample loading procedures were used. Some samples were loaded at a rate of 14 MPa/min, other samples were loaded incrementally i.e. increment of load 14 MPa/min was used and was kept constant in a period of 1 min. The linear or incremental load was increased until failure. The measurements of acoustic emission as dependent on the rate of sample loading were performed in the frequency range from 1.5 to 150 KHz.

The results obtained show that at slow loading rate (incremental) of the samples, more small amplitude events is observed since fractures propagate at a lower velocity, and dimensions of the AE sources are smaller, e.g. sample No 12 (Fig. 4). At a faster loading rate, the events of larger energy are observed and the rock failure process is quicker, e.g. sample No 13 (Fig. 4).

In the AE investigation, also the influence of the frequency response of the AE channel on the plot of AE maximum burst amplitude and event rate was examined. The measurements of AE of some samples were performed in a low frequency range i.e. 0.5–15 KHz and for some other samples in a higher frequency range i.e. 15–150 KHz. In these cases the load was increased incrementally.

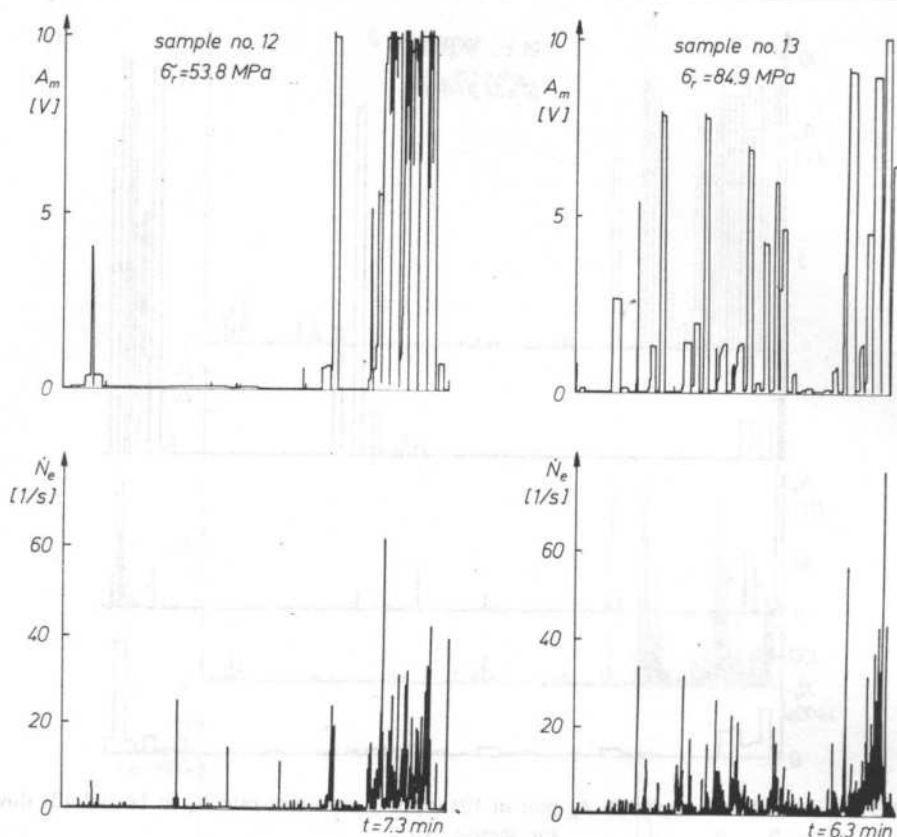


FIG. 4. AE maximum burst amplitude A_m plot in 10s and event rate N_e in 1s as a function of incremental loading (sample No 12) and linear (sample No 13)

Summarizing, the results obtained indicate that for dolomite higher maximum amplitudes were observed in the low frequency range (0.5–15 KHz), e.g. sample No 8a. However, the event rates in this range were smaller than in the high frequency range (15–150 KHz) e.g. sample No 8b (Fig. 5). The samples No 8a and No 8b were obtained by dividing the sample No 8 into two separate equal parts.

For sandstone, higher values of maximum amplitudes as well as event rates were observed in the low frequency range. These results indicate that the sandstone AE frequency spectrum is shifted downwards relative to the AE frequency spectrum of dolomite, and are in good agreement with the measurements of the AE spectra for these rocks [7].

No significant influence of sample dimensions on the character of maximum amplitude and event rate under compressive load, for the rocks tested, was observed. However, higher event rates were observed in the samples of larger dimensions.

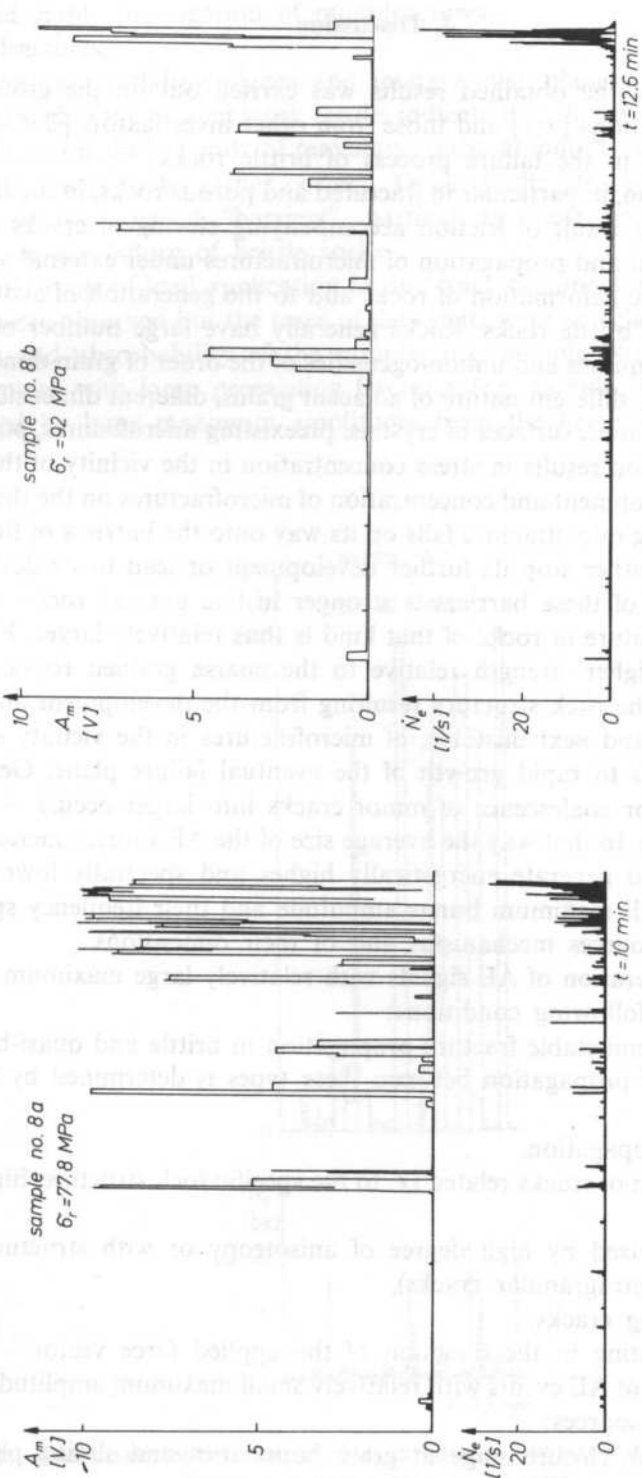


Fig. 5. The plot of AE maximum burst amplitude A_m and event rate N_e in frequency range 0.5 to 15 KHz (sample No 8a) and 15 to 150 KHz (sample No 8b)

4. Discussion

Interpretation of the obtained results was carried out on the grounds of the earlier own observations [1,7] and those from other investigators [2-5, 8-10] both relating to the AE in the failure process of brittle rocks.

Acoustic emission, in particular in fractured and porous rocks, in the first stage of loading occurs as a result of friction accompanying closing of cracks and pores.

The development and propagation of microfractures under external stress which leads to the inelastic deformation of rocks and to the generation of acoustic waves results in failure of brittle rocks. Rocks generally have large number of structural defects like discontinuities and unhomogeneities of the order of grain dimensions. To this class belong e.g. different nature of adjacent grains, different dimensions of these grains, grain boundaries, surfaces of crystals, preexisting microfissures, pores and the like. Load application results in stress concentration in the vicinity of these defects, leading to the development and concentration of microfractures on their surfaces.

The propagating microfracture falls on its way onto the barriers of the discussed nature which can either stop its further development or lead to its deviation. The stoppage influence of these barriers is stronger in fine grained rocks. The energy required for the rupture of rocks of that kind is thus relatively larger. Fine grained rocks have thus higher strength relative to the coarse grained rocks.

Weakening of the rock structure resulting from the development and propagation, firstly stable and next unstable, of microfractures in the vicinity of the most strong defects leads to rapid growth of the eventual failure plane. Generation of larger cracks and/or coalescence of minor cracks into larger occurs — leading to macroscopic failure. In that way the average size of the AE sources increases. Larger AE sources tend to generate energetically higher and spectrally lower frequency events. Both the AE maximum bursts amplitude and their frequency spectrum are functions of AE sources mechanisms and of their dimensions.

In general, generation of AE signals with relatively large maximum amplitudes occurs under the following conditions:

- unstable and semi-stable fracture propagation in brittle and quasi-brittle rocks, classification of propagation between these types is determined by the Griffith criterion,
- macrocrack propagation,
- fast propagation of cracks related i.e. to the specific rock structure, high load rate etc.,
- rocks characterized by high degree of anisotropy or with structural defects,
- grain failure (intragranular cracks),
- large preexisting cracks,
- cracks propagating in the direction of the applied force vector.

The generation of AE events with relatively small maximum amplitudes occurs in the following AE sources:

- friction in crack closure stage at grain boundaries and sliding planes,
- twinnings,

- slow and stable propagation of microfractures,
- ductile fractures,
- microfractures in sliding planes and intergranular planes.

The obtained in the present work results indicate that the general qualification of the AE sources on the grounds of maximum burst amplitude values, generated by these sources seems to be rather correct. These results also seem to support the hypothesis of the role of "barriers", particularly these concerning the grain boundaries, in the failure of brittle rocks.

In the first stage of load application i.e. in "crack closure stage" small amplitude AE events were observed but the rates of the events were correlated with the degree of porosity and absorbability of the samples (e.g. sample No 7, Fig. 7).

The samples with large preexisting fractures (e.g. sample No 15, Fig. 6) were characterized by large maximum amplitudes from the beginning of loading.

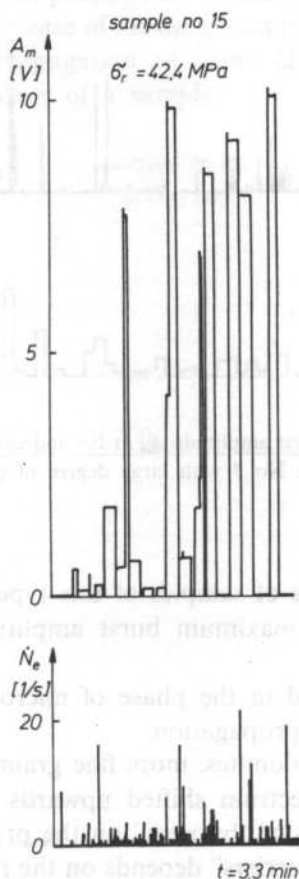


FIG. 6. The plot of AE maximum burst amplitude A_m in 10s and event rate N_e in 1s for dolomite sample No 15 with large preexisting fractures

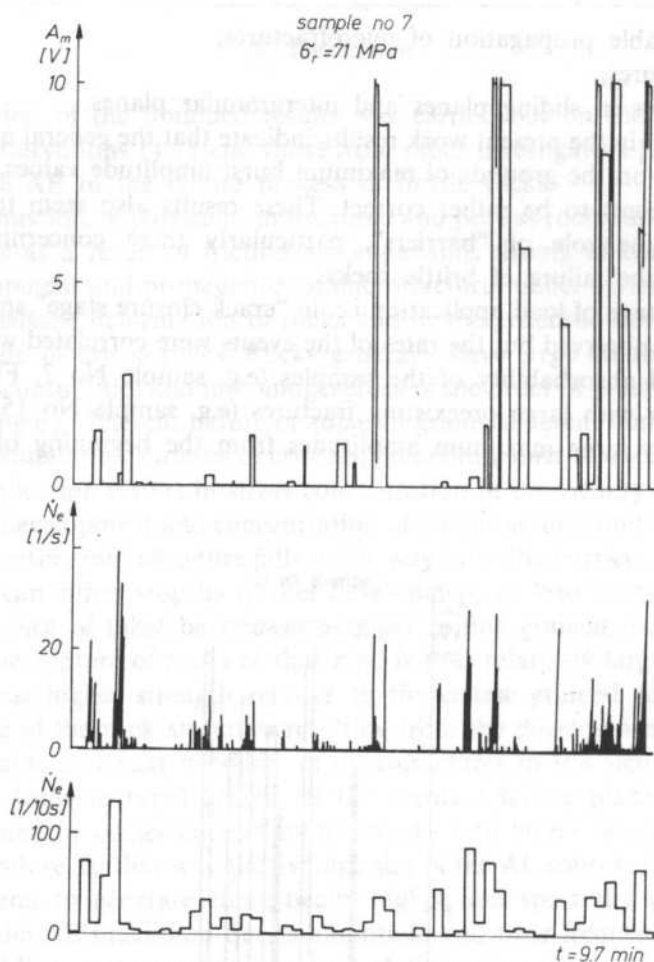


FIG. 7. The plot of AE maximum burst amplitude A_m in 10s and event rate N_e in 1s and 10s for dolomite sample No 7 with large degree of porosity

Monitoring of failure process of samples of this type and burst prediction on the grounds of the plot of AE maximum burst amplitude and event rate is rather difficult.

High amplitudes observed in the phase of microfractures seems to signal the beginning of their unstable propagation.

It has been found that dolomites, more fine grained relative to sandstones, are characterized by the AE spectrum shifted upwards and also by higher strength resulting from stronger effect of "barriers" on the propagation of fractures. It was also found that the role of "barriers" depends on the rate of loading. In case of slow loading rate they have stronger suppressing effect on fracture propagation, which

leads to the decrease of average AE source dimensions and eventually to generation of events of higher frequencies and smaller amplitudes e.g. sample No 12 (Fig. 4).

Increase of the loading rate on the other hand, leads to the generation of larger AE amplitude events, e.g. sample No 13 (Fig. 4), as a consequence of higher velocity of microfracture propagation and accompanying increase of the average AE source dimensions.

The present results indicate that brittle rocks can be divided in general into two groups i.e. rocks characterized by explosive failure and non-explosive failure (unstable type and Mogi-type) which is in support of Lord's data [4].

In samples of unstable type the increase of maximum amplitudes and also of event rate is observed only directly prior to their failure. A rather characteristic plot of maximum amplitude and event rate for this type of failure was observed in homogeneous samples of fine-grained sandstone, e.g. sample No 11p (Fig. 7). The prediction of failure in such a case was not possible. However, for the majority of dolomite and sandstone samples examined, as a result of their substantial heterogeneity, a development and stable propagation of microfractures prior to their failure is observed (Mogi-type). An increase of maximum amplitudes indicates the initiation of semi-stable or unstable propagation of some of the microfractures, i.e. the beginning of uncontrolled failure of a sample.

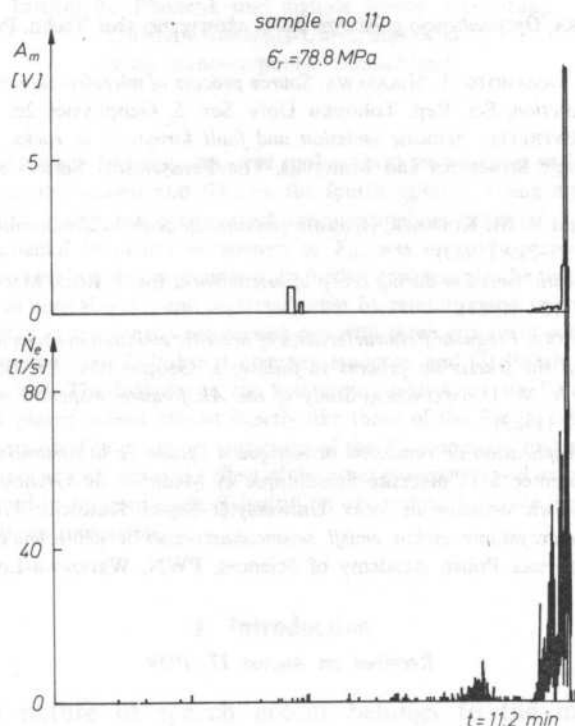


FIG. 8. The plot of AE maximum burst amplitude A_m in 10s and event rate N_e in 1s for sandstone sample No 11p, characterized by explosive failure

Statistical analysis of the results obtained shows that 50% of samples tested had AE maximum amplitude characteristic which was in a high degree similar to their characteristic of event rate. Correlation coefficient between the discussed characteristics was larger than 0.8 for each of these 50% of samples.

However, for 40% of the samples tested the prediction of failure was difficult without information contained in the maximum amplitude plot. Correlation coefficient for this part of samples was smaller than 0.5.

Prediction of failure was practically impossible for the remaining 10% of samples characterized by explosive failure (unstable type) both on the grounds of N_e and A_m .

The performed laboratory experiments seem to support the hypothesis that the AE maximum burst amplitude is not only a parameter which can be measured with the least error introduced by the equipment used or caused by sample dimensions, but firstly it is a parameter which depends significantly on the mechanism of the AE source.

The plot of AE maximum burst amplitude contains information which can be used in predicting impending failure of dolomite and sandstone in situ.

References

- [1] A. M. JAROSZEWSKA, *Optymalizacja pomiarów emisji akustycznej skal*, Techn. Poszuk. Geolog. **26**, 4-5, 25-28 (1987).
- [2] K. KUSUNOSE, K. YAMAMOTO, T. HIRASAWA, *Source process of microfracture in granite with reference to earthquake prediction*, Sci. Rep. Tohoku Univ. Ser. 5, Geophysics **26**, 3-4, 111-121 (1980).
- [3] D. LOCKNER, J. BYERLEE, *Acoustic emission and fault formation in rocks*, Proc. First. Conf. on AE/MA in Geologic Structures and Materials, The Pennsylvania State University, Trans. Tech. Publ. 1977, p. 13.
- [4] A. E. LORD, Jr and R. M. KOERNER, *Acoustic emission in geological materials*, Journal of Acoustic Emission, **2**, 3, 195-219 (1983).
- [5] M. OHNAKA, *Acoustic emission during creep of brittle rock*, Int. J. Rock Mech. Min. Sci. Geomech. Abstr. **20**, 3, 121-134 (1983).
- [6] M. OHNAKA, K. MOGI, *Frequency characteristics of acoustic emission in rocks under axial compression and its relation to the fracturing process to failure*, J. Geoph. Res., **87**, B5, 3873-3884 (1982).
- [7] M. C. REYMOND, A. M. JAROSZEWSKA, *Study of the AE frequency spectra of some rocks*, Arch. of Acoustics, **14**, 1-2 (1989).
- [8] M. THIERCELIN, *Application de l'émission acoustique à l'étude de la fissuration et de la rupture des roches*. Thèse présentée à l'Université Scientifique et Médicale de Grenoble 1980.
- [9] W. ZUBEREK, *Acoustic emission in rocks*, Uniwersytet Śląski, Katowice 1984.
- [10] W. ZUBEREK, *Wykorzystanie efektu emisji sejsmoakustycznej w geotechnice*. Publications of the Institute of Geophysics Polish Academy of Sciences, PWN, Warszawa-Lódź 1988.

Received on August 17, 1989

PERCEPTION OF POLISH ACCENT IN A RE-SYNTHESIZED SPEECH SIGNAL

W. JASSEM

Acoustic Phonetics Department, Institute of Fundamental Technological Research
Polish Academy of Sciences
(61-704 Poznań, Noskowskiego 10)

W. VAN DOMMELEN

Institut für Phonetik und digitale Sprachverarbeitung
Christian-Albrechts-Universität • Kiel
(Kiel, Bundesrepublik Deutschland)

The utterance /vidziŋeteras/ was spoken, in three versions, with the accent (I) on the first, (II) on the second and (IV) on the fourth syllable. Using a package of computer programs for speech processing which executes analysis and synthesis by linear prediction, the fundamental frequency parameter, or F_0 , was mutually exchanged among the three versions, in two listening experiments. In further experiments, the time variations of F_0 were averaged in several ways, and replaced either by random noise or by a constant F_0 value. The listening experiments were carried out with three groups of subjects, viz. (1) German University students, (2) Polish University students, and (3) Polish research workers and technical staff. The listeners in the first group, who knew no Polish, but specialized in phonetics, placed accent almost exactly like those of the Polish subjects whose reactions were systematic. The temporal variations of the F_0 parameter had a decisive effect on the perception of accent, whilst the effect of the other parameters was extremely limited when F_0 was replaced by random noise. Substitution of constant F_0 made the localization of accent almost totally impossible.

1. Introduction

The acoustical nature of speech accent belongs to the most controversial problems of contemporary experimental phonetics. An academic textbook of phonetics, still regarded as standard (LADEGOGED [9]) contains the following

definition of accent: "A stressed (i.e. accented, W. J.) syllable is pronounced with greater amount of energy than an unstressed syllable." (p. 222). In a terminological glossary in the same work, the description of accent (or stress) also relies on "extra respiratory energy during a syllable" (p. 281). Ladefoged adduces no experimental support, not even by way of a convincing illustration, for his concept of accent (or, using his term, "stress"), which — by the way — is widely accepted in linguistic circles.

Over the last thirty years or so, three general descriptions of contemporary Polish pronunciation have appeared: WIERZCHOWSKA ([16, 17, 18]). In all these works, the Polish accent (stress) is defined as "dynamic" or "expiratory", implying and increase of "force" (or vocal effort) within that part of an utterance which bears accent (WIERZCHOWSKA [16], p. 157; [17], p. 17; [18], p. 133–134). Translating this into acoustic terms, it should be expected that an accented syllable, other things being equal, would be signalled by relatively high intensity level compared with an unaccented (unstressed) syllable.

About thirty year ago, one of the present authors (JASSEM 1959, 1962), using measurements of three time-variable acoustic-phonetic parameters — fundamental frequency, intensity level envelope and segmental duration — attempted to show that the location of accent in Polish is essentially determined by the temporal variations of F_0 (not necessarily its maximum). Subsequently, JASSEM, MORTON and STEFFEN-BATÓG [8] presented the results of their experiments, performed with speech-like stimuli, which appeared to demonstrate that the F_0 parameter was decisive for the perception of accent (stress) by Polish listeners. Yet, 10 years later, DOBROGOWSKA [3] stated, on the basis of F_0 measurements, that this parameter was not unambiguously related to speech accent. The problem of the **acoustic** nature of accent (stress) thus remained open. The present investigation attacks this issue once again as it is currently especially acute in view of the needs of **speech synthesis** and computerized **recognition of the speech signal**.

A side-product of the study (not, apparently, devoid of some general interest), is the finding that in perceptual experiments in which acoustic-phonetic features are being examined, it is necessary to ensure homogeneity of subjects' responses.

2. Potential and real accent

In the phonetic literature, the traditional terms "word stress" and "sentence stress" are still very much in use. Relating as they do to a specified syllable within a word or a sentence, they are not appropriate, primarily because these two linguistic units are not phonetic entities. They belong to morphology and syntax, and therefore to a different plane of analysis and description. JASSEM and GIBBSON [7] proposed the introduction into phonetic and phonological analysis of the English terms "stress" and "accent" in a sense of essentially new (though related to Bolinger's work:

1955a, b; 1958) definitions. The notions are independent of the word and the sentence, but are associated with them — more strictly, with the word and the intonation phrase respectively. Stress was defined as the **potential location** of accent, whilst the latter as the **real** fact of a syllable standing out in some specific way. In the special case of English, certain durational relations and certain F_0 features determine accent.

In the present study we shall use the terms "stress" and "accent" as defined in JASSEM and GIBBON [7].

3. Experimental material

The utterance *widzićeteraz/* was spoken by WJ (one of the present authors) in a sound-proof studio, and tape-recorded with high-quality instruments, in three versions, varying the location of accent, which fell, in version I on the first, in version II on the second and in version IV on the fourth syllable. These phrases may correspond either to the orthographic form **Widzi cię teraz** or **Widzicie teraz**. In either case, there are two stresses: on /vi/ and /te/ or on /dzi/ and /te/.

We used a package of programmes for the analysis and synthesis of speech developed in the Institute of Phonetics and Digital Speech Processing of the University of Kiel, which are based on linear prediction and have been described in RATHJEN [13], Schäfer-Vincent 1972 and BARRY et al. [1]). The three original phrases were analyzed and processed in various ways described below, to obtain the output signals constituting our experimental material. This material was used in six experimental designs, each including a number of stimuli. Within each design, each stimulus was preceded by a brief 200 Hz beep of 100 ms duration and followed by a 4 s silent interval, this interval being later used by the listeners to make a decision as to the location of accent in the stimulus just heard. For the listeners' convenience, additional brief sinusoidal audio signals were recorded before every tenth stimulus.

Experiment 1

Three different stimuli were prepared: I_I — a re-synthesis of version I with the values of all analysis parameters unaltered, I_{II} — version I re-synthesized, with all parameters unaltered except F_0 which — after minor linear adjustments — was transplanted from version II, and I_{IV} — version I re-synthesized with all parameters unaltered except F_0 which — again after minor adjustments — was transplanted from version IV. Each of the three new stimuli: I_I , I_{II} and I_{IV} was copied 10 times to a total of 30 stimuli. Figure 1 shows the results of the LPC analysis of version I (with the first syllable accented). The phonetic parameters are: F_0 , the frequency and bandwidth of F_1 , F_2 , F_3 , F_4 , and F_5 , (the local spectrum level maxima) and time envelope of the intensity level (the LPC residue).

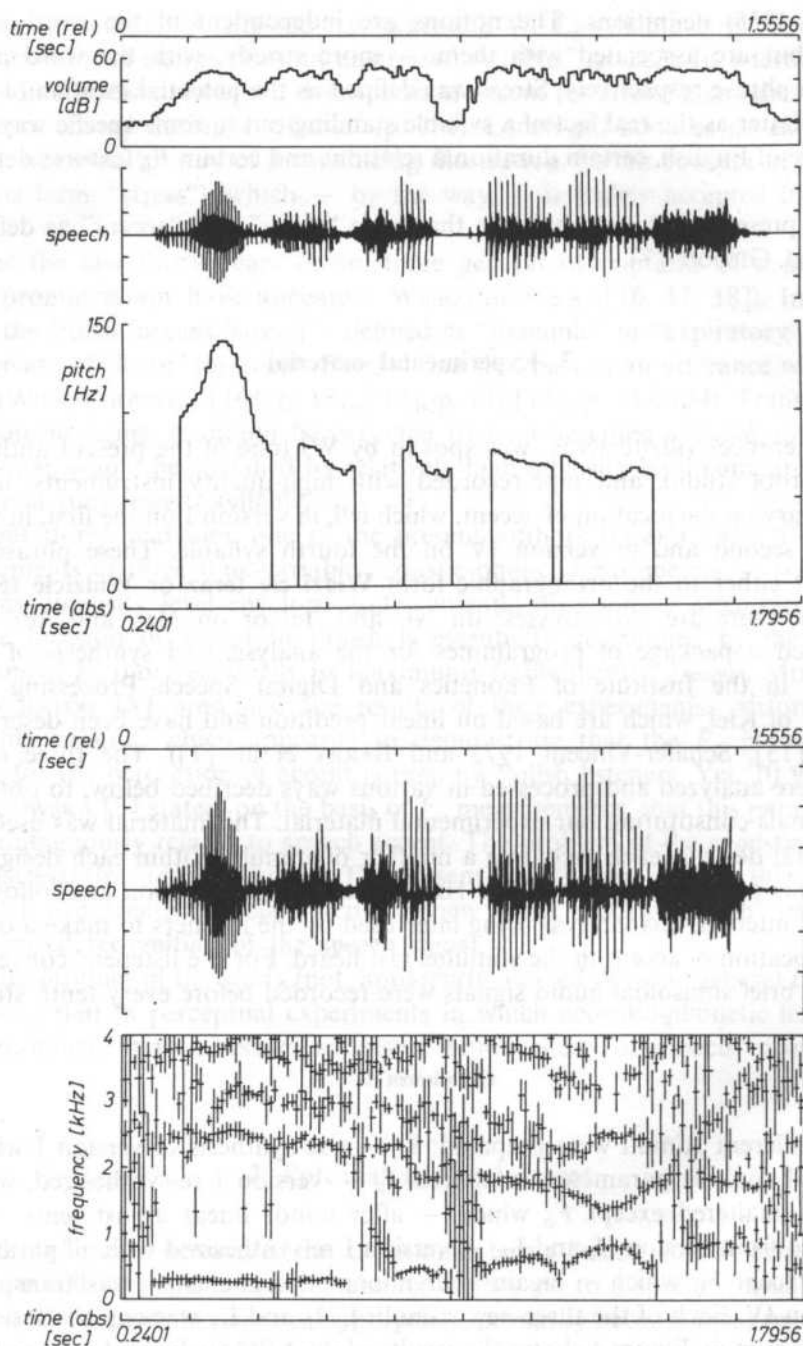


FIG. 1. The acoustic-phonetic parameters extracted by LPC from the utterance **Widzi cię teraz**

Experiment 2

In all the three original versions, the F_0 parameter was replaced by white noise. Each new stimulus was copied 10 times to a total of 30. The new stimuli were denoted as I_S , II_S , IV_S .

Experiment 3

The stimuli were here analogous to those in Experiment 1 with the addition of F_0 from utterance I and II transplanted into IV and utterances II and IV unaltered. As a result of these manipulations 9 different stimuli were obtained: I_I , I_{II} , I_{IV} ; II_I , II_{II} , II_{IV} ; IV_I , IV_{II} and IV_{IV} . Each of these was copied 10 times making up 90 stimuli in this experiment.

Experiment 4

The original versions were set in three pairs: (1) I_I and I_{II} , (2) I_I and I_{IV} , and I_{II} and I_{IV} . Within each pair, additional three intermediate versions were synthesized. These represented gradual transitions from the first to the second member of the pair with respect to F_0 . Three sets of stimuli were thus produced, each including five items: the extreme ones (e.g. I_I and I_{IV}) and three intermediate ones. Each element of each set was denoted as in the following example: I_I , $(I_I: I_{IV})_2$, $(I_I: I_{IV})_3$, $(I_I: I_{IV})_4$, I_{IV} . As before, the Roman number on the line indicated which syllable was accented in the original, the subscript Roman number refers to the transplanted syllable, and the subscript Arabic number indicates the successive graded transitions from the initial to the final item. All the remaining parameters of the original remained unaltered, whilst the intermediate F_0 values were obtained, for each successive time interval of LPC (10 ms) according to the following simple expressions:

$$F_0(I_I: I_{II})_2 = F_0 \left(I_I + \frac{1}{4} |I_I - I_{II}| \right),$$

$$F_0(I_I: I_{II})_3 = F_0 \left(I_I + \frac{1}{2} |I_I - I_{II}| \right),$$

$$F_0(I_I: I_{II})_4 = F_0 \left(I_I + \frac{3}{4} |I_I - I_{II}| \right), \text{ and analogously}$$

for $F_0(I_I: I_{IV})_{2,3,4}$ and $F_0(I_{II}: I_{IV})_{2,3,4}$.

Experiment 5

This experiment is an expansion of experiment 2, with the volume parameter from I transplanted to II, and then to IV. Each of the 5 different stimuli: I_S , II_S , IV_S , $II_{S(II)}$, $IV_{S(IV)}$ was copied 5 times resulting in a total of 25 stimuli in the experiment.

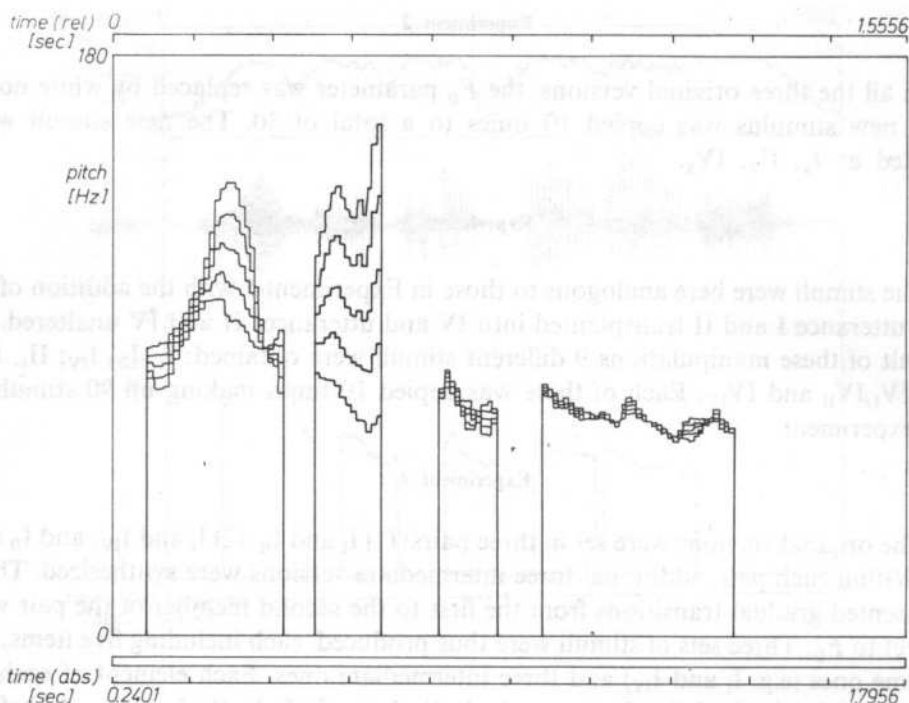


FIG. 2. F_0 in version I, I_{II} and three intermediate stimuli

Experiment 6

In all the three originals, the time-variable F_0 values were replaced by a constant $F_0 = 100$ Hz. 10 replications were produced.

Within each experiment, all final stimuli were randomized.

4. The listening test

The resynthesized experimental material described in the preceding Section was subjected to listening tests performed by three groups of subjects:

(1) Group (A) — 8 German students of phonetics at the University of Kiel. They had all had an experience of two or more years of phonetic training, but had no knowledge of the Polish language and were unfamiliar with the theory of Polish accentuation.

(2) Group (B) – 9 students of the A. Mickiewicz University of Poznań, all native Poles, specializing in various subjects, but with no knowledge of either phonetics or linguistics (apart from perhaps faint vestiges of such knowledge from primary or secondary schools).

(3) Group (C) – 10 research workers and technicians including subjects with and without previous phonetic training.

With one exception, none of the subjects in any of the three groups had any known hearing problem. The one exception belonged to Group (C). This subject had a unilateral hearing impairment, but his results did not evidently differ from those of the others in the Subgroup which was later distinguished on other evidence (the Systematic Group, see below).

The tests were carried out according to the same design in all three groups: Each subject received a set of answer sheets on which each stimulus, in each Experiment was marked by a successive number. Next to each number, there were five long horizontal dashes, each dash corresponding to one syllable, like this:

1.	_____	_____	_____	_____	_____
2.	_____	_____	_____	_____	_____
3.	_____	_____	_____	_____	_____
⋮					
40.	_____	_____	_____	_____	_____
⋮					

The listeners were asked to mark the syllable, or syllables, in each stimulus, which they heard as accented, according to the following instructions: If there is one accented syllable in a 5-syllable stimulus, mark it with a cross. If you hear two syllables as accented, you have a choice: If you hear both as being equally strongly accented, mark each of the two with a cross. If you hear one as being more strongly accented than the other, mark the former with a cross and the latter with a stroke. If you cannot make up your mind as to the location of the accent, make a random decision and mark any of the syllables (not more than just one) with a cross. The crosses were subsequently counted as primary accents, and the strokes as secondary accents.

5. Results of the tests

5.1. Homogeneity of responses

The arithmetic details of the analysis of response homogeneity are contained in Appendix A. We shall here confine ourselves to a general statement that Group (A) responded sufficiently systematically and consistently for us to regard it as

homogeneous. In Group (B), 3 subjects behaved consistently, and the others erratically in that the responses to identical stimuli within an Experiment were random. Consequently, only the former three subjects' responses were included in the subsequent statistical analysis. We would repeat here that (like the others in this Group) the three subjects had no previous phonetic training. Therefore, the drastic difference in the results should be attributed to such added psychological factors as motivation, concentration, interest, etc. In Group (C), again two subgroups could clearly be distinguished: 7 subjects behaved consistently and 3 erratically. This time, however, the first subgroup consisted of specialists — phoneticians, linguists and persons with experience with phonetic listening tests. The remaining 3 subjects did not have such qualifications.

Thus, from the original three groups, two final ones were created, *G* (German) and *P* (Polish) both homogeneous in the sense of consistency of responses. Group *P* included 10 subjects.

5.2. Statistical analysis of the consistent responses

The random variable is here the perceptual location of accent on the respective syllables. It comes in three values: primary accent denoted ***, secondary accent **, and no accent, denoted *. The distribution of the variable values has to be examined as an effect of three conditions assumed to be independent: (1) The subject's native language — two states: *G* and *P*; (2) the position of the syllable in the utterance — five states: syllable 1, ..., 5; (3) modification of the F_0 parameter in the re-synthesis: 3, 4 or 5 states, depending on the kind of modification (or transplantation) of the F_0 parameter in the individual Experiments, as described in Section 3 above.

From the point of view of conditions (1) and (2), the results of the listening tests were analyzed separately for each state. Condition (3) was treated as the independent variable and the distribution of the random variable relative to the individual states of condition (3) was tested using a modified χ^2 test for independence in contingency tables. The design of the contingency tables may be illustrated by the following examples:

Experiment 1				Experiment 1			
Group <i>G</i> /syllable 1				Group <i>G</i> /syllable 2			
	***	**	*		***	**	*
I	70	0	10	I	3	6	71
I _{II}	1	2	77	I _{II}	79	0	1
I _{IV}	6	13	61	I _{IV}	12	1	67

Experiment 1
Group G/syllable 3

	***	**	*
I	6	1	73
I _{II}	0	2	78
I _{IV}	3	3	74

Experiment 1
Group G/syllable 4

	***	**	*
I	3	6	69
I _{II}	4	11	65
I _{IV}	62	9	9

Experiment 1
Group G/syllable 5

	***	**	*
I	0	13	67
I _{II}	1	16	63
I _{IV}	0	3	77

As explained above, in the contingency tables, I_I refers to version I with unaltered parameters, I_{II} — to version I with F_0 transplanted from version II to version I and the remaining parameters unaltered, and I_{IV} — to version I with F_0 transplanted from version IV and the other parameters unaltered.

The results shown in the above contingency tables can be described as follows:

- (1) Syllable 1 is strongly biased towards *** (primary accent) under condition I_I and strongly biased towards * (no accent) under conditions I_{II} and I_{IV}.
- (2) Syllable 2 is strongly biased towards *** under condition I_{II} and towards * under conditions I_I and I_{IV}.
- (3) Syllable 3 is strongly biased towards * under all three conditions.
- (4) Syllable 4 is strongly biased towards *** under condition I_{IV} and towards * under conditions I_I and I_{II}.
- (5) Syllable 5 is strongly biased towards * under all conditions.

It follows from the above observations that syllables 1, 2 and 4 are marked by the listeners as accented (primary accent) as an effect of F_0 since the transplantation of F_0 from versions II and IV into version I, with the remaining parameters of version I unaltered resulted in the location of accent by the listeners as, respectively, in versions II and IV. Syllables 3 and 5 were perceived as unaccented no matter which of the three possible variations of F_0 the re-synthesized utterances contained.

Although the numbers in the contingency tables lead to an intuitively indubitable conclusion that the descriptions under points 1, ..., 5 above are correct, it may be interesting to define the statistical probability of the null hypothesis on the

non-dependence of the distribution of the three values of the variable under analysis on the conditions under (3) above (p. 9). Such non-dependence can be tested by using the χ^2 test. The application of this test to a full contingency table is, in its classical form, contingent on the individual cells including values not less than 8 (see, e.g., GREŃ [4]; 131) or — according to other authors — not less than 5 (see, e.g., VOLK [15]; 95). If this condition is not fulfilled, it becomes necessary, in the traditional usage, to combine classes in the contingency table, which leads to loss of information. As each of our tables above — like most the remaining ones — failed to meet the condition, a modification was introduced as described by NASS [11] and POTTHOFF & WITTINGHILL [12]. The appropriate algorithm and computer program for the modified χ^2 test was presented by DOBEK & KIELCZEWSKA [2], and the program was implemented on a computer of the JS system (Riad 32) in the Computer Centre of the Mickiewicz University in Poznań. The substance of the modified χ^2 test is presented here in Appendix B.

Experiments 1, ..., 5 were carried out with Group G, and Experiments 1, ..., 6 with Group P. For the former Group 45 contingency tables were constructed, and 48 for Group P. Each table was subjected to the modified χ^2 test. On the basis of the test values for each table, together with the corresponding value of the degrees of freedom (see Appendix B), the significance level for the rejection of the null hypothesis could be found in standard statistical tables.

In overall terms, for Group G, the null hypothesis of independence of the distribution of the random variable of the conditions (3) above, i.e., of the transformations of F_0 , was rejected, for 2 tables, on a significance level of $\alpha = 0.01$, and for 19 tables it was impossible to give reliable significance level values because the modified number of degrees of freedom was less than 1. With respect to the remaining 24 tables, the null hypothesis was rejected at the level of $\alpha = 0.001$. In the case of Group P, the null hypothesis was rejected at $\alpha = 0.01$ once. Again, for 19 tables the number of degrees of freedom was less than 1, making it impossible to define the significance level, whilst for the remaining 28 tables the null hypothesis was, in this Group, rejected at $\alpha = 0.001$.

In both Groups, almost all the tables with the number of degrees of freedom below 1 pertained to syllables 3 and 5. Those are the **unstressed** syllables (i.e. the syllables without potential accent) /tce/ and /ras/. In all three versions: I, II and IV, these syllables bore no accent. In these cases, the χ^2 test, or in fact any statistical test, is not really necessary, because the result is self-evident, as can be seen from the following typical examples:

Experiment 1

Group P/syllable 5

	***	**	*
I	0	1	99
I _{II}	0	0	100
I _{IV}	0	0	100

No comment is necessary on the dependence on condition (3) in a case like this. In other cases of syllable 3 or 5 the contingency tables were mostly as in the following example:

Experiment 2

Group *P*/syllable 5

	***	**	*
I	0	0	100
I _{II}	0	0	100
I _{IV}	0	0	100

5.3. Results of the listening tests

Experiment 1 (Fig. 3)

In Fig. 3, the horizontal axis refers to the successive syllables. The vertical axis indicates the percentage of the three possible reactions (i.e., ***, **, and *) out of a total of 80. The thick line connects the "primary accent" judgments, the thin line connects the secondary accent" judgments, while the dashed line pertains to "no accent". The three upper graphs refer to Group *G*. The successive graphs, both in the upper and the lower row, relate to I_I, I_{II} and I_{IV}. **The shift of the accent location (primary accent) from the first syllable in I_I through the second syllable in I_{II} to the fourth syllable in I_{IV} is visible quite clearly.**

Experiment 2 (Fig. 4)

Figure 4 as well as all the remaining Figures relating to the Experiments, are analogous to Fig. 3 with respect to the design and the meaning of the connecting lines. In Fig. 4, in both rows, the successive graphs refer to I_S, II_S and IV_S. The results differ as between the three levels of condition (3). There is, on the other hand, a fair similarity between the two Groups, *G* and *P*, though weaker than in Experiment 1. **The location of the accent, in this experiment, is evidently ambiguous.** For version I_S, there are two maxima at 1 and 4, for version II_S the maxima are at 2 and 4. Version IV_S exhibits a strong maximum at 4 with a weaker one at 2. Thus, **the replacement of the variable F_0 by noise (see p. 6) considerably reduces the possibility of unambiguously locating accent.**

With respect to the secondary accent, the two Groups *G* and *P* differ

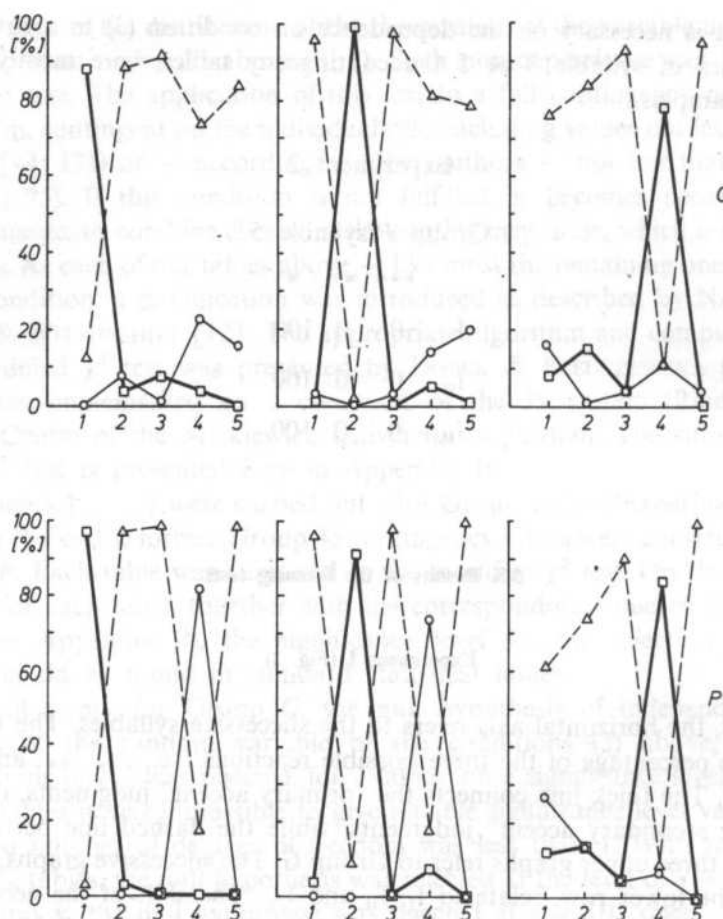


FIG. 3. Utterances I_I , I_{II} and I_{IV} . Results of the listening test in Experiment 1

considerably in Experiment 1 as well as in Experiment 2. In both Experiments the minima for primary accent (with the simultaneous maxima for no accent) lie at syllables 3 and 5.

Experiment 3 (Fig. 5)

Figure 5.1 refers to versions I_I , I_{II} and I_{IV} , Fig. 5.2 to versions II_I , II_{II} and II_{IV} , and Fig. 5.3. to versions IV_I , IV_{II} and IV_{IV} . All the three parts of Fig. 5 show very distinctly that the **location of accent is exclusively dependent on the course of F_0** , no matter whether the re-synthesized utterances were the originals (I_I , II_{II} , IV_{IV}) or had their F_0 transplanted from the other versions.

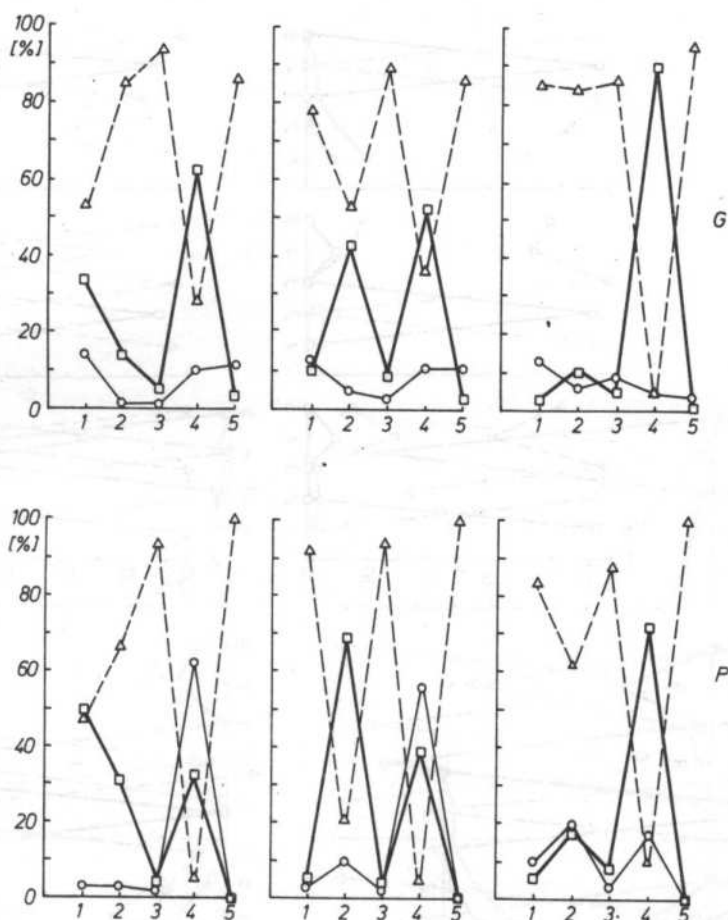
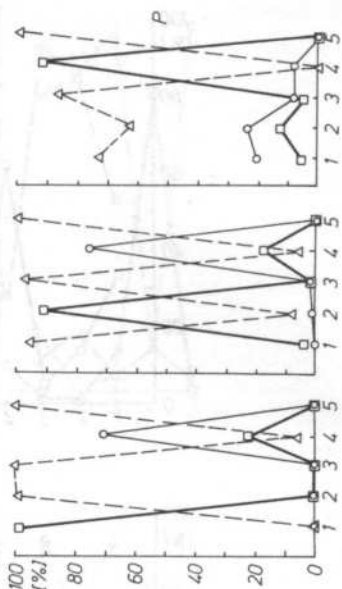
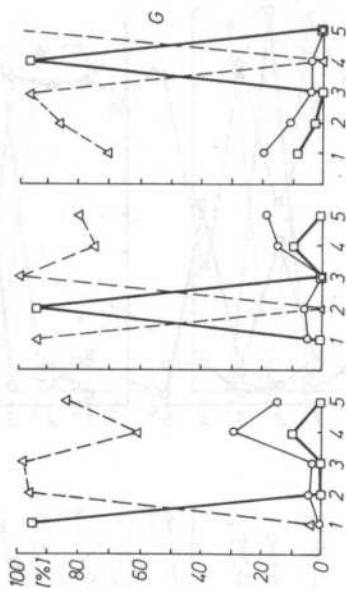
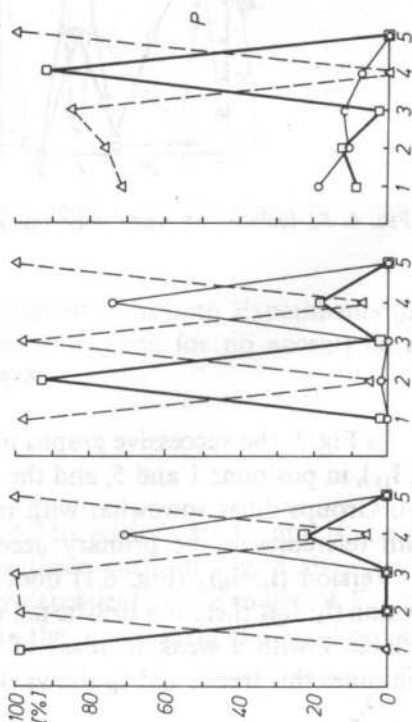
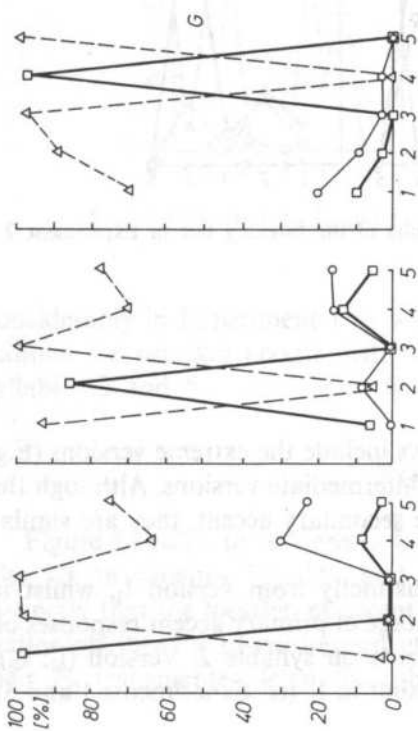


FIG. 4. F_n replaced by white noise (unmodulated). Results of the listening test in Experiment 2

Experiment 4 (Fig. 6)

In Fig. 6, the successive graphs in the two rows include the extreme versions (E.g. I_1 , I_{IV}), in positions 1 and 5, and the consecutive intermediate versions. Although the two Groups differ somewhat with respect to the secondary accent, they are similar with reference to the primary accent. Thus:

Version (I_1 : I_{II})₂ (Fig. 6.1) does not differ distinctly from version I_1 , whilst in version (I_1 : I_{II})₃ there is a drastic fall in the percentage of primary accent responses on syllable 1 with a weak increase of these judgments on syllable 2. Version (I_1 : I_{II})₄ continues this trend, and I_{II} shows the complete shift in I_{II} (cf. Experiments 1 and 3).



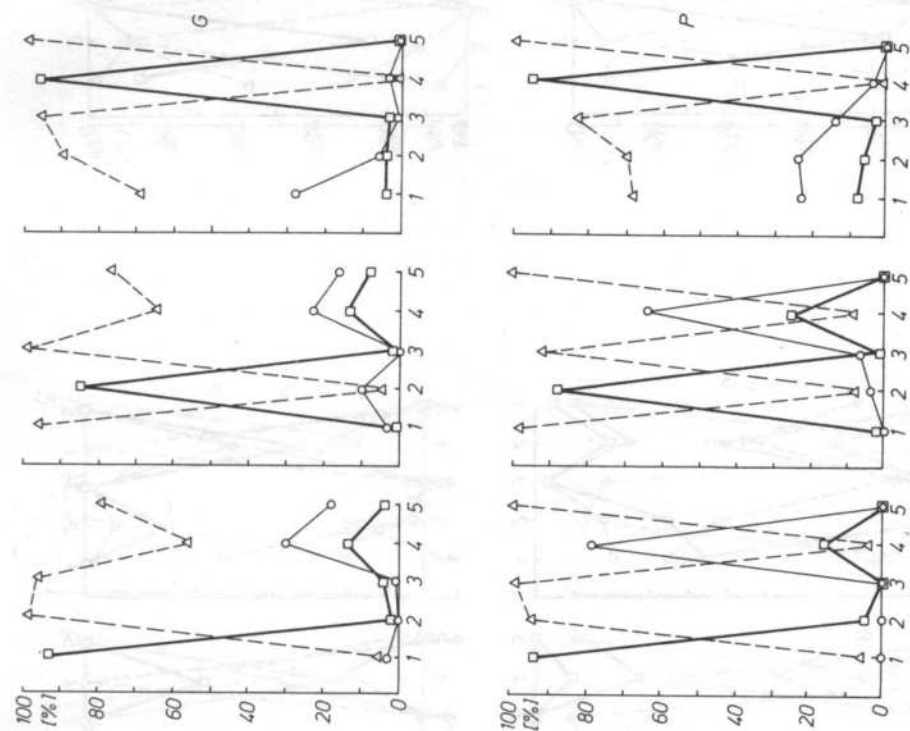
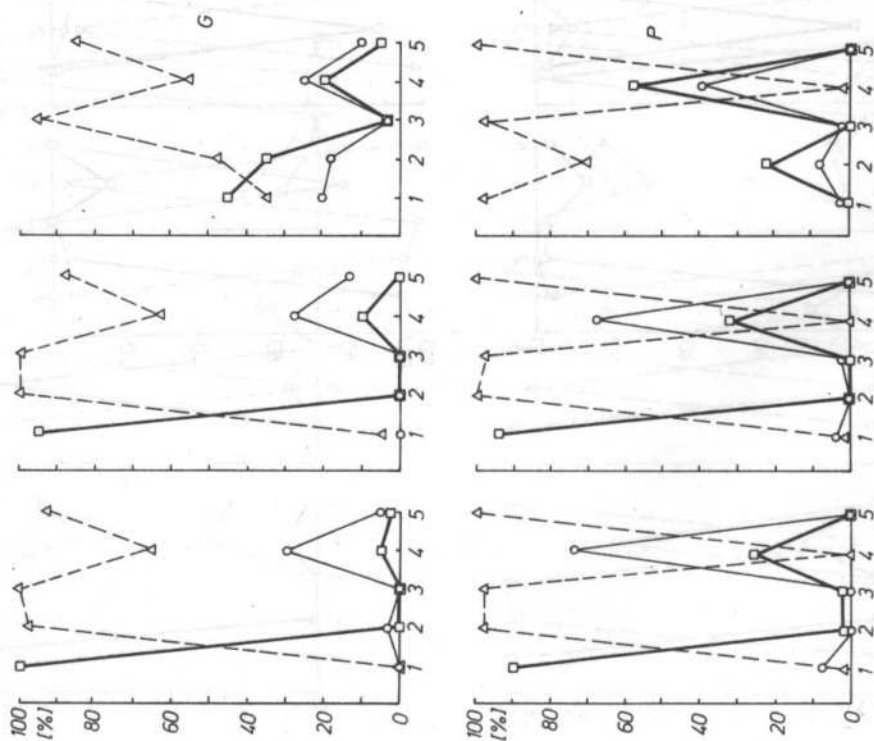
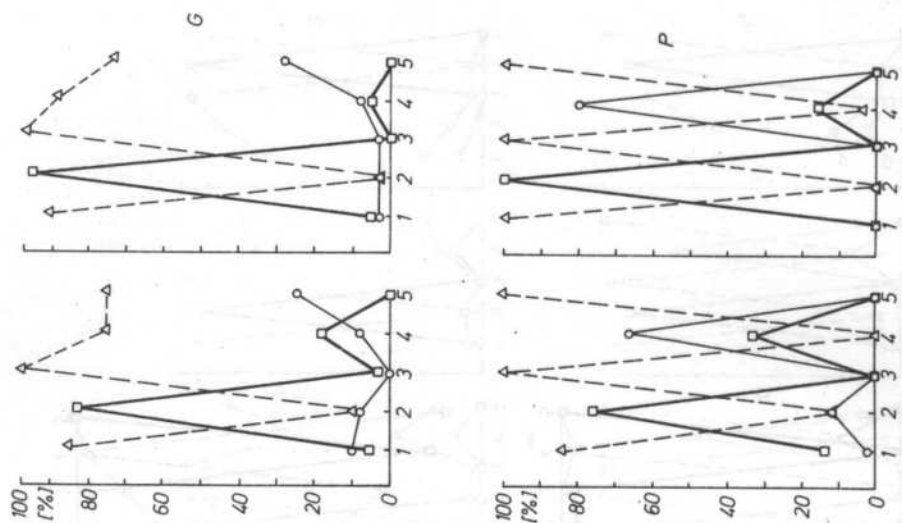
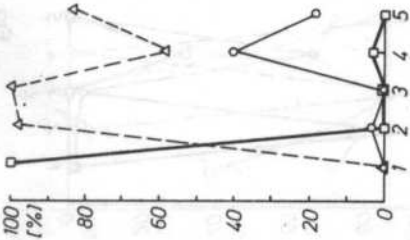
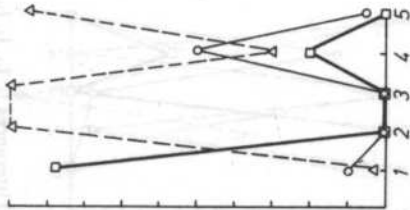
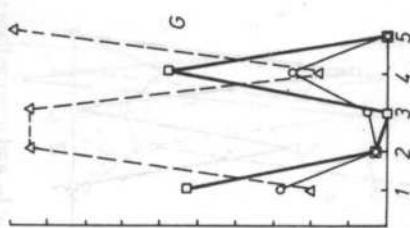
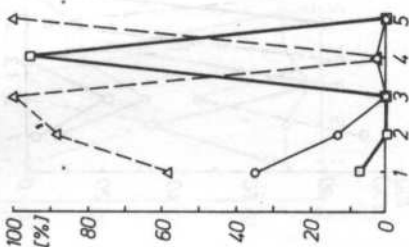
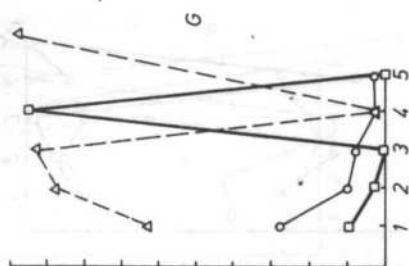
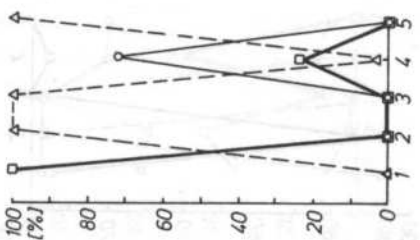
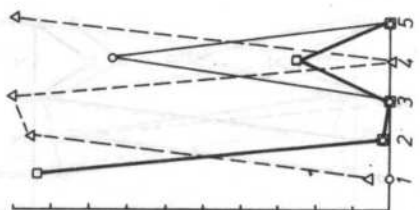
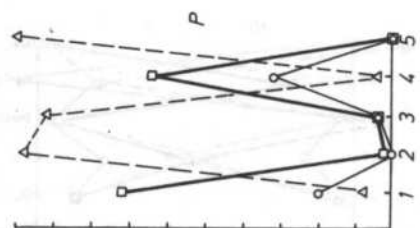
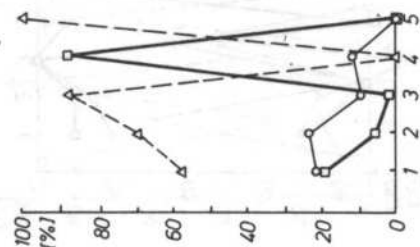
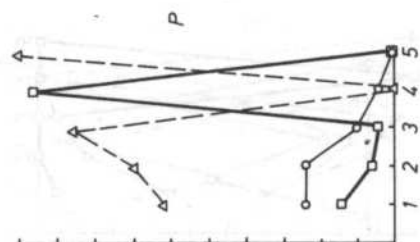


FIG. 5. Utterances I, I_{II}, I_{IV}; II, II_I, II_{II}, II_{IV}; IV, IV_I, IV_{II} and IV_{IV}. Results of the listening test in Experiment 3





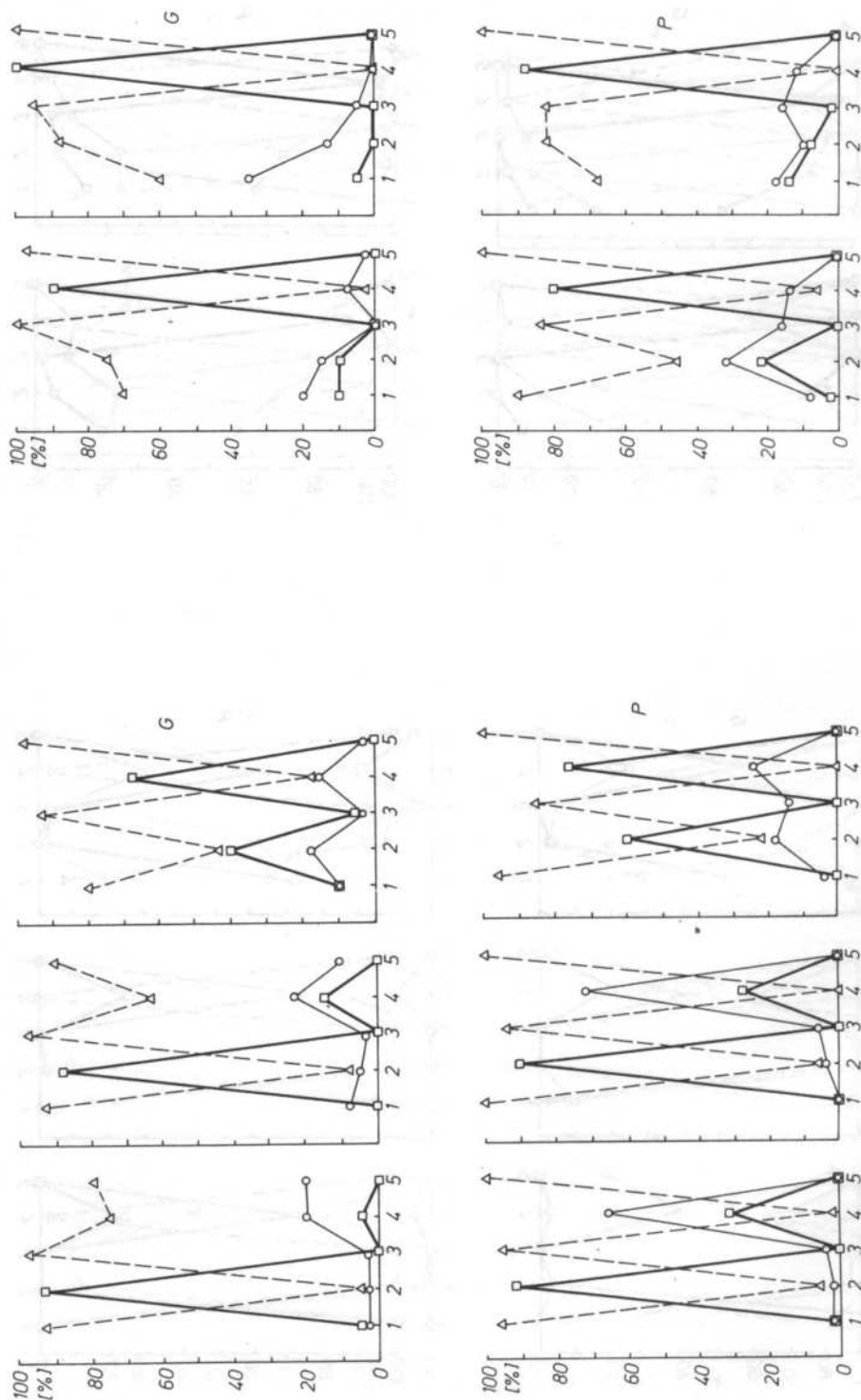


FIG. 6. Utterances I₁; I_{IV}; I_{IV}; I_{IV}; I_{IV}: Results of the listening test in Experiment 4

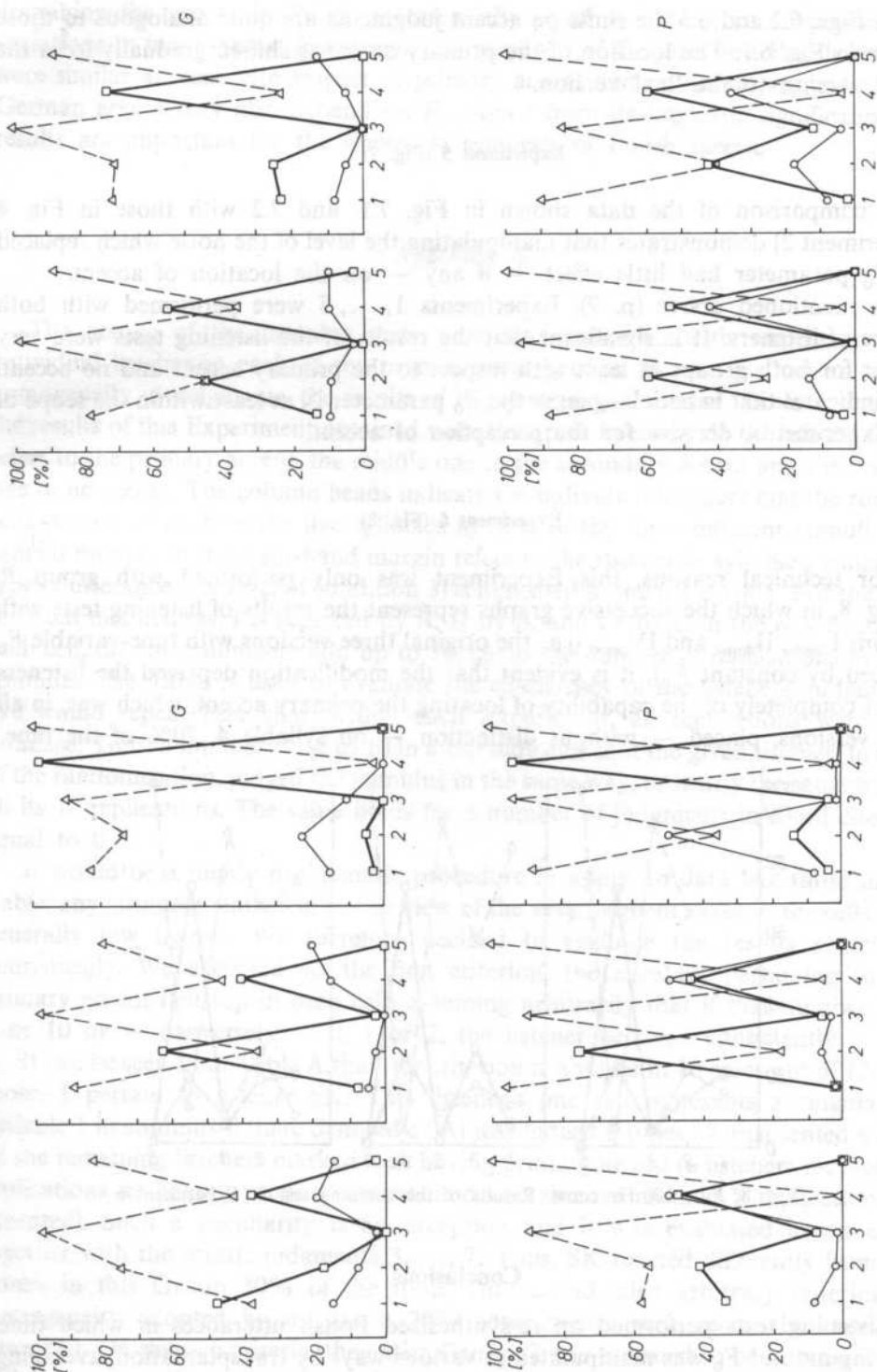


FIG. 7. F_0 replaced by noise (level-modulated). Results of the listening test in Experiment 5

In Figs. 6.2 and 6.3 the shifts on accent judgments are quite analogous to those shown in Fig. 6.1. The location of the primary accent is shifted gradually from the initial version to the final version.

Experiment 5 (Fig. 7)

A comparison of the data shown in Fig. 7.1. and 7.2 with those in Fig. 4 (Experiment 2) demonstrates that manipulating the level of the noise which replaced the F_0 parameter had little effect — if any — on the location of accent.

As mentioned above (p. 7), Experiments 1, ..., 5 were performed with both groups of listeners. It is significant that the results of the listening tests were very similar for both groups at least with respect to the primary accent and no accent. This indicates that in both languages the F_0 parameter is, at least within the scope of the Experiments, **decisive for the perception of accent.**

Experiment 6 (Fig. 8)

For technical reasons, this Experiment was only performed with group P. In Fig. 8, in which the successive graphs represent the results of listening tests with versions I_{const} , II_{const} and IV_{const} (i.e., the original three versions with time-variable F_0 replaced by constant F_0), it is evident that the modification deprived the listeners almost completely of the capability of locating the primary accent, which was, in all three versions, placed — without distinction — on syllable 4, 70% of the time.

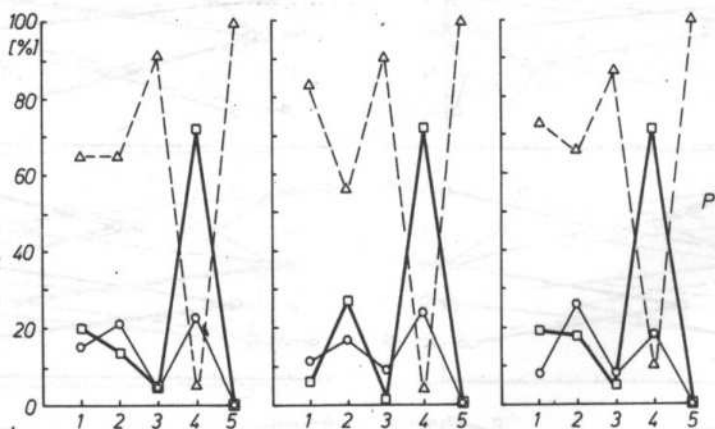


FIG. 8. $F_0 = 100$ Hz const. Results of the listening test in Experiment 6

Conclusions

Listening tests performed on re-synthesized Polish utterances in which time-varying natural F_0 was manipulated in various ways by transplantation, averaging, replacement by noise and converting to constant gave strong support to the theory

describing the accent in Polish as essentially tonal in nature, i.e., dependent on variations in fundamental frequency. The reactions of German and Polish listeners were similar at least with respect to primary accent and no accent suggesting that German accent may also depend on F_0 . Apart from its linguistic significance, the results are important for the **electronic synthesis of Polish speech**.

Appendix A

The results of the listening tests were first examined with respect to each individual listener in each of the original three groups. For an evaluation of the homogeneity of judgments, the results of Experiment 1 were used. Table A sums up the results of this Experiment obtained with Group G. In each cell, the left-top figure refers to the primary accent, the middle one to the secondary accent and the bottom one to no accent. The column heads indicate the individual listeners and the rows of cells pertain to each of the five syllables in each of the three different stimuli. The ordinal number in the right-hand margin refers to the successive syllables, whilst the type of utterance (the level of condition 3) is indicated in the left margin. For the sake of visual distinctness, I is replaced by A, II by B, and IV by C in the row heads. In each cell, the three numbers add up to 10, i.e. to the number of replications of each stimulus. The Table is used to evaluate the **consistency** of the listeners' judgments. We would repeat here that, within each Experiment, all replications were randomized. Thus, a number close to 10 in a cell indicates that the given listener, in spite of the randomization, judged the stimulus in the same way, or nearly the same way in all its 10 replications. The same holds for a number of judgments in a cell close or equal to 0.

It would be a highly problematic procedure to apply, to data like those in the Table, any stringent statistical test in view of the very frequent zeros in the cells, and generally low figures. We therefore decided to evaluate the results somewhat heuristically. We accepted, as the first criterion, the numbers pertaining to the primary accent (left-top in each cell) assuming arbitrarily that if that number is 8, 9 or 10 or — conversely — 0, 1 or 2, the listener behaved consistently.

It can be seen from Table A that our criterion is not met in 10 cases out of 120. Of those, 5 pertain to listener SK. This listener's one cell represents a singularity: Syllable 1 in stimulus I₁ (here denoted as A) was judged 8 times as unaccented whilst all the remaining listeners marked it as having primary accent (6 listeners marked all replications as having primary accent, and one listener marked 8 replications as accented). Such a peculiarity is an exception and it was evaluated as an error together with the erratic judgments 3, ..., 7. Thus, SK reacted differently from the others in this Group 30% of the time. The second, also arbitrary criterion of homogeneity adopted by us was a 70% concurrence, such as in the case just described. On the two criteria, the entire Group G was assumed to be homogeneous with respect to the reactions to the stimuli.

	BK	CR	EB	FR	HW	MT	RD	SK	
A	2 10 1 0 0 0	10 0 0 0 0 0	10 0 0 0 0 0	8 0 0 2 0 0	10 0 0 0 0 0	10 0 0 0 0 0	10 0 0 0 0 0	2 0 0 8 0 10	1
A _B	2 1 1 1 0 0	0 0 0 10 0 10	0 0 0 10 0 10	0 0 0 10 0 10	0 0 0 10 0 10	0 0 0 10 0 10	0 1 0 9 0 10	0 0 0 10 0 10	
A _C	2 0 1 2 0 0	0 0 0 8 0 10	0 3 0 7 0 7	0 3 0 7 0 7	1 1 0 8 0 8	0 1 0 9 0 9	5 3 2 2 0 10	0 0 0 10 0 10	
A	2 0 1 1 0 0	0 0 0 10 0 10	0 0 0 10 0 10	0 0 0 10 0 10	0 3 0 7 0 7	0 0 0 10 0 10	0 2 0 8 0 7	3 0 0 7 0 1	2
A _B	2 1 1 0 0 0	0 0 0 0 0 0	0 0 0 0 0 0	0 0 0 0 0 0	0 0 0 0 0 0	0 0 0 0 0 0	0 0 0 0 0 0	9 0 0 1 0 1	
A _C	2 6 1 0 0 0	0 0 0 10 0 10	2 0 0 8 0 10	0 0 0 10 0 10	2 0 0 8 0 10	0 0 0 10 0 10	0 2 0 10 0 10	0 1 0 7 0 7	
A	2 0 1 0 0 0	0 0 0 10 0 10	0 0 0 10 0 10	2 0 0 8 0 8	0 1 0 9 0 10	0 0 0 10 0 10	0 4 0 10 0 10	0 6 0 1 0 8	3
A _B	2 0 1 1 0 0	0 0 0 10 0 10	0 0 0 10 0 10	0 0 0 10 0 10	0 0 0 10 0 10	0 0 0 10 0 10	0 1 0 10 0 10	1 8 0 7 0 7	
A _C	2 2 1 0 0 0	0 0 0 10 0 10	2 0 0 8 0 10	0 0 0 10 0 10	2 0 0 8 0 10	0 0 0 10 0 10	0 3 0 10 0 10	0 7 0 7 0 7	
A	2 0 1 1 0 0	0 0 0 10 0 10	0 5 0 5 0 5	1 1 0 8 0 8	0 0 0 10 0 10	0 6 0 4 0 9	0 1 0 2 0 3	2 3 0 5 0 5	4
A _B	2 1 1 0 0 0	0 0 0 10 0 10	0 7 0 3 0 3	0 0 0 10 0 10	0 0 0 10 0 10	2 2 0 6 0 6	0 1 0 9 0 7	2 1 0 7 0 3	
A _C	2 4 1 3 0 0	10 0 0 0 0 0	8 2 0 0 0 0	10 0 0 0 0 0	7 0 0 3 0 0	10 0 0 0 0 0	6 4 0 0 0 0	7 0 0 3 0 3	
A	2 0 1 1 0 0	0 0 0 10 0 10	0 0 0 10 0 10	0 0 0 10 0 10	0 7 0 3 0 3	0 0 0 10 0 10	0 2 0 8 0 10	0 0 0 10 0 10	5
A _B	2 1 1 1 0 0	0 0 0 10 0 10	0 2 0 8 0 10	0 0 0 10 0 10	0 5 0 5 0 5	0 0 0 10 0 10	0 8 0 2 0 10	0 0 0 10 0 10	
A _C	2 0 1 1 0 0	0 0 0 10 0 10	0 1 0 9 0 10	0 0 0 10 0 10	1 1 0 8 0 10	0 0 0 10 0 10	0 0 0 10 0 10	0 0 0 10 0 10	

Table A. Reactions of the German listeners in Experiment 1

The same, informal test was applied to Group B and it was found that on the above combined criterion only 3 subjects behaved consistently, so the remaining 6 were eliminated from further analysis as being outside the homogeneous panel.

In Group C consisting of 10 subjects, 3 were eliminated on the same basis. The three subjects from Group B were then combined with the three subjects of Group C obtaining a homogeneous group of consistent respondents, and this new Group was denoted by P. As in the case of Group G (the entire panel of German students), the homogeneity test was based on Experiment 1.

As none of the Polish students (the original Group B) had any phonetic training, whilst — on the other hand — some of the subjects belonging to Group C had at least had some experience with phonetic experiments, our results permit no generalization as to the effect of such experience on the results of phonetic listening tests. But

a comparison of the results of all the three original Groups strongly suggests that such factors as motivation, concentration and other psychological conditions, which have so far received little attention in phonetic literature, may be significant.

Appendix B

The procedure applied by us here in order to analyze statistically the contingency tables does not put any constraints on the numbers in the individual cells apart from an obvious case like the one quoted above with reference to Experiment 2/Group P/syllable 5 (p. 13).

Symbolically, a contingency table may be represented as follows:

x_{11}	x_{1j}	x_{1m}	z_1
.....	
x_{i1}	x_{ij}	x_{im}	z_i
x_{n1}	x_{nj}	x_{nm}	z_n
<hr/>						
y_1		y_j		y_m		N

In the above table, x_{ij} denotes the number of observations in the i -th row and j -th column, i.e., the size of the sub-class (i, j) in a double classification with the value of z_i as a marginal sum for the i -th row and y_j as the marginal sum for the j -th column. The probability of the sub-class (i, j) is defined by the corresponding marginal sums and the grand sum N .

The null hypothesis on the independence of the features may be written as follows:

$$H_0: = p_i p_j \quad \text{for} \quad i = 1, 2, \dots, n \quad \text{and} \quad j = 1, 2, \dots, m.$$

The classical test of this hypothesis is based on the statistic

$$G = N \sum_{i=1}^n \sum_{j=1}^m x_{ij}^2 / (y_j z_i) - 1,$$

where

$$N = \sum_{i=1}^n \sum_{j=1}^m x_{ij}, \quad y_j = \sum_{i=1}^n x_{ij}, \quad z_i = \sum_{j=1}^m x_{ij}.$$

If the null hypothesis is true, then the statistic G has a distribution which is approximately that of χ^2 with $v = (n-1)(m-1)$ degrees of freedom.

If the numbers in the individual cells are small, failing to meet the classical condition (see above p. 12), the test is subject to modification. The G statistic is

replaced by the G_1 statistics:

$$G_1 = cG, \quad \text{where}$$

$$c = 2E(G)/\text{Var}(G),$$

where $E(G)$ is the expected value of G and $\text{Var}(G)$ is the variance of the statistic G . The calculation of the value of the G_1 statistic is somewhat complex. The appropriate numerical methods are presented in DOBEK & KIELCZEWSKA ([2]). The procedure calculates the modified χ^2 value as well as the modified value of the number of degrees of freedom:

$$v_1 = c(m-1)(n-1)/(N-1).$$

References

- [1] W. J. BARRY, W. van DOMMELEN, H. JANSSEN, K. J. KOHLER, K. SCHÄFER W. THON, G. TIMMERMAN, *Phonetic data processing*, Kiel University, Arbeitsberichte Nr. 18, Inst. f. Phonetik 1982.
- [2] A. DOBEK, H. KIELCZEWSKA, *Testing independence and homogeneity of samples for small expected frequencies* (in Polish). *Algorytmy biometryczne i statystyczne*, 6, 163–174 1979.
- [3] K. DOBROGOWSKA, *Investigation of the relations between accent and intonation in unemotional speech* (in Polish). *Lingua Posnaniensis* 21, 65–75 (1978).
- [4] J. GREŃ, *Mathematical statistics, models and exercises 4th ed* (in Polish) PWN, Warszawa 1974.
- [5] W. JASSEM, *The phonology of Polish stress*, 15, 252–269 (1964).
- [6] W. JASSEM, *The accent in Polish* (in Polish) *Prace Językoznawcze* No. 31, Komitet językoznawstwa PAN, 1962.
- [7] W. JASSEM, D. GIBBON, *Re-defining English accent and stress*, *Journal of the International Phonetic Association* 10, 2–16 (1980).
- [8] W. JASSEM, J. MORTON, M. STEFFEN-BATOGOWA, *The perception of stress in speech-like stimuli by Polish listeners*, in: *Speech analysis and synthesis* ed. W. Jassem PWN, Warszawa 1968 vol. 1 pp. 289–308.
- [9] P. LADEFOGED, *A course in phonetics*, Harcourt, Brace, Jovanovich Inc., New York 1975.
- [10] O. LANCASTER, *The chi-squared distribution*, Wiley and Sons, New York 1969.
- [11] C. A. D. NASS, *The χ^2 Test for small expectations in contingency tables with special reference to accident and absenteeism*, *Biometrika* 46, 365–385 (1959).
- [12] F. POTTHOFF, M. WITTINGHALL, *Testing for homogeneity. The binomial and multinomial*, *Biometrika* 53, 167–182 (1966).
- [13] G. RATHJEN, *Numerische und experimentelle Methoden der lineären Prädiktion zur Datenreduktion von Sprachsignalen* Arbeitsberichte Nr 11, Inst. f. Phonetik, Kiel 1979, 3–133.
- [14] K. SCHÄFER, *Concepts in the SSP Programme*, Arbeitsberichte Nr. 18, Inst. f. Phonetik, Kiel 1982, 11–126.
- [15] W. VOLK, *Mathematical statistics for engineers*, (in Polish) Wyd. Nauk.-Techn, Warszawa 1965.
- [16] B. WIERZCHOWSKA, *Polish pronunciation* (in Polish) Państw. Zakł. Wyd. Szkol. Warszawa 1965.
- [17] B. WIERZCHOWSKA, *A phonetic description of Polish* (in Polish) PWN, Warszawa 1987.
- [18] B. WIERZCHOWSKA, *The phonetics and phonology of Polish* (in Polish), Zakł. Nar. im. Ossolińskich, Wrocław 1980.

ULTRASONIC STUDIES OF THE HYDRATION OF AMINO ACIDS AND OLIGOPEPTIDES

A. JUSZKIEWICZ

Faculty of Chemistry, Jagiellonian University
(30-060 Kraków, ul. Karasia 3)

Hydration number of selected amino acids, their hydrochlorides and their oligopeptides with glycine were determined by the ultrasonic method. Assuming additivity of contributions of ionic and non-ionic groups to the total hydration of the studied substances, the hydration numbers of the free amino acids were calculated. The results obtained are interpreted on the basis of the pseudocrystalline model of water structure.

1. Introduction

In the model of interactions of biologically active substances such as amino acids, peptides and proteins, hydration numbers of these substances are of fundamental importance. In the previous paper [1] the hydration numbers of selected water-soluble amino acids and peptides were presented. This paper is an extension of this study into amino acids slightly soluble in water. In order to evaluate the hydration numbers of these amino acids the hydration numbers of their hydrochlorides and their dipeptides with glycine were determined first. Both the hydrochlorides and dipeptides are soluble in water. Assuming additivity of contributions of ionic and non-ionic groups to the total hydration of a given compound, the hydration number of the free amino acid can be calculated. The ultrasonic method of hydration number determination consists in determination of the maximum of the parabola-like dependency of ultrasonic velocity on ethanol concentration in both water-ethanol and water-ethanol-cosolvent systems [2, 3]. Introduction of a third component to a water-ethanol solution leads to a shift of this maximum. The value, n_p , of this shift (expressed in moles of H_2O per mole of solute) is a measure of hydration and is described by the following formula:

$$n_t = \frac{1000(m_0 - m_1)}{m_0 m_s m_w} \quad (1)$$

where: m_0 and m_1 are the molal concentrations (mole $\text{kg}^{-1} \text{H}_2\text{O}$) of ethanol at the maxima of ultrasonic velocity in binary and ternary systems, respectively; m_s is the molal concentration of the solute; M_w is the molecular weight of water. With use of the above method the hydration numbers of the following substances were determined: carboxylic acids, amino acids and peptides [1], 1-1 and 2-1 electrolytes [4-6], non-electrolytes [7-9], sugars and their derivatives [10, 11], nucleosides [12], nucleotides and nucleic acids [13, 14], and macromolecules [15, 16].

For some of the above listed substances the measurements were performed not only in aqueous ethanolic solutions but also in solutions of other cosolvents such as propanol, acetone, dioxane, tetrahydrofuran, dimethylformamide and dimethylsulphoxide [6-8]. In the case of substances slightly soluble in water, the above method gives results with a high error, because the shifts of maximum velocities are usually small, often lying within the experimental error. The proposed procedure of determination of hydration numbers of amino acids slightly soluble in water through measurements in solutions of their derivatives is an attempt to eliminate this limitation.

2. Experimental

The examined amino acids and oligopeptides were from Sigma (USA). Hydrochlorides of the amino acids were obtained through the reaction of these amino acids with 1 M HCl. Triply distilled water and 99.8% ethanol, analytically pure (POCH, Gliwice) were used. The measurements of ultrasonic velocity were carried out at $25 \pm 0.01^\circ\text{C}$ with use of "sing around" gauge. The details of the experimental procedure were described previously [10, 17]. The obtained results are listed in Tables 1-3. These results are mean of 4-6 measurements. For comparison the hydration numbers of amino acids and peptides obtained previously [1] are also included in the Tables.

Table 1. Hydration numbers of amino acids determined in aqueous-ethanolic solutions at 20°C

Compound	$n_{25^\circ\text{C}}$	n^0
Glycine ^(a)	5.7 ± 0.2	3.9
α -alanine ^(a)	7.8 ± 0.2	6.0
DL- α -amino butyric acid ^(a)	9.9 ± 0.4	8.1
DL-valine ^(a)	13.6 ± 0.6	11.8
DL-lysine ^(a)	12.8 ± 0.6	11.0
DL-proline ^(a)	7.9 ± 0.4	6.0
DL- β -phenylalanine	14.1 ± 1.0	12.3
DL-serine	6.9 ± 1.0	5.1
D- β -asparagine	4.3 ± 1.0	2.5
DL-ornithine	11.0 ± 1.0	9.2
L-arginine	6.9 ± 1.0	5.1

^(a) — Ref. [1]

Table 2. Hydration numbers of amino acids monohydrochlorides in aqueous-ethanolic solutions at 25°C

Compound	$n_{25^{\circ}\text{C}}$	n^0
L-arginine monohydrochloride	8.6 ± 1	6.8
DL-ornithine monohydrochloride	12.2 ± 1	10.4
L-lysine monohydrochloride	13.6 ± 1	11.8
DL- β -phenylalanine monohydrochloride	15.5 ± 1	13.7
L-leucine monohydrochloride	17.2 ± 1	15.4
D- β -asparagine monohydrochloride	5.4 ± 1	3.6
DL-tryptophan monohydrochloride	11.2 ± 1	9.4
DL-methionine monohydrochloride	11.7 ± 1	9.9
L-histidine monohydrochloride	6.5 ± 1	4.7
L-iso-leucine monohydrochloride	15.4 ± 1	13.6

Table 3. Hydration numbers of oligopeptides determined in aqueous-ethanolic solutions at 25°C

Compound	$n_{25^{\circ}\text{C}}$	n^0
Diglycine ^(a)	8.9 ± 0.5	7.1
triglycine ^(a)	12.8 ± 1.0	11.0
glycyl-L- α alanine ^(a)	11.0 ± 0.5	9.2
glycyl-DL- α -alanyl glycine ^(a)	13.5 ± 1.0	11.7
L-alanylglycine ^(a)	10.8 ± 0.5	9.0
DL-alanyl-DL-alanine ^(a)	12.8 ± 0.5	11.0
glycyl-L-proline ^(a)	10.7 ± 0.5	8.9
glycyl-L-valine ^(a)	17.6 ± 1.0	15.8
glycyl-L-leucine	20.0 ± 1.5	18.2
DL-leucylglycine	20.0 ± 1.5	18.2
D-leucylglycylglycine	25.0 ± 1.0	23.2
glycyl-L-asparagine	6.8 ± 1.0	5.0
glycyl-L-methionine	14.0 ± 1.5	12.2
glycyl-L-tyrosine	11.0 ± 1.0	9.2

^(a) — Ref. [1]

3. Results and discussion

The values of n^0 corresponding to hydration numbers at 0°C are listed in Tables 1–3. These values were obtained on the assumption that the temperature dependence of the hydration numbers n_i of the studied amino acids, their hydrochlorides and their oligopeptides with glycine is of the same type as that obtained previously for simple amino acids and peptides [1], 1–1 electrolytes [4, 5], sugars [10, 11],

non-electrolytes [7, 8] and macromolecules [15, 16]:

$$n_t = n^0 + At + Bt^2, \quad (2)$$

where: A and B are coefficients equal to $0.0383 \text{ mole } ^\circ\text{C}^{-1}$ and $0.0013 \text{ mole } ^\circ\text{C}^{-2}$, respectively; t is temperature in $^\circ\text{C}$. Assuming that at 0°C all water molecules are fixed in the pseudocrystalline, ice-like water structure, the value of n^0 can be interpreted as a number of water molecules of the ice-like net which constitute the closest vicinity of a solute molecule. The remaining fragment of eq. (2) $At + Bt^2$ is dependent on the properties of water irrespective of the type of solute and determines the population of "free" water at different temperatures. At 25°C $At + Bt^2 = 1.8$. By subtracting this value from experimental results n_t at 25°C the values of n^0 were obtained. The values of this parameter were calculated for the free amino acids which in the study were used in the form of hydrochlorides and oligopeptides with glycine. For this calculation it was assumed that n^0 is an additive function of contributions of ionic and non-ionic groups of these substances. In the case of the hydrochlorides the hydration number of Cl^- , n_{Cl}^0 — obtained previously from the study of hydration of 1-1 electrolytes [5, 4] was used, and it was assumed that hydration within the pairs

Table 4. Hydration numbers n^0 of amino acids obtained from direct measurements and calculated from measurements of hydration numbers of hydrochlorides of amino acids and oligopeptides of amino acids with glycine

	Values obtained from direct measurements	Values calculated	
		from measurements in hydrochlorides of amino acids under assumption $n_{\text{Cl}}^0 = 2$	from measurements in oligopeptides of amino acids with glycine under assumption $n_{\text{glyc}}^0 = 3$
	n^0	n_c^0	n_p^0
glycine	3.9		4.0
α -alanine	6.0		6.0
DL-proline	6.0		5.9
DL-valine	11.8		12.8
L-arginine	5.1	4.8	
D- β -asparagine	2.5	1.6	2.0
DL-ornithine	9.2	8.4	
DL-lysine	11.0	10.0	
DL-phenylalanine	12.3	11.7	
L-leucine		13.4	15-16
L-isoleucine		11.6	
DL-serine	5.1		
DL-methionine		7.9	9.2
DL-tryptophan		7.4	
L-histidine		2.7	
L-tyrosine			6.2

of groups $-\text{NH}_3^+ - -\text{NH}_2$ and $-\text{COO}^-$, $-\text{COOH}$ is of the same order. In the case of the dipeptides of the amino acids with glycine it was assumed that hydration of glycine group in all dipeptides is the same as that of glycine group in diglycine. For diglycine $n^0 = 7$ and for glycine $n^0 = 4$. Therefore it can be assumed that 3 water molecules correspond to glycine group in a dipeptide i.e. $n_{\text{glyc.}}^0 = 3$. Correctness of this assumption was confirmed by the results obtained for glycylalanine, alanyl-glycine and glycylproline for which the values of n^0 obtained this way for alanine and proline are in agreement with the values of n^0 obtained directly for these amino acids in free state. The results of the performed measurements are listed in Table 4. It follows from these results that the values of hydration numbers n^0 calculated by the proposed method for the other amino acids under study are in agreement with each other within the experimental error. Therefore it seems that the proposed method is a useful way of determination of hydration numbers of amino acids slightly soluble in water, for which other methods fail.

This study was partially supported by the Polish Academy of Sciences (programme CPBP 02.03.)

References

- [1] A. JUSZKIEWICZ, *Ultrasonic studies on hydration of carboxylic acids, aminoacids and peptides in aqueous ethanolic solutions*, Arch. of Acoust., **10**, 151–160 (1985).
- [2] T. YASUNAGA, Y. HIRATA, Y. KAWANO, M. MIURA, *Ultrasonic studies of the hydration of various compounds in an ethanol-water mixed solvent. Hydration of inorganic compounds*, Bull. Chem. Soc. Japan **37**, 867–871 (1964).
- [3] T. YASUNAGA, I. USUI, K. IWATA, M. MIURA, *Ultrasonic studies of the hydration of various compounds in an ethanol-water mixed solvent. II. The hydration of organic compounds*, Bull. Chem. Soc. Japan, **37**, 1658–1660 (1964).
- [4] A. JUSZKIEWICZ, *Hydration numbers of electrolytes determined by the ultrasonic method*, Pol. J. Chem., **58**, 1115–1123 (1984).
- [5] A. JUSZKIEWICZ, *Ultrasonic studies on hydration of tetraalkylammonium halides in aqueous ethanolic solutions*, Pol. J. Chem., **59**, 1209–1215 (1985).
- [6] A. JUSZKIEWICZ, *Ultrasonic study on hydration of 2–1 electrolytes*, Pol. J. Chem., **62**, 495–501 (1988).
- [7] A. JUSZKIEWICZ, *Study on hydration of urea and amides by use of the ultrasonic method*, Zeit. Phys. Chem. N. F., **158**, 87–98 (1988).
- [8] A. JUSZKIEWICZ, *Ultrasonic studies on hydration of non-electrolytes*, Ultrasonics, **27**, 131–139 (1989).
- [9] A. JUSZKIEWICZ, *Molal volume and compressibility in non-electrolyte aqueous solutions*, Arch. of Acoust., in press.
- [10] A. JUSZKIEWICZ, *Ultrasonic velocity measurements of hydration numbers of sugars in alcohol-water solutions*, Arch. of Acoust., **6**, 307–319 (1981).
- [11] A. JUSZKIEWICZ, J. ANTOSIEWICZ, *Ultrasonic velocity studies on carbohydrates in aqueous ethanolic solutions*, Zeit. Phys. Chem. N. F., **148**, 185–195 (1986).
- [12] J. ANTOSIEWICZ, A. JUSZKIEWICZ, D. SHUGAR, *Ultrasonic studies on hydration of pyrimidine nucleosides in aqueous ethanolic solutions*, J. Phys. Chem., **86**, 4831–4834 (1982).

- [13] A. JUSZKIEWICZ, *Determination of the hydration of DNA and its subunits: nucleosides and nucleotides using acoustical method*, *Akustyka molekularna i kwantowa*, **3**, 37–43 (1982).
- [14] A. JUSZKIEWICZ, *Hydration of nucleic acids and nucleotides in aqueous ethanolic solutions determined by ultrasonic method*, *Archives of Acoust.*, **11**, 89–96 (1986).
- [15] A. JUSZKIEWICZ, J. POTACZEK, *Investigations of the hydration of dextran using an acoustic method*, *Arch. of Acoust.*, **6**, 401–408 (1981).
- [16] A. JUSZKIEWICZ, *Hydration of ions, molecules and macromolecules in aqueous ethanolic solutions*, *IFTR Reports*, 31/1985.
- [17] A. JUSZKIEWICZ, J. RANACHOWSKI, *Ultraschallmessungen zur Untersuchung verschiedener physikalisch-chemischer Prozesse in Flüssigkeiten und Lösungen*, *Wiss. Zeit. TH Leuna-Merseburg*, **24**, 275–286 (1982).

Received on August 14, 1989

DIGITAL VELOCITY PROFILE ESTIMATOR OF BLOOD FLOW IN THE HEART AND LARGE BLOOD VESSELS

P. KARŁOWICZ, J. LIWSKI, M. PIECHOCKI, W. SECOMSKI, A. NOWICKI

Institute of Fundamental Technological Research of the Polish Academy of Sciences
(00-049 Warszawa, ul. Świętokrzyska 21)

The paper discusses principles of a digital multigate system for Doppler frequency measurements. The conception of a system with serial data processing, based on the Doppler frequency measurement with the "zero crossing" method, is described. Problems with the recognition of the direction of flow in the digital system are presented, as well as two solutions, tested in practice, which limit occurring measuring errors. An example of an actual flow measurement made with the application of a model of the presented device is described, and possible errors resulting from the "zero crossing" technique are given. In order to improve properties of the system the use of a digital low-pass filter is proposed. The conception of such a filter is described.

W artykule omówiono podstawy cyfrowego systemu wielobramkowego pomiaru częstotliwości dopplerowskiej. Opisano koncepcje układu z przetwarzaniem szeregowym opartego o pomiar częstotliwości dopplerowskiej metodą „zero crossing”. Przedstawiono problemy z rozpoznawaniem kierunku przepływu w systemie cyfrowym oraz dwa praktyczne wypróbowane rozwiązania pozwalające ograniczyć występujące błędy pomiaru. Pokazano przykład pomiaru rzeczywistego przepływu z wykorzystaniem modelu opisywanego urządzenia oraz mogące występować błędy wynikające z techniki „zero crossing”. Zaproponowano zastosowanie cyfrowego filtra dolnoprzepustowego do polepszenia własności układu i opisano koncepcje takiego filtra.

1. Introduction

As in many other fields, the development of ultrasonic Doppler apparatus is related with the widespread of digital technique application. It makes possible the construction of multigate systems and construction apparatus for colour flow visualization, i.e. colour Doppler on their basis.

The simultaneous measurement of blood flow velocity at many different depths (at different distances from the ultrasonic probe is called a multigate system [1]. In a traditional pulse flowmeter the receiver's gate is switched with certain delay after every pulse of the transmitter. This is a cyclic process and the received signal is used

to determine the Doppler frequency. If we would accept such a receiving system as a single channel and would build several such channels for which the gate of the receiver is switched on with different delays in relation too the transmitter, then we would obtain a multichannel system. Results of a multichannel measurements of Doppler frequency can be presented in terms of depth in the patient's body as a so-called velocity profile, or it can undergo further processing. Information processing in every gate takes place at different time intervals, so the process of Doppler frequency measurement can be performed by one measuring system. The system functions in cycles repeated for all successive gates. Such a system is called a system with serial processing [2]. If we accept a rather general assumption that the range of investigated depths is of about 10 cm and resolution in depth (thickness of a layer in which a measurement in one gate is performed) is of the order of 1 mm, then we reach the number of 100 necessary gates (channels) with opening time of each for average velocity of an ultrasonic wave in a human body (1540 m/s) of approximately 1.5 μ s. Only digital technique makes the realization of such a system possible, because it makes it possible to process signals in one system not only for successive value in one gate, but also values from other gates which can be considered as absolutely independent. A digital solution also ensures the identity of all channels as well as small dimensions of the device.

2. Multichannel system with serial processing

Ultrasonic signals are reflected in a human body from boundaries of tissues with different acoustic impedance and are scattered on blood particles. Signals reflected from motionless or slow moving structures can be more than a hundred times larger from signals dissipated in blood. These last signals contain a Doppler information about flow velocity. Hence, to fish out the information about the flow we either need a signal's path with very high dynamics prevent small components from the flow distortion of, or the method of elimination of stationary echoes has to be applied. This second solution is much better from the first one — it significantly simplifies the further part of the path of the signal, because processing of signals with low dynamics decrease the essential number of bits of signal's digital representation. Therefore, the elimination of constant echoes is practically an essential element of a multigate system.

We can come across two fundamental types of eliminators: digital and analogue [3, 4]. Digital systems require very fast elements including big (e.g. 12 bit) a/d converters — expensive and attainable with difficulty (embargo). An analogue suppression stationary echoes canceller (SEC) system was previously developed in the Department of Ultrasonics and it is applied in the UDP-30-TES flowmeter, produced by Experimental Department "Venpan". A version of a pulse Doppler flowmeter, equipped with a SEC system, for heart examinations was created in the Department of Ultrasonics during the last five years. This flowmeter will be used as

an analogue block (flowmeter system and constant echo eliminator system included, Fig. 1) of the developed apparatus for colour flow visualization. At this stage it is advisable to base the multigate system on an analogue eliminator of constant echoes. After the signals from the receiving unit pass through demodulation and through the eliminator, they have to be changed into digital form. Then the Doppler frequency in

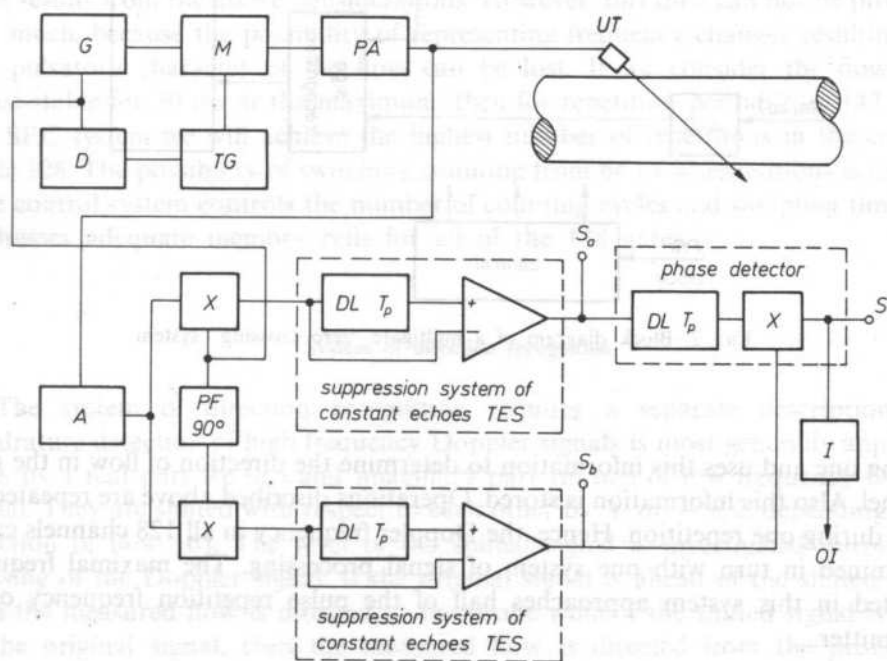


FIG. 1. Block diagram of the SEC system

individual gates has to be determined in the multigate system. The method of counting the number of crossings through zero "zerocrossing" [5] is the method of determining frequency most generally applied in classical Doppler flowmeters. In the "zerocrossing" method the detected frequency is defined by the number of crossings of the signal through the zero level, counted in a definite period of time. Figure 2 presents a general block diagram of a zerocrossing system adapted to a multigate system.

Doppler signals in a quadrature (shifted with respect to each other by $+\pi/2$ or $-\pi/2$, depending on the direction of flow) are changed into digital form. One of them is delayed by the pulse repetition time of the transmitter T_p . The so obtained value S_1 is compared by the system of detection of crossings through zero with the actual, not delayed value S_2 (Fig. 2). If a crossing through zero occurred, then the number of crossings through zero in a given channel, stored in the memory, is increased by one. At the same time the system of sign recognition determines which signal was the

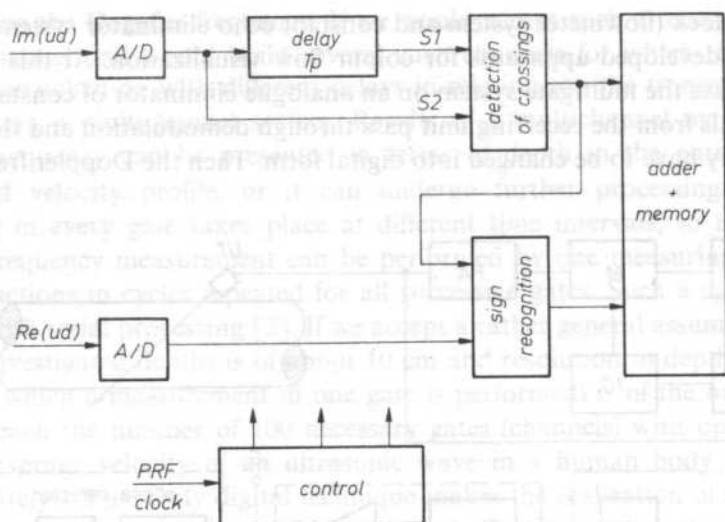


FIG. 2. Block diagram of a multigate "zero crossing" system

leading one and uses this information to determine the direction of flow in the given channel. Also this information is stored. Operations described above are repeated 128 times during one repetition. Hence, the Doppler frequency in all 128 channels can be determined in turn with one system of signal processing. The maximal frequency detected in this system approaches half of the pulse repetition frequency of the transmitter.

Detection system of crossings through zero

There are two methods of counting crossings through zero. We either only count the number of crossings through zero of a signal in one direction (e.g. from minus to plus), or in both. When the method of counting the number of crossings through zero in both directions is applied, then measured frequency remains unchanged while measuring accuracy, determined by the so-called quantization grain increases. Therefore, both directions of crossings through zero will be counted. The function of output a/d converters will be fulfilled by comparators, because a one bit information about the signal is sufficient to determine the sign of the signal. Their hysteresis are so chosen, that crossings through zero resulting from noises generated in earlier elements of the system are not recognised. The delay by repetition time is realized by the memory consisting of 128 storage cells, which stores during the period of repetition time the information about the sign of the signal for individual channels. The 128 storage cells are also used during counting. In every repetition cycle the information about the number of counted so far crossings through zero in a given

gate is read-out in turn and if a crossing is detected it is increased by one and stored anew. The detection of a crossing through zero consists in the determination whether S_1 and S_2 are different (Fig. 2). This is continued during the entire counting time, which is a multiplicity of the repetition time T_p . After the counting time, the numbers crossings through zero in individual channels are read-out and the memory is cleared. A dependence between the accuracy of frequency detection and counting time results from the above considerations. However, this time can not be prolonged too much, because the possibility of representing frequency changes resulting from the pulsatory character of the flow can be lost. If we consider the flow to be quasi-stable for 20 ms at the maximum, then for repetition period $T_p = 147.5 \mu\text{s}$ in the SEC system we will achieve the highest number of repetitions in the counting cycle 128. The possibility of switching counting from 64 to 32 repetitions is foreseen. The control system controls the number of counting cycles and sampling times, and addresses adequate memory cells for all of the 128 gates.

System of direction recognition

The system of direction recognition requires a separate description. The quadrature detection of high frequency Doppler signals is most generally applied. It gives us a real part $\text{Re}(u_d)$ and imaginary part $\text{Im}(u_d)$ of low frequency Doppler signal. They are shifted with respect to each other by $+\text{ or }-\pi/2$, depending on the direction of flow [6]. The level of the shifted signal is investigated during zero crossing of the Doppler signal. If the original signal is ahead of the shifted signal, then the measured flow is directed to the probe while if the shifted signal is ahead of the original signal, then the measured flow is directed from the probe. The information about the Doppler signal comes from sampling (during the opening of the gate) in a pulse flowmeter. In analogue systems signals from sample and hold systems are passed through low pass filters which approximately reproduce their waveform. In a digital system the information about a zero crossing comes from two successive samples; the sampling time is accepted in the moment of zero crossing.

By adding crossings through zero in successive gates, taking into account the sign obtained from the phase shifted signal during the counting period we reach the value of velocity of the flow together with its direction. However because of the determination of crossings through zero on the basis of samples only the interpretation of the direction is correct for Doppler frequencies below $1/4$ of the repetition frequency (while Doppler frequencies are measured unambiguously up to $1/2$ of the repetition frequency). Figure 3 presents an example to explain this effect. It shows components of two Doppler signals with frequencies equal to $1/5$ (signal U_{d1}) and $1/3$ (signal U_{d2}) of the repetition frequency. Phases of these signals were chosen in such a manner that an error occurs in the determination of the direction of flow. Sampling times and values of signal samples have been marked. Samples S_1 and S_2 for both signals differ with the sign — the detection system of crossings through zero will state

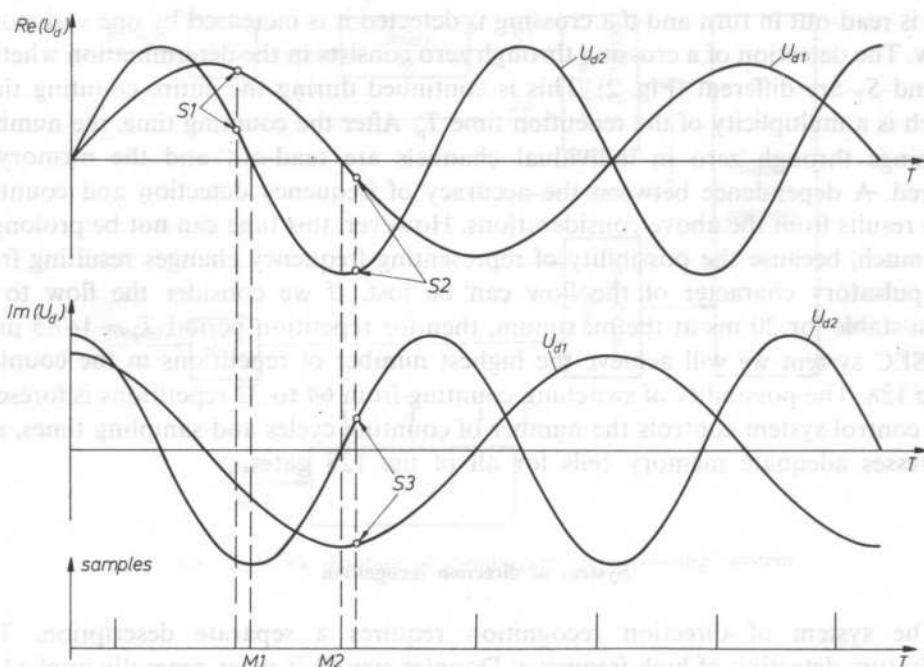


FIG. 3. Example of Doppler signal with frequency $1/3$ and $1/5 f_p$

a zero crossing but samples S_3 in these cases are different. The system for direction determination will state different directions of flow. This is a result of a too great delay of sampling with respect to the actual crossing through zero of the signal $\text{Re}(U_{d1})$ time M_1). We should notice that in an analogue system described above problems do not have place, because the determination of direction occurs practically at the same time as the actual crossing through zero (times M_1 and M_2 in Fig. 3). The only situation in which the sign can be determined falsely is when the Doppler signal has enough time to change by more than a quarter of a period between successive samples: so its frequency has to exceed $1/4$ of the pulse repetition frequency. Moreover we should notice that the effect of false determination of direction of flow occurs randomly with probability the greater, the higher the Doppler signal frequency. The probability distribution function of the above phenomenon is presented in Fig. 4.

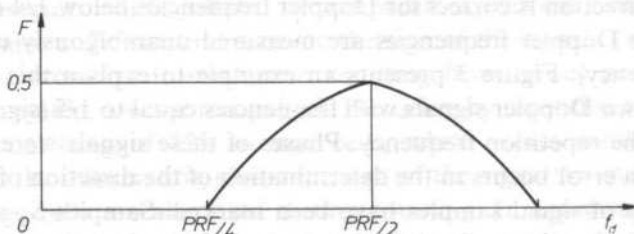


FIG. 4. Probability distribution function of the occurrence of a false sign of the direction of flow

Two solutions limiting the described above drawback have been analysed and tested in practice. The first one is based on the observation that the recognition of the direction of flow is correct up to $1/4$ of the repetition frequency. Up to a frequency, called threshold frequency, somewhat lower than $1/4$ of the repetition frequency, the system's functioning remained unchanged. Whereas, when the threshold frequency was exceeded, the sign of the previously occurring direction was maintained artificially. This was carried out on the basis of an assumption that it is impossible in such a short period of time (shorter than the accepted counting time) for a quick flow to change rapidly into an equally quick one but moving in the opposite direction. Forces necessary to perform such a change do not occur in the blood-vascular system. Unfortunately however velocities with Doppler frequencies exceeding the repetition frequency can occur, here. The sign maintaining system can only function correctly for Doppler frequencies which do not exceed the repetition frequency minus threshold frequency (Figs. 5 and 6). This significantly limits the application of the above system.

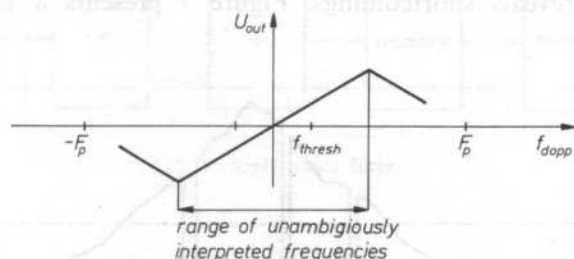


FIG. 5. Frequency characteristic of system with the maintenance of the sign of the direction of flow for $f < F_p - f_{\text{thresh}}$

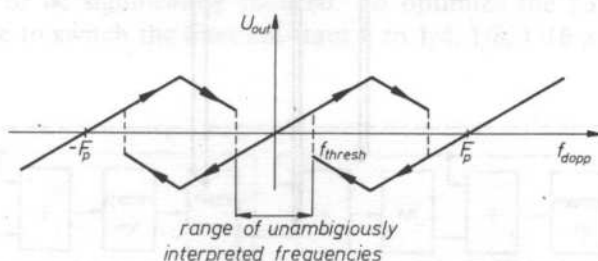


FIG. 6. Frequency characteristic of system with the maintenance of the sign of the direction of flow for $f > F_p - f_{\text{thresh}}$

The second absolutely original solution is based on a different observation. An increase of the Doppler frequency was accompanied by an increase of signs of the phase shifted signal, read-off for zero crossings, and causing misinterpretation of direction. Yet, incorrect signs appeared more rarely than correct ones up to $1/2$ of the repetition frequency, for which their number becomes equal. Therefore, a certain

trend of the direction of flow can be observed for obtained signs. And this was the origin of the idea of "averaging of signs". The system based on this idea functions as follows. One path was used to sum up zero crossings, which determine the velocity modulus after counting time. In the second path signs obtained during zero crossings were summed. If the number of positive signs exceeds the number of negative ones during counting time, then the direction of flow was accepted as positive. In a contrary case the direction is negative. The information about the direction and the absolute value of the flow are joined together on the output of the system after every counting cycle.

3. Modification of the system

During measurements of actual flows, when the relation between the useful signal, and noise and disturbances changes, the frequency measurement with the zero crossing method reveals shortcomings. Figure 7 presents a Doppler frequency

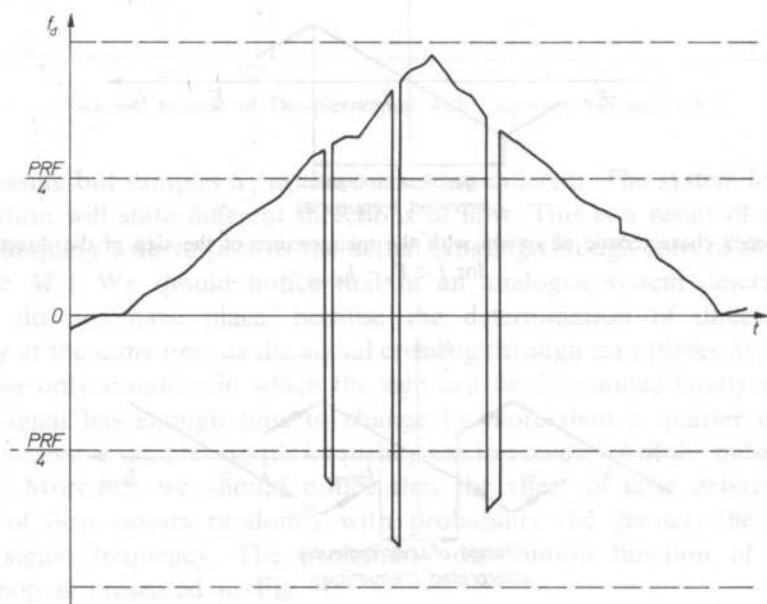


FIG. 7. Example of actual in one gate

measurement in one out of 128 gates for an exemplary actual flow, with visible measuring errors. Thus, trials have been undertaken of improving the functioning of the system. To this end a digital low-pass filter is foreseen in the described system. Such a filter can operate with a directional Doppler signal. Also two filters can be applied — one in the velocity modulus path, the other in the path of direction

determination, and then both filtered informations can be joined together. Figure 8 presents the method of forming a digital filter. The memory acts as a delay element and the filter constant k is realized by binary division (shift of bits). The configuration of a second order filter, formed from a connection in series of two first order filters, is

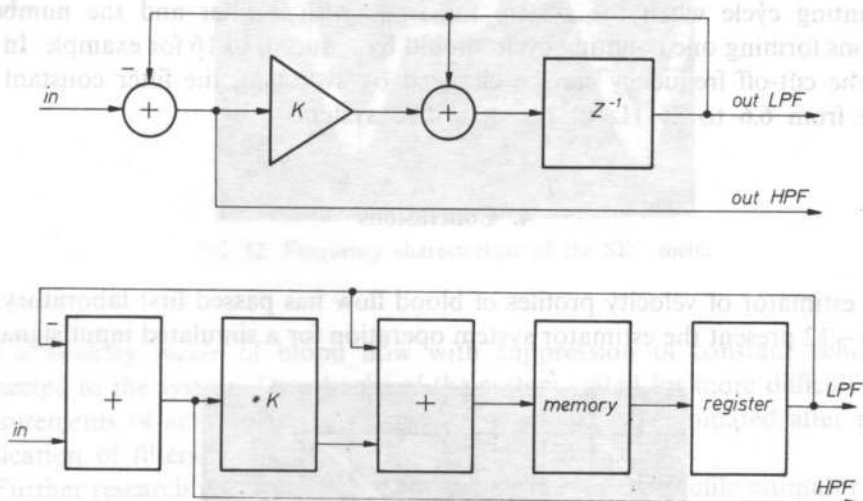


FIG. 8. First order filter

shown in Fig. 9a. The application of adequately fast digital systems makes it possible to realize such a filter as a filter functioning in series in time, i.e. with repeated information cycle in it's loop. We can see from Fig. 9 b that this allows the number of essential elements to be significantly reduced. To optimize the parameters of the system it is possible to switch the filter constant k to $1/4$, $1/8$, $1/16$ and what follows

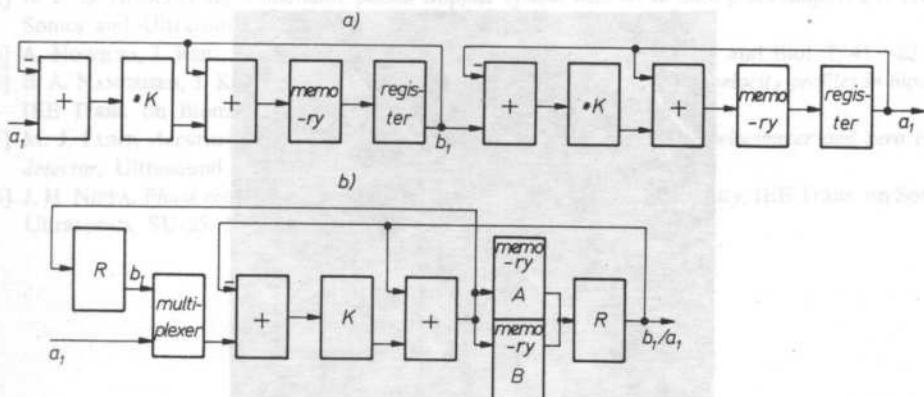


FIG. 9. Second order filter forming

cut-off frequency is then defined by

$$f_c = k \cdot \frac{f_{\text{repetition}} \cdot \text{number of repetitions in a cycle}}{4} \quad (1)$$

As we can see from expression (1) the cut-off frequency depends on the length of the counting cycle when the system functions with a filter and the number of repetitions forming one counting cycle should be reduced, to 16 for example. In such a case the cut-off frequency can be changed by switching the filter constant k in a range from 6.6 to 26 Hz in the described system.

4. Conclusions

The estimator of velocity profiles of blood flow has passed first laboratory tests. Figs. 10–12 present the estimator system operation for a simulated input signal and

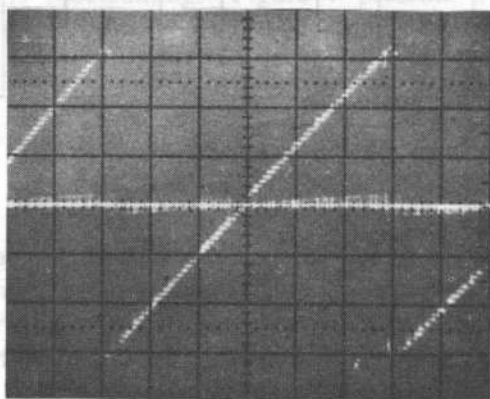


FIG. 10. Frequency characteristic of the estimator

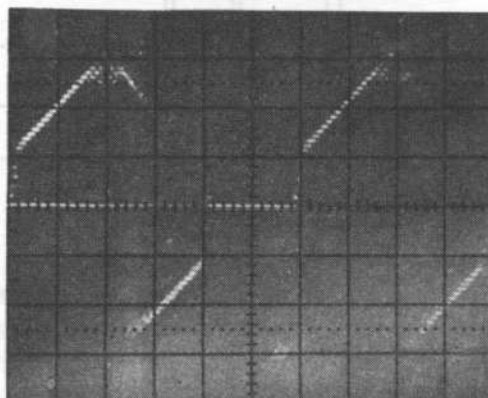


FIG. 11. Frequency characteristic of the estimator connected with flowmeter SEC

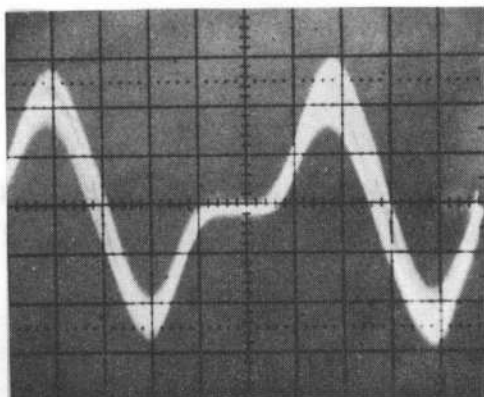


FIG. 12. Frequency characteristic of the SEC meter

with a velocity meter of blood flow with suppression of constant echoes SEC connected to the system. Drawbacks of the system stated for more difficult cases of measurements of actual signals, in particular, should be eliminated after practical application of filters.

Further research will be aimed at the connection of the profile estimator with an ultrasonocardiograph in order to present the flow on the background of echoes from body structures in the *M*-mode system. The dynamic development of the "colour Doppler" technique in the world confirms the purposefulness of these studies.

References

- [1] F. D. MC LEOD, M. ANLIKER, *Multichannel pulsed Doppler velocimeter. Principle and operation*, NASA Report 1972.
- [2] A. P. G. HOEKS et al., *A multigate pulsed Doppler system with serial data processing*, IEEE Trans. on Sonics and Ultrasonics, SU-28, 4, 242–247 (1981).
- [3] A. NOWICKI, J. REID, *An infinite gate pulse Doppler*, Ultrasound in Med. and Biol. 7, 41–50 (1981).
- [4] B. A. NANGEISEN, J. KRISTOFFERSEN, *On ultrasonic MTI measurement of velocity profiles in blood flow*, IEE Trans. on Biomedical Engn. BME, 26, 12, 665–671 (1979).
- [5] M. J. LUNT, *Accuracy and limitations of the ultrasonic Doppler blood velocimeter and zero crossing detector*, Ultrasound in Med. and Biol. 2, 4–10 (1975).
- [6] J. H. NIPPA, *Phase rotation for separating forward and reverse blood, velocity*, IEE Trans. on Sonic and Ultrasonics, SU-25, 5.

Received on June 1, 1987

MAKING USE OF BRAGG'S DIFFRACTION FOR INVESTIGATIONS OF THE ACOUSTIC ACTIVITY OF BISMUTH-GERMANIUM OXIDE

Z. KLESZCZEWSKI

Institute of Physics, Silesian Technical University
(44-100 Gliwice, ul. Krzywoustego 2, Poland)

The essence of the acoustic activity of crystals has been discussed. A measuring system for the investigation of this activity has been presented. The measuring method makes use of Bragg's type diffraction of laser light in an acoustic wave. Measurements of the gyration constant G_{23} for bismuth-germanium oxide have been made.

1. Acoustic activity of crystals

Acoustic activity of crystals is the result of the existence of the dispersion phenomenon, i.e., the dependence of the velocity wave propagation, and thus the elastic constants on the wave vector k . Assuming that $c_{ijkl} = c_{ijkl}(k)$, we can write Hooke's law, with an accuracy of the second order terms, in the form:

$$\sigma_{ij} = c_{ijkl}s_{kl} + b_{ijklm} \frac{\partial s_{kl}}{\partial x_m}, \quad (1)$$

where σ_{ij} is the stress tensor, c_{ijkl} — the tensor of elastic constants, s_{kl} — deformation tensor, b_{ijklm} — tensor of acoustic activity. As this is the tensor of the odd rank, the phenomenon of the acoustic activity occurs only in the crystals with no centre of symmetry. It may be shown [1] that its numerical value is of the order $c_{ijkl} \cdot a$, where a is the lattice constant. In view of this, taking into account dependence (1), we infer that dispersion, and thus also the acoustic activity, may appear at frequencies of at least 10^8 Hz and higher.

The tensor of acoustic activity b_{ijklm} is usually written in the form:

$$b_{ijklm} = \delta_{ijq} G_{qklm}, \quad (2)$$

where G_{qklm} is the tensor of acoustic gyration, whereas δ_{ijq} is a unitary tensor defined

as follows:

$$\delta_{ijq} = \begin{cases} 1 & \text{with } ijq = 123, 231, 312, \\ -1 & \text{with } ijq = 132, 213, 321, \\ 0 & \text{in remaining cases.} \end{cases}$$

If the dependence expressed by formula (2) is substituted in the equation of motion

$$\varrho \frac{\partial^2 u_i}{\partial t^2} = \frac{\partial \sigma_{ij}}{\partial x_j} \quad (3)$$

we obtain

$$\varrho \frac{\partial^2 u_i}{\partial t^2} = c_{ijkl} \frac{\partial^2 u_k}{\partial x_l \partial x_j} + b_{ijklm} \frac{\partial^3 u_k}{\partial x_l \partial x_j \partial x_m}. \quad (4)$$

Assuming the solution from equation (4) in the form of a plane wave

$$u_i = u_{oi} e^{i(k_l x_l - \omega t)} \quad (5)$$

we obtain Christoffel equation

$$(c_{ijkl} k_l k_j + i b_{ijklm} k_l k_j k_m - \varrho \omega^2 \delta_{ik}) u_{ok} = 0 \quad (6a)$$

and respectively

$$|c_{ijkl} \kappa_l \kappa_j + i b_{ijklm} \kappa_l \kappa_j k_m - \varrho v^2 \delta_{ik}| = 0, \quad (6b)$$

where k_m is the component of the wave vector, κ_l — component of the unitary vector in the direction of wave propagation, v — the velocity of wave propagation, δ_{ik} — Kronecker delta.

After making use of the definition of the gyration tensor equation (6b) will be written in the form:

$$|\Gamma_{ik} + ik G_{ik} - \varrho v^2 \delta_{ik}| = 0, \quad (7)$$

where $\Gamma_{ik} = c_{ijkl} \kappa_j \kappa_l$, $G_{ik} = \delta_{ikp} G_{mpjl} \kappa_m \kappa_l$.

Let us now consider the effect of the acoustic activity of a crystal on the propagation of an acoustic wave. By the way of an example let us take a crystal of cubic structure in which an acoustic wave is propagated in one of the principal directions. We then have:

$$\Gamma_{11} = c_{11}, \quad (8a)$$

$$\Gamma_{12} = \Gamma_{13} = \Gamma_{23} = 0, \quad (8b)$$

$$\Gamma_{22} = \Gamma_{33} = c_{44}, \quad (8c)$$

$$G_{12} = G_{31} = 0, \quad (8d)$$

$$G_{23} = -G_{32} = G. \quad (8e)$$

In such case, the determinant of Christoffel equation assumes the form:

$$\begin{vmatrix} c_{11} - \rho v^2 & 0 & 0 \\ 0 & c_{44} - \rho v^2 & ikG \\ 0 & -ikG & c_{44} - \rho v^2 \end{vmatrix} = 0. \quad (9)$$

Solving equation (9) we obtain the expressions for the velocity of propagation of longitudinal wave $v_L = (c_{11}/\rho)^{1/2}$, and of two transverse waves

$$v_{T1} = \sqrt{\frac{c_{44} + kG}{\rho}} \cong v_{T0} \left(1 + \frac{1}{2} \frac{kG}{c_{44}} \right), \quad (10a)$$

$$v_{T2} = \sqrt{\frac{c_{44} - kG}{\rho}} \cong v_{T0} \left(1 - \frac{1}{2} \frac{kG}{c_{44}} \right), \quad (10b)$$

where $v_{T0} = \sqrt{\frac{c_{44}}{\rho}}$.

Substituting the velocities determined in Christoffel equation we may determine the polarization of the wave of the velocity given. For the waves v_{T1} and v_{T2} we shall get respectively:

$$u_y = iu_z, \quad (11a)$$

$$u_y = -iu_z. \quad (11b)$$

This means that these waves have circular laevorotatory and dextrorotatory polarization.

If we put together two waves of circular laevorotatory and dextrorotatory polarization, we obtain a linearly polarized wave of the amplitude twice higher the amplitude of each of the components.

In the case when $v_{T1} = v_{T2}$, there is no phase difference between the waves, and the vector of polarization has a constant direction in space (Fig. 1a). However, if

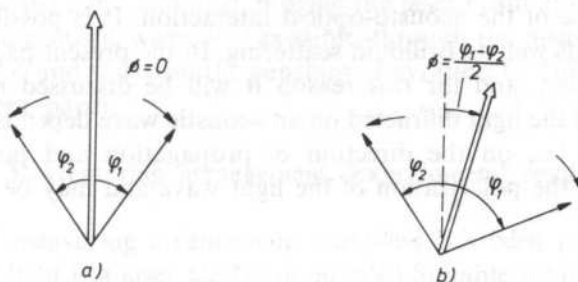


FIG. 1. Direction of wave polarization in the case when: a) $v_{T1} = v_{T2}$, b) $v_{T2} \neq v_{T1}$

dispersion occurs in the medium, that is $v_{T1} \neq v_{T2}$, a difference of phases will be created between the waves (Fig. 1b). After the waves have travelled path l , the phases will be

$$\varphi_1 = \frac{\omega}{v_{T1}} l, \quad (12a)$$

$$\varphi_2 = \frac{\omega}{v_{T2}} l, \quad (12b)$$

whereas the difference of phases $\Delta\varphi$ and the rotation of the polarization plane Φ are respectively

$$\Delta\varphi = \varphi_1 - \varphi_2 = \omega l \left(\frac{1}{v_{T1}} - \frac{1}{v_{T2}} \right), \quad (13a)$$

$$\Phi = \frac{\varphi_1 - \varphi_2}{2} = \frac{\omega l}{2} \frac{v_{T1} - v_{T2}}{v_{T1} v_{T2}} \cong \frac{\omega l}{2} \frac{\Delta v}{v_{T0}^2}. \quad (13b)$$

Considering that

$$v_{T1} - v_{T2} = \frac{kG}{c_{44}} v_{T0} = \frac{\omega G}{\rho v_{T0}^2}, \quad (14)$$

we finally obtain

$$\Phi = \frac{\omega^2 l}{2 \rho v_{T0}^4} G. \quad (15)$$

This means that there occurs a change of the plane of polarization of the transverse acoustic wave.

2. Acousto-optical interaction in acoustically active crystals

A very useful method of investigating the acoustic activity of crystals is the method making use of the acousto-optical interaction. It is possible to apply here Bragg's diffraction as well as Brillouin scattering. In the present paper use was made of Bragg's diffraction, and for this reason it will be discussed more fully.

The intensity of the light diffracted on an acoustic wave depends on the geometry of the diffraction, i.e., on the direction of propagation and polarization of the acoustic wave and the polarization of the light wave and may be expressed by the dependence [2]

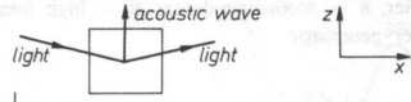
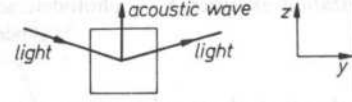
$$\frac{I}{I_0} \sim (p_{ijkl} \alpha_i \beta_j \alpha_k \gamma_l)^2, \quad (16)$$

where p_{ijkl} are the components of the tensor of photoelastic constants, α_i, β_j — constants of the unitary vector determining the polarization of incident and diffracted light, κ_k, γ_l — unitary vectors in the direction of propagation and polarization of an acoustic wave. This means that in the particular crystal, and thus in the determined form of the tensor p_{ijkl} , diffraction is possible only for a certain polarization of the diffracted and incident light, and for a certain polarization and direction of propagation of an acoustic wave. A change of the plane of polarization of an acoustic wave, which is what takes place in acoustically active crystals, results in the change of the intensity of the diffracted light. In particular, this intensity may be equal to zero.

In table 1 are given, as an example, some possible geometries of diffraction at a particular direction of propagation of an acoustic wave for a cubic system.

Table 1.

diffraction of light in acoustic waves in crystals of cubic system

polarization of acoustic wave	 $x = (0, 0, 1)$		 $x = (0, 0, 1)$			
	polarization of light : incident / diffracted (α_i / β_j)					
	α_y / β_y	α_z / β_z	α_z / β_y	α_x / β_x	α_z / β_z	α_z / β_x
\hat{j}_x	$p_{25} = 0$	$p_{35} = 0$	$p_{45} = 0$	$p_{15} = 0$	$p_{35} = 0$	$p_{55} \neq 0$
\hat{j}_y	$p_{24} = 0$	$p_{34} = 0$	$p_{44} \neq 0$	$p_{14} = 0$	$p_{34} = 0$	$p_{54} = 0$

The idea of applying Bragg's diffraction arises already from the data above. It is known that in the acoustically active crystals the direction of polarization of the transverse wave is changed. This means that there is also a change of the intensity of the diffracted light with a particular geometry of diffraction. This intensity will be changed periodically with the period of changes corresponding to the change of the phase $\phi = \pi$, or $I(\phi) = I(\phi + n\pi)$. Thus, determining the plane of polarization of the incident and diffracted light, and next, moving the laser beam along the direction of propagation of the acoustic wave, it is possible, through the measurement of $I(l)$ or $I(\phi)$, to determine ϕ and thus also the constant of gyration G . This method has been used in the present paper.

3. Measuring arrangement. Experimental results

A diagram of measuring arrangement compiled has been presented in Fig. 2.

The source of light is a laser He-Ne of 50 mW. Suitable rotators, polarizers and analyzers provide suitable polarization of the incidence and diffraction light. The

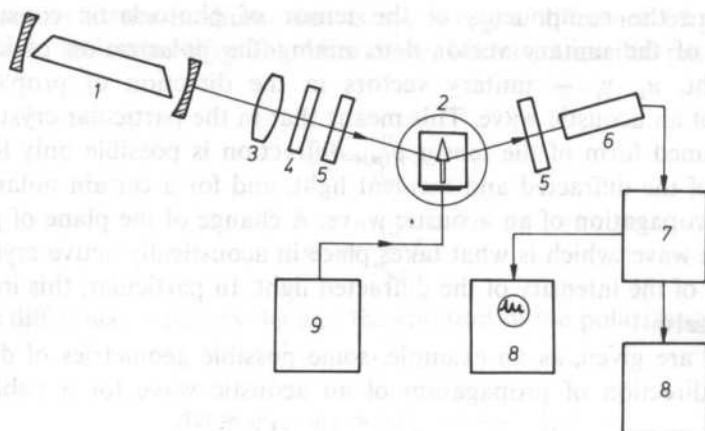


FIG. 2. Diagram of the measuring arrangement for the testing of the acoustic activity of crystals. 1 — laser, 2 — goniometric table with a shift, 3 — system of beam formation, 4 — rotator, 5 — polarizer and polarization analyzer, 8 — photodetector, 7 — amplifier, 8 — recording device, 9 — high frequency generator and power generator

samples tested are placed on a geometric table which may be moved in a horizontal plane by means of a motor, in the direction of propagation of an acoustic wave with the speed of about 1 cm/min. The diffracted light is registered by means of a photoelectric multiplier, amplifier, oscilloscope and recorder. Piezoelectric transducers are activated by means of high frequency generators G3-20 and G4-37A.

Measurements were made for the crystals of bismuth-germanium oxide $\text{Bi}_{12}\text{GeO}_{20}$ (BGO). The crystals cut along principal directions were in the shape of rectangular prisms of the dimensions $8 \times 8 \times 60$ mm, LiNbO_3 transducers of the X cut were glued on the butting faces of the crystal so that the direction of polarization of the acoustic wave at the transducer was in the diffraction plane (Fig. 3). The sample

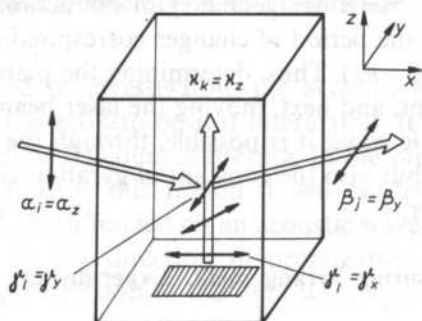


FIG. 3. Geometry of the experiment

was placed between the intersecting polarizer and analyzer, i.e., diffraction was studied while changing the plane of polarization. The initial conditions are thus as follows $\alpha_i = \alpha_z$, $\beta_j = \beta_y$, $\kappa_k = \kappa_z$, $\gamma_l = \gamma_x$. The photoelastic constant corresponding to these conditions is $p_{3231} = p_{45}$. For the crystal BGO (cubic structure) $p_{45} = 0$ [3]. This means that the initial intensity of the diffracted light $I(z = 0) = 0$. When moving the crystal along the direction of propagation of an acoustic wave (with an immobile laser beam) there is a diffraction of light in the transverse wave of the polarization γ_y which appears as a result of the rotation of the polarization plane. Responsible for this diffraction is the photoelastic constant $p_{3232} = p_{44}$ which is, for the BGO crystals, different from zero.

The measurements were made for two frequencies: $f_1 = 360$ MHz and $f_2 = 450$ MHz. The measurement results are given in Fig. 4.

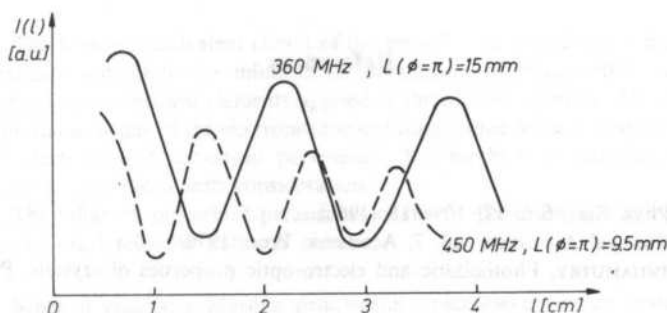


FIG. 4. Dependence of the intensity of the diffracted light on the distance from the transducer

From the measurements made it results that the intensity of the diffracted light reaches the successive maxima and minima with the distance between the maxima being $l_1 = 15$ mm for the frequency $f_1 = 360$ MHz and $l_2 = 9.5$ mm for the frequency $f_2 = 450$ MHz. Assuming that to these l values corresponds $\phi = \pi$, we may determine, on the basis of formula (15), the constant G which is:

$$G = \frac{\rho v_{T0}^4}{2\pi l f^2}. \quad (20)$$

Substituting in formula (20) the experimental values obtained, as well as the material constants: $\rho = 9.252 \cdot 10^3 \text{ kg} \cdot \text{m}^{-3}$, $v_{T0} = 1662 \text{ m} \cdot \text{s}^{-1}$, we obtain the numerical value of the constant $G = 5.8 \text{ N m}^{-1}$. Taking into account the accuracy of the determination L which is mainly dependent on the diameter of the laser beam and is about 0.5 mm, we may write that the constant of acoustic gyration $G = G_{23}$ for the crystals BGO is $(5.8 \pm 0.8) \text{ Nm}^{-1}$.

4. Summary

The measurements made have shown that Bragg's diffraction of laser light in an acoustic wave is very useful for the investigating of the acoustic activity of crystals.

The investigation of the acoustic activity, or in general, of the polarization effects with the propagation of acoustic waves makes it possible to obtain significant information in the field of the acoustics of solids. In particular, it is possible to analyze dispersion and influence of acoustic waves, acoustic anisotropy, non-linear effects, accuracy of orientation of crystals.

It seems that of particular importance is the investigation of forced activity and of forced polarization effects since in this way it is possible to obtain information about the stresses and deformations in crystals which is of partial significance. Further research will be made in this direction.

References

- [1] G. KLUGE, *Phys. Stat. Sol.* **17**, 109-118 (1966).
- [2] V. MASON, *Physical Acoustics*, vol. 7, Academic Press 1970.
- [3] T. S. NARASIMHAMUTRY, *Photoelastic and electro-optic properties of crystals*, Plenum Press 1981.

Received on September 28, 1989

DESIGN OF ULTRASONIC PROBES FOR MEDICAL DIAGNOSTICS

G. ŁYPACEWICZ, E. DURIASZ

Ultrasonics Department, Institute of Fundamental Technological Research, Polish Academy of Sciences
(00-049 Warszawa, Świątokrzyska 21)

The Mason's equivalent circuit of the piezoelectric transducer is modified in order to investigate separately the influence of parameters of piezoelectric material as well as electrical and acoustical elements applied in the ultrasonic probe. All values transferred to the mechanical side of the electromechanical transformer let us introduce the relative values both electrical and acoustical parameters. The mechanical and dielectric losses of the transducer are taken into consideration.

The influence of various parameters of the probe on input admittance and reflected from an ideal reflector pulses is shown.

Schemat zastępczy Masona przetwornika piezoelektrycznego został zmodyfikowany w sposób umożliwiający badanie oddzielnie wpływu zarówno parametrów piezoelektrycznego materiału, jak również elektrycznych i akustycznych elementów zastosowanych w głowicy. Wszystkie wielkości przeniesiono na stronę mechaniczną transformatora elektromechanicznego, co pozwoliło na wprowadzenie wartości względnych zarówno elektrycznych, jak i akustycznych parametrów. W układzie zastępczym uwzględniono straty mechaniczne i dielektryczne przetwornika.

Pokazano wpływ różnych parametrów głowicy na admitancję wejściową i impulsy odbite od idealnego reflektora.

Notation

- A surface of transducer
- c_a velocity of ultrasonic wave in medium loading the back surface of transducer
- c_b velocity of ultrasonic wave in investigated medium
- c_p velocity of ultrasonic wave in transducer
- c_{01} velocity of ultrasonic wave in first matching layer
- c_{02} velocity of ultrasonic wave in second matching layer
- C_0 clamped capacitance of transducer
- C_m capacitance in equivalent series resonance system of transducer
- d thickness of transducer
- d_{01} thickness of first matching layer

- d_{02} thickness of second matching layer
- E_t voltage of transmitter
- E'_t relative voltage of transmitter
- E_r voltage of pulse reflected from an ideal reflector
- E'_r relative voltage of pulse reflected from an ideal reflector
- f frequency
- f_e electric resonance frequency of transducer
- f_m mechanical resonance frequency of transducer
- F_t acoustic force radiated by the transducer
- F_r acoustic force reflected from ideal reflector
- k parameter describing capacitance in compensating circuit
- k_t electromechanical coupling coefficient
- l parameter describing series inductance in compensating circuit
- l_c length of cable
- L_m inductance in equivalent series resonance circuit of transducer
- m parameter describing parallel inductance in compensating circuit
- N turns ratio of electromechanical transformer
- n parameter describing thickness of first matching layer
- p parameter describing thickness of second matching layer
- Q_m mechanical factor of transducer
- R_a relative acoustic resistance of back loading of transducer
- R_b relative acoustic resistance of investigated medium
- R_e relative acoustic resistance of dielectric losses
- R_m relative acoustic resistance of mechanical losses
- R_{oc} characteristic impedance of cable
- R_p acoustic resistance of transducer
- R_r resistance of receiver
- R'_r relative resistance of receiver
- R_t resistance of transmitter
- R'_t relative resistance of transmitter
- R_A acoustic resistance of back loading of transducer
- R_B acoustic resistance of investigated medium
- R_F acoustic impedance of transducer at resonance frequency f_e
- R_{01} relative acoustic impedance of first matching layer
- R_{02} relative impedance of second matching layer
- t time
- T_m period of transducer mechanical vibrations
- w_c coefficient describing characteristic impedance of cable
- W_m coefficient describing resistance of mechanical losses in terms of frequency
- x relative frequency
- x_e relative frequency of electric resonance
- x_m relative frequency of mechanical resonance
- X_{in} imaginary part of relative mechanical impedance of transducer
- Y_{in} relative input admittance of transducer
- Z_E input impedance of transducer
- Z_{in} relative input impedance of transducer
- Z_M mechanical impedance of transducer
- Z_m relative mechanical impedance of transducer
- Z_{ck} relative capacitance impedance in compensating circuit
- Z_{L1} relative impedance of a series coil in compensating circuit
- Z_{Lm} relative impedance of series coil in compensating circuit
- β phase constant of lines (matching layers)

δ_e	angle of dielectric losses
δ_m	angle of mechanical losses
ϵ^S	dielectric constant
φ_c	coefficient describing length of cable
λ_e	length of acoustic wave for electric resonance of transducer
λ_m	length of acoustic wave for mechanical resonance of transducer
λ_{el}	length of electromagnetic wave in cable
ρ_a	density of back loading of transducer
ρ_b	density of investigated medium
ρ_p	density of transducer
ρ_{01}	density of first matching layer
ρ_{02}	density of second matching layer
ω	pulsation
ω_e	pulsation of electric resonance of transducer
ω_m	pulsation of mechanical resonance of transducer

1. Introduction

Ultrasonic medical diagnostics have been developing during the last 30 years. A clear progress can be noted in the past several years. It results from computerization on one hand and perfection of ultrasonic transmitting-receiving systems on the other. For example an increase of general sensitivity led to an increase of operating frequency of ultrasonographs for abdominal examinations from 2.5 MHz to 3.5 MHz, and this, in turn, improved resolution. The progress in this field is conditioned by the construction of adequate ultrasonic probes. Sensitivity is increased by eliminating or decreasing loading of the back surface, by using layers matching acoustic impedance of the acoustic transducer to the human body and by matching electric impedance of the probe to that of echograph transmitting-receiving systems.

The following quantities influence the shape and size of received ultrasonic pulses: voltage exciting the transducer, electric and acoustic systems, parameters of piezoelectric materials and the transducer dimensions.

In order to investigate the influence of these parameters separately, the transducer equivalent circuit was modified by introducing relative quantities and by including dielectric and mechanical losses (what is essential when piezoelectric film is applied). Also quantities describing the compensating system, cable, transmitter and receiver were introduced into the model.

Designers of ultrasonic probes generally tend to achieve flat amplitude and linear phase characteristics of the transmitting-receiving path and to minimize losses due to processing. However it is difficult to describe the pulse response dependence on amplitude-phase characteristics, therefore the influence of individual parameters of the system on its operation was usually illustrated with pulses reflected from an ideal reflector.

The analysis is carried out on the basis of the four-terminal theory and FFT techniques.

2. Equivalent circuit of an ultrasonic probe

The equivalent circuit of an ultrasonic probe is presented in Fig. 1. Many authors [8], [15], [16] apply the KLM equivalent circuit. However, here we accepted Mason's equivalent circuit [13], because in the KLM model the turns ratio of an

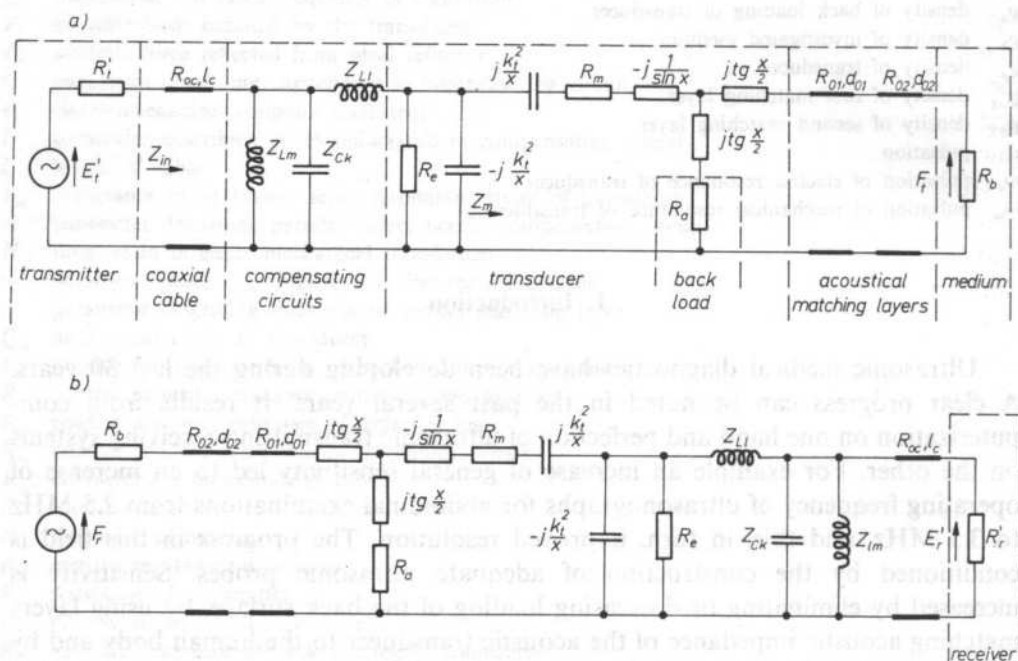


FIG. 1. Equivalent circuit of ultrasonic probe: a — transmitting, b — receiving (parameters described in paper)

electromechanical transformer is frequency dependent. It is possible to calculate the transducer input impedance and the electric resonance frequency f_e — electromechanical coupling coefficient k_t relationship [10] directly from Mason's model.

All quantities describing the probe and input transmitting-receiving systems have been transferred in the model to the mechanical side of the electromechanical transformer (comparative with Fig. 9), and at the same time relative values of parameters were introduced:

- frequency $x = \Pi f / f_m$
- acoustic resistance of transducer $R_p / R_p = 1$ where $R_p = A Q_p c_p$
- resistance of dielectric and mechanical losses R_e and R_m
- acoustic resistance of back loading $R_a = A Q_a c_a / R_p$
- acoustic resistance of investigated medium $R_B = A Q_b c_B / R_p$
- parameters describing matching layers R_{01} , n and R_{02} , p

- parameters describing the coaxial cable R_{0c}, l
- impedances of compensating system Z_{Ll}, Z_{Ck}, Z_{Lm}
- voltage of transmitter $E'_t = E_t N$
- voltage of pulse reflected from an ideal reflector $E'_r = E_r N$
- resistance of transmitter and receiver $R'_t = R_t N^2 / R_p, R'_r = R_r N^2 / R_p$, where f_m — frequency of transducer mechanical resonance, A — surface of transducer, $q_p c_p, q_a c_a, q_b c_b$ — acoustic resistances of transducer, loading of transducer back surface and investigated medium, respectively, R_t, R_r — input impedances of transmitter and receiver, $N^2 = 2 k_t^2 f_m C_0 R_p$ turns ratio of electromechanical transformer, C_0 — clamped capacitance of transducer, k_t — electromechanical coupling coefficient for thickness vibrations, E_N — voltage of incident wave, E_r — voltage of reflected wave.

Additional elements can be included in the probe equivalent circuit (subject to its construction), such as e.g. layers matching back loading to transducer, or transformer matching the electrical impedance of the probe to the transmitting-receiving circuit. Such an equivalent circuit with all these relative quantities can be used to investigate the influence of individual parameters of piezoelectric ceramics, as well as of other elements of the probe, on the size and shape of reflected pulse, independently of the transducer diameter and its resonance frequency.

2.1 Dielectric and mechanical losses of the transducer

L. F. BROWN and D. L. CARLSON [1] have investigated polymer piezoelectric films with high dielectric and mechanical losses, and proved that the actual input impedance of the transducer can be modelled with 1% accuracy when resistances of these losses in the form as in Fig. 1 are included in Mason's model. Thus, according to results of their papers, relative quantities can be introduced as follows.

Dielectric losses are described with $\text{tg } \delta_e$ which represents the ratio of the conduction current to the displacement current in a dielectric, so

$$\text{tg } \delta_e = \frac{1}{R_e \omega C_0}. \quad (1)$$

Because in the modified Mason's model (Fig. 1) the impedance of C_0 is represented as

$$\frac{1}{\omega C_0} \Rightarrow \frac{k_t^2}{x}$$

then the resistance expressing losses is

$$R_e = \frac{k_t^2}{x \text{tg } \delta_e}. \quad (2)$$

In order to introduce element R_m , which describes mechanical losses, let us consider mechanical impedance Z_m of a not loaded transducer ($R_a = R_b = R_{01} = R_{02} = 0$).

It will have the form as in Fig. 2a, b.

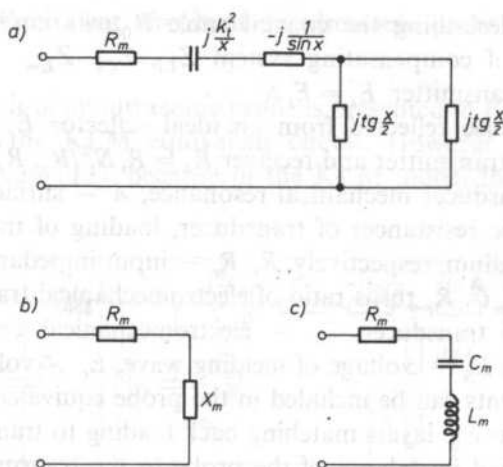


FIG. 2. Equivalent circuit of mechanical part of transducer (not loaded): a and b according to Mason's model, c near electric resonance

Hence, we can write

$$Z_m = R_m + jX_m, \quad (3)$$

where

$$X_m = \frac{k_t^2}{x} - \frac{1}{\sin x} + \frac{1}{2} \operatorname{tg} \frac{x}{2} = \frac{k_t^2}{x} - \frac{1}{2} \operatorname{ctg} \frac{x}{2}. \quad (4)$$

The electric resonance of a transducer occurs at frequency, for which $X_m = 0$. This leads to expression

$$k_t^2 = \frac{x_e}{2} \operatorname{ctg} \frac{x_e}{2}, \quad (5)$$

where $x_e = f_e/f_m$, f_e — frequency of electric resonance. As we can see, the relative frequency of electric resonance of a not loaded transducer is a function of the electromechanical coupling coefficient only (Fig. 3).

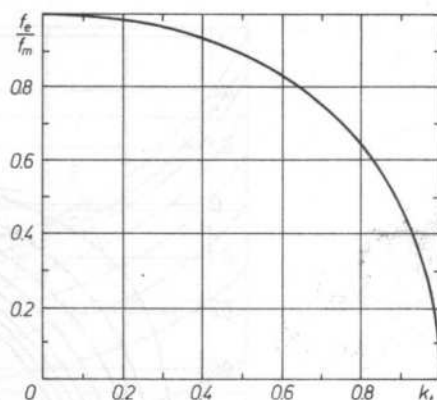
Near electric resonance mechanical impedance of the transducer can be substituted with good accuracy with a series resonance circuit R_m , C_m , L_m (Fig. 2c). Thus

$$X_m = \omega L_m - \frac{1}{\omega C_m}. \quad (6)$$

The following expressions can be written for this circuit

$$Q_m = \frac{1}{R_m \omega_e C_m}, \quad (7)$$

FIG. 3. The electric resonance frequency f_e to mechanical resonance frequency f_m ratio in terms of electromechanical coupling coefficient k_t



where $\omega_e = 2\pi f_e$

$$\omega_e = 1/\sqrt{L_m C_m} \quad (8)$$

and thus

$$X_m = \frac{1}{C_m \omega_e} \left(\frac{\omega}{\omega_e} - \frac{\omega_e}{\omega} \right). \quad (9)$$

Figure 4 presents values of X_m calculated in accordance with formula (4) (Fig. 4a) and formula (9) (Fig. 4b). Values X_m have been equalized here for frequencies x_e and $1.25 x_e$. As we can see these curves are identical with an accuracy of the drawing in the frequency range of the relative band $\Delta f/f_e \approx 0.5$.

If we accept, as L. F. BROWN and D. L. CARLSON [1] did, that factor Q_m can be assumed independent of frequency, then it will be the inverse of the mechanical losses tangent

$$Q_m = 1/\text{tg} \delta_m. \quad (10)$$

From expressions (4), (5), (7) and (10) we obtain the formula for R_m in the following form

$$R_m = W_m \text{tg} \delta_m, \quad (11)$$

where

$$W_m = X_m(x)/(x/x_e - x_e/x) = \frac{1}{2} \left(\frac{x_e}{x} \text{ctg} \frac{x_e}{2} - \text{ctg} \frac{x}{2} \right) / (x/x_e - x_e/x). \quad (12)$$

Figure 5 presents diagrams of coefficient W_m in terms of frequency for various k_t values. Points mark frequencies of electric resonance (f_e/f_m). Knowing the value of

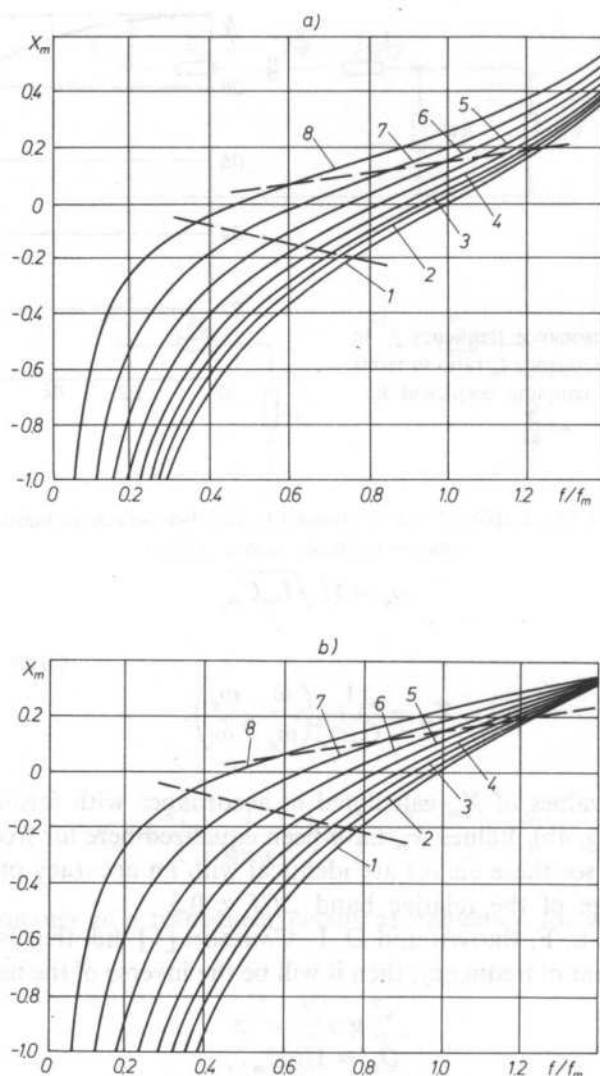


FIG. 4. The imaginary part of mechanical impedance of transducer not loaded in terms of frequency to mechanical resonance frequency f_m ratio, resulting from: a — Mason's equivalent circuit, b — equivalent series resonance circuit for: 1 — $k_t = 0.1$, 2 — $k_t = 0.3$, 3 — $k_t = 0.4$, 4 — $k_t = 0.5$, 5 — $k_t = 0.6$, 6 — $k_t = 0.7$, 7 — $k_t = 0.8$, 8 — $k_t = 0.9$. Broken lines mark the range with frequency band $\Delta f/f_e$ equal to 0.5

the mechanical losses tangent $\operatorname{tg} \delta_m$, we can include the resistance of losses R_m in the equivalent transducer circuit Fig. 1.

It should be noted that a different dependence of R_e and R_m on frequency could be used in formulae (2) and (11) — a dependence defining losses in various piezoelectric materials more accurately.

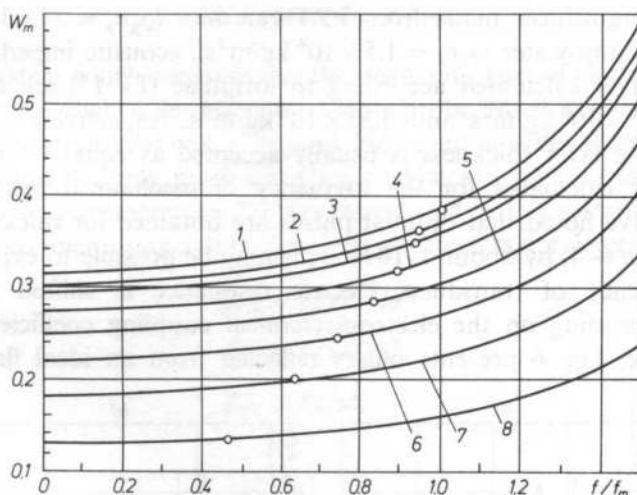


FIG. 5. W_m coefficient (describing mechanical losses according to expression (12)) in terms of frequency to mechanical resonance frequency f_m ratio for: 1 — $k_t = 0.1$, 2 — $k_t = 0.3$, 3 — $k_t = 0.4$, 4 — $k_t = 0.5$, 5 — $k_t = 0.6$, 6 — $k_t = 0.7$, 7 — $k_t = 0.8$, 8 — $k_t = 0.9$. Points mark the electric resonance frequencies f_e/f_m

2.2 Acoustic matching layers

Acoustic layers matching the acoustic impedance of the transducer to the impedance of investigated medium (or back loading of transducer) are described with two parameters — acoustic characteristic impedance of line $R_{01} = A\varrho_{01}c_{01}/R_p$ and parameter n corresponding with layer thickness constant phase line β in accordance with formula $n = \lambda_m/d_{01}$, where λ_m — wave length for transducer mechanical resonance frequency, d_{01} — thickness of layer (length of line). Because $\beta = 2\pi d_{01}/\lambda$ and $\lambda = c_{01}/f$, $\lambda_m = c_{01}/f_m$, then $\beta = 2\pi n$.

Parameters of the second matching layer, R_{02} and p are determined by analogy. Naturally, an arbitrary number of layers can be introduced into the system.

Characteristic impedances of lines are generally determined from Czebyszew's formulae (geometric mean) [3]. Other authors calculate acoustic impedance of matching layers on the basis of various premises. DE SILETS et al. [15], [16] have proved that the shape of received pulses is optimal when the acoustic resistance of matching layers is calculated according to the binominal criterion. SOUQUET et al. [17], [4] have derived formulae for acoustic impedance of these layers assuming an equality of Q factors of the electric and mechanical branch of the equivalent circuit.

Formulae for acoustic impedance of a single matching layer are as follows

$$\text{according to CZEBYSZEW} \quad \varrho_{01}c_{01} = \sqrt{(\varrho_p c_p)(\varrho_b c_b)}, \quad (13)$$

$$\text{according to DE SILETS} \quad \varrho_{01}c_{01} = \sqrt[3]{(\varrho_p c_p)(\varrho_b c_b)^2}, \quad (14)$$

$$\text{according to SOUQUET} \quad \varrho_{01}c_{01} = \sqrt[3]{2(\varrho_p c_p)(\varrho_b c_b)^2}, \quad (15)$$

And so, for a transducer made from PZT ceramics ($\varrho_p c_p = 34 \times 10^6 \text{ kg/m}^2\text{s}$) and investigated medium-water ($\varrho_b c_b = 1.5 \times 10^6 \text{ kg/m}^2\text{s}$), acoustic impedances $\varrho_{01} c_{01}$ of the matching layer calculated according to formulae (13–15) are equal to $7.14 \times 10^6 \text{ kg/m}^2\text{s}$, $4.25 \times 10^6 \text{ kg/m}^2\text{s}$ and $5.35 \times 10^6 \text{ kg/m}^2\text{s}$, respectively.

The matching layer thickness is usually accepted as equal to one fourth of the wave length — calculated for the frequency of mechanical resonance. Certain authors [16] have noted that optimal pulses are obtained for thicknesses of layers exceeding $\lambda_m/4$ ($n = 4$) by about 4–10%. This may be possible to explain by the fact that the frequency of transducer electric resonance is shifted towards lower frequencies, depending on the electromechanical coupling coefficient k_t .

For example, Fig. 6 presents pulses reflected from an ideal flat reflector, for

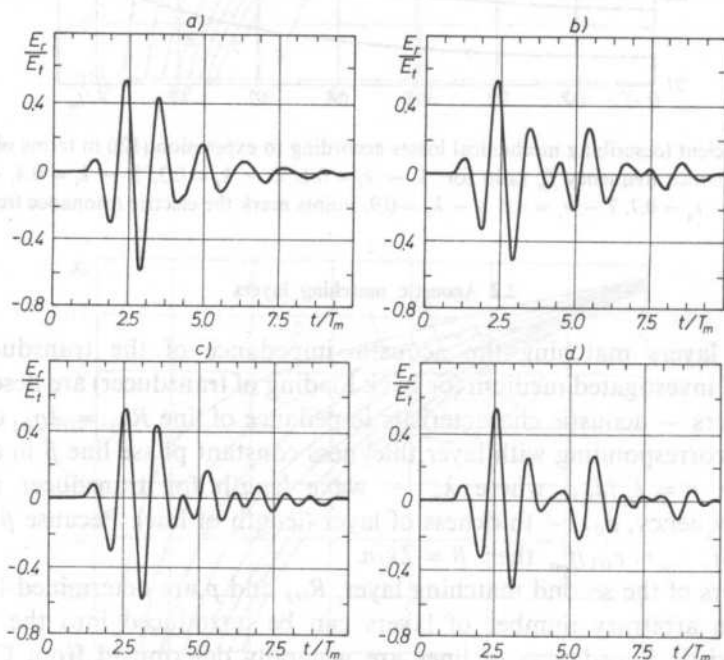


FIG. 6. Pulses reflected from ideal reflector for PZT I ceramic transducer with two matching layer for excitation voltage $E_i = \delta(t)$, $k_t = 0.5$, $R_a = 0$, $R_b = 0.044$

- a) $R_{01} = 0.262$, $R_{02} = 0.069$, $n = p = 4$
- b) $R_{01} = 0.36$, $R_{02} = 0.122$, $n = p = 4$
- c) $R_{01} = 0.262$, $R_{02} = 0.069$, $n = p = 3.55$
- d) $R_{01} = 0.36$, $R_{02} = 0.122$, $n = p = 3.55$

where $T_m = 1/f_m$

a transducer from PZT ceramics with two matching layers with acoustic impedances calculated according to the binomial criterion (a, c) and Czebyszew's formulae (b, d), and thickness equal to one fourth of wave length calculated for mechanical resonance frequency $\lambda_m/4$ (a, b) and electric resonance frequency λ_e (c, d). We can see that these parameters only slightly influence the pulse amplitude, while it has significant influence on its shape.

2.3. Compensating system

Usually a system which compensates the imaginary part of electric impedance or admittance is applied when designing ultrasonic probe. Most frequently the simplest system — a series or parallel coil — is used. However, in order to improve the pulse shape certain authors apply more complicated systems, such as the one shown in Fig. 1 for example. Parameters m , l , k are introduced in this system. Impedances of elements of the compensating system for these parameters are determined as follows

$$Z_{Lm} = k_l^2 x / \pi^2 m^2,$$

$$Z_{Ll} = k_l^2 x l^2 / \pi^2,$$

$$Z_{Ck} = k_l^2 / x k.$$

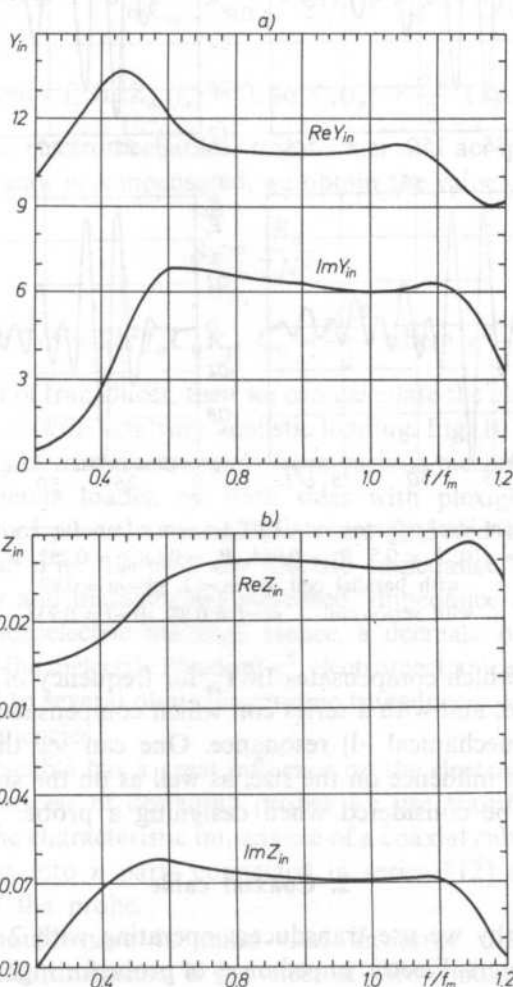


FIG. 7. Diagrams: a) — of relative input admittance Y_{in} , b) — of relative input impedance Z_{in} of transducer with two matching layers. $k_l = 0.5$, $R_h = 0.044$, $R_a = 0$, $R_{01} = 0.262$, $R_{02} = 0.069$, $n = p = 3.55$

The inductance of a parallel coil Z_m compensates the transducer clamped capacitance for frequency equal to mf_m , i.e. for transducer mechanical resonance $m = 1$, while for electric resonance $m = f_e/f_m$.

Figure 7 presents the admittance (a) and impedance (b) of a transducer from PZT I ceramics with matching layers, calculated according to the binomial criterion, with thickness equal to one fourth of wave length for electric resonance frequency. These diagrams were used to calculate parameters m and l .

In Fig. 8 we can see pulses reflected from an ideal reflector for a probe as in Fig. 7,

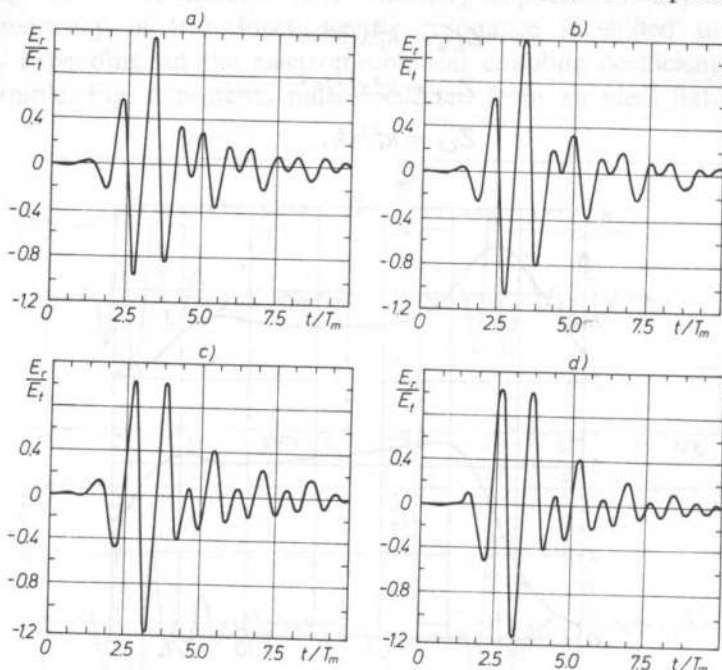


FIG. 8. Pulses reflected from ideal reflector for a PZT I ceramic transducer with two matching layers for excitation voltage $E_i = \delta(t)$, $k_t = 0.5$, $R_b = 0.044$, $R_a = 0$, $R_{01} = 0.262$, $R_{02} = 0.069$, $n = p = 3.55$
with parallel coil a) $-m = 1$, b) $-m = 0.89$
with series coil c) $-l = 0.98$, d) $-l = 0.938$

with a parallel coil which compensates $\text{Im}Y_{in}$ for frequency of a mechanical (a) and electric (b) resonance; and with a series coil which compensates $\text{Im}Z_{in}$ for frequency of electric (c) and mechanical (d) resonance. One can see that the compensating system has a distinct influence on the size, as well as on the shape, of the pulse and therefore it has to be considered when designing a probe.

2. Coaxial cable

In ultrasonography we use transducers operating with 2–10 MHz frequencies and 3–50 mm diameters. Electric impedances of probe for high frequencies and large diameters are equal to several ohms. Let us consider for example a transducer loaded symmetrically with acoustic impedance $R_B = A \rho_b c_b$ (Fig. 9).

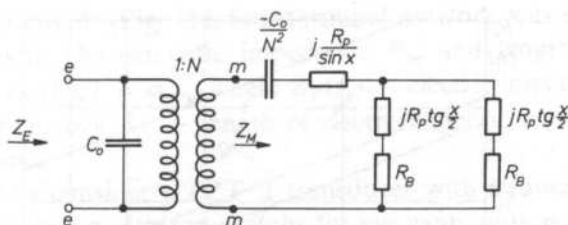


FIG. 9. Equivalent circuit of transducer loaded symmetrically with acoustic impedance R_B

The transducer mechanical impedance is then expressed by

$$Z_M = -j \frac{N^2}{\omega C_0} + j \frac{R_p}{\sin x} + \frac{1}{2} \left(j R_p \tan \frac{x}{2} + R_B \right).$$

For resonance frequency f_e $\text{Im } Z_M(f_e) = 0$, so $Z_M(f_e) = \frac{R_B}{2}$. Transposing all terms to the electric side of the electromechanical transformer and accepting the assumption that clamped capacitance is compensated, we obtain the value of electric impedance

$$R_E = \frac{R_B}{2 N^2}.$$

If we remember that $N^2 = 2k_t^2 f_m C_0 R_p$, $C_0 = \frac{A \varepsilon^S}{d}$ where ε^S — dielectric constant, $d = \lambda_m/2$ — thickness of transducer, then we can calculate the electric impedances for an arbitrary transducer with arbitrary acoustic loading. Fig. 10 presents diagrams of electric impedance R_E of transducers made from various piezoelectric materials with 5 and 20 mm diameters loaded on both sides with plexiglass ($\rho_b c_b = 3.2 \times 10^6$ kg/m²s). Parameters of piezoelectric materials are gathered in Table 1.

We can see from Fig. 10 that the electric impedance decreases when the transducer frequency and diameter are increased. Impedance is also influenced by parameters of the piezoelectric material. Hence, a decrease of impedance accompanies an increase of the dielectric constant ε^S , electromechanical coupling coefficient k_t . And so, it is equal to several ohms for ceramic transducers with 20 mm diameters and 5–10 MHz frequencies.

In these cases the cable has a great influence on the electric characteristic of the transducer. In the process of designing probes we use transformers matching the probe resistance to the characteristic impedance of a coaxial cable; or, sometimes, we divide the transducer into n parts connected in series [12] and obtain n^2 times greater resistance of the probe.

However, we should have in mind that an error may be made during measurements of such transducers, if the effect of wire conductors is not included. The influence of these conductors has to be also considered during the process of designing ultrasonic probes.

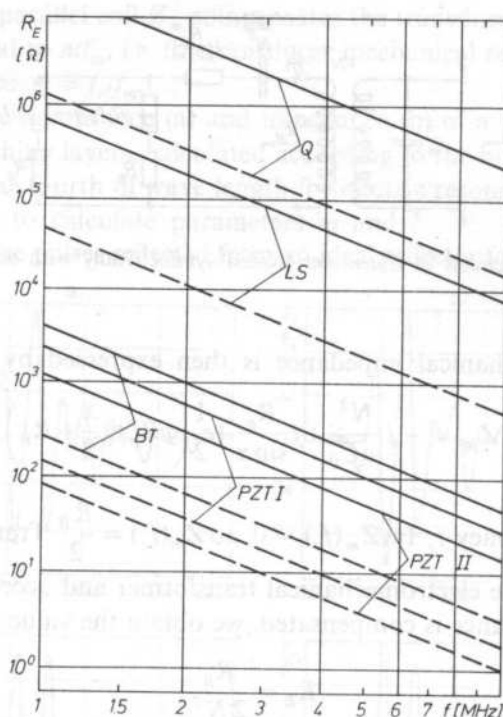


FIG. 10. Electric impedance of transducers loaded on both sides with plexiglass ($\rho_b c_b = 3.2 \cdot 10^6 \text{ kg/m}^2\text{s}$) in terms of their resonance frequencies (compensated clamped capacitance) Q — quartz, LS — lithium sulphate, BT — titaniabate ceramics, PZT I, PZT II — PZT type ceramics, full line — diameter of transducer — 5 mm, broken line — diameter of transducer — 20 mm

Table 1. Parameters of piezoelectric materials

Material		Density $\times 10^3 \text{ kg/m}^3$	Relative dielectric constant ϵ^s	Coupling coefficient k_t
Quartz	*	2.65	4.6	0.095
Lithium sulphate	*	2.06	10.3	0.38
Barium titanate	*	5.6	1200	0.3
PZT I	**	7.5	500	0.5
PZT II	**	7.5	500	0.7

* According to G. BRADFIELD, Ultrasonics 1970 [2].

** According to measurements of domestic ceramics prod. CERAD.

In the equivalent circuit (Fig. 1) a four-terminal network was included to define the coaxial cable with characteristic impedance R_{oc} and length l_c , expressed as follows: $R_{oc} = w_c R_e Z_E(f_e)$, $l_c = \varphi_c \lambda_{el}$ where $Z_E(f_e)$ — electric impedance of probe for electric resonance frequency, λ_{el} — length of electromagnetic wave in the cable, w_c and φ_c — coefficients.

For example let us consider a PZT II transducer with frequency $f_e = 10$ MHz, diameter 20 mm (applied in ultrasonographs for eye examinations), loaded on both sides with plexiglass. Electric impedance equal to $R_E = 1\Omega$ results from the diagram in Fig. 10. If we consider wire conductors as a long line with wave impedance of $R_{oc} = 300\Omega$ and $\lambda_{el} = 30$ m, then $w_c = 300$, $\varphi_c = 0.0005$ (for connectors with length $l_c = 1.5$ cm) and $\varphi_c = 0.0001$ (for $l_c = 3$ cm). It becomes clear that the cable influences the admittance value, as well as the shift of transducer resonance frequency (Fig. 11).

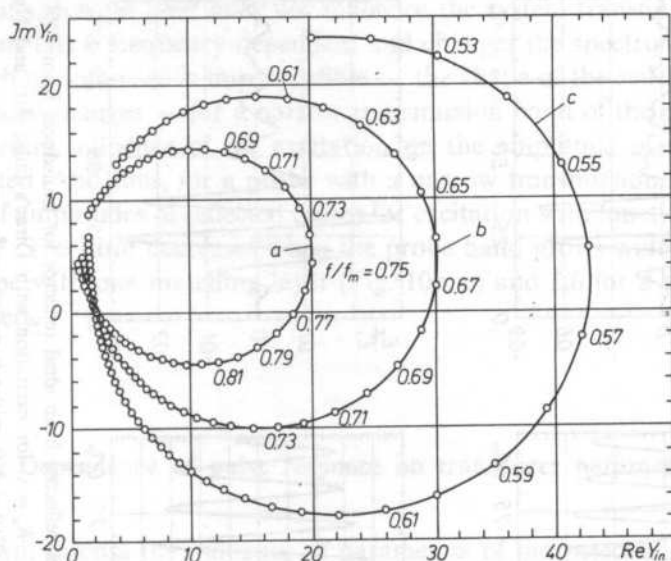


FIG. 11. Circles of relative input admittance of transducer from PZT II ceramics, with diameter equal to 20 mm and frequency equal to 10 MHz, loaded on both sides with plexiglass, $k_t = 0.7$, $R_a = R_b = 0.1$

- a) — without cable supply conductors,
 - b) — with cable $l_c = 1.5$ cm, $\varphi_c = 0.0005$, $w_c = 300$,
 - c) — with cable $l_c = 3$ cm, $\varphi_c = 0.001$, $w_c = 300$,
- f/f_m — parameter

3. Transmitting-receiving system

The design of the transmitting-receiving system and the transmitter, in particular, significantly influences the size and shape of the pulse transmitted, as well as the received pulse. However, it is much easier to use a simple system, such as in Fig. 1, in the process of designing ultrasonic probes. Here, the transmitter is presented as

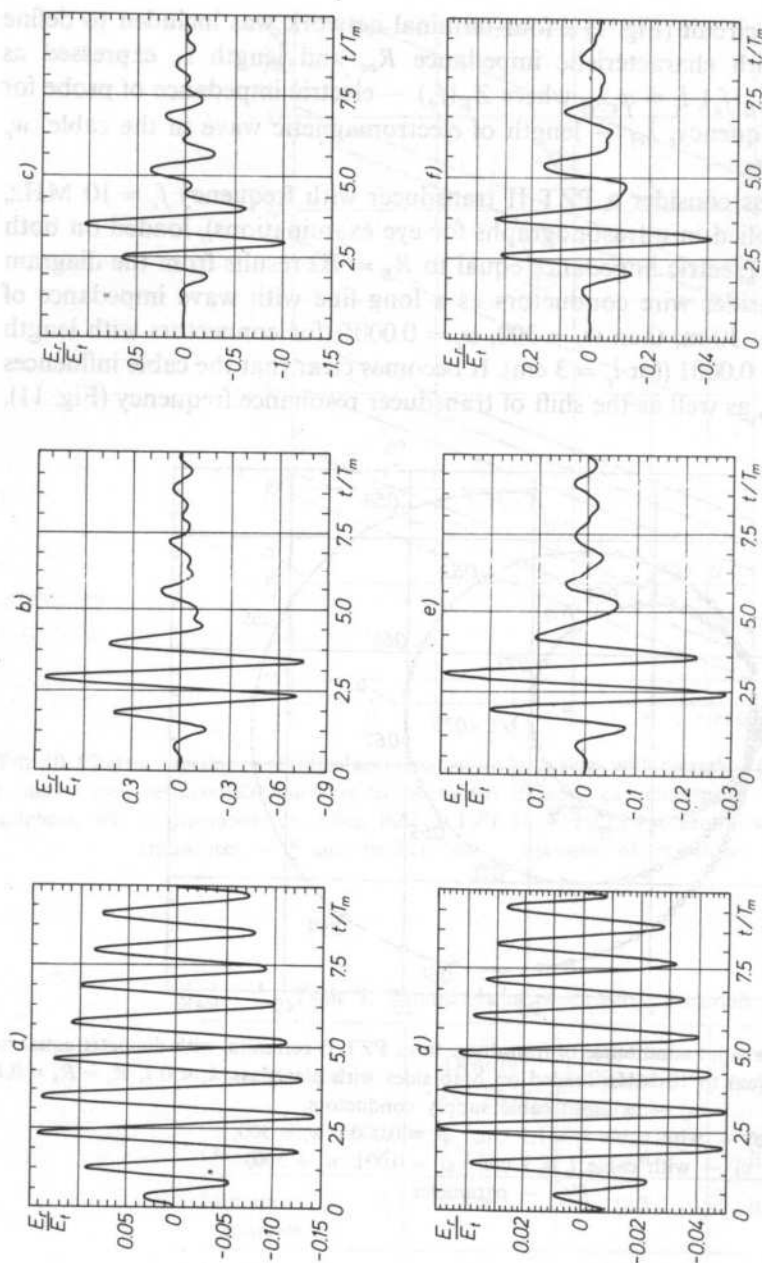


Fig. 12. Pulses reflected from ideal reflector for transducer from PZT I ceramics, $k_t = 0.5$, $R_b = 0.044$, $R_a = 0$ for excitation with Dirac's pulse $\delta(t)$ and Heaviside pulse $1(t)$

- a) — $E(t) = \delta(t)$, without matching layers
- b) — $E(t) = \delta(t)$, with one matching layer $R_{01} = 0.122$, $n = 3.55$
- c) — $E(t) = \delta(t)$, with two matching layers $R_{01} = 0.262$, $R_{02} = 0.069$, $n = p = 3.55$
- d) — $E(t) = 1(t)$ without layers
- e) — $E(t) = 1(t)$ with one layer $R_{01} = 0.122$, $n = 3.55$
- f) — $E(t) = 1(t)$ with two layers $R_{01} = 0.262$, $R_{02} = 0.069$, $n = p = 3.55$

source E_i' and resistance R_i' ; receiver as resistance R_r' , as it was described in Sect. 2. It is easier to design the ultrasonic probe, including the ratio of probe impedance to source and receiver impedance when electric quantities are transferred to the mechanical side of the electromechanical transformer.

The excitation voltage can be defined with any function containing Fourier's transform. Most frequently Heviside's function $1(t)$ or Dirac's function $\delta(t)$ with unitary amplitude is used in the course of designing probes. Figure 12 presents pulses reflected from an ideal reflector for a PZT I transducer with a parallel coil, without matching layers (a, d) with one matching layer (b, e) and with two matching layers (c, f), excited with voltage $\delta(t)$ (a, b, c) and $1(t)$ (d, e, f).

The application of matching layers widens the probe transmission band. This is why here we see a change of the reflected pulse shape (see Figs. 10b and 10e, 10c and 10f) depending on the used excitation voltage. This is justifiable because function $\delta(t)$ has a constant spectrum (and does not influence the system transmission function), while spectrum $1(t)$ is frequency-dependent and changes the spectrum of the system response. Such an influence is imperceptible — the shape of the reflected pulse does not undergo any changes — for a narrow transmission band of the probe (Fig. 10a, d). Also a certain influence of the excitation on the amplitude of reflected pulses should be noted. And thus, for a probe with a narrow transmission band (Fig. 10a, d), the ratio of amplitudes of reflected pulses for excitation with function $\delta(t)$ and $1(t)$ is equal to 2.8. The ratio decreases when the probe band grows wider. It is equal to 2.7 for a probe with one matching layer (Fig. 10b, e) and 2.6 for a probe with two matching layers.

4. Dependence of pulse response on transducer parameters

Here we will discuss the influence of parameters of piezoelectric materials, $q_p c_p$ and k_t on the shape and size of pulses reflected from an ideal reflector, for probes with and without matching layers, and with and without a parallel compensating coil. Transducers from PZT type ceramics lead metaniobate ceramics and quartz (only for comparison, because quartz is not used in ultrasonography due to difficulties with electric matching) were analysed.

The following assumptions were made to eliminate from discussion the influence of parameters of the transmitting-receiving system and matching layers:

- the excitation voltage is defined by Dirac's function $\delta(t)$
- $R_i = 0.01 \ 1/Re \ Y_{in}(x_e) \quad R_r = 10 \ 1/Re \ Y_{in}(x_e)$
- acoustic impedances of matching layers were calculated according to the binomial criterion
- the thickness of matching layers is equal to $1/4$ of wave length for electric resonance

- the inductance of the parallel coil compensates the imaginary part of the input admittance for electric resonance
- acoustic impedance of examined medium (soft tissue) $\varrho_b c_b = 1.5 \times 10^6 \text{ kg/m}^2\text{s}$
- the back surface of the transducer is not loaded ($R_a = 0$).

4.1. Reflected pulses, conclusions

The size of pulses for quartz is by an order of magnitude smaller than of those for ceramic materials in a case of transducers without matching layers and without a coil (Fig. 13a, b, c, d). The amplitude is first of all influenced by the electromechanical coupling coefficient k_t . With a parallel coil added (Fig. 13e, f, g, h), sizes of pulses for quartz and lead metaniobate ceramics are comparable, while for PZT ceramics they are twice as small and longer. This can be explained by better acoustic matching of quartz and lead metaniobate ceramics to the examined medium than in case of PZT.

For transducers with one matching layer and without a coil (Fig. 14a, b, c, d) the shortest pulse is observed for quartz. This is an evidence for very good acoustic matching. It is worth noting that the pulse amplitude for PZT II is four times larger than for lead metaniobate ceramics. This means that k_t has greater influence on the pulse size when transducers are acoustically matched. The attachment of a coil (Fig. 14e, f, g, h) has the greater effect, the smaller coefficient k_t is. For quartz the amplitude increases about 10 times yet the shape of the pulse worsens; for PZT II it practically does not change at all.

The application of two matching layers (Fig. 15) makes the amplitude smaller and worsens the pulse shape for quartz, hardly changes the pulse for lead metaniobate ceramics; increases the amplitude for PZT which has the greatest acoustic resistance. This is strictly related to acoustic matching of the transducer itself to the medium.

To sum up we can state that the pulse size and shape is influenced by the transducer acoustic resistance, as well as by the electromechanical coupling coefficient k_t . The choice of ceramics for the design of ultrasonic probes should depend on the possibility of electric matching (in ultrasonography frequency and, frequently, diameter of the transducer — and the electric impedance as a result — is imposed depending on the examined organ) and construction restrictions (greater difficulties with making two matching layers). However, it should be noted that largest amplitudes are achieved for PZT ceramics with two matching layers.

5. Conclusions

The proposed equivalent circuit of an ultrasonic probe with all quantities describing electric, as well as mechanical parameters of the transducer transferred to one side of the electromechanical transformer can be used to design probes, taking into account the influence of all of these quantities.

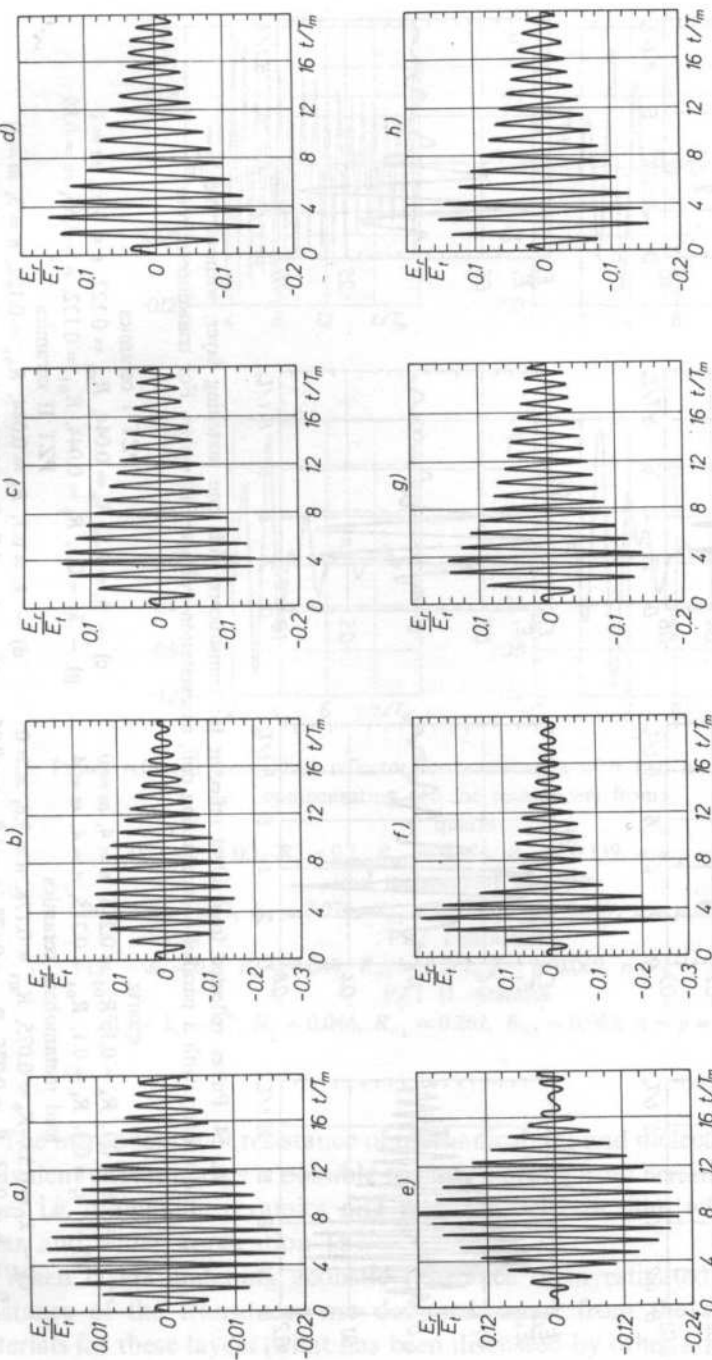


FIG. 13. Pulses reflected from ideal reflector for transducers without matching layers, without and adequately with a parallel compensating coil, at excitation voltage $E(t) = \delta(t)$. For transducers from:

PZT I ceramics transducers

- c) $-k_t = 0.5$, $R_b = 0.044$, $m = 0$
- g) $-k_t = 0.5$, $R_b = 0.044$, $m = 0.89$

PZT II ceramics transducers

- d) $-k_t = 0.7$, $R_b = 0.044$, $m = 0$
- h) $-k_t = 0.7$, $R_b = 0.044$, $m = 0.75$

quartz

- a) $-k_t = 0.1$, $R_b = 0.1$, $m = 0$
- e) $-k_t = 0.1$, $R_b = 0.1$, $m = 1$

lead metaniobate ceramics transducers

- b) $-k_t = 0.33$, $R_b = 0.075$, $m = 0$
- f) $-k_t = 0.33$, $R_b = 0.075$, $m = 0.95$

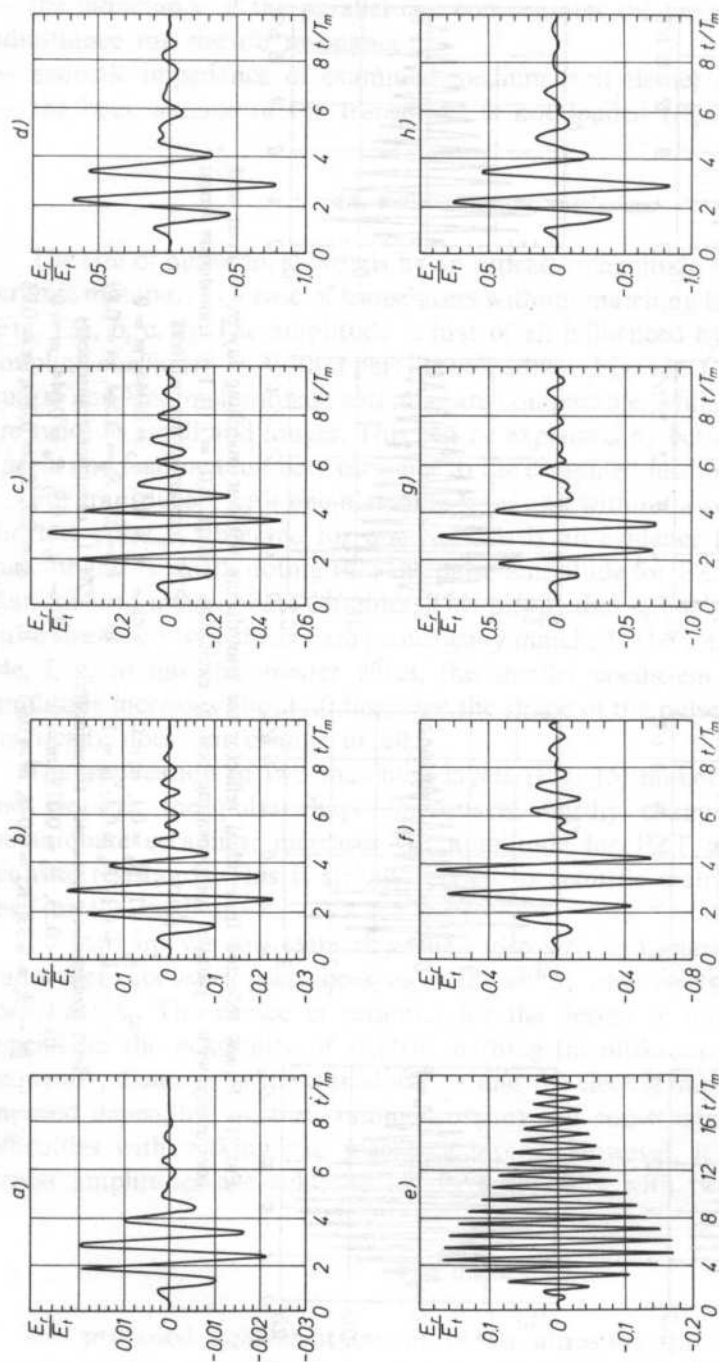


Fig. 14. Pulses reflected from ideal reflector for transducers with one matching layer, without and adequately with a parallel compensating coil, at excitation voltage $E(t) = \delta(t)$. For transducers from:

quartz

a) — $k_t = 0.1$, $R_b = 0.1$, $R_{01} = 0.215$, $n = 4$, $m = 0$

e) — $k_t = 0.1$, $R_b = 0.1$, $R_{01} = 0.215$, $n = 4$, $m = 4$

lead metaniobate ceramics

c) — $k_t = 0.33$, $R_b = 0.075$, $R_{01} = 0.178$, $n = 3.8$, $m = 0$

h) — $k_t = 0.33$, $R_b = 0.075$, $R_{01} = 0.178$, $n = 3.8$, $m = 0.95$

PZT I ceramics

c) — $k_t = 0.5$, $R_b = 0.044$, $R_{01} = 0.122$, $n = 3.55$, $m = 0$

g) — $k_t = 0.5$, $R_b = 0.044$, $R_{01} = 0.122$, $n = 3.55$, $m = 0.89$

PZT II ceramics

d) — $k_t = 0.7$, $R_b = 0.044$, $R_{01} = 0.122$, $n = 3$, $m = 0$

h) — $k_t = 0.7$, $R_b = 0.044$, $R_{01} = 0.122$, $n = 3$, $m = 0.75$

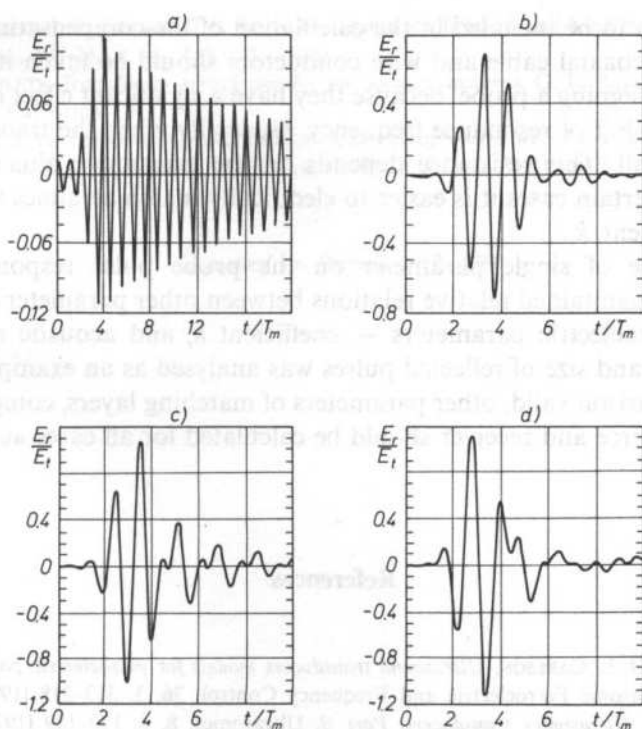


FIG. 15. Pulses reflected from ideal reflector for transducers with two matching layers and parallel compensating coil for transducers from:

quartz

a) — $k_t = 0.1$, $R_b = 0.1$, $R_{01} = 0.374$, $R_{02} = 0.139$, $n = p = 4$, $m = 1$

lead metaniobate ceramics

b) — $k_t = 0.33$, $R_b = 0.075$, $R_{01} = 0.329$, $R_{02} = 0.109$, $n = p = 3.8$, $m = 0.95$

PZT I ceramics

c) — $k_t = 0.5$, $R_b = 0.044$, $R_{01} = 0.262$, $R_{02} = 0.069$, $n = p = 3.55$, $m = 0.89$

PZT II ceramics

d) — $k_t = 0.7$, $R_b = 0.044$, $R_{01} = 0.262$, $R_{02} = 0.069$, $n = p = 3$, $m = 0.75$

The introduction of resistance of mechanical, R_m and dielectric losses, R_e , into the equivalent circuit makes it possible to design probe from ceramics with high internal losses i.e. niobianate ceramics and pvdf piezoelectric film which are now finding wider and wider application [6].

When layers matching acoustic resistance of investigated medium to acoustic resistance of the transducer are designed, apart from the selection of adequate materials for these layers (what has been discussed by other authors), the shift of the transducer electric resonance, depending on the electromechanical coupling coefficient k_p , has to be taken into account when the thickness of these layers is determined.

This shift has to be included in the calculation of the compensating system. The influence of the coaxial cable and wire conductors should be taken into account in the process of designing a probe, because they have a significant effect on the value of admittance and shift of resonance frequency, especially when the transducer electric resistance is small. This resistance depends on the transducer dimensions and its parameters. In certain cases it is easier to electrically match ceramics with a smaller, coupling coefficient k_t .

The influence of single parameter on the probe pulse response should be compared with maintained relative relations between other parameters. In this paper influence of piezoelectric parameters — coefficient k_t and acoustic resistance $\rho_p c_p$ — on the shape and size of reflected pulses was analysed as an example. In order to make this comparison valid, other parameters of matching layers, compensatory coil, resistances of source and receiver should be calculated for all cases according to the same formulae.

References

- [1] J. F. BROWN, D. L. CARLSON, *Ultrasound transducers models for piezoelectric polymer films*, IEEE Trans on Ultrasonic Ferroelectric and Frequency Control, **36**, 3, 313–318 (1989).
- [2] G. BRADFIELD, *Ultrasonics transducers, Part B*, Ultrasonics, **8**, 3, 177–189 (1970).
- [3] J. H. GOLL, *The design of broad-band fluid-loaded ultrasonic transducers*, IEEE Trans on Sonics and Ultrasonic, **SU-26**, 6, 385–393 (1979).
- [4] J. H. HUNT, M. ARDITI, F. S. FOSTER, *Ultrasound transducers for pulse-echo medical imaging*, IEEE Trans on Biomedical Engineering, **BME-30**, 8, 453–473 (1983).
- [5] T. INQUE, M. OHTA, S. TAKAHASHI, *Design of ultrasonic transducers with multiple acoustic matching layers for medical application*, IEEE Trans on Ultrasonics Ferroelectrics and Frequency Control **UFFC-34**, 1, 8–14 (1987).
- [6] V. P. JACKSON, E. KELLY-FRAY, P. A. ROTHSLD, R. W. HOLDEN, S. A. CLARC, *Automated breast sonography using a 7.5-MHz PVDF transducer: preliminary clinical evaluation*, Radiology **159**, 3, 679–684 (1986).
- [7] C. T. LANCEE J. SOUQUET, H. OHIGASHI, N. BOM, *Ferro-electric ceramics versus polymer piezoelectric materials*, Ultrasonics, **23**, 3, 138–142 (1986).
- [8] D. LEEDOM, H. KRIMHOLTZ, G. MATTHAEI, *Equivalent, circuits for transducers having arbitrary even-or odd-symetry piezoelectric excitation*, IEEE Trans **Su-18**, 128–141 (1971).
- [9] G. ŁYPACEWICZ, E. DURIASZ, *Application of one and two matching layers in ultrasonic medical probes (in Polish)*, Proc. IV Symposium "Hydroacoustics" W.Sz.M.W., Gdynia 1987, 177–184.
- [10] G. ŁYPACEWICZ, L. FILIPCZYŃSKI, *Measurements of the clamped capacitance C_0 and the electromechanical coupling coefficient k_t of piezoelectric ceramic transducers under mechanical load*, Acoustica, **25**, 1, 64–68 (1971).
- [11] G. ŁYPACEWICZ, E. DURIASZ, *Dependence of pulse response on parameters of transducer (in Polish)*, XXXV Open Seminar on Acoustics, 118–123, Warszawa 1989.
- [12] A. MARKIEWICZ, *Analysis of pulse transmitting receiving ultrasonic systems for medical diagnostics (in Polish)*, Doctor's thesis, IFTR PAS Warszawa 1978.
- [13] W. P. MASON, *Physical acoustics*, vol. 1 part A, Academic Press, New York 1964.
- [14] H. W. PERSSON, C. H. HERTZ, *Acoustic impedance matching of medical ultrasound transducers*, Ultrasonics **23**, 2, pp. 83–89 (1985).

- [15] C. S. DE SILETS, J. D. FRASER, G. S. KINO, *The design of efficient broad-band piezoelectric transducers*, IEEE Trans., SU-25, 3, pp. 115-125 (1988).
- [16] C. S. DE SILETS, *Transducers arrays suitable for acoustic imaging*, G. L. Report No 2833, Stanford University California 1978.
- [17] J. SOUQUET, P. H. DEFRANOULD and J. DESBOIS, *Design of lowloss wide band ultrasonic transducers for noninvasive medical application*, IEEE Trans. SU-26, 2, pp. 75-81 (1979).

Received on December 12, 1989

1. Introduction

It is well known that the Gaussian distribution of a group of independent random variables tends to a standard normal probability distribution as the number of random variables increases, not only in the domain, but also in the tails. In this paper, the authors will show that the Gaussian distribution is a good approximation for the probability of the sound intensity in the domain and in the tails. A new method will be presented to obtain the

UNIFICATION OF VARIOUS TYPE EXPRESSIONS FOR PROBABILITY DISTRIBUTION OF ARBITRARY RANDOM NOISE AND VIBRATION WAVES BASED ON THEIR ACTUAL FLUCTUATION RANGES (THEORY AND EXPERIMENT)

MITSUO OHTA*, NOBORU NAKASAKO**, YEGUI XIAO***

*Faculty of Engineering, Kinki University
5-1-3, Hiro-Koshinkai, Kure City, 737-01

**Dept. of Electrical Engineering, Hiroshima Institute of Technology
(725 Miyake, Itsukaichi-cho, Saiki-ku, Hiroshima 731-51 Japan)

***Faculty of Engineering, Hiroshima University
(Shitani, Saijo-cho, Higashi-Hiroshima City 724 Japan)

In the measurement of actual random phenomena, the observed data often result in a loss or a distortion of information due to the existence of a definite dynamic range of measurement equipments. In this paper, a unified expression of the fluctuation probability distribution for an environmental noise or vibration wave is proposed in an actual case when this wave has a finite range of amplitude fluctuation in itself or is measured through the usual instruments (e.g., sound level meter, level recorder, etc.) with a finite dynamic range. The resultant expression of the probability distribution function has been derived in a form of the statistical Jacobi series type expansion taking a Beta distribution as the 1st expansion term and Jacobi polynomial as the orthogonal polynomial. This unified probability expression contains the well-known statistical Gegenbauer series type probability expansion as a special case, and the statistical Laguerre and Hermite series type probability expansions as two special limiting cases. Finally, the validity of the proposed theory has been experimentally confirmed by applying to the actually observed data of a road traffic noise. This statistical Jacobi series expression shows good agreement with experimentally sampled points as compared with other types of statistical series expression.

1. Introduction

It is well-known that the Gaussian distribution is of essential importance as a standard type probability distribution expression of random noise or vibration, not only in the outdoor but also in the indoor acoustics. Moreover, not inferior to the Gaussian distribution, as a probability distribution for the fluctuation of the sound intensity — for instance in the diffused sound field, the Gamma distribution plays an

important role, as seen in the studies by WATERHOUSE [1], LUBMAN [2] and so forth [3, 4]. For the road traffic noise, the Gamma distribution is widely known as the distribution of sound intensity, the sound energy density or the distance between two vehicles (involving the Erlang distribution [5] as a special case). In general, the Gamma distribution can be employed as the first order approximation to the arbitrary type probability distribution expression of a positive random variable. However, the field of environmental noise or vibration seems to be more complex due to the physical, social and human psychological causes. So, in such a field, the observed random wave shows a complicated fluctuation pattern with arbitrary distribution forms apart from a usual Gaussian or Gamma distribution. Furthermore, in the actual observation, it very often happens that the recorded pattern of an objective random wave has a limited fluctuation amplitude domain owing to the dynamic range of measurement device — its probability distribution has to change naturally in its functional shape from an original one with non constrained amplitude fluctuation.

As is well-known, as the general type probability distribution expression for non-Gaussian and non-Gamma variables, the statistical Hermite expansion series type expression [6] including the well-known Gram-Charlier A type expansion [7] defined within a fluctuation domain $(-\infty, \infty)$ and taking the Gaussian distribution as the first expansion term, and the Laguerre one within a fluctuating domain $[0, \infty]$ and taking the Gamma distribution as the first expansion term have been not only theoretically proposed but also frequently applied to the indoor or outdoor actual sound or vibration environment. For example, as reported [1], when the input wave of sound pressure or vibration acceleration with the statistical Hermite type arbitrary distribution passes through the mean-squared circuit of sound level meter or vibration meter, the fluctuation of its output response wave can be described by the statistical Laguerre expansion series type probability expression.

The fluctuating amplitude of the actual phenomenon can not take every value within all parts of the theoretically defined ideal range $(-\infty, \infty)$ or $[0, \infty)$ but has some kind of limited fluctuation range. Additionally, its fluctuation range is usually constrained by the existence of dynamic range of measuring equipments. Therefore, when only the above two kinds of statistical Hermite or Laguerre type orthonormal expansion series type expressions are applied to the actual situations, there remains some discrepancy between theory and experiment, especially at the tips of the fluctuation amplitude (for example, corresponding to evaluation indices L_5 , L_{10} , L_{95} , L_{90} and so on). And, in case of using the theoretical expansion type expressions with no matching to the objective phenomena, many expansion terms had to be introduced for the purpose of reflecting the higher order moments directly connected with the tips of the fluctuation. From the above practical points of view, the limitation of amplitude should be actively introduced into the present theoretical consideration from the starting point of study and calls for a new distribution expression which involves the above two kinds of Hermite and Laguerre type probability expressions as two special cases.

In this paper, in order to obtain a better adaptation to the limitation of amplitude fluctuation and a wider application, it is more important in the actual sound or vibration environment to grasp more correctly the diversified fluctuation distribution forms of input, before considering the effect of various type characteristics of sound system itself. Thus, this study is first on how to find a new kind of unified probability distribution expression of the random fluctuation appearing in the complicated sound or vibration environment. More concretely, the unified probability density function is newly derived in a form of statistical Jacobi expansion series type expression (including the Gegenbauer expansion series type expression) taking the well-known Beta distribution as the first expansion term and the higher order moments as the Jacobi polynomial type statistics in each expansion coefficient. Finally, the effectiveness of the proposed method is experimentally confirmed by applying it to the digital simulation data and to the actually observed road traffic noise data.

2. Theoretical consideration

2.1. Probability density expression with the limitation of amplitude fluctuation range

2.1.1. A probability density expression in a unified form

Statistical Jacobi expansion series type. Now, an arbitrary variable X fluctuating only within a finite interval $[a, b]$ is taken into consideration. It is necessary to normalize the fluctuation range so as to investigate generally the influence of the limitation of the fluctuation amplitude on the resultant probability expression in a unified form. Hereupon, let us first pay attention to the variable fluctuating within the interval $[0, 1]$. Introducing an arbitrary weighting function $p(x)$ defined within the interval and the orthonormal polynomials based on $p(x)$, a probability density function (abbr., p.d.f) $P(x)$ can be expressed by the following distribution expansion

$$P(x) = \sum_{n=0}^{\infty} A_n p(x) \Phi_n^*(x), \quad (1)$$

where $\{\Phi_n^*(x)\}$ forms a complete set of orthonormal function with respect to $p(x)$

$$\int_0^1 \Phi_m^*(x) \Phi_n^*(x) p(x) dx = \delta_{mn}. \quad (2)$$

Then, by use of this relationship, every expansion coefficient can be immediately calculated in the following:

$$A_n \triangleq \langle \Phi_n^*(x) \rangle = \int_0^1 \Phi_n^*(x) P(x) dx, \quad (3)$$

where $\langle \cdot \rangle$ denotes the statistical averaging operation with respect to the distribution P . The weighting function $p(x)$ can be set arbitrarily in advance so as to satisfy the

following fundamental properties of p.d.f.

$$\int_0^1 p(x) dx = 1. \quad (4)$$

Since weighting function defined within $[0, 1]$, the well-known Beta distribution can be reasonably chosen,

$$p(x) = \frac{1}{B(\gamma, \alpha - \gamma + 1)} x^{\gamma-1} (1-x)^{\alpha-\gamma}, \quad (5)$$

$$B(p, q) \triangleq \int_0^1 t^{p-1} (1-t)^{q-1} dt \quad (6)$$

Then, from Eq. (2), the orthonormal function can be determined as

$$\Phi_n^*(x) = \sqrt{\frac{(\alpha+2n)\Gamma(\alpha-\gamma+1)\Gamma(\alpha+n)\Gamma(\gamma+n)}{\Gamma(\alpha+1)n!\Gamma(n+\alpha-\gamma+1)\Gamma(\gamma)}} G_n(\alpha, \gamma; x), \quad (7)$$

where $\Gamma(z)$ is the Gamma function and $G_n(\alpha, \gamma; x)$ is the Jacobi polynomial defined by:

$$G_n(\alpha, \gamma; x) \triangleq \frac{\Gamma(\gamma)}{\Gamma(\gamma+n)} x^{1-\gamma} (1-x)^{\gamma-\alpha} \left(\frac{d}{dx} \right)^n [x^{\gamma+n-1} (1-x)^{\alpha+n-\gamma}]. \quad (8)$$

The employment of Jacobi polynomial at the beginning of analysis brings some generality to the resultant expressions. That is, this Jacobi polynomial coincides with the other types of orthogonal polynomials, e.g., Gegenbauer polynomial, Legendre polynomial, Tchebycheff polynomial, etc., when α and γ take certain particular values. Consequently, substituting Eqs. (5) and (7) into Eq. (1), the p.d.f. for x is derived in a general form of the expansion series as:

$$P(x) = \frac{1}{B(\gamma, \alpha - \gamma + 1)} x^{\gamma-1} (1-x)^{\alpha-\gamma} \left\{ 1 + \sum_{n=1}^{\infty} A_n \sqrt{\frac{(\alpha+2n)\Gamma(\alpha-\gamma+1)\Gamma(\alpha+n)\Gamma(\gamma+n)}{\Gamma(\alpha+1)n!\Gamma(n+\alpha-\gamma+1)\Gamma(\gamma)}} \times G_n(\alpha, \gamma; x) \right\}. \quad (9)$$

From Eq. (3), the expansion coefficient A_n in the above expression can be immediately calculated by using from the 1st to the n th order moment statistics

$$A_n \triangleq \langle \Phi_n^*(x) \rangle = \sqrt{\frac{(\alpha+2n)\Gamma(\alpha-\gamma+1)\Gamma(\alpha+n)\Gamma(\gamma+n)}{\Gamma(\alpha+1)n!\Gamma(n+\alpha-\gamma+1)\Gamma(\gamma)}} \langle G_n(\alpha, \gamma; x) \rangle. \quad (10)$$

Thus, the p.d.f. of the variable x confined within a finite fluctuation range $[0, 1]$ is expressed by the orthonormal series with the Beta distribution being as the first term of expansion and with expansion coefficients which can be estimated through the statistics in the form of the empirical averages of consecutive Jacobi polynomials.

The use of Jacobi polynomials having two parameters α and γ is advantageous in expressing roughly the shape of the p.d.f. by lower order approximations because it is fundamentally important to catch first the statistical information on two lower order moments like the mean and variance. The dominant part of the expansion (9) can be reflected by few first terms due to the proper adjustment of these two parameters α and γ . It is easy to transform the above representation of p.d.f. with a normalized fluctuation interval $[0, 1]$ to the general case with an arbitrary fluctuation interval $[a, b]$ by means of a transformation of variables

$$x \triangleq (X-a)/(b-a). \quad (11)$$

Namely, the p.d.f. $P_x(X)$ of the actual variable X can be directly derived by using the measure-preserving transformation of probability:

$$P_x(X) = P(x) \left| \frac{dx}{dX} \right|_{x=(X-a)/(b-a)} = \sum_{n=0}^{\infty} A_n P_0(X) \Phi_n(X), \quad (12)$$

where

$$P_0(X) = \frac{1}{B(\gamma, \alpha - \gamma + 1)(b-a)^\alpha} (X-a)^{\gamma-1} (b-X)^{\alpha-\gamma}, \quad (13-a)$$

$$\begin{aligned} \Phi_n(X) &= \Phi_n^*(x) \Big|_{x=(X-a)/(b-a)} \\ &= \sqrt{\frac{(\alpha+2n)\Gamma(\alpha-\gamma+1)\Gamma(\alpha+n)\Gamma(\gamma+n)}{\Gamma(\alpha+1)n!\Gamma(n+\alpha-\gamma+1)\Gamma(\gamma)}} G_n\left(\alpha, \gamma; \frac{X-a}{b-a}\right), \end{aligned} \quad (13-b)$$

$$A_n = \sqrt{\frac{(\alpha+2n)\Gamma(\alpha-\gamma+1)\Gamma(\alpha+n)\Gamma(\gamma+n)}{\Gamma(\alpha+1)n!\Gamma(n+\alpha-\gamma+1)\Gamma(\gamma)}} \left\langle G_n\left(\alpha, \gamma; \frac{X-a}{b-a}\right) \right\rangle. \quad (13-c)$$

Here, it may be advantageous to impose the additional conditions $A_1 = A_2 = 0$ upon the expansion coefficients. These constants determine α and γ uniquely. The unknown parameters α, γ resulting from the above assumption can be explicitly determined by means of mean μ_x and variance σ_x^2 of the actually observed variable X , respectively, as follows (i.e. moment method):

$$\left. \begin{aligned} \alpha &= \frac{(\mu_x - a)(b - \mu_x)}{\sigma_x^2} - 2, \\ \gamma &= \frac{\mu_x - a}{b - a} \left\{ \frac{(\mu_x - a)(b - \mu_x)}{\sigma_x^2} - 1 \right\}. \end{aligned} \right\} \quad (14)$$

2.1.2 A probability density expression in a symmetrical form

Statistical Gegenbauer expansion series type. Let us consider a special case of choosing a p.d.f. symmetrical with respect to the center $(a+b)/2$ of the amplitude fluctuation interval. According to the above symmetrical property, two parameters $\alpha,$

γ must satisfy first the following relation

$$\alpha = 2\gamma - 1. \quad (15)$$

In order to investigate the effect of the symmetry on the resultant probability distribution form, let us introduce the following parameter

$$v = \gamma - 1/2 (v > -1/2). \quad (16)$$

[A] Eq. (13-a) as the first term of expansion series type expression in Eq. (12) can be transformed, as follows:

$$\begin{aligned} P_0(X) &= \frac{1}{B(v+1/2, v+1/2)(b-a)} \left(\frac{X-a}{b-a} \right)^{v-1/2} \left(1 - \frac{X-a}{b-a} \right)^{v-1/2} \\ &= \frac{1}{B(v+1/2, v+1/2)(b-a)/2 \cdot 2^{2v}} \left[1 - \left\{ \frac{X-(a+b)/2}{(b-a)/2} \right\}^2 \right]^{v-1/2}. \end{aligned} \quad (17)$$

Then, the duplication formula of Gamma function [8]:

$$\Gamma(2Y) = \frac{2^{2Y}}{2\sqrt{\pi}} \Gamma(Y) \Gamma(Y+1/2) \quad (18)$$

and equality $\Gamma(1/2) = \sqrt{\pi}$ give

$$B(v+1/2, v+1/2)2^{2v} = B(v+1/2, 1/2). \quad (19)$$

Substituting Eq. (19) into Eq. (17) leads to:

$$P_0(X) = \frac{1}{B(v+1/2, 1/2)(b-a)/2} \left[1 - \left\{ \frac{X-(a+b)/2}{(b-a)/2} \right\}^2 \right]^{v-1/2}. \quad (20)$$

[B] In the same way, Eq. (13-b) can be transformed by use of the above symmetrical property, and Eqs. (15) and (16).

$$\begin{aligned} \Phi_n(X) &= \sqrt{\frac{(2v+2n)\Gamma(v+1/2)\Gamma(2v+n)\Gamma(v+n+1/2)}{\Gamma(2v+1)n!\Gamma(n+v+1)\Gamma(v+1/2)}} G_n\left(2v, v+1/2; \frac{X-a}{b-a}\right) \\ &= (-1)^n \sqrt{\frac{2(v+n)n! [\Gamma(2v)]^2}{\Gamma(2v+1)\Gamma(2v+n)}} (-1)^n \frac{\Gamma(n+2v)}{n!\Gamma(2v)} \times \\ &\quad \times G_n\left(2v, v+1/2; \frac{1}{2} \left\{ 1 + \frac{X-(a+b)/2}{(b-a)/2} \right\} \right). \end{aligned} \quad (21)$$

Then, based on a relationship:

$$\frac{2[\Gamma(2v)]^2}{\Gamma(2v+1)} = B(v+1/2, 1/2) \frac{2^{2v-1} [\Gamma(v)]^2}{\pi}, \quad (22)$$

Eq. (21) can be rewritten as

$$\begin{aligned} \Phi_n(X) = & (-1)^n \sqrt{B(v+1/2, 1/2)} \frac{(v+n)n! 2^{2v-1} [\Gamma(v)]^2}{\pi \Gamma(2v+n)} \\ & \times (-1)^n \frac{\Gamma(n+2v)}{n! \Gamma(2v)} G_n \left(2v, v+1/2; \frac{1}{2} \left\{ 1 + \frac{X-(a+b)/2}{(b-a)/2} \right\} \right). \end{aligned} \quad (23)$$

In the sequel, by virtue of the relationship between Jacobi and Gegenbauer polynomials

$$(-1)^n \frac{\Gamma(n+2v)}{n! \Gamma(2v)} G_n \left(2v, v+1/2; \frac{1+x}{2} \right) = C_n^v(x), \quad (24)$$

the above $\Phi_n(X)$ can be finally expressed as follows:

$$\Phi_n(X) = (-1)^n \sqrt{B(v+1/2, 1/2)} \frac{(v+n)n! 2^{2v-1} [\Gamma(v)]^2}{\pi \Gamma(2v+n)} C_n^v \left(\frac{X-(a+b)/2}{(b-a)/2} \right), \quad (25)$$

where $C_n^v(X)$ is the Gegenbauer polynomial.

[C] The expansion coefficient A_n can also be immediately calculated by the statistics:

$$A_n \triangleq \langle \Phi_n(X) \rangle = (-1)^n \sqrt{\frac{B(v+1/2, 1/2)(v+n)n! 2^{2v-1} [\Gamma(v)]^2}{\pi \Gamma(2v+n)}} \langle C_n^v \left(\frac{X-(a+b)/2}{(b-a)/2} \right) \rangle. \quad (26)$$

Thus, the p.d.f. of the random variable X with an arbitrary fluctuation amplitude $[a, b]$ is given by the following expression in the form of the statistical Gegenbauer expansion series:

$$\begin{aligned} P(X) = & \frac{1}{B(v+1/2, 1/2)(b-a)/2} \left[1 - \left\{ \frac{X-(a+b)/2}{(b-a)/2} \right\}^2 \right]^{v-1/2} \left\{ 1 + \sum_{n=1}^{\infty} A_n \times \right. \\ & \left. \times (-1)^n \sqrt{\frac{B(v+1/2, 1/2)(v+n)n! 2^{2v-1} [\Gamma(v)]^2}{\pi \Gamma(2v+n)}} C_n^v \left(\frac{X-(a+b)/2}{(b-a)/2} \right) \right\}. \end{aligned} \quad (27)$$

And, from Eq. (14), the mean and the variance are expressed respectively as follows:

$$\mu_x = (a+b)/2, \quad \sigma_x^2 = \left(\frac{b-a}{2} \right)^2 \frac{1}{2(v+1)}. \quad (28)$$

2.2. Probability density expression with an infinite amplitude fluctuation range

Connection with the well-known generalized p.d.f. expressions. As is well-known, the standard Gaussian distribution with amplitude domain $(-\infty, \infty)$ has been applied to many kinds of statistical problems on the random waves. With the same fluctuation domain, the statistical Hermite expansion series type expression (for instance, the Gram-Charlier A type of expansion expression) has been used to

express an arbitrary distribution expression of non-Gaussian type. In the field of environmental noise or vibration, the above generalized distribution expression and approximately its first expansion term, the Gaussian distribution, have been both very frequently used to describe the p.d.f. of the sound pressure, vibration acceleration and/or level fluctuation. On the other hand, there is a generalized statistical Laguerre expansion series type expression for the random waves fluctuating only within a positive interval $[0, \infty)$ (e.g., the energy fluctuation in the same field), whose first term of expansion is the Gamma distribution. Even though it seems apparently true that the infinite domain $(-\infty, \infty)$ involves domain $[0, \infty)$ and a finite one $[a, b]$, the distribution expression, which is defined within the domain $[a, b]$ and reflects much more strictness of restrictions in theoretical analysis, can contain the probability expression defined within $(-\infty, \infty)$ or $[0, \infty)$ as two special cases where the restrictions are loosened. Therefore, the probability density expression in Eqs. (12), (13) or (27) must agree as special cases with the statistical Hermite and statistical Laguerre expansion series type expressions previously reported. Through such a theoretical consideration, the validity of the proposed expression can be shown within the theoretical extent as follows:

2.2.1. Relation to the statistical Hermite series expansion type expression. First, let us consider the usual case when the random variable originally fluctuates freely in both positive and negative intervals $(-\infty, \infty)$ under no constraint of amplitude limitation, and first focus on the statistical Gegenbauer series type expression of Eq. (27) having a symmetrical property with respect to the center of the fluctuation domain.

By solving Eq. (28) with respect to a and b , the following relationship can be derived.

$$\begin{aligned} a &= \mu_x - \sqrt{2(v+1)}\sigma_x, \\ b &= \mu_x + \sqrt{2(v+1)}\sigma_x. \end{aligned} \quad (29)$$

Substituting Eq. (29) into Eqs. (20), (25) and (26), the first expansion term $P_0(X)$, the orthogonal polynomial $\Phi_n(X)$ and the expansion coefficient A_n could be rewritten respectively as follows:

$$P_0(X) = \frac{1}{\sqrt{2\pi}\sigma_x} \frac{\Gamma(v)}{\Gamma(v+1/2)\sqrt{v+1}} \left[1 - \frac{(X-\mu_x)^2/2\sigma_x^2}{v+1} \right]^{v+1-3/2}, \quad (30-a)$$

$$\Phi_n(X) = (-1)^n \sqrt{B(v+1/2, 1/2)} \frac{(v+n)! 2^{2v-1} [\Gamma(v)]^2}{\pi \Gamma(2v+n)} C_n^v \left(\frac{X-\mu_x}{\sqrt{2(v+1)}\sigma_x} \right), \quad (30-b)$$

$$A_n = (-1)^n \sqrt{B(v+1/2, 1/2)} \frac{(v+n)! 2^{2v-1} [\Gamma(v)]^2}{\pi \Gamma(2v+n)} \left\langle C_n^v \left(\frac{X-\mu_x}{\sqrt{2(v+1)}\sigma_x} \right) \right\rangle. \quad (30-c)$$

Here, the limiting case with no amplitude constraint: $a \rightarrow -\infty$ and $b \rightarrow \infty$ can be obtained in the case when $v \rightarrow \infty$ (from Eq. (29)).

[A] First of all, let us consider $P_0(X)$. From the Stirling's formula [8]:

$$\Gamma(v) \sim \sqrt{2\pi} e^{-v} v^{v-1/2} (v \rightarrow \infty), \quad (31)$$

the following relationship can be derived.

$$\frac{v\Gamma(v)}{\Gamma(v+1/2)\sqrt{v+1}} \sim 1 \quad (v \rightarrow \infty). \quad (32)$$

Furthermore, the well-known property $(1+1/y)^y \rightarrow e$ ($y \rightarrow \infty$) gives

$$\left[1 - \frac{(X - \mu_x)^2 / 2\sigma_x^2}{v+1}\right]^{v+1-3/2} \rightarrow e^{-(x-\mu_x)^2/2\sigma_x^2} (v \rightarrow \infty). \quad (33)$$

When $v \rightarrow \infty$, the first expansion term $P_0(X)$ asymptotically approaches to the Gaussian distribution with mean μ_x and variance σ_x^2 .

$$P_0(X) = \frac{1}{\sqrt{2\pi}\sigma_x} e^{-(x-\mu_x)^2/2\sigma_x^2}. \quad (34)$$

[B] $\Phi_n(X)$ in Eq. (30-b) can be rewritten as follows:

$$\Phi_n(X) = \frac{(-1)^n}{\sqrt{n!}} \sqrt{\frac{\Gamma(v+1/2)\sqrt{\pi}(v+n)2^{2v-1}[\Gamma(v)]^2}{\Gamma(v+1)\pi\Gamma(n+2v)(2v)^{-n}}} n!(2v)^{-n/2} C_n^v\left(\frac{X-\mu_x}{\sqrt{2(v+1)}\sigma_x}\right). \quad (35)$$

Using the relationship:

$$\frac{\Gamma(v+1/2)\sqrt{\pi}(v+n)2^{2v-1}[\Gamma(v)]^2}{\Gamma(v+1)\pi\Gamma(n+2v)(2v)^{-n}} \rightarrow 1 (v \rightarrow \infty) \quad (36)$$

and considering the limiting property related to Hermite polynomial $H_n(\cdot)$:

$$n!(2v)^{-n/2} C_n^v\left(\frac{X-\mu_x}{\sqrt{2(v+1)}\sigma_x}\right) \rightarrow H_n\left(\frac{X-\mu_x}{\sigma_x}\right) (v \rightarrow \infty), \quad (37)$$

the orthonormal polynomial $\Phi_n(X)$ in Eq. (35) asymptotically changes as:

$$\Phi_n(X) = \frac{(-1)^n}{\sqrt{n!}} H_n\left(\frac{X-\mu_x}{\sigma_x}\right). \quad (38)$$

[C] Through the same asymptotical procedure as in Eq. (37), the expansion coefficient can be also rewritten as follows:

$$A_n = \frac{(-1)^n}{\sqrt{n!}} \left\langle H_n\left(\frac{X-\mu_x}{\sigma_x}\right) \right\rangle. \quad (39)$$

Therefore, by use of the asymptotical relationships of Eqs. (34), (38) and (39), it could be proved that the statistical Gegenbauer expansion series type expression completely agrees with the well-known statistical Hermite expansion series type

expression defined within $(-\infty, \infty)$. From the proof process, it can be easily noticed that if the values of μ_x and σ_x^2 are employed as arbitrary parameters in advance, Eq. (14), of course, is not necessary to be satisfied (when μ_x and σ_x^2 are adopted as the mean and the variance of X respectively under the conditions $A_1 = A_2 = 0$, the statistical Hermite expansion series type expression could coincide with the Gram-Charlier A series type expression).

2.2.2. Relation to the statistical Laguerre series expansion type expression. By introducing two kinds of new parameters m and s satisfying the relationships: $\gamma = m$, $a = 0$, $b = \alpha s$, Eqs. (13-a), (13-b) and (13-c) can be rewritten as:

$$P_0(X) = \frac{1}{B(m, \alpha - m + 1) \alpha s} \left(\frac{X}{\alpha s} \right)^{m-1} \left(1 - \frac{X}{\alpha s} \right)^{\alpha - m}, \quad (40-a)$$

$$\Phi_n(X) = \sqrt{\frac{\Gamma(\alpha - m + 1)(\alpha + 2n) \Gamma(\alpha + n) \Gamma(m + n)}{\Gamma(\alpha + 1) n! \Gamma(n + \alpha - m + 1) \Gamma(m)}} G_n(\alpha, m; X/\alpha s), \quad (40-b)$$

$$A_n = \sqrt{\frac{\Gamma(\alpha - m + 1)(\alpha + 2n) \Gamma(\alpha + n) \Gamma(m + n)}{\Gamma(\alpha + 1) n! \Gamma(n + \alpha - m + 1) \Gamma(m)}} \left\langle G_n(\alpha, m; X/\alpha s) \right\rangle. \quad (40-c)$$

[A] First, we pay our attention to $P_0(X)$ and rewrite Eq. (40-a) as:

$$P_0(X) = \frac{\Gamma(\alpha + 1)}{\Gamma(\alpha - m + 1) \alpha^m \Gamma(m) s^m} \left(1 - \frac{X}{\alpha s} \right)^{\alpha - m}. \quad (41)$$

By using the Stirling's formula, the coefficient in Eq. (41) becomes

$$\frac{\Gamma(\alpha + 1)}{\Gamma(\alpha - m + 1) \alpha^m} \sim 1. \quad (42)$$

Therefore, the first term of expansion in Eq. (12) approaches asymptotically to the well-known Gamma distribution when $\alpha \rightarrow \infty$

$$P_0(X) = \frac{X^{m-1}}{\Gamma(m) s^m} e^{-X/s}. \quad (43)$$

[B] Secondly, Eq. (40-b) can be rewritten as

$$\Phi_n(X) = \sqrt{\frac{\Gamma(m) n! \Gamma(\alpha - m + 1)(\alpha + 2n) \Gamma(\alpha + n) \Gamma(m + n)}{\Gamma(m + n) \Gamma(\alpha + 1) \Gamma(n + \alpha - m + 1) n! \Gamma(m)}} G_n(\alpha, m; X/\alpha s). \quad (44)$$

Considering the asymptotical relationship:

$$\frac{\Gamma(\alpha - m + 1)(\alpha + 2n) \Gamma(\alpha + n)}{\Gamma(\alpha + 1) \Gamma(n + \alpha - m + 1)} \rightarrow 1 (\alpha \rightarrow \infty) \quad (45)$$

and the limiting property related to a Laguerre polynomial $L_n^{(m-1)}(\cdot)$:

$$\frac{\Gamma(m+n)}{n! \Gamma(m)} G_n(\alpha, m; X/\alpha s) \rightarrow L_n^{(m-1)}(X/s) (\alpha \rightarrow \infty), \quad (46)$$

Eq. (44) becomes

$$\Phi_n(X) = \sqrt{\frac{\Gamma(m)n!}{\Gamma(m+n)}} L_n^{(m-1)}(X/s). \quad (47)$$

[C] Through the same asymptotical procedure as in the previous orthonormal polynomial, the expansion coefficient can be also rewritten as follows when $\alpha \rightarrow \infty$.

$$A_n = \sqrt{\frac{\Gamma(m)n!}{\Gamma(m+n)}} \langle L_n^{(m-1)}(X/s) \rangle. \quad (48)$$

Therefore, the statistical Jacobi expansion series type expression in Eq. (12) agrees completely with the well-known statistical Laguerre one in the asymptotic case when $\alpha \rightarrow \infty$.

3. Experimental consideration

In the actual field of noise or vibration the statistical Hermite and Laguerre expansion series type expression are very often used as the p.d.f. for many kinds of random fluctuations, e.g. the road traffic noise or vibration, the sound pressure level and the sound intensity in a room. Accordingly, many results reported in the previous papers by applying the statistical Hermite and Laguerre expansion series type expressions to the actual environment can also be recognized as the experimental confirmation of the proposed method. In this paper, through the experimental results on the application to the actual data, it has been confirmed that the statistical Jacobi expansion series type expression is best matched to the actual phenomena with constraint of their fluctuating amplitude limitation. First of all, the effectiveness of the statistical Gegenbauer expansion series type expression has been confirmed by means of the digital simulation technique. Then, the statistical Jacobi expansion series type expression has been applied to the actually observed road traffic noise.

3.1. Digital simulation

In this section, the proposed Gegenbauer expansion series type expression (a special case of the Jacobi expansion series type expression) is experimentally compared with the well-known statistical Hermite expansion series type expression.

[i] Establishment of random model (a distribution with axial symmetry)

In order to investigate how the limitation of fluctuating amplitude interval affects

the resultant p.d.f., the saturating non-linear system

$$X = \begin{cases} \frac{s}{A} U(|U| < A), \\ s \cdot \text{sgn } U(|U| \geq A), \end{cases} \quad (49)$$

is adopted as the random where U is an idealized "true" value and X is the observed model. Concretely, the nonlinear property of this system is changed by selecting a threshold value A as 0.25, 1.0 and so on.

As a random system input U , the following four cases have been adopted:

Case A normal random numbers (mean = 0, variance = 1);

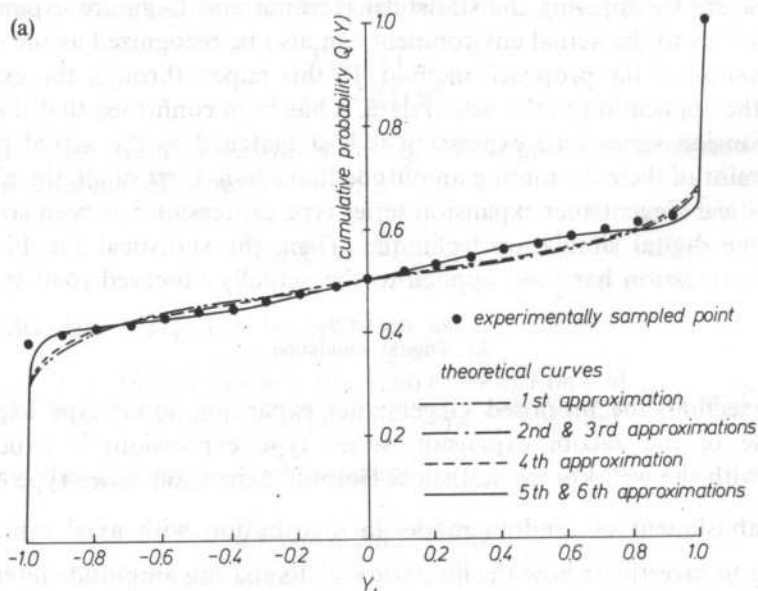
Case B (as a model reflecting the actual situation to some extent) a sum of normal random numbers (mean = 0, variance = 0.25) and a sine wave with amplitude 1 and frequency 10;

Case C (as an extreme example of non-Gaussian input) random numbers uniformly distributed within $[-2, 2]$;

Case D the same random input as in Case C and a sine wave with amplitude 1 and frequency 10.

[ii] Experimental results and discussions

Figure 1 (a) shows a comparison between the cumulative distribution function $Q(Y) = \left(\int_{-\infty}^Y P(Y) dY \right)$ of Gegenbauer expansion series type expression and experimentally sampled points for Case D. The abscissa has been normalized by $Y = \{X - (a+b)/2\} / \{(b-a)/2\}$. The deviation $\varepsilon(Y)$ of the cumulative probability distribution from a Beta distribution is shown in Fig. 1 (b). From these figures, it is



obvious that the successive addition of higher order expansion terms moves theoretical curves close to the experimentally sampled points. Fig. 1 (c) shows the result of the Hermite expansion series type expression applied to the same experimental data. As for the saturated nonlinear phenomenon, these experimental results obviously clarify that the proposed Gegenbauer expansion series type

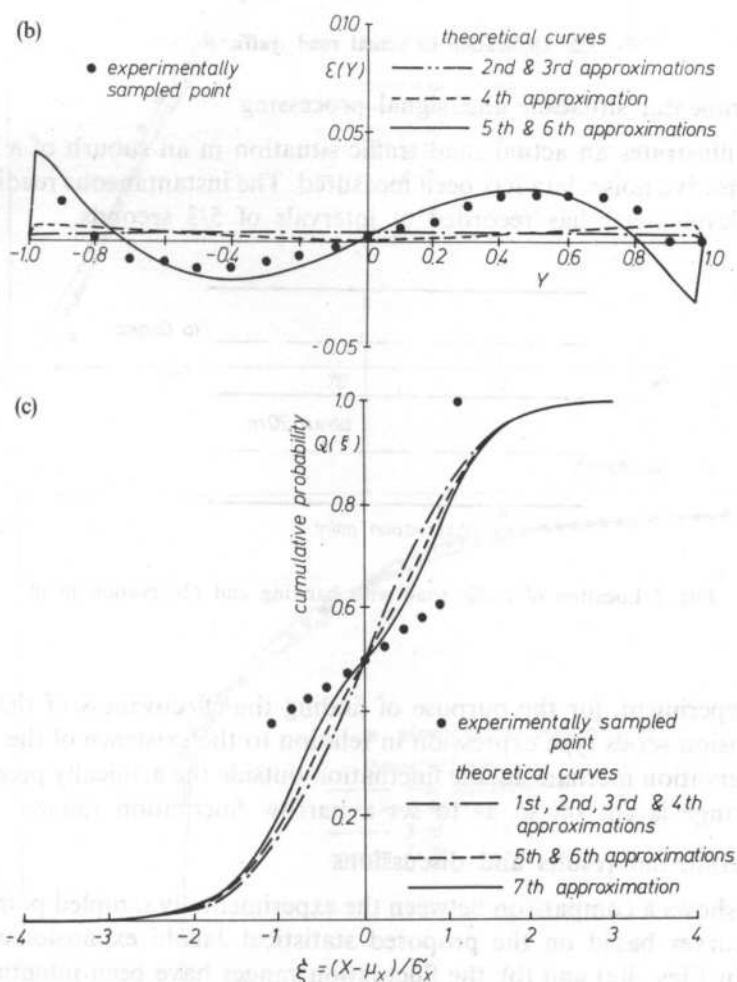


FIG. 1. A comparison between theory and experiment for a Case D ($A = 0.25$, $v = -0.395$)

FIG. 1(a) comparison between theoretical curves and experimentally sampled points for cumulative distribution function ($A_1 = 1.26 \times 10^{-2}$, $A_2 = 0.0$, $A_3 = 4.09 \times 10^{-1}$, $A_4 = -6.8$, $A_5 = -2.65 \times 10^{-1}$)

FIG. 1(b) comparison between theoretical curves and experimentally sampled points for deviation $\varepsilon(Y)$ from the Beta distribution

FIG. 1(c) comparison between theoretical curves of the statistical Hermite series expansion type and experimentally sampled points for cumulative probability distribution ($A_1 = A_2 = 0.0$, $A_3 = 1.8 \times 10^{-2}$, $A_4 = -7.7 \times 10^{-2}$, $A_5 = -6.4 \times 10^{-4}$, $A_6 = 1.9 \times 10^{-2}$)

expression has more flexibility necessary for applications than the well-used Hermite expansion series type expression.

Results for the other cases cited in [i] which have also given a good agreement between theory and experiment have been omitted.

3.2. Application to actual road traffic noise

[i] Experimental situation and signal processing

Figure 2 illustrates an actual road traffic situation in an suburb of a large city, where the objective noise data has been measured. The instantaneous reading (in dB) of a sound level meter has recorded at intervals of $5/3$ seconds.

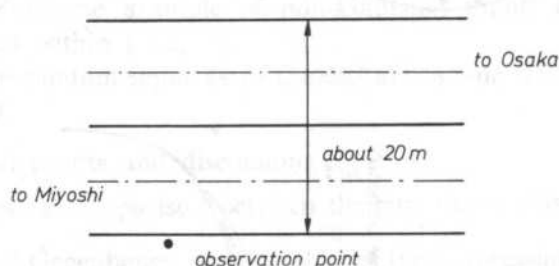


FIG. 2 Location of traffic road with banking and observation point

In this experiment, for the purpose of finding the effectiveness of the proposed Jacobi expansion series type expression in relation to the existence of the dynamical range of observation mechanism, the fluctuation outside the artificially preestablished dynamical range is cut off so as to set a narrow fluctuation range.

[ii] Experimental results and discussions

Figure 3 shows a comparison between the experimentally sampled points and the theoretical curves based on the proposed statistical Jacobi expansion series type expression. In Figs. 3(a) and (b), the fluctuation ranges have been intentionally and artificially set as $[50, 100]$ and $[60, 90]$ (dBA), respectively, to confirm the actual effectiveness of the proposed method.

Figure 4 shows a comparison between the experimentally sampled points and the theoretical curves based on the statistical Jacobi, Hermite and Laguerre expansion series type expressions. The fluctuation range has been purposely confined within $[50, 100]$ (dBA) in advance and all of the theoretical curves have been drawn by employing the first 3 expansion terms. From Fig. 4, though the noise level completely fluctuates only within the preestablished range, it can be easily found that the

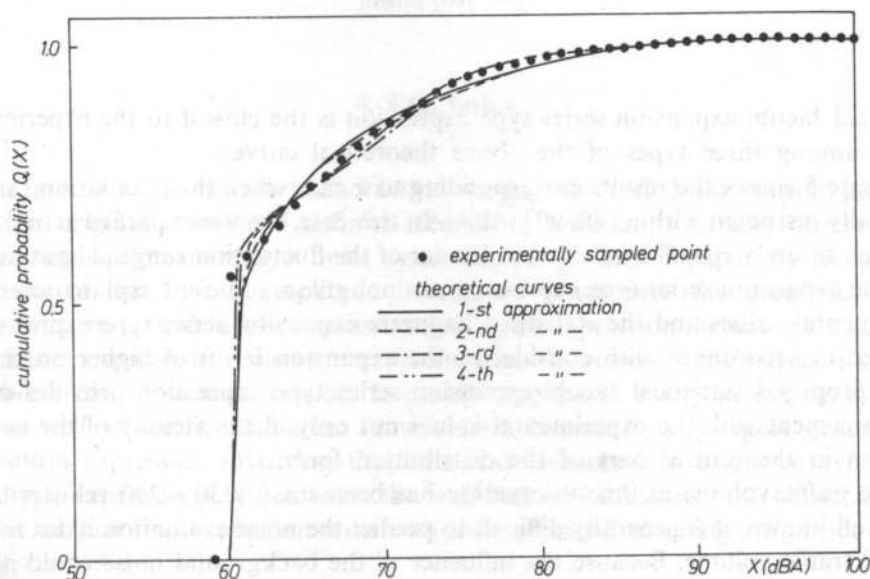
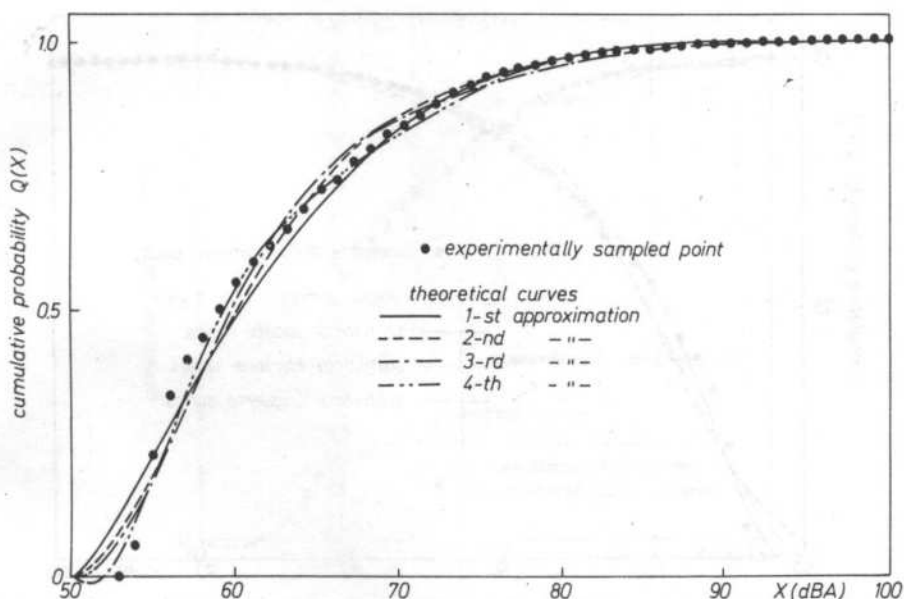


FIG. 3. A comparison between the experimentally sampled points and the theoretical curves based on the proposed statistical Jacobi expansion series type probability expression

FIG. 3(a) a case with a fluctuation domain [50, 100] (dBA)

FIG. 3(b) a case with a fluctuation domain [60, 90] (dBA)

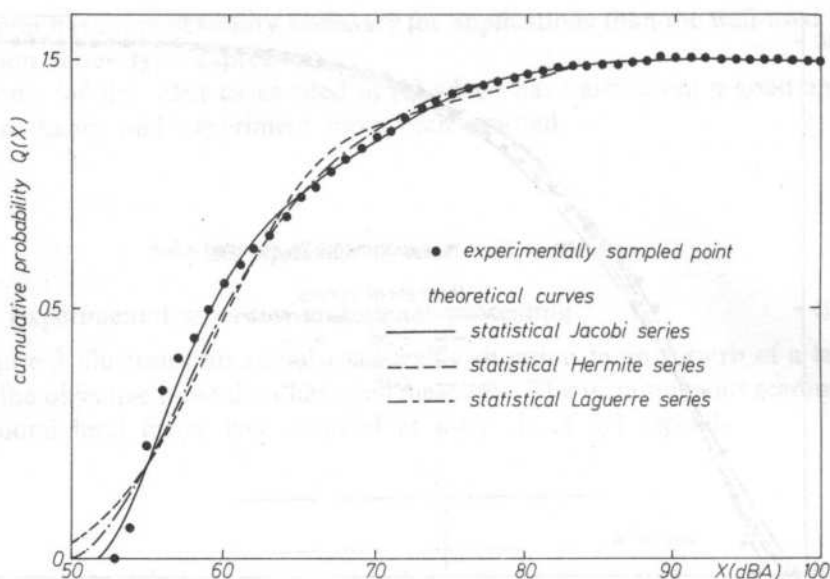


FIG. 4. A comparison between three types of series expansion expression and experimentally sampled points for cumulative probability distribution for an actual road traffic noise (the fluctuation domain is [50, 100] (dBA))

statistical Jacobi expansion series type expression is the closest to the experimental values among three types of the above theoretical curves.

Figure 5 shows the results corresponding to a case when the fluctuation range is artificially restricted within [60, 90] (dBA). In this case, the lower part of actual wave has been severely cut off by the lower border of the fluctuation range. The statistical Hermite expansion series type expression can not give a sufficient explanation of the experimental values and the statistical Laguerre expansion series type expression is diverged in accordance with considering the expansion terms of higher order. The newly proposed statistical Jacobi expansion series type expression provides us the best agreement with the experimental values not only in the vicinity of the borders but also in the central part of the distribution form.

The traffic volume in this observation has been small (230 ~ 240 vehicles/hour). As is well-known, it is generally difficult to predict the noise evaluation index in such a small traffic volume. Because the influence of the background noise could not be neglected, the cumulative level distribution has shown a rapid ascent and it is very difficult to make a sufficient approximation by means of only the usual Gaussian distribution. However, since the proposed unified expression involves originally the statistical Hermite and Laguerre expansion series type expressions as special cases, there is no doubt that the statistical Jacobi expansion series type expression can be sufficiently applied to the situation of large traffic volume too.

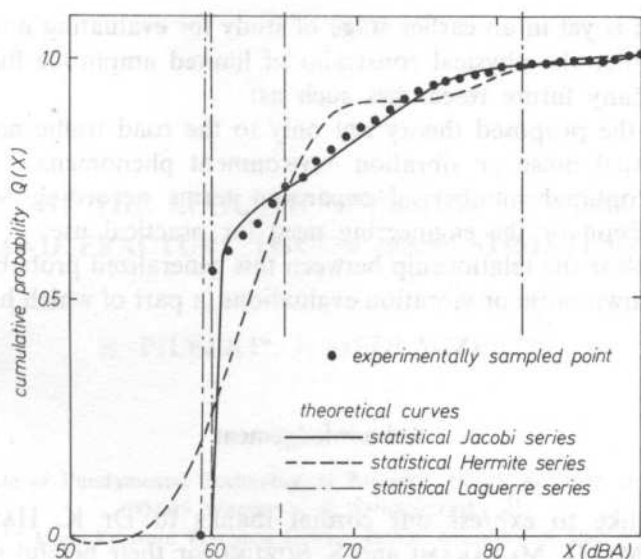


FIG. 5 A comparison between three types of series expansion expression and experimentally sampled points for cumulative probability distribution for an actual road traffic noise (the fluctuation domain is [60, 90] (dBA))

4. Conclusion

The actual environment phenomenon having diversified fluctuation patterns fluctuates originally within a definite interval in itself or is usually observed by a measuring equipment with a finite dynamical range. In this paper, by taking this constraint of the limited amplitude fluctuation range into the theoretical consideration, a statistical Jacobi expansion series type expression including a statistical Gegenbauer expansion series type expression has been newly derived as a unified probability distribution expression. It can be applied to many actual engineering fields as well as the field of noise or vibration, because it is a highly generalized distribution expression involving the statistical Hermite and Laguerre expansion series type expressions which take the well-known Gaussian and Gamma distribution as their first expansion term with their proper fluctuating amplitude range $(-\infty, \infty)$ and $[0, \infty)$.

To confirm the validity of the proposed theory, a digital simulation technique has been applied by employing the random numbers having axial symmetry. Then, the proposed theory has been also applied to the actual road traffic noise which can be poorly approximated by the ordinary Gaussian distribution in case of small traffic volume. The proposed theory has shown a good agreement with the experiment, in comparison with all the previously reported evaluation methods.

This research is yet in an earlier stage of study for evaluating noise or vibration environment under the physical constraint of limited amplitude fluctuation. Thus there remain many future researches such as:

- 1) to apply the proposed theory not only to the road traffic noise but also to many other actual noise or vibration environment phenomena;
- 2) to find optimal number of expansion terms according to the required prediction precision or the engineering need for practical use;
- 3) to make clear the relationship between this generalized probability expression and the well-known noise or vibration evaluations (a part of which has been already presented [9]).

Acknowledgement

We would like to express our cordial thanks to Dr K. HATAKEYAMA and Dr. A. IKUTA, Mr. O. MURAKAMI and S. SUZUKI for their helpful discussions and valuable assistance.

References

- [1] R. V. WATERHOUSE, *Statistical properties of reverberant sound field*, J. Acoust. Soc. Am., **43**, 1436-1444 (1968).
- [2] D. LUBMAN, *Fluctuations of sound with position in a reverberation room*, J. Acoust. Soc. Am., **44**, 1491-1502 (1968).
- [3] K. BODLUND, *Statistical characteristics of some standard reverberant sound field measurements*, J. Sound Vib., **45**, 539-557 (1976).
- [4] K. J. EBELING and K. FREUDENSTEIN, *On spatial averaging of sinusoidal sound intensities in reverberant rooms: exact distribution functions*, Acustica, **46**, 18-25 (1980).
- [5] D. E. BLUMENFELD and G. H. WEISS, *Effects of headway distributions on second order properties of traffic noise*, J. Sound Vib., **41** (1), 93-102 (1975).
- [6] M. OHTA and T. KOIZUMI, *General statistical treatment of response of nonlinear rectifying device to stationary random input*, IEEE Trans. Inf. Theory IT-14, 595-598 (1968).
- [7] B. V. GNEDENKO and A. N. KOLMOGOLOV, *Limit distribution for sums of independent random variables* (Translated into English by K. L. Chung. Addison-Wesley Pub. Co., Massachusetts, 1954), Chap. 8.
- [8] S. MORIGUCHI, K. UTAGAWA and S. HITOTSUMATSU, *Mathematical Formula* (Iwanami, Tokyo, 1977), Vol. III, 95, 1, 86, 5 (in Japanese).
- [9] M. OHTA and Y. MITANI, *The effect of the restricted fluctuation range in the actual random noise on the transformation of evaluation indices from L_x to L_{eq}* , J. Acoust. Soc. Jpn., **43**(3), 143-151 (1987) (in Japanese).

Received on December 18, 1988

APPLICATION OF THE ACOUSTIC EMISSION METHOD IN FATIGUE CRACKING AND FRACTURE TOUGHNESS ESTIMATION FOR STEEL

S. PILECKI*, J. SIEDLACZEK**

* Institute of Fundamental Technological Research, Polish Academy of Sciences
(00-049 Warszawa, ul. Świętokrzyska 21)

** High Pressure Research Center, Polish Academy of Sciences
(01-142 Warszawa, ul. Sokołowska 29)

The present paper consists of the confirmation of previous works where the great variety of the acoustic emission (AE) characteristics of different metals have been found. Based on the experiments conducted for the St90PA steel, possibilities of the fatigue cracks initiation detection by use of the AE method are discussed herein. Relations between the fatigue crack length and AE count rate or count sum have been determined and the possibilities of the application of AE in fracture toughness estimation as well as in critical stress intensity factor K_{Ic} calculations have been presented. It has been stated that creation of the fatigue cracks in steel can be detected much earlier by use of the AE method than it was possible by use of the classical optical method. AE method also makes the estimation of the propagating crack length easier as well as it can make the estimation of the fracture toughness more accurate.

Kontynuując wcześniejsze prace, w których stwierdzono dużą różnorodność charakterystyk akustycznych różnych metali, w niniejszej pracy na przykładzie stali St90PA zbadano możliwości wykrywania inicjacji pęknięć zmęczeniowych metodą EA, wyznaczono zależność między długością pęknięcia zmęczeniowego a gęstością i sumą zliczeń EA oraz naświetlono możliwości wykorzystania EA w wyznaczaniu odporności na pękanie i obliczaniu wartości krytycznego współczynnika intensywności naprężeń K_{Ic} . Zostało wykazane, że powstawanie pęknięć zmęczeniowych w stali może być metodą EA wykryte znacznie wcześniej niż metodą optyczną. Metoda EA ułatwia też ocenę długości propagującego się pęknięcia, jak również może uściślić ocenę odporności na pękanie.

1. Introduction

In the case of cyclic as well as static loading the quantitative significance of results obtained in the experimental measurements carried out for given conditions can only be estimated with their reference to the acoustic characteristic of tested

material. It is well known [1] that significant differences can be observed in the case of acoustic emission (AE) of different materials and the AE measurements usually allow rather for the comparison.

2. Acoustic emission phenomenon in fatigue cracking process

The simplest relations between AE and rate of cracking were first detected in 1964 [4]. In 1967 relations between the AE count sum and load were given for aluminum alloys and steel [5]. In 1976 BAILEY et al. [8] stated that there exists a very good correlation of the AE count sum with the fatigue crack length. Relation between the stress intensity factor K and AE per unit crack length was also shown in [6, 7].

The main reference for the acoustic investigations of a given material tested for cyclic loading is its dynamic acoustic emission characteristic. Determination of the complete characteristic is a time-consuming process. It happens because this characteristic depends on many parameters, such as range and history of loading, geometry of specimen, its material properties, kind of specimen's mechanical and heat treatment and, eventually, existence of notch. With regard to the qualitative correlation of the AE phenomenon and the cracking process of dynamically loaded material, the AE measurement allows for a more precise estimation of crack initiation and crack growth than the commonly used optical method.

Establishment of the moment of fatigue crack initiation is a very difficult task. This difficulty comes out of two reasons. The first one is connected with establishing of synonymous definition of a damage dimension big enough to be treated as the initial crack. Localization (detection) of the crack tip is the second reason. When the optical method of measurement is used, appearance of the crack can only be established for cracks visible on the outer surface of the specimen. In reality, especially for specimens with A -shape notch, the crack can initiate within the invisible part of the specimen. For this reason the supposition on the crack initiation based on the AE measurements seems to be more objective than the standard optical observation*.

Three fundamental stages can be distinguished in the process of fatigue cracking, namely: I. Incubation of the crack. Characteristic features of this stage are the saturation of dislocation structures and arising of the roughnesses on the outer surface; II. Crack growth to the visually perceptible dimensions (initiation); III. Further crack growth (propagation) from the moment of its initial perception to the final destruction of the specimen. The AE method is peculiarly useful in the last two stages. It makes the

* Development of new methods of crack measurements observed recently (electromagnetic or electric resistance method) does not change the fact that the optical method is still the most popular one used in practice.

estimation of real initiation of the fatigue crack growth more accurate. It should be noticed that the first optical observation of the crack on the specimen's surface can not be connected with the initiation of the cracking process but it usually indicates that the process is already in progress. It happens also, when the crack tip has been geometrically situated on the visible surface. Precise observation of the moment of crack initiation is usually impossible because the resolving power of optical instruments is not too big and the conditions for observation of the specimen are rather difficult due to its vibrations. On the other hand, just for the reason of specimen vibrations, increase of the resolving power of the optical instruments seems to be aimless.

The acoustic effect produced in the third stage of cracking generally depends on the volume of plastic zone, that is on the length of the crack front and the stress level as well as on the kind of cracking material. The first two factors are important for a given material. In the case of notched specimens with a rectangular cross-section subjected to a cyclic bending with constant amplitude, it can be assumed that at the beginning of cracking, growth of the crack front takes place for constant stresses acting in the cracked region. In this phase increase of AE is connected only with the growth of the crack front length. It happens until the entire specimen's cross-section width is cracked, since from this moment the front length remains constant. It means that now the change of AE depends only of the stress amplitude. In this way correlations between the acoustical effects of tested materials, its fatigue properties and velocity of the crack growth within the structure can be made. The large number of data obtained by measurements is necessary to do it.

Touching the problem of the usefulness of obtained results it should be noticed that the appropriate regulation of the measuring equipment plays a very important role in the AE method [2]. The appropriate total amplification and discrimination levels of the electric signal are the most important factors [2]. Obtained results depend a lot on those parameters and the final success of the experiment is greatly influenced by their proper choice. This problem has been discussed in details in references [1-3] where the results of the AE measurements in the St90PA steel were described.

3. Specimens and testing procedure

Tests were carried out on the normalized carbon-manganese St90PA steel specimens of a following average percentage composition: C 0.68; Mn 1.11; Si 0.24; Cr 0.01; Ni 0.01; Mo 0.10; V 0.02; S 0.027; P 0.026; Fe — the rest. Ultimate strength of this steel equals 1010 MPa and its yield stress is 600 MPa.

The normalized cylindrical specimens with reduced section 5 mm in diameter and 55 mm in gauge length were used for tension. The rectangular specimens were prepared for 3-point bending in three kinds of dimensions: $20 \times 30 \times 250 \text{ mm}^3$

with straight notch for fatigue crack initiation test; $20 \times 50 \times 220 \text{ mm}^3$ with A -shape notch for fatigue crack propagation, and $20 \times 40 \times 180 \text{ mm}^3$ with A -shape notch according to ASTM E-399-77 for determining fracture toughness and the K_{Ic} factor. Cylindrical specimens were obtained from new railway rails as well as from the 10 years old rails of the railway track, exhibiting the fatigue cracks of a brittle nature. Rectangular specimens descended from the new and exploited rails and a part of the specimens was additionally annealed for 1 hour at the temperature 600°C in open-air conditions and next cooled together with a furnace. Elimination of internal stresses and softening of the material were the basic aims of this heat treatment. Rectangular specimens for a fracture toughness measurements descended only from new rails.

Main investigations were preceded by determination of the AE characteristics of a new and exploited material. These characteristics were obtained for cylindrical specimens stretched to the rupture. Test conditions and obtained results were not different from those described in [1].

Washers were used between the specimen and all the holders or rollers for electric and acoustic isolation of the specimen and for damping of noise of the mechanical nature. Experimental tests were carried out on test stand No. 1 described in [1, 3], that is on the Instron-1251 fatigue testing machine and on the 4 channel AE analyser, type E1, made in Institute of Nuclear Research, Poland. The DZM 180 printer was also used. The AE transducer was located on upper wall of the specimen, in its central part.

The 20 Hz frequency sinusoidally changing loads were used in initiation tests and the 25 Hz frequency was used in other tests. Total amplification of the analyser E1 was 80 dB, its level of discrimination was 1 V and the transmitted frequency band was 65...250 kHz. The high-pass filter used has had the limit frequency equal to 260 Hz. The line printer recorded maximum load value and the AE count rate and count sum. In the AE measurements accompanying the crack initiation the 20 s time base was used, whereas in the measurements of the crack propagation the 1...100 s base was used.

Initiation and growth of the crack length were the additionally inspected and recorded parameters. Stereoscopic optical microscope together with the millimetre mesh marked on both sides of the specimen in the vicinity of the growing crack (or notch) were used in these measurements.

Investigations concerning initiation of a fatigue crack were done for two groups of specimens of the total number of 9. Since such experiments were never carried out before, initially 5 specimens of the pilot group were used in diagnostic investigations. Their basic aim was the appropriate choice of loading parameters and the AE analyser regulation. Estimation of the influence of external disturbances on the measured parameters and the characteristic of the change of these disturbances in time were also the aim of the diagnostic tests. Tests on the main group of specimens done according to the established procedure were the next step of investigations.

4. Results and discussion

Before the beginning of cycling each specimen was quasistatically loaded to $F_{\max} = 11.42$ kN with the simultaneous AE recording. The aim of experiment was to check up if the stresses near the notch tip produced by this load were not greater than the yield stress; none of the samples exhibited acoustic activity during this loading. Investigations of the acoustic effects for various load values (Table 1) and the relation of these effects with crack growth were the reason for changing the load. The most important test data are given in Table 2 and Fig. 1. For each specimen it was found that AE produced by cycling was observed much earlier than the crack could be optically discovered on one of the lateral surfaces of the specimen (interval A).

Table 1. Values of cyclic load in particular test intervals

Test intervals Load	A	B	C
F_{\max} [kN]	11.42	5.30	8.16
F_{\min} [kN]	0.80	0.80	0.80
$R = F_{\min}/F_{\max}$	0.07	0.15	0.10

Table 2. Testing of fatigue crack initiation

Specimen No	Cycle number to appearance/ of intensive AE	Cycle number to optical detection of crack	AE counts to optical detection of crack	Specimen endurance [cycles]	Crack length [mm]	Fatigue crack area [%]
1	2	3	4	5	6	7
1	40 000	50 000	850 000	106 000	2.0	7.3
2	10 200	45 000	461 495	61 500	1.9	7.0
3	18 200	52 000	426 755	58 700	1.9	7.0
4	30 200	52 000	1 342 978	82 600	2.8	10.5
5	33 100	72 000	991 508	86 200	2.0	7.5
6	29 300	63 400	561 500	62 800		
7	21 600	49 500	426 800	60 400		
8	25 500	57 300	860 600	81 600		
9	42 900	65 600	628 900	87 600		

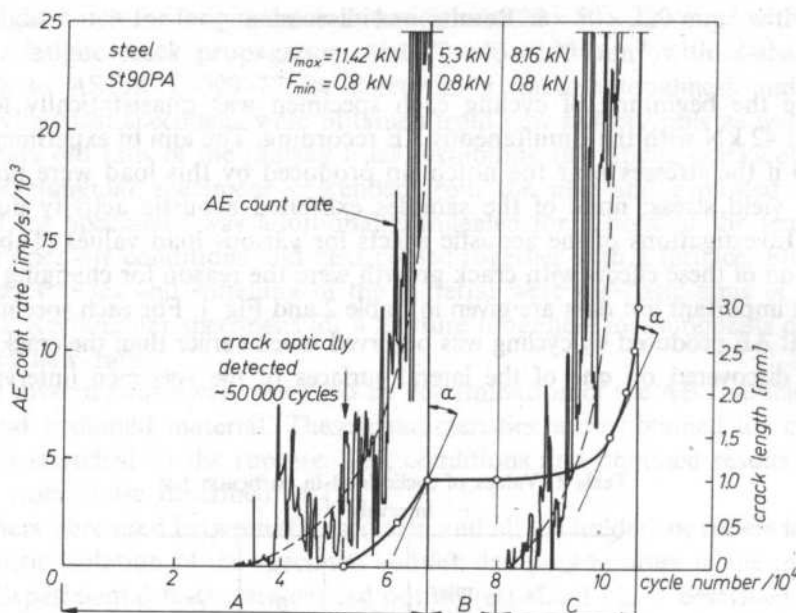


FIG. 1. Acoustic emission count rate and crack length versus cycle number by different load value

If we assume that this activity is produced by crack initiation and its initial growth, then we should say that the acoustic method of detection of appearing cracks is much more effective than the optical method commonly used in practice nowadays. In the successive stage of the process, AE is growing progressively (broken line) together with the crack length growth (solid line).

To investigate AE in the interval B, the maximum cyclic load F_{\max} was reduced to 5.30 kN. For this load, AE did not appear. Fatigue crack growth was neither observed, too. This phenomenon was detected every time when F_{\max} was reduced. It was observed also in crack propagation tests done for specimens with a A -shape notch.

In the interval C the load F_{\max} was increased to the value which evoked a distinct AE effect, but which was less by 3.26 kN (about 28%) than in the interval A. Magnification of the specimen's endurance and prolongation of the observation time of a fatigue crack growth together with the accompanying acoustic activity were the reasons for such load changing. When the AE count rate in the interval C reaches the maximum value from the interval A, then the same rate of fatigue crack growth is reached. Direction of tangential lines drawn in the proper points of the crack growth curve indicates for this phenomenon.

Four samples (No. 6 to 9) of the main group were tested for a procedure shown in Fig. 2 (see Sect. 2). Values used in tests were: $F_{\max} = 11.2$ kN, $F_{\min} = 5.2$ kN, $R = 0.46$. From Figs. 1 and 2 it can be seen that the superiority of the AE method with respect to the optical detection of a fatigue crack initiation is evident.

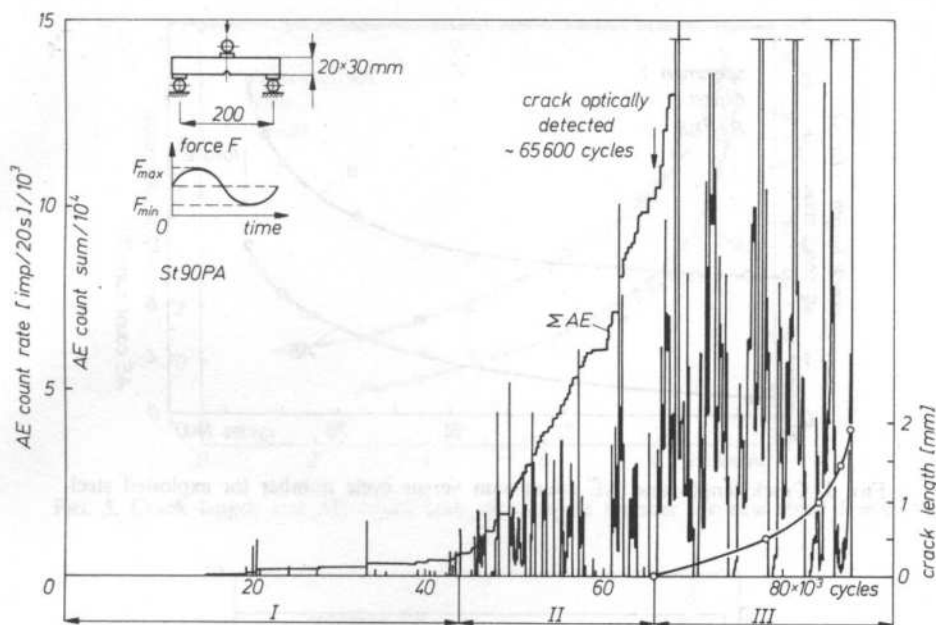


FIG. 2. Acoustic activity of a specimen No. 9 by 3-point cyclic bending

A slightly different procedure was applied in main measurement of the crack propagation. Initial maximum load of a cycle was 24 kN and it was held constant until crack appeared on the lateral surface of the sample. A high initial load was applied in order to reduce the incubation time. The AE measurements conducted in this part of the experiment were only used for qualitative estimation of crack existence. Maximum load was reduced to 14 kN when the crack became visible and could be optically observed on a surface of the sample. Afterwards, both crack development and AE were carefully measured. These results are marked by sample number and a letter *A*. Measurements were conducted to the moment when the crack length reached ca 10 mm. Then load was reduced to 8 kN in order to delay specimen's failure and to obtain second series of results, marked by a letter *B*. For this load, samples were cycled until they were broken; an increment of the crack length attained an average value of 12 mm. Thus, average total crack length reached ca 22 mm. Each change of the maximum load was accompanied by the change in the minimum load of the cycle, because we wanted to keep the assumed value of the stress ratio R constant.

Totally 12 series of measurements for 7 specimens were done. Relations presented in Figs. 3 to 6 were obtained for samples 1, 3A, 4A and 7B in three already mentioned (Section 3) states of the material and for different values of the stress ratio R in the cases when a new material has been used (4A, 7B). Curves "a" for the crack length and "AE" for count sum plotted as the function of load cycles are of the

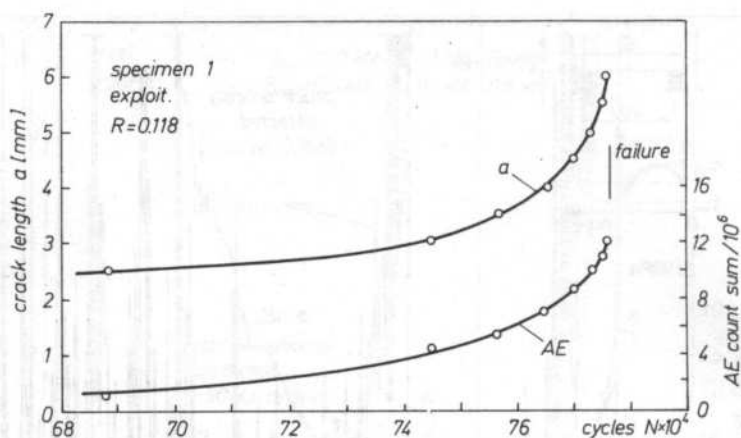


FIG. 3. Crack length and AE count sum versus cycle number for exploited steel

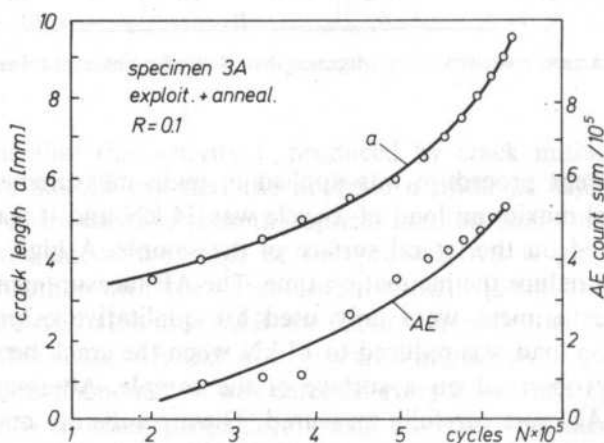
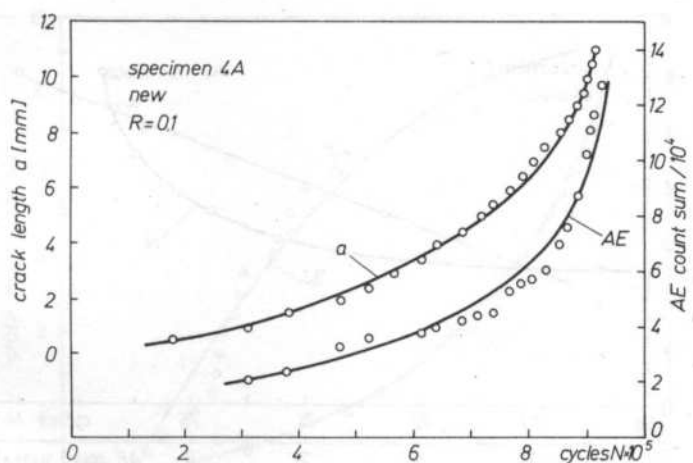
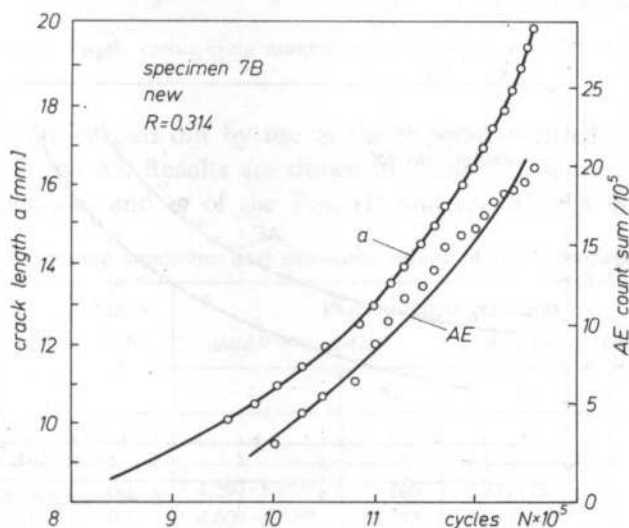


FIG. 4. Crack length and AE count sum versus cycle number for exploited and annealed steel

similar nature, especially by small crack lengths. Differences in the state of the material and in obtained crack lengths can be the reasons for the observed absence of the full parallelism of the curves plotted for greater crack lengths.

Differences which are significant in further interpretation of the obtained results can be observed in the subsequent presentation of the experimental data (see Figs. 7–9). Three characteristic relations between the crack length and the AE counts sum can be distinguished here, namely the linear dependence (Fig. 7, sample 1), the progressively growing nonlinear dependence (Fig. 8, sample 3A) and the regressively growing nonlinear dependence (Fig. 9, sample 4A).

FIG. 5. Crack length and AE count sum versus cycle number for new steel, $R = 0.1$ FIG. 6. Crack length and AE count sum versus cycle number for new steel, $R = 0.314$

We can notice that there is a certain relation between the crack length and the AE count sum. This relation can be seen in both coordinate systems: crack length and the count sum as a function of the number of cycles as well as crack length as a function of the AE count sum and number of cycles. In accordance with this relation the count sum can be treated as a parameter of the meaning similar to the number of load cycles. The well known Paris' equation for crack growth rate reads as follows.

$$da/dN = c_1(\Delta K)^{n_1}, \quad (1)$$

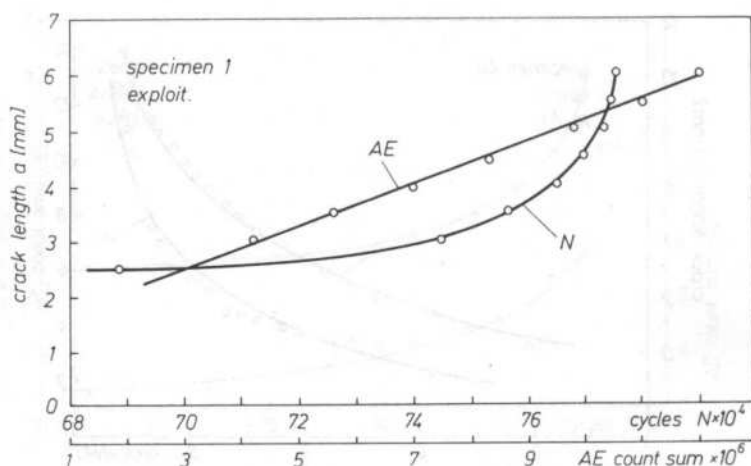


FIG. 7. Crack length versus cycle number and AE count sum for exploited steel

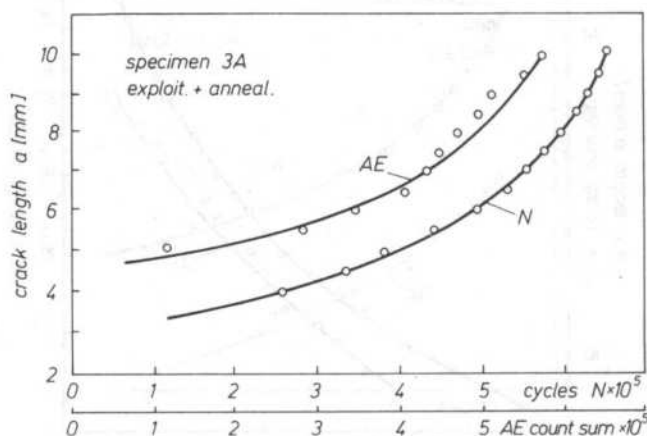


FIG. 8. Crack length versus cycle number and AE count sum for exploited and annealed steel

where da/dN — increment of fatigue crack per cycle, c_1, n_1 — material constants, ΔK — range of the stress intensity factor.

It seems to be reasonable to use a similar formula for describing the crack growth in terms of AE parameters

$$da/dn = c_2 (\Delta K)^{n_2}, \quad (2)$$

where da/dn — increment of fatigue crack per AE count.

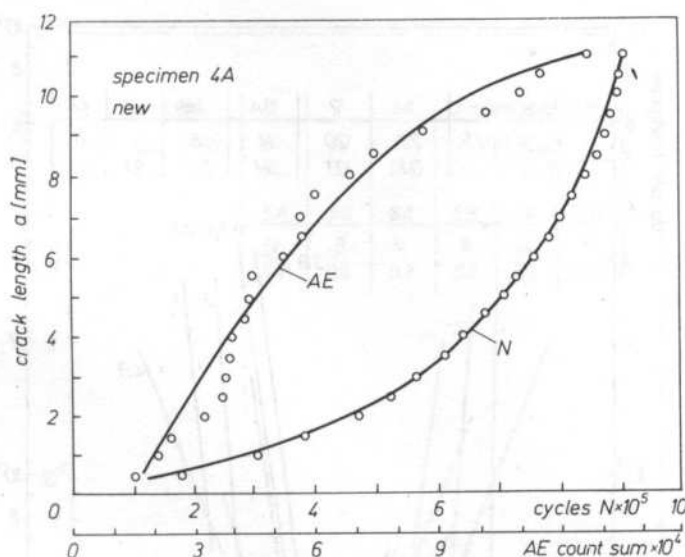


FIG. 9. Crack length versus cycle number and AE count sum for new steel

Calculations were carried out by use of the program written according to the standard ASTM E 746-83. Results are shown in Table 3. Columns 4 to 7 give the estimated coefficients c_i and n_i of the Eqs. (1) and (2). Results of the numerical

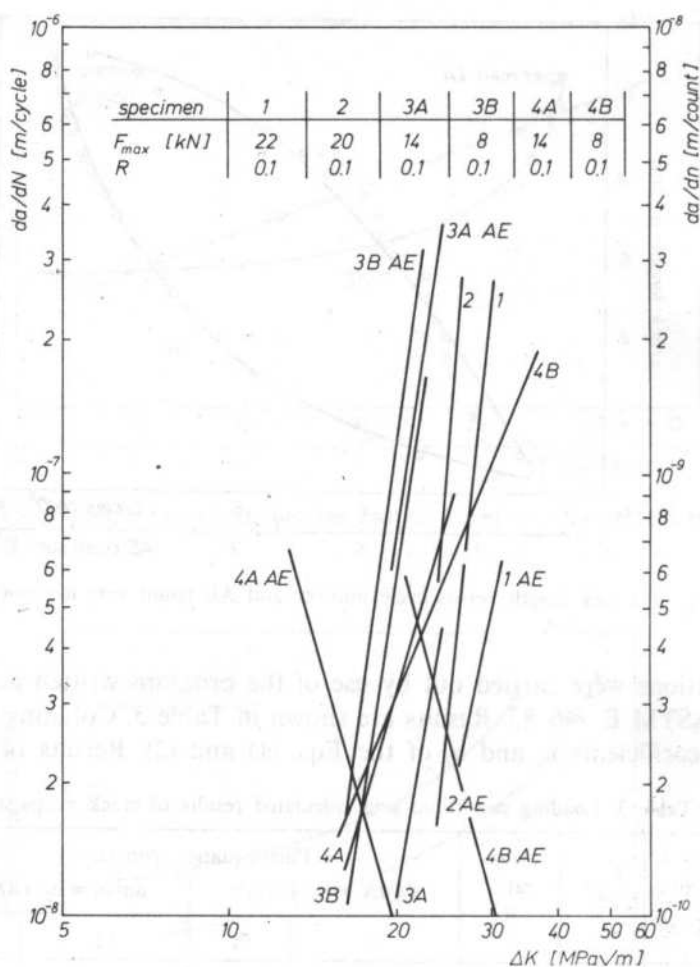
Table 3. Loading conditions and calculated results of crack propagation

No	F_{\max} kN	Stress ratio R	Paris' equation constants			
			$da/dN = c_1 \cdot (\Delta K)^{n_1}$		$da/dn = c_2 \cdot (\Delta K)^{n_2}$	
			c_1	n_1	c_2	n_2
1	2	3	4	5	6	7
1 ^e	22	0.1	$4.297 \cdot 10^{-21}$	9.266	$5.772 \cdot 10^{-17}$	4.650
2 ^e	20	0.1	$4.009 \cdot 10^{-24}$	11.753	$3.840 \cdot 10^{-25}$	10.709
3A ^a	14	0.1	$5.667 \cdot 10^{-18}$	7.132	$3.005 \cdot 10^{-18}$	6.492
3B ^a	8	0.1	$2.593 \cdot 10^{-18}$	7.919	$3.377 \cdot 10^{-16}$	4.977
4A ^a	14	0.1	$2.939 \cdot 10^{-13}$	3.829	$3.501 \cdot 10^{-2}$	-4.262
4B ^a	8	0.1	$4.124 \cdot 10^{-12}$	2.981	$3.901 \cdot 10^{-3}$	-3.756
5A ^a	14	0.3	$3.088 \cdot 10^{-11}$	2.542	$7.227 \cdot 10^{-18}$	6.778
5B ^a	8	0.3	$1.983 \cdot 10^{-10}$	1.780	$7.780 \cdot 10^{-13}$	2.045
6A ^a	14	0.3	$3.172 \cdot 10^{-11}$	2.567	—	—
6B ^a	8	0.3	$5.806 \cdot 10^{-12}$	3.062	—	—
7A ^a	14	0.3	$3.102 \cdot 10^{-11}$	2.606	$1.070 \cdot 10^{-12}$	2.140
7B ^a	8	0.3	$5.544 \cdot 10^{-11}$	2.262	$9.813 \cdot 10^{-12}$	2.198

(^e) Exploited steel.

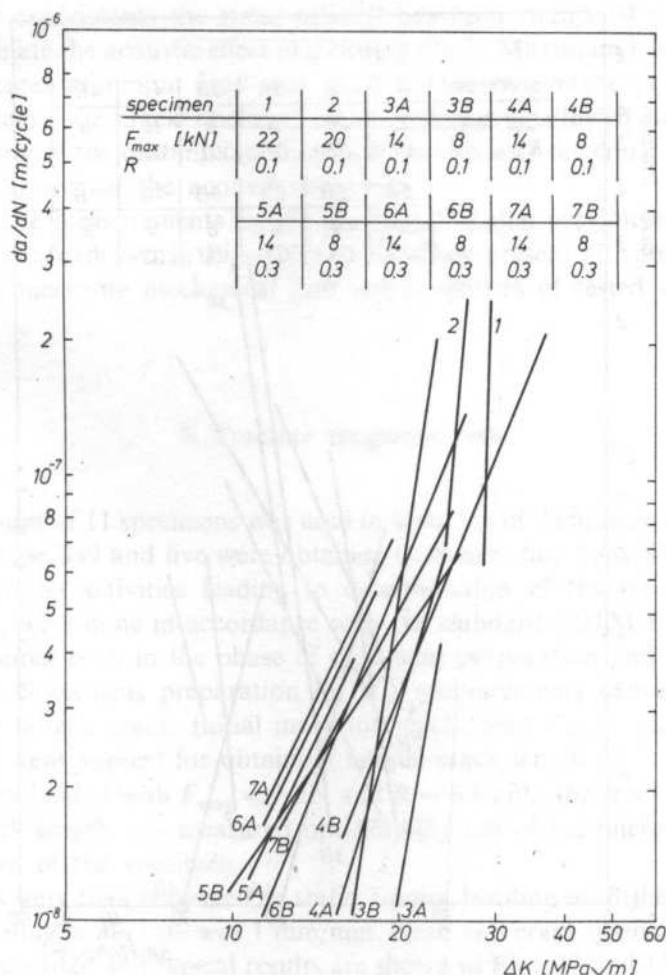
(^a) Exploited and annealed steel.

(ⁿ) New steel.

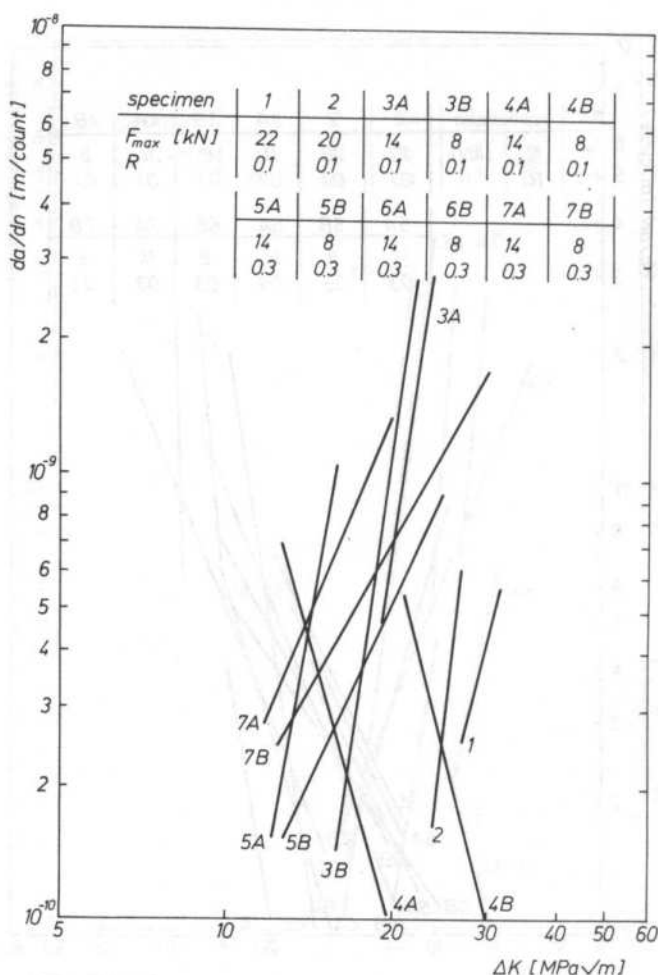
FIG. 10. da/dN and da/dn versus ΔK

analysis are plotted in the doubly logarithmic system in Figs. 10 and 12. They form the most synthetic picture of the results obtained by our measurements. Fig. 10 shows that the AE estimations are in a good conformity with the results obtained with the use of fracture mechanics methods. Nonconformity of the load cycles with the AE count per unit increment of crack length is the reason that explains the shifting of corresponding lines 1 – 1AE, 2 – 2AE, 3A – 3A AE, 3B – 3B AE, etc. It should be noticed that 10 to 100 of the AE counts correspond to one load cycle. Presented results also suggest that the value of load applied for the constant stress ratio R (see Table 3) does not influence the conformity of acoustical and mechanical results.

Results obtained for the specimen No. 4 (new railway rail) are not similar (Fig.

FIG. 11. da/dN versus ΔK

10). Although loading conditions applied here have been the same as in the specimen 3, AE measurements are qualitatively different. This difference is invisible when the relation between crack length and the number of load cycles of Fig. 5 is considered. It becomes evident both for the relation expressing the increment of crack length as a function of AE count sum (see the regressively growing "AE" curve from Fig. 9) and for the results of numerical analysis. Straight lines 4A-AE and 4B-AE in Fig. 10 are descending lines (they have inverse inclination). This result seems to be illogical when the fracture mechanics viewpoint is applied. Relation $da/dN = c_1(\Delta K)^n$ can be represented in a double logarithmic system by a straight line inclined with respect to

FIG. 12. da/dn versus ΔK

the ΔK axis by an angle less than 90° . It follows from the rule that stress increments are usually accompanied by a growth of the fatigue crack propagation velocity but the inverse statement is never true. When da/dn is measured, it can sometimes happen that crack length growth implies growth of dn/da , that is growth of the count number per unit crack length increment and the decrease of da/dn . This result can be explained if we assume that there exists an additional AE source. Acoustic activity of this source grows with fatigue crack length growth. Friction occurring on newly created surfaces in crack opening and closure can be regarded as this additional source. Activity of this source can be much greater than activity of sources directly connected with crack growth, that is with expansion of a plastic zone near the crack tip and with creation of a new surface.

In further experiments the stress ratio R has been changed from 0.1 to 0.3 in order to eliminate the acoustic effect of a closing crack. Maximum load of a cycle was constant whereas minimum load was made higher in every experiment. It gave occasion to leave the crack unclosed in unloading and allowed us to reduce the acoustic activity of the rubbing crack surfaces. In this way the crack growth was the predominant source of the acoustic emission.

Results of AE measurements for the specimen 5–7 after previous magnification of the stress ratio are shown in Figs. 11 and 12. They present all results obtained in experiments concerning mechanical and AE properties of tested specimens.

5. Fracture toughness tests

Total amount of 11 specimens was used in tests. Six of them were made from new railway rails type S49 and five were obtained from new rails type S60 with thermal treatment. All the activities leading to determination of the fracture toughness coefficient K_{Ic} were done in accordance with the standard ASTM E399. Moreover, AE was measured both in the phase of specimens preparation and in the phase of their fracture. Specimens preparation for K_{Ic} measurements consisted in making a preliminary fatigue crack. Initial maximum cyclic load $F_{max} = 10$ kN and stress ratio $R = 0.1$ were applied for obtaining fatigue crack length of $3^{\pm 1}$ mm and then specimens were loaded with $F_{max} = 7$ kN and $R = 0.1$ until the crack length reached $5^{\pm 1}$ mm. Crack length was measured optically (by use of the microscope) on both lateral surfaces of the specimen.

Specimens were then subjected to static 3-point bending until their final fracture occurred. Bending strain rate was 1 mm/min. Load and crack opening displacement (COD) were recorded and typical results are shown in Figs. 13 and 14. Fig. 15 shows surface of specimens 27 and 28. Majority of obtained fractures is of the same nature as for the specimen No. 27. An important feature of the fracture is its shape and position of a boundary between extemporary and fatigue regions. It should have a shape of a straight line and it should be symmetric with respect to the axis of symmetry of a cross-section. Fracture obtained for the specimen 28 is the example of the improper boundary between these two regions, as it is inclined and bent.

Linear dependence of the crack opening and the applied load and step increment of crack length by the load F_Q has been observed for all tested specimens except the specimen 27 (cf Fig. 14a), where points F_Q and F_{max} coincided. Specimens from rails without heat treatment fractured with much higher crack opening than specimens with heat treatment. Mean crack opening typical for the first case was ca 0.32 mm whereas in the second case it was ca 0.16 mm.

This retardation in fracture of specimens without a heat treatment is represented in Fig. 13 by the curve segment between points F_{max} and K . Moreover, one or even

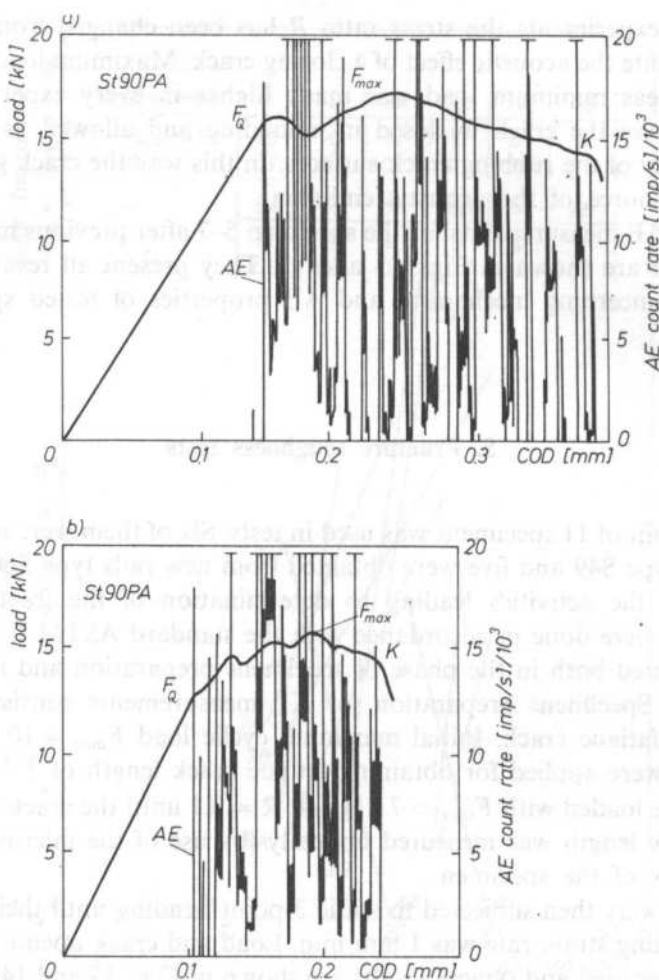


FIG. 13. Bending load value and AE count rate versus COD (rail type S49)

more distinct minima can be seen for specimens made from S49 rails. Curves plotted for specimens made from S60 rails did not exhibit this feature. These differences, except the calculated values of K_{IC} , allow us to distinguish both materials with regard to their inclination to brittle fracture.

Differentiation of both materials with respect to their brittle fracture toughness seems to be even more evident when measurements of the AE counts are taken into account. Specimens made from rails without heat treatment, in spite of different shape of their load curve (Fig. 13), exhibit acoustic activity in fracture contained between points F_Q and K . The most important result of the AE measurement is the coincidence of the beginning of acoustic activity with the initiation of crack growth. Both processes had begun in point F_Q . In this way the AE result confirms the

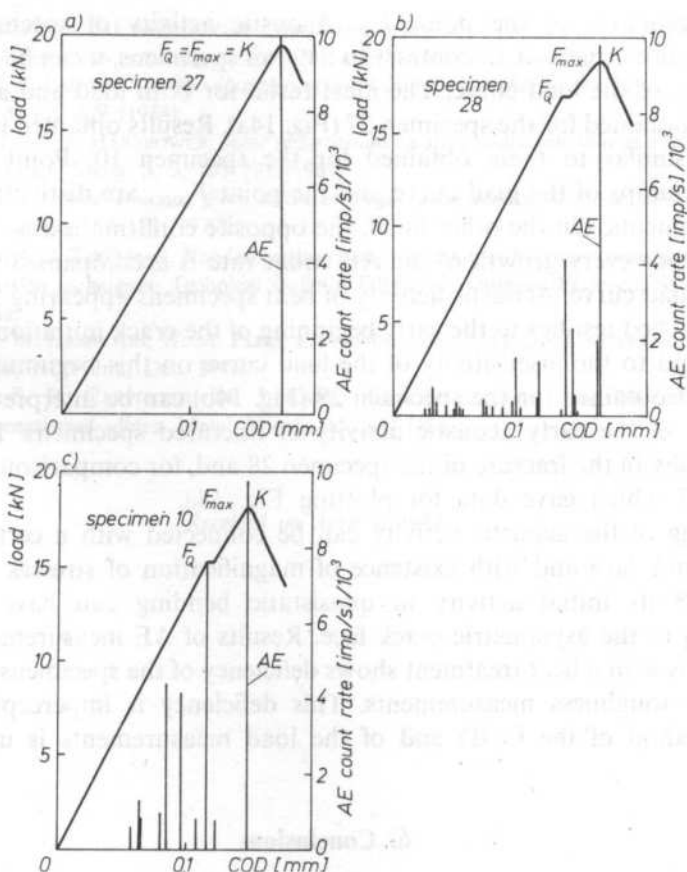


FIG. 14. Bending load value and AE count rate versus COD (rail type S60, annealed)

specimen 27

specimen 28

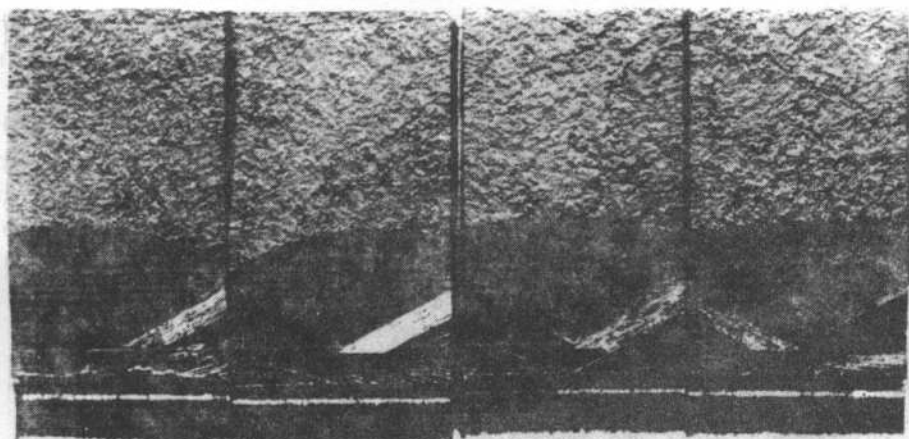


FIG. 15. Fracture surface of fatigued specimens. Boundary between extemporary and fatigue regions is well visible

practical usefulness of the point F_Q . Acoustic activity of specimens with heat treatment is not large and, in contrast to S49 rail specimens, it can be observed below the point F_Q of the load curve. The ideal result for both load and acoustic activity curves was obtained for the specimen 27 (Fig. 14a). Results obtained in the remaining tests were similar to these obtained for the specimen 10. Point F_Q as well as subsequent jumps of the load curve and the point F_{\max} , are distinctly confirmed by AE measurements. On the other hand, the opposite confirmation is not observed. It means that not every growth of the AE count rate is accompanied by a significant step of the load curve. Acoustic activity of bent specimens appearing before point F_Q has been reached testifies to the early beginning of the crack initiation process on the one hand and to the insensitivity of the load curve on this beginning on the other hand. Result obtained for the specimen 28 (Fig. 14b) can be interpreted as a certain explanation of the early acoustic activity of fractured specimens. Fig. 15a shows a photography of the fracture of the specimen 28 and, for comparison, fracture of the specimen 27 which gave data for plotting Fig. 14a.

Beginning of the acoustic activity can be connected with a certain features of a fatigue crack face and with existence of magnification of stresses. In the case of specimen 28 its initial activity in quasistatic bending can have its source in equalization of the asymmetric crack face. Results of AE measurements conducted for specimens with a heat treatment shows deficiency of the specimens preparation to the fracture toughness measurements. This deficiency is imperceptible when the classical method of the COD and of the load measurements is used.

6. Conclusions

Results of the presented experiments show that

1. Before using AE method to quantitative tests of structures, one must know AE characteristics of a material from which the structure is made.
2. Beginning of the fatigue cracking can be discovered by AE method much earlier than by optical method, and crack growth rate can be estimated more precisely.
3. AE measurements can be helpful in precise estimation of crack length.
4. AE method is able to make an estimation of fracture toughness more precise than optical method and it can indicate when cracking of particular microregions occurs.

References

- [1] S. PILECKI, J. SIEDLACZEK, *Acoustic activity of some metals determined by the acoustic emission method*, Arch. of Acoust. **14**, 3-4, 261-281 (1989).
- [2] S. PILECKI, *Wykorzystanie emisji akustycznej w badaniach własności mechanicznych i pękania ciał stałych*, Arch. Akust. **21**, 109 (1986).

- Received on April 4, 1989*

REMOTE SENSING OF THE SEA OIL POLLUTION BY MEANS OF HIGH FREQUENCY SURFACE SCATTERING (*)

S. J. POGORZELSKI

Environmental Laboratory of Acoustic and Spectroscopy University of Gdańsk
(80-952 Gdańsk, ul. Wita Stwosza 57)

The statistical properties of the ultrasonic signal scattered at a rough surface of both clean water and water covered with a layer of oil substance in an outdoor pond were examined. The results obtained by means of free-floating acoustic buoy-like system confirmed all the laboratory results and predictions of high-frequency scattering theory. The proposed system enables the remote, contactless sensing and determination of the principal physical properties of the oil substance spread on the rough water surface on the basis of scattered signal statistics considerations.

Introduction

An application of acoustic surface scattering as a suitable tool for remote sensing and determination of the sea-atmosphere interaction process has been becoming more and more often used since last ten years [1, 2]. A high-frequency acoustic scattering system (i.e. one with a large value of Rayleigh parameter) enables investigation of small scale processes and objects in the sea like: bottom microrelief [3, 4], wave breaking [1], propagation of capillary waves and surface currents, Langmuir circulation, gas bubbles and plankton population [2]. A layer of an oil substance on the sea surface strongly influences the field of wind waves particularly from short gravity and capillary range [5, 6].

In modern oceanography the study of this variability is closely connected with the problem of remote sensing of ocean processes by their manifestation on the surface. Capillary wind waves are characterized by a particular shape, have a large steepness and small amplitude [7, 8]. In high-frequency scattering, the scattering function of

(*) Carried out under the research programme CPBP 02.03 II/2.16, coordinated by the Polish Academy of Sciences.

the acoustic waves depends only on the mean square slope of the surface [9]. Therefore an acoustic system of such properties constitutes a most suitable tool for investigation of scattering on the surface of the type described. All systematic changes of the rough water surface undulation, for example due to the presence of a layer of oil substance, express themselves in corresponding changes of the scattered signal statistics as shown in the laboratory measurements [10, 11]. The aim of this paper is to present the new acoustic system for remote sensing and monitoring of the surface oil pollution in natural conditions. Some preliminary results of the outdoor pond measurements by means of buoy-like acoustic system and artificial oil slick spread on the surface are also presented. The properties of the used system and obtained results are discussed in terms of high-frequency surface scattering theory [3, 12].

2. Statistical parameters of acoustic signals scattered at rough surface. Theory

Essential characteristics of the fluctuations of the scattered acoustic signal i.e. autocorrelation functions, the magnitude of amplitude fluctuations, and the form of probability density function (p.d.f.) depend on the value of Rayleigh parameter [13, 14]:

$$R_a = 2 k h \cos \theta, \quad (1)$$

where $k = 2\pi/\lambda$ — wavenumber of the acoustic wave of length λ , h — height of surface irregularities, θ — incident angle of the acoustic wave.

At small values of $R_a (\ll 1)$, autocorrelation functions of the scattered signal amplitude are identical with the same functions of the undulated surface, and probability density function has the form of Gaussian distribution [13, 14, 15]:

$$p_n(X_a) = \frac{1}{\sqrt{2\pi}\sigma} \exp[-(X_a - \bar{X}_a)^2/2\sigma^2], \quad (2)$$

where X_a , \bar{X}_a — temporal and mean amplitudes, σ — standard deviation.

At large values of $R_a (\gg 1)$, the periodic character of the signal autocorrelation function is disturbed and does not exhibit any connections with the autocorrelation function of the rough surface. The statistical distribution of signal amplitude has the form of Rayleigh distribution [15, 16, 17]:

$$p_r(X_a) = (X_a/\sigma^2) \exp[-X_a^2/2\sigma^2]. \quad (3)$$

At intermediate values of R_a , the Rayleigh-Rice distribution, gamma distribution, three-parameter log-normal distributions, etc. are obtained [13, 15, 16, 18]. A variety of the distribution functions observed in many experiments results from different character of wave motion in each case [15].

A good approximation of the experimental distribution is obtained by expanding the Gaussian-distribution into Gram-Charlier series up to the fourth statistical moment

[19]. The p.d.f. of polynomial distribution has the following form [20]:

$$p(X_a) = p_n(X_a) \left[1 + \frac{A_1}{6} H_3(m) + \frac{A_2}{24} H_4(m) + \dots \right], \quad (4)$$

where $m = \frac{X_a - \bar{X}_a}{\sigma}$ — normalized random variable, $H_3(m) = m^3 - 3m$, $H_4(m) = m^4 - 6m^2 + 3$ — Hermite's polynomials, $A_2 = (\mu_4/\sigma^4) - 3$ — flattening coefficient, $A_1 = \mu_3/\sigma^3$ — asymmetry coefficient, μ_3, μ_4 — third and fourth central moments. The A_1 and A_2 parameters describe in a regular manner deviations of the experimental distribution from the Gaussian one, in which values of \bar{X}_a and σ are introduced from the experimental data. A fluctuation coefficient is a measure of the signal amplitude variability, and defined by equation [14, 15, 17]:

$$\eta = \sigma / \bar{X}_a. \quad (5)$$

Fig. 1 presents theoretically computed η (R_a) dependence [17], which has an asymptotic character in the range of large R_a values. A high-frequency acoustic surface scattering is characterized by means of acoustic surface scattering cross section (also called the wave scattering function) [3, 14]:

$$S_{hf} = r^2 I_s / I_0 A, \quad (6)$$

where I_0, I_s — intensity of the incident and scattered waves, r — distance between the transducer and the center of irradiated surface, A — area of the irradiated surface.

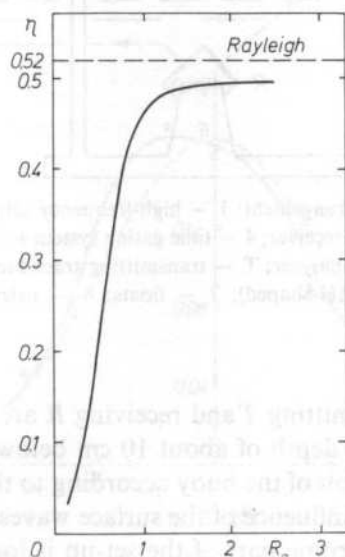


FIG. 1. Fluctuation coefficient of the scattered signal amplitude as a function of Rayleigh parameter with data taken from [17]

S_{hf} depends only on the mean square slope of the rough surface [9], and does not depend on driving wave frequencies, significant wave heights or correlation radius of rough surface undulation.

3. Experimental set-up and methodology

Scattering measurements of the ultrasound waves were carried out in an outdoor pond of small dimensions i.e. 5×5 m, under conditions of wind speed ranging from 0.5 to 2 m/s.

Fig. 2 presents a block diagram of the experimental arrangement. The ultrasonic

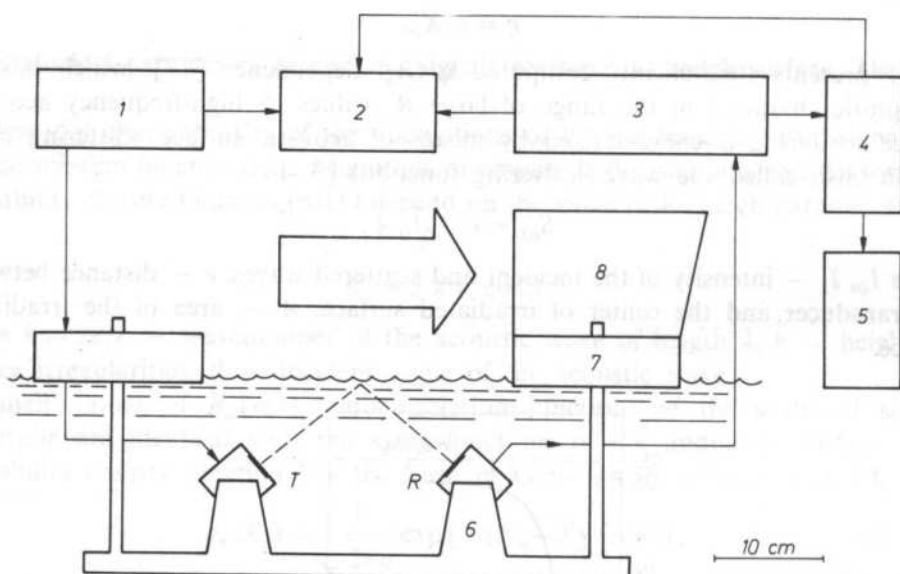


FIG. 2. Diagram of the experimental arrangement: 1 — high-frequency ultrasonic transmitter; 2 — oscilloscope; 3 — high-frequency ultrasonic receiver; 4 — time gating system + signal envelope and peak value detectors; 5 — statistical distribution analyzer; T — transmitting transducer; R — receiving transducer; 6 — buoy support (H-shaped); 7 — floats; 8 — orienting wings

quartz transducers: both transmitting T and receiving R are situated on the support of the free-floating buoy at the depth of about 10 cm below the water surface. Two float wings enable self-orientation of the buoy according to the actual wind direction, which significantly reduces the influence of the surface waves reflected from the floats on the measurement. The electronic part of the set-up is located on the pond bank and connected to the buoy using cables. The ultrasonic transmitter operating under pulse regime with the 3 kHz repetition frequency forms series of pulses lasting few μ s.

Each pulse has a rectangular envelope and is filled with a sine wave of 10 MHz frequency. An incident angle of the acoustic beam is equal to 60° . The scattered signal is registered in the specular reflection direction. A time gate of the electronic circuit 4 enables the envelope detection and measurement of peak value of the signal part corresponding only to surface scattering. Then the statistical analysis of the signal was performed using a Statistical Distribution Analyzer (Type 4420, Brüel and Kjaer) which measured the amplitude every 0.1 s and the p.d.f. of signal distribution was determined on the basis of 1800 counts. The scattering measurements were carried out for both clean water surface and water surface covered with a layer of gasoline 96. This gasoline has the following physical properties: density 760 kg/m^3 , viscosity $0.6 \text{ mPa} \cdot \text{s}$, and surface tension 20.3 mN/m has got of a positive spreading coefficient value against water and spontaneously forms an uniform layer (see Tab. 1 in [10]).

4. Results discussion

Figs 3 and 4 present examples of probability distributions $P(m)$ of amplitudes of the acoustic signal scattered from a rough surface of clean water and water covered with the gasoline 96 film, respectively. They also include two theoretical forms of p.d.f: Rayleigh distribution (solid line) and Gaussian distribution (dotted line), in which \bar{X}_a and σ values are introduced from the experimental data. In order to make the comparison between the experimental distribution and the theoretical ones easier, the distributions are presented as functions of normalized random variable m .

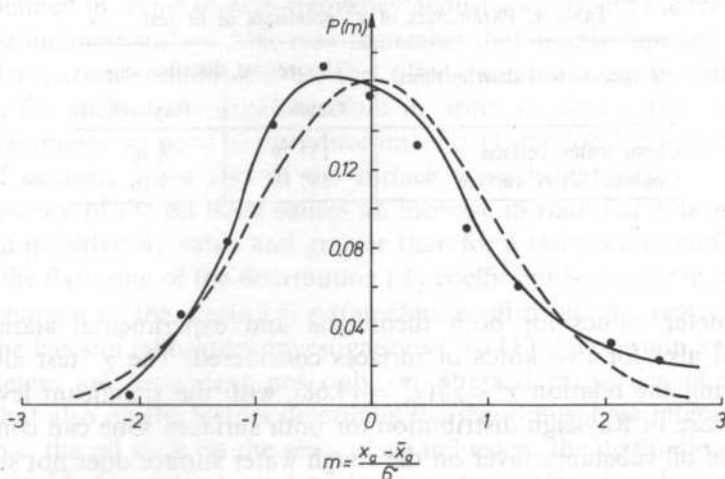


FIG. 3. Theoretical and experimental probability distributions of amplitudes of acoustic signal scattered from a rough water surface. ● — experimental points, theoretical Rayleigh (—) and Gaussian (----) functions, in which \bar{X}_a and σ values are introduced from the experimental data

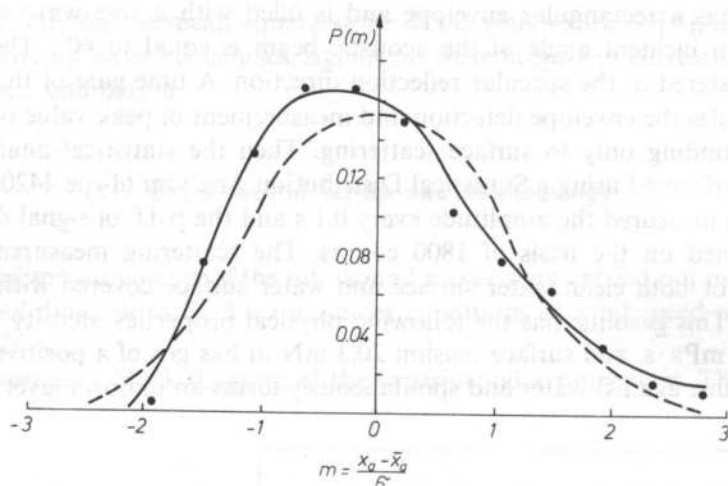


FIG. 4. Theoretical and experimental probability distributions of amplitudes of acoustic signal scattered from a rough water surface covered with a layer of gasoline 96. ● — experimental points, theoretical Rayleigh (—) and Gaussian (----) functions, in which \bar{x}_a and σ values are introduced from the experimental data

The experimental points in the case of both surfaces considered are much closer to the Rayleigh distribution than to Gaussian one, which is in agreement with the results of other authors and high-frequency surface scattering theory [12, 13, 15, 18, 21]. This remark can be confirmed by the χ^2 goodness of fit test [20]. Tab. 1 collects

Table 1. Parameters of χ^2 goodness of fit test

Experimental distributions	Theoretical distributions	
	Gaussian	Rayleigh
Clean water surface	137.79	8.46
Covered water surface	147.18	9.16

the χ^2 parameter values for both theoretical and experimental statistical distributions, and also for two kinds of surfaces considered. The χ^2 test always gives results satisfying the relation $\chi^2 < \chi_0^2$ ($\chi_0^2 = 14.68$), with the significant level fixed at 10% only in case of Rayleigh distribution for both surfaces. One can conclude that the presence of oil substance layer on the rough water surface does not significantly change the form of p.d.f. of the scattered signal amplitude, although leads to noticeable changes of the statistical distribution parameters as shown in Table 2. Changes of the statistical parameter values taken into consideration, observed for

Table 2. Statistical parameters of the distribution of the scattered signal amplitudes

Surface	\bar{X}_a	η	A_1	A_2
Clean water	0.1876	0.3209	0.4748	-0.2290
Covered water	0.1746	0.3315	0.5126	-0.2946

both clean and covered water surfaces give a quantitative measure of the distribution deviations which can not be simply noticed on visual inspection of Figs. 3 and 4. It can be seen that for the covered surface the mean amplitude is lower and fluctuation coefficient is greater which well corresponds to higher surface wind waves (the rough surface scatters ultrasonic waves more effectively). The water surface covered with the light oil substance film is probably much more susceptible to deformation caused by wind. This substance is characterized by density, viscosity and surface tension much smaller than water. However, such explanation seems to be a bit simplified because of a very complicated influence of the oil slick on the field of wind waves, which also depends on wind-waves range considered. Generally, the presence of oil film suppresses the wind waves from short gravity and capillary range but for waves of decimetre length an opposite effect is observed, and such waves are amplified [5].

The fluctuation coefficient in the case of the both surfaces reaches only slightly over 60 per cent of the asymptotic theoretical value ($= 0.5227$, see Fig. 1) expected for high-frequency surface scattering. Waves of the height equal to few cm were observed in the pond, which in the case of the applied acoustic system results in Rayleigh parameter values of the order of 100. On the other hand, the measured η values correspond to 0.6–0.7 of asymptotic R_a values. This apparent disagreement can be explained in terms of high-frequency acoustic scattering theory for two-scale composite-roughness surface. One may remember that mainly capillary waves, which occur under natural conditions on the tilted faces of long gravity waves, are responsible for such scattering. Therefore in order to obtain the "true" value of Rayleigh parameter we have to introduce into Eq. (1) the local values of the angle of incident of acoustic wave and of the surface wave height [3].

The presence of the oil layer causes an increase in right-hand asymmetry of the distribution (positive A_1 value and greater than for a clean water surface), and also intensifies the flatterness of the distribution (A_2 coefficient is greater in modulus). The observed changes of the statistical parameters confirm all the remarks previously made on the basis of laboratory investigations [10, 11]. The certain values taken by the parameters are dependent not only on physical properties of the given oil substance but also on the factors describing the sea-atmosphere interaction process. For example, the oil slick on the sea surface influences the dissipation rate of wind waves energy [5, 6], vertical wind profile near the surface (see Fig. 9 in [6]), and mean slope of water surface (Eq. (15) in [22]). It may be helpful to add that in the outdoor pond measurements the ratio h/λ (significant wave height to ultrasonic

wavelength) took on values similar, for example, to those of an acoustic experiment with acoustic waves of 80–100 kHz frequency at open sea. Fig. 5 presents a time record of the scattered signal temporal amplitude. The passage of the slick edge is clearly seen (and indicated by the arrow) as a rapid drop of the signal.

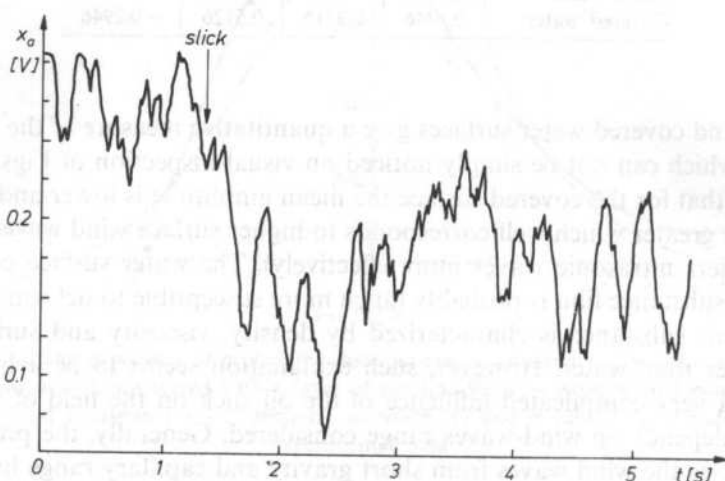


FIG. 5. Time record of the scattered signal amplitude. An arrow indicates the passage of the oil slick edge

The signal consists of the short-time oscillations of the frequency ranging from 3 to 15 Hz, which correspond to the gravity-capillary range of wind waves [13]. The spectrum range of the signal fluctuation frequencies is connected with the properties of the used acoustic system, especially with the ratio of linear dimension of the irradiated surface area A to the length of surface wave. The area of the irradiated region of elliptic shape is equal to $A = \pi XY = 0.645 \times 10^{-4} \text{ m}^2$ ($2X = 1.3 \text{ cm}$ and $2Y = 0.6 \text{ cm}$, see [10]). The value of $2X$ is comparable to the length of surface wave of 30 Hz frequency of the clean water surface ($\approx 1.2 \text{ cm}$, [13]). Since the scattered signal is averaged over the whole element of the area A , the dynamics of the recorded signal and sensitivity of the system to changes of surface roughness decreases with an increase of surface wave frequency (decrease of its length). It is accepted that the surface waves of the length equal to $4X$ and larger are registered with maximum dynamics [12]. The properties of the applied acoustic system allow recording surface waves of frequency of 15 Hz or smaller as shown in Fig. 5.

5. Conclusions

An outdoor pond surface scattering measurements by means of free-floating buoy-like acoustic system showed that a probability density function of the signal amplitude distribution has a Rayleigh form for both clean water surface and water

surface covered with oil substance layer. The presence of the oil substance film does not change the signal distribution form although leads to significantly different values of the statistical distribution parameters as compared to the clean surface scattering. The changes in the parameters values are related to physical properties of the oil substance spread on the rough surface as mentioned previously on the basis of the laboratory measurements [10, 11]. The results obtained in a small tank can not be directly applied to situation existing in natural conditions. A reliable acoustic method for remote sensing requires careful and extensive measurements of the air-sea interface properties and other factors describing the interaction process between atmosphere and sea in conjunction with measurements of acoustic scattering. In order to test the system presented here and theory developed in this and previous papers [10, 11], additional experiments with surface films of different chemical structure have to be performed. The described system seems to be suitable for continuous long-term monitoring for regions not so far from shore at limited state of undulation.

References

- [1] S. O. MC CONNELL, *Remote sensing of the air-sea interface using microwave acoustics*, Proceedings of Oceans, Institute of Electrical and Electronic Engineers, **1**, 85-92, (1983).
- [2] T. K. STANTON, C. S. CLAY, *Sonar echo statistics as a remote sensing tool: volume and seafloor*, IEEE Journal of Ocean Engineering, **OE-11**, 79-96, (1986).
- [3] D. R. JACKSON, D. P. WINEBRENNER, A. ISHIMARU, *Application of the composite roughness model to high-frequency bottom backscattering*, J. Acoust. Soc. Am. **79**, 1410-1422, (1986).
- [4] T. K. STANTON, *Echo fluctuations from the rough sea floor: predictions based on acoustically measured microrelief properties*, J. Acoust. Soc. Am. **78**, 715-721, (1985).
- [5] D. M. BRAVO-ZHIVOTOVSKY, L. S. DOLIN, S. A. ERMAKOV, E. M. ZUJKOVA, A. G. LUCHININ, V. I. TITOV, *The effect of the amplification of decimeter wind waves in the region of an oil slick*, Dokl. Akad. Nauk SSSR, **276**, 1243-1246, (1984).
- [6] S. A. ERMAKOV, E. M. ZUJKOVA, A. R. PANCHENKO, S. G. SALASHIN, T. G. TALIPOVA, V. I. TITOV, *Surface film effect on short wind waves*, Dynamics of Atmospheres and Oceans, **10**, 31-50, (1986).
- [7] C. S. COX, *Measurements of slopes of high-frequency wind waves*, J. Mar. Res. **16**, 199-225, (1958).
- [8] A. H. SCHOOLEY, *Profiles of wind-created water waves in the capillary-gravity transition region*, J. Mar. Res. **16**, 100-108, (1958).
- [9] I. TOLSTOY, C. S. CLAY, *Ocean acoustic*, Mc Graw-Hill, New York 1966.
- [10] S. J. POGORZELSKI, *Examination of the processes resulting from the presence of oil-derivative substance on the water surface by acoustical methods*, Ph. D. Thesis, University of Gdańsk, 1985.
- [11] S. J. POGORZELSKI, B. LINDE, A. ŚLIWIŃSKI, *Investigation of undulated water surface covered with different oil layers, by statistical analysis of scattered acoustic signals*, Acoust. Letters, **9**, 190-195, (1986).
- [12] S. T. MC DANIEL, A. D. GORMAN, *Acoustic and radar sea surface backscatter*, J. Geophys. Res. **87**, 4127-4136, (1982).
- [13] L. M. BREKHOVSKICH, *Akustika Okeana*, Nauka, Moscow 1974.
- [14] C. S. CLAY, H. MEDWIN, *Acoustical oceanography: principles and applications*, Wiley, New York 1977.

- [15] C. S. CLAY, H. MEDWIN, W. H. WRIGHT, *Specularly scattered sound and the probability density function of a rough surface*, J. Acoust. Soc. Am. **53**, 1677-1682, (1973).
- [16] L. FORTUIN, *Survey of literature on reflection and scattering of sound waves at the sea surface*, J. Acoust. Soc. Am. **47**, 1209-1228, (1970).
- [17] C. GAZANHES, J. LEANDRE, *Some aspects of the surface scattering of underwater sound*, J. Sound Vibration, **70**, 11-27, (1980).
- [18] C. W. HORTON, *A review of reverberation, scattering and echo structure*, J. Acoust. Soc. Am. **51**, 1049-1061, (1972).
- [19] M. BRZOWSKA, *An influence of undulated sea surface and bottom on sound propagation in the shallow sea*, Ph. D. Thesis, Institute of Oceanology of the Polish Academy of Sciences, Sopot 1977.
- [20] H. CRAMER, *Mathematical methods of statistics*, University Press, Princeton 1946.
- [21] J. A. OGILVY, *Wave scattering from rough surfaces*, Reports on Progress in Physics, **50**, 1553-1608, (1987).
- [22] H. MITSUYASU, T. HONDA, *The effects of surfactant on certain air-sea interaction phenomena*, in: Wave Dynamics and Radio Probing of the Ocean Surface, O. M. Phillips, K. Hasselman, [Eds.], Plenum, New York 1986, p. 95-115.

Received on June 21, 1989

INVESTIGATIONS ON AUDITORY SPACIOUSNESS OF LARGE ACOUSTIC SOURCES WITHIN A ROOM⁽¹⁾

K. RUDNO-RUDZIŃSKI, J. RENOWSKI

Institute of Telecommunication and Acoustics, Technical University of Wrocław
(50-370 Wrocław, Wybrzeże St. Wyspiańskiego 27)

This paper presents results of a psychoacoustic experiment which consisted in length estimation of a quasi-linear horizontal sound source, performed by listeners. At preserved similarities of obtained dependences, considerable differences between responses of individual listeners were stated. Size evaluations did not reflect the source's length, but were in linear dependence with the maximal value of a normalized cross correlation function of signals reaching the listener's left and right ear. An increase of sound level caused an increase of the source's apparent length within the given series of estimations.

Measurement results presented on the background of investigations on sound volume and sound spaciousness in concert halls indicate that volume and auditory spaciousness are different forms of the same impression quantity.

W pracy przedstawiono wyniki eksperymentu psychoakustycznego, w którym słuchacze oceniali długość quasi-liniowego, poziomego źródła dźwięku. Stwierdzono znaczne różnicowanie odpowiedzi pomiędzy poszczególnymi słuchaczami przy zachowaniu podobieństwa uzyskanych zależności. Oceny rozległości nie odzwierciedlały długości źródła, natomiast wykazywały liniową zależność od maksymalnej wartości unormowanej funkcji korelacji wzajemnej sygnałów docierających do lewego i prawego ucha słuchacza. Wzrost poziomu dźwięku powodował zwiększenie pozornej długości źródła w ramach danej serii ocen.

Wyniki pomiarów, które przedyskutowano na tle dotychczasowych badań nad wolumenem dźwięku oraz przestrzennością dźwięku w salach koncertowych, wskazują, że wolumen i rozległość słuchowa są różnymi formami tej samej wielkości wrażeniowej.

1. Introduction

A. Auditory spaciousness

Besides sound localization auditory spaciousness is the second feature of sound related with the interpretation of auditory impressions on the background of

⁽¹⁾ Research was performed within programme CPBP 02.03 and Institute's own studies.

surrounding three-dimensional space. Problems of spaciousness have been studied much more rarely than problems of sound localization. This last group of problems has been theoretically founded and descriptive, as well as explanatory, investigations have been carried out (see eg. BLAUERT [5]).

Contemporary knowledge on sound spaciousness perception comes from studies on sound quality in concert halls, mainly. These studies have been performed during the last twenty five years [2, 15, 16]. For the impression of sound spaciousness has been found to be one of the fundamental criteria for sound quality evaluation in concert halls [1, 6, 21].

The problem of sound spaciousness is also found in other fields of psychoacoustics. Changes of impressions of sound spaciousness in binaural fusion investigations are due to differentiation of signals in the left and right ear of the earphones [7]. The impression of spaciousness is a significant factor also in quality estimations of sound transmitted in an electroacoustic system. Thus, many methods of sound transmission have been developed in order to increase the impression of spaciousness (see eg. GARDNER [9]). It is still a live issue [12].

According to the systematics of motions, related to the impression of spaciousness, defined by BLAUERT [6], the conception of the type and size of space formed spontaneously by a listener in a given sound field is called the auditory spatial impression. Two main factors constitute the auditory spatial impression. Namely reverberance and auditory spaciousness. Reverberance, which is related to changes of auditory events in time, is influenced by reverberation and late reflections. Where as, auditory spaciousness is the spatial characteristic of auditory events. It results from early lateral reflections (i.e. delayed not more than about 80 ms with respect to direct sound).

Two physical measures can be found in literature which have been proved to reflect the psychological measure of sound extensity adequately. The ratio energy of early lateral reflections and total sound energy reaching the listener during the first 80 ms is the first measure [2]. While the second one is the absolute maximum value of the interaural cross correlation function of signals reaching both ears, normalized in relation to the total energy of signals [15, 21]. It is sometimes called the degree of coherence [5]. The lower is the degree of coherence of signals, the higher spaciousness is.

The spaciousness estimation depends also on sound level [2]. In Keet's paper a 10 dB increase of sound level caused an increase of angular dimensions of an apparent sound source of 16° [15].

In investigations on sound spaciousness in concert halls auditory spaciousness depends on the particular space and given positions of primary and secondary sound sources [16]. Sometimes spaciousness judgements are expressed in terms of angular measure, as the extension of an apparent sound source [15]. Listeners have the ability of estimating two dimensions of an apparent source—width and depth [6].

B. Sound volume

There is a notion of sound volume in classical psychoacoustics which is one of four attributes of tone (loudness, pitch, volume, density) related to its spaciousness, [22].

Stumpf is considered to be [4, 23] the first one to describe extension (*Ausdehnung*) as a subjective tone property in 1883. From that time many psychoacoustics have dealt with this aspect of auditory impression which has been called "volume".

It seems characteristic of results of early studies on volume that on one hand its existence as the attribute of tone was not questioned, whereas on the other hand significant differences between estimations of individual listeners were indicated, as well as a strong relation between estimations of volume and loudness [13, 22].

Volume was finally considered an independent attribute of tone when Stevens developed a new research method consisting in volume levelling of two different tones by a listener. THOMAS [23] applied this method in his extensive measurements of equal-volume curves. Thomas, as well as other researchers before him, have stated that tone volume increases with an increase of its intensity and a frequency decrease. These properties of tone volume have been also confirmed by results of investigations on volume scaling with the method of magnitude estimation [18] and the fractionation method [13].

The physiology of hearing explains basic attributes of tone, such as loudness and pitch. A similar explanation was sought for volume. Bekesy, among others, was a supporter of the Lehmann's hypothesis concerning the relation between tone volume and basilar membrane excitation [4]. Earlier James set forth a hypothesis, in which the ability of sound spaciousness estimation is a learned ability based on the fact that large acoustic sources more frequently produce low frequency and high level sounds, while small sources on the contrary - high frequency and low level sounds. However, results of comparative examinations of the ability of volume estimations of persons with congenial blindness and persons with good sight did not differ and thus did not confirm James's hypothesis [20].

The notion of volume was also applied in estimations of noise spaciousness [24]. It was stated that an increase of noise volume accompanied an increase of sound level, duration and differentiation between signals reaching both ears [20].

As it results from the above discussion volume as a sound attribute was considered in the classical approach separately from spatial features of the sound and its source. Volume assessments were comparative assessments, or they were expressed in arbitrary scale. Only Bekesy from among other authors related volume estimations with space in which the sound source was located and expressed the assessment of an apparent sound source in meters. At the same time he found that the estimation of the source's dimensions does not depend on the width of the sound producing loudspeaker [3].

Such two notions as sound volume and auditory spaciousness give rise to the

following questions. What mutual relation is there between these psychoacoustic terms? Are these two different quantities, or is there a definite relation between them? Is the size of an apparent sound source a constant value in Euclidean space for given conditions? Is auditory measurement of spaciousness in meters or degrees worth-while? Can the size of a real sound source be estimated directly? Is the estimation of spaciousness equivalent with blurring of sound source localization? A psychoacoustic experiment concerning sound spaciousness estimation was to answer these questions. A sound source with adjustable length was applied in order to determine the influence of dimensions of the source on the estimation of its extension, and to compare spaciousness estimations in conditions characteristic for volume examinations (point source) and spaciousness investigations (horizontally arranged sources).

2. Psychoacoustic experiment

A. Apparatus

A previously developed system for spaciousness examinations of sound produced by a quasi-linear source [10] was used in the experiment.

A system of 30 loudspeakers mounted along the axis of a 300×75 cm acoustic baffle was used as a sound source with adjustable length. There was a distance of 7.5 cm between centres of adjacent loudspeakers. Every loudspeaker had its own closed enclosure. Loudspeakers have been chosen from among a greater lot of loudspeakers with respect to the repeatability of their frequency responses. The three last loudspeakers on one side and four on the other side were dummies. The acoustic baffle was perpendicular to the floor. Loudspeakers were on listener's ear level. A distance of 1.5 m divided the listener from the acoustic baffle. The listener's seat was located symmetrically with respect to the system of the 23 loudspeakers used in the experiment. A pink noise generator with a system of filters on the output was the source of signals.

A band noise with mid-band frequency of 1000 Hz and band width equal to a $1/3$ octave and $1/1$ octave was used, as well as pink noise with band width limited by the loudspeakers frequency response to the 200–8000 Hz interval. The signal from the generator was transmitted to the system of 23 loudspeaker amplifiers (Fig. 1).

Every loudspeaker could be switched off with an electronic key contained by every amplifier. Keys were microcomputer controlled. Thus, any number of loudspeakers from among the 23 of them could be switched on. In this experiment symmetrical systems of sources, consisting of 1, 3, 5, 9, 15 and 23 loudspeakers, were used.

Double level balancing of sound produced at listening point was applied in the experiment. First of all sound levels were balanced inside the loudspeaker system –

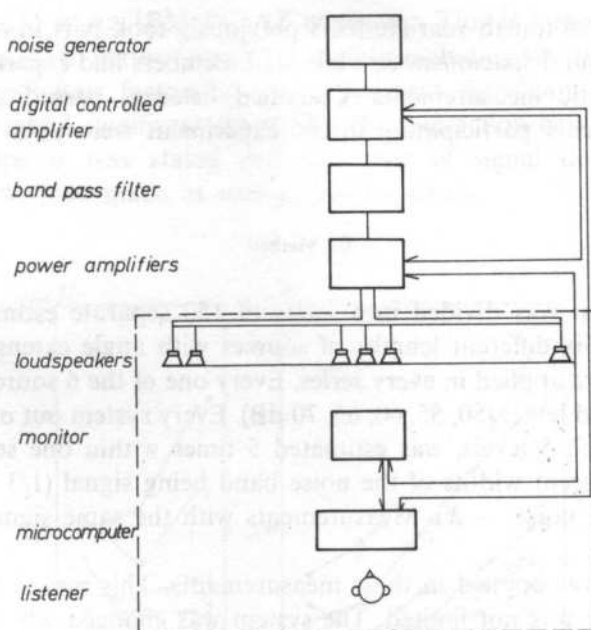


FIG. 1. Block diagram of the measuring system

every loudspeaker in a given system produced a sound with equal level at the listening point. Secondly, systems were balanced — the resultant sound level did not depend on the number of switched on loudspeakers.

Notations on the acoustically transparent fabric covering the loudspeakers were to enable listeners to estimate sound extensity by giving coordinates of boundaries of the apparent sound source. Coordinates could be determined with 1.25 cm accuracy, corresponding to about 0.5° in the central area of the source. Answers of the listener concerning the position of the left and right boundary of the apparent sound source were introduced into a microcomputer from the keyboard. Results of every series of measurements were recorded on a floppy disc.

Monitors within listeners sight, but out of the path of waves travelling from loudspeakers to the observation point, displayed information about takes to be performed by listeners at a given moment.

Measurements were conducted in an audiomonitoring studio with 25 m² surface, 92 m³ volume and reverberation time of about 0.4 s [25].

B. Listeners

6 listeners participated in investigations — students and staff members of the Institute of Telecommunications and Acoustics. Listeners had various previous experience concerning psychoacoustic experiments: two third-year students had no

such experience two fourth-year students previously took part in other experiments concerned with sound spaciousness, while staff members had experiences from many other psychoacoustic measurements. Classified listeners passed audiometric tests successfully. Students participating in the experiment were paid on an hour rate basis.

C. Method

The experiment was divided into series of 150 separate estimations of source extensions each. Six different lengths of sources with angle extension in the range from 3° to 60° were applied in every series. Every one of the 6 sources was presented at 5 different sound levels (50, 55, 60, 65, 70 dB). Every system out of the 30, resulting from 6 sources and 5 levels, was estimated 5 times within one series. Subsequent series applied different widths of the noise band being signal (1/3 octave — *T*, 1/1 octave — *O*, pink noise — *R*). Measurements with the same signal were repeated, also.

Free rhythm was applied in these measurements. This means that the listening and response time was not limited. The system was changed when the answer was introduced into the microcomputer. The duration of a single series of measurements varied from 20 to 40 minutes for different listeners. The sequence of presentation of sources with different levels and lengths was randomly chosen at the beginning of each series.

3. Results

A. Analysis of collected results

Answers of listeners concerning the position of the left and right boundary of the sound source have been converted into angular values. They form a set of values of the *Y* dependent variable. Every spaciousness estimation Y_i was obtained for a definite combination of independent variables. The angle extension of the sound source (variable *P6*) and sound level produced by the source (variable *P5*) were the independent variables. They were randomized within one measurement series. Furthermore, there were two independent variables which were the parameters of a given series. These were: listeners number (variable *P2*) and symbol of noise bands (variable *P4*).

For such a great number of factors in the experiment it becomes a problem to present the effect of individual independent variables on the result of measurements and interactions between variables. These problems were solved by using the ANOVA analysis of variance [8] in statistic elaborations of results. However, a four-factor analysis of variance, including all possible interactions, requires over

1100 KByte of RAM in an IBM PC AT computer. This is impossible to achieve. However, it is possible to perform variance analysis including two factor interactions. ANOVA proved all four factors of the experiment significant. Also two-factor interactions were found significant, except for the interaction between variables $P4$ and $P5$. Therefore, it was stated that the type of signal does not influence spaciousness estimations made at various sound levels.

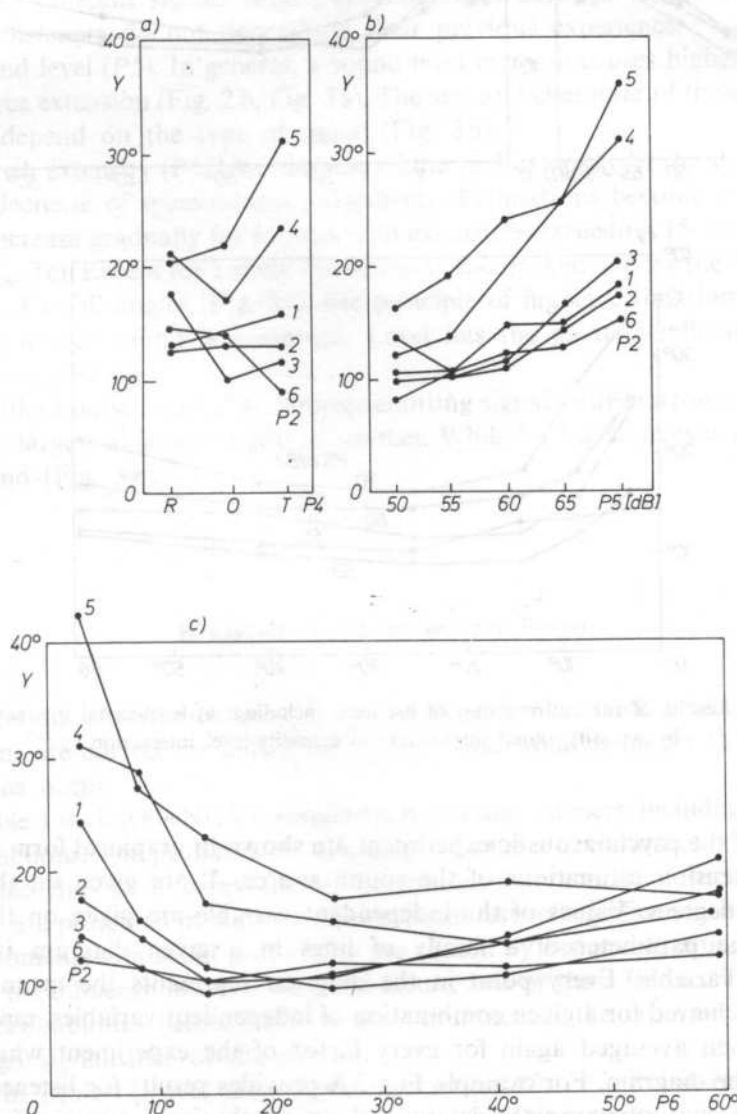


FIG. 2. Measurement results for individual listeners in terms of: a) type of signal $P4$, b) sound level $P5$, c) extensity of the sound source $P6$

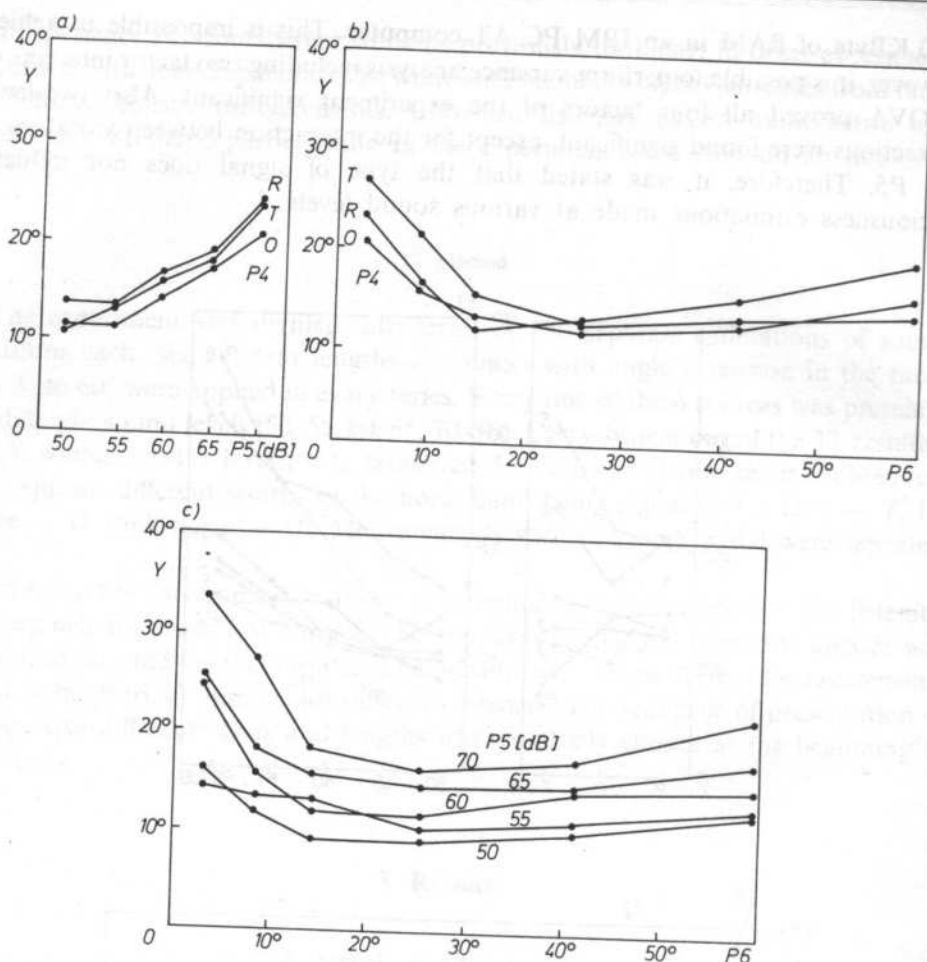


FIG. 3. Results of the entire group of listeners, including: a) level-signal interaction, b) extent-signal interaction, c) extent-level interaction

Results of the psychoacoustic experiment are shown in graphical form in Figs. 2, 3 and 4. Extension estimations of the sound source, Y , are given on the axis of ordinates in degrees. Values of the independent variable are given on the axis of abscissae. The parameter of a family of lines is given on the axis of independent variable. Every point in the diagram represents the mean value of estimations achieved for a given combination of independent variables, repeated five times, and then averaged again for every factor of the experiment which is not included in the diagram. For example Fig. 2A provides results for listener 4 in the form of lines connecting points determined on the basis of answers for various signals. The average estimation marked by every point was obtained from five times repeated spaciousness estimations made for six different lengths of the source. Then,

every one out of these thirty combinations had to be included for every one out of five values of sound level. Therefore, it is an average of 150 answers.

The effect of individual factors on estimations can be described on the basis of data from Figs 2 and 3:

1. Listeners (*P2*). In spite of differences in absolute values of estimations between individual listeners, the arrangement of estimations was similar with respect to source extensity (Fig. 2 c), as well as sound level (Fig. 2 b). No regularity was noticed for lines for different signals (Fig. 2 a). Differences between estimations made by individual listeners do not depend on their previous experience.

2. Sound level (*P5*). In general, a sound level increase causes higher judgements of the source extension (Fig. 2 b, Fig. 3 a). The size and character of these judgements does not depend on the type of signal (Fig. 3 a).

3. Source extensity (*P6*). An increase of the real extensity of the source initially causes a decrease of spaciousness judgements. Estimations become stable or even begin to increase gradually for sources with extensities exceeding 15° to 20° (Fig. 2 c, Fig. 3 b Fig. 3 c). Except for a small distortion of the broken line for the 55 dB level in the range of small angles (Fig. 3 c), the principle of higher estimations for sources generating louder sound is preserved. Level has the greatest influence for small extensities of sources.

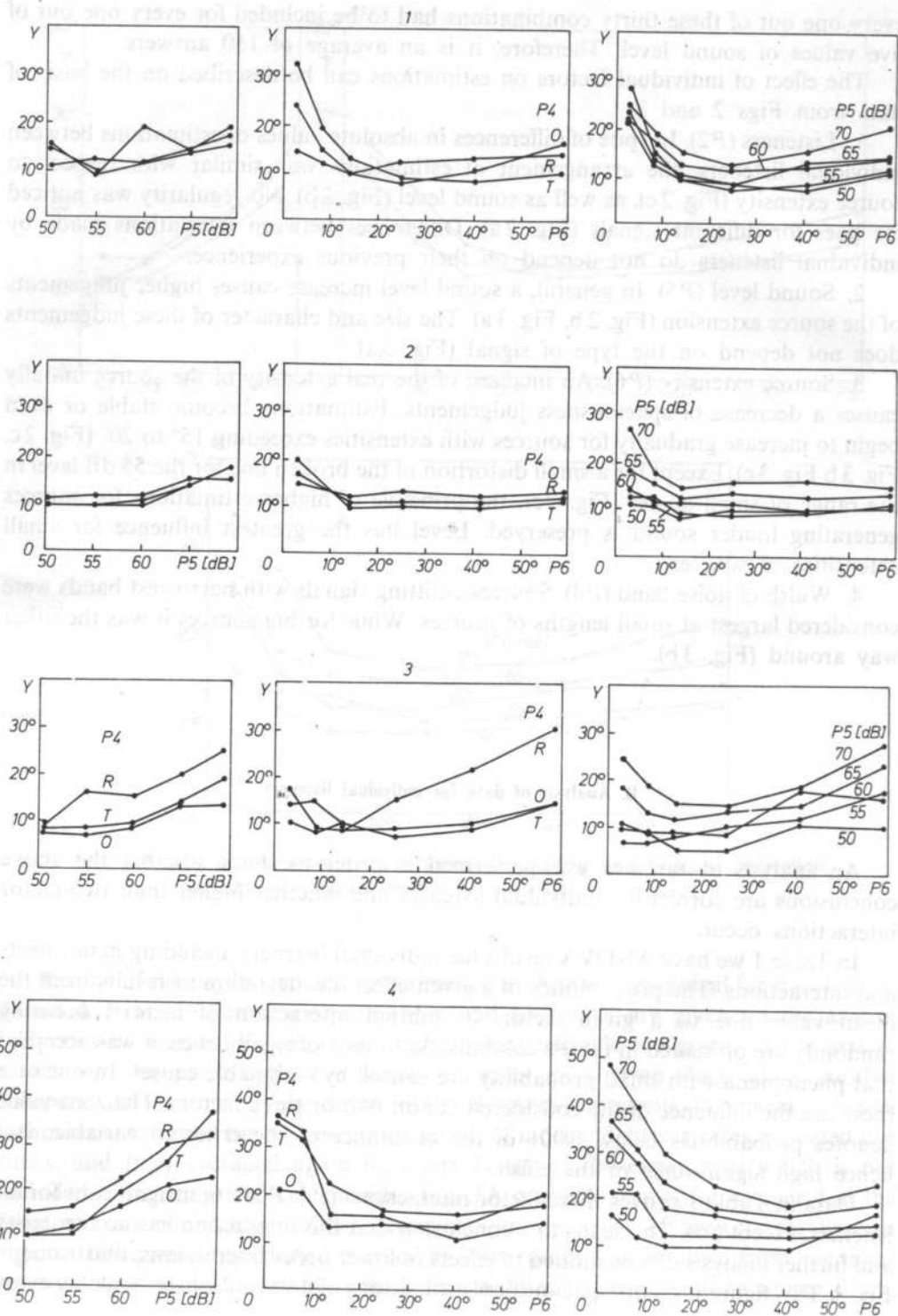
4. Width of noise band (*P4*). Sources emitting signals with narrowest bands were considered largest at small lengths of sources. While for big sources it was the other way around (Fig. 3 b).

B. Analysis of data for individual listeners

An analysis of variance was performed in order to check whether the above conclusions are correct for individual listeners and whether higher than two-factor interactions occur.

In Table 1 we have ANOVA results for individual listeners, including main effects and interactions. The probabilities of a given effect (i.e. deviation of results from the mean value due to a given factor, or mutual interaction of factors) occurring randomly are presented in table's columns. As in tests of significance, it was accepted that phenomena with small probability are caused by assignable causes. In our case these are the influence of the considered factor, two or three factors. The zero value denotes probabilities below 0.001 of the occurrence of the criterion variable, and hence high significance of the effect.

Data in Table 1 proves three-factor interactions (*P4-P5-P6*) insignificant for all listeners, except one. This leads to a conclusion that this interaction has no regularity and further analysis can be limited to effects of lower order interactions, illustrated in Fig. 4. This figure presents spaciousness estimations of a sound source made by every



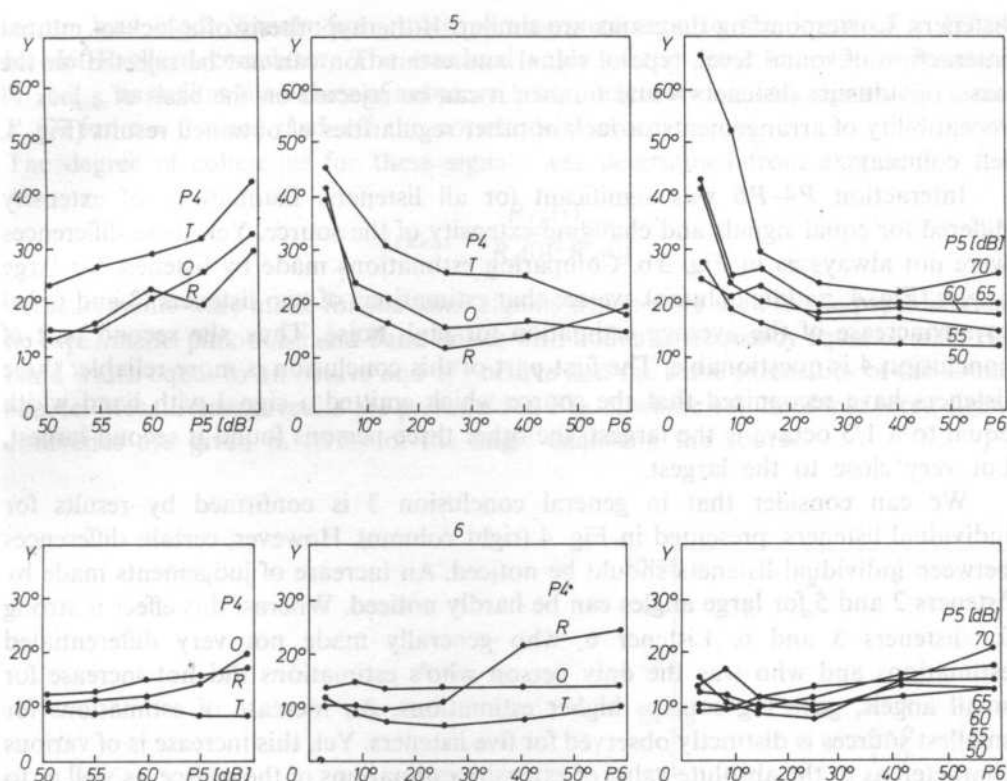


FIG. 4. Individual results for 6 listeners: left column — in terms of level and signal, middle column — in terms of extensity of source and signal, right column — in terms of extensity of source and level

Table 1. ANOVA results for individual listeners

nr	Listener effect/interaction						
	P4	P5	P6	P4-P5	P4-P6	P5-P6	P4-P5-P6
1	0,002	0	0	0,760	0	0,834	0,31
2	0,704	0	0	0,116	0	0	0,232
3	0	0	0	0,082	0	0,452	0,589
4	0	0	0	0	0	0	0,558
5	0	0	0	0,607	0	0	0
6	0	0	0	0	0	0,533	0,037

listener separately, in terms of sound level (left column) and extensity of the source (middle and right column). The type of signal (left and middle column) and sound level (right column) are parameters of families of lines in diagrams.

Conclusions made previously find a confirmation in data for individual listeners. The influence of the P4-P5 interaction is statistically insignificant for a majority of

listeners. Corresponding diagrams are similar. If the hypothesis of a lack of mutual interaction of sound level, type of signal and estimation can not be rejected on the basis of statistics (listeners 4 and 6), then it can be rejected on the basis of a lack of repeatability of arrangements or lack of other regularities of obtained results (Fig. 4, left column).

Interaction $P4-P6$ was significant for all listeners. Estimations of extensity differed for equal signals and changing extensity of the source. Yet, these differences were not always as in Fig. 3b. Comparing estimations made by listeners for large angles (Fig. 4, middle column), we see that estimations of two listeners (3 and 6) led to an increase of the average estimation for pink noise. Thus, the second part of conclusion 4 is questionable. The first part of this conclusion is more reliable: three listeners have recognized that the source which emitted a signal with band width equal to a $1/3$ octave is the largest, the other three persons found it second largest, but very close to the largest.

We can consider that in general conclusion 3 is confirmed by results for individual listeners, presented in Fig. 4 (right column). However, certain differences between individual listeners should be noticed. An increase of judgements made by listeners 2 and 5 for large angles can be hardly noticed. Whereas, this effect is strong for listeners 3 and 6. Listener 6, who generally made not very differentiated estimations and who was the only person who's estimations did not increase for small angles, gave big sources higher estimations. An increase of estimations for smallest sources is distinctly observed for five listeners. Yet, this increase is of various character, as to the absolute value of extensity estimations of the source, as well as to the relations between estimations of sources with different level. A lack of significance of interaction $P5-P6$ (in Table 1) for listeners 1, 3 and 6 results from limitations of the analysis of variance method. ANOVA does not take into account the arrangement or mutual numerical relations between levels of the factor. Information on values of factors (angle extensity of the source in this case) is limited to the level of nominal scale. The stated regularity becomes visible when results are presented in the form of a diagram, in terms of angle, measured in ratio scale.

4. Measurements of the coefficient of interaural correlation

Practically a lack of a relation of extensity evaluations with actual dimensions of the sound source, or even the occurrence of reverse estimations for small sources is the most distinct characteristic of obtained results. In order to explain this effect, the value of the parameter related with the evaluation of sound spaciousness in concert halls was measured. The absolute value of the maximum interaural cross correlation function of signals reaching both ears of the listener, related to the total energy of these signals, is this parameter. A pair of microphones, 18 cm from each other and placed in the spot where the listener's head was during psychoacoustic measure-

ments, was used. Signals from microphones were sent to the input of a 3721A Hewlett-Packard correlator. The maximal value of the cross correlation function $R_{LR}(\tau)_{\max}$ as well as the values of autocorrelation functions for both signals $R_L(0)$ and $R_R(0)$ for $\tau = 0$ were read off the correlator's screen.

The degree of coherence for these signals was determined from expression:

$$Q_{LR\max} = \frac{R_{LR}(\tau)_{\max}}{R_L(0) \cdot R_R(0)} \quad (1)$$

Measurements were made for the same signals which were used in the psychoacoustic experiment: pink noise and band noises with midband frequency equal to 1000 Hz, band width equal to an octave and 1/3 octave and the same extensities of the sound source. Measurement results are presented in Fig. 5, where values of measured signal coherence are given in terms of the angle enclosing the source.

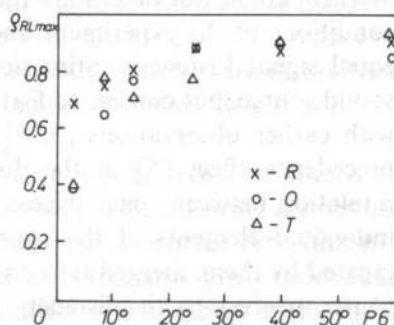


FIG. 5. Results of measurements of the maximum normalized interaural correlation function for three signals: R — pink noise, O — octave band, T — 1/3 octave band

We can see from the Figure that there are no principal differences between results for various signals. All results lie on a line resembling a mirror reflection, with respect to a line parallel to the x-axis, of lines shown in Fig. 3b. Therefore, a suggestion can be made that there is a simple dependence between the maximum value of the normalized function of interaural correlation and the estimation of the sound source extension. Figures 3b and 5 are parametric diagrams of this dependence. Just like Keet [5], we have assumed a linear dependence between $(1 - Q_{LR\max})$ and the estimation of the source's width Y in the following form

$$Y = k \cdot (1 - Q_{LR\max}) + Y_0, \quad (2)$$

where k is the slope of a straight line, Y_0 is the minimal value of estimation for identical signals in both ears. Values of coefficients k and Y_0 were determined by means of the least square method and introduced to expression (2), giving

$$Y = 30.5 - 18.75 Q_{LR\max}. \quad (3)$$

For k on the 0.95 significance level, the confidence interval is equal to $2 \cdot 1.75$. The value of the coefficient of correlation r was calculated in order to check the power of the relation between $(1 - \varrho_{RL\max})$ and Y . It was equal to 0.67.

From equation (3) we can see that estimations of sources extension vary in a range from 11.75° for fully coherent signals to 30.5° for non-correlated signals. However, it should be noticed that this is data averaged for a definite group of listeners, who gave very differentiated estimations of spaciousness, but had a common general trend. A comparison between lines presented in Figs. 3b and 5 leads to a suggestion that there is still another factor, apart from coherence of signals, which influenced spaciousness estimations. This is indicated also by a distinct increase of estimations for the largest sources.

5. Discussion and conclusions

With reference to questions formulated in the introduction we can state that listeners could not determine the position of the actual limits of a sound source in conditions of the experiment and with all elements of the source supplied with an equal signal. Listener's estimations did not concern physical characteristics of the sound source, but concerned features of the impression. This conclusion is consistent with earlier observations [3, 11, 19]. The effect of summing localization and the precedence effect [5] in the discussed experiment are the reasons for a lack of a relation between spaciousness estimations and length of the source. Signals from individual elements of the source were so similar that the auditory impression, created by them, merged into one image located in the middle of a symmetric sound source nearest to the listener.

Spaciousness estimations were made according to an imposed ratio scale identical for all listeners. The differentiation of individual estimations (see Fig. 2 and 4) proves that a given sound created a different impression of spaciousness for individual listeners. The differentiation of values of estimations at their similar character for different listeners at the same time leads to a conclusion that this psychoacoustic experiment should be interpreted as scaling of auditory spaciousness with the method of magnitude estimation. Here we have an analogy to other psychoacoustic experiments aimed at the investigation of dependences between the quantitative attribute of impression and physical quantities, such as for loudness scaling [18].

A comparison of results of the experiment with listeners, with results of measurements of the correlation function proves that the statistic similarity of signals reaching the listener's ears and expressed by the maximum of a normalized cross-correlation function was decisive to spaciousness evaluations. From the linear dependence between Y and $\varrho_{RL\max}$, expressed by equation (3), we can see that when the correlation coefficient is changed by 0.1 then the evaluation of the sound source's width changes by about 1.9° on the average. This change was equal to 3.8° for

sounds with 70 dB level. It is similar to the value of 5.4° achieved by Keet for the 73 dB (A) level [15].

Sound level was the second important factor which influenced evaluations. A linear model of evaluation changes due to extensity in terms of sound level was accepted. In order to compare our results with results of other authors, the average and greatest slopes were calculated. They were equal to $0.55^\circ/\text{dB}$ and $0.93^\circ/\text{dB}$ for a single loudspeaker source ($q_{RL\max} = 0.5$) respectively. As it was mentioned before, Keet obtained a slope of $1.6^\circ/\text{dB}$. However, a power function analogic to that accepted by Stevens for loudness [22] between spaciousness evaluations and acoustic pressure seems more suitable here. Calculated values of the exponent varied from 0.18 for a signal from a single loudspeaker source to about 0.13 for sources radiating signals with degree of coherence equal to about 0.9

In order to fully determine the relation between spaciousness evaluations and level, we should notice that within one series of measurements sound level was changed, as well as extensity of the source. In experiments previously conducted by the authors [11] sound level within one series was constant. In such a case listeners did not relate spaciousness evaluations with the value of sound level. Differences in evaluations between individual series, i.e. for different sound levels were of random character and proved that there was no constant standard which would connect sound level with estimations of spaciousness [11].

Presented properties of sound source extensity evaluation are similar to results of investigations on sound volume and auditory spaciousness. The following properties are characteristic of volume: independence of evaluations of sources type (dimensions), increase of evaluations accompanying sound level increase, great individual variability of evaluations. Then, the similarity to auditory spaciousness evaluations consists in: the dependence of evaluations on the interaural correlation of signals, proportionality between evaluations and sound level, consideration and evaluation of width changes of the apparent sound source due to independent variables. Hence, it seems that we can consider volume as well as auditory spaciousness as various forms of the same impression quantity. It is a multidimensional quantity, dependent on an entire set of physical factors.

The stated lack of dependence between dimensions of the source and extension evaluations is in conflict with James'es hypothesis, presented in the introduction and concerned with the practical foundation of volumen's properties consisting in the evaluation of the sound source's size.

In order to explain the mechanism of forming an impression of spaciousness, on the basis of stated dependence on interaural correlation, a binaural correlation model of signal processing has to be applied (e.g. [17]). Because of the dependence of evaluations on sound level, the model has to include the intensity of the stimulus, may be in relation with the excitation surface of the basilar membrane. The necessity of assuring the functioning of the model for monaural hearing results from the existence of such an ability of man [20].

6. Summary and final remarks

Performed research has led to the determination of characteristics of sound volume as well as auditory spaciousness in listener's evaluations.

Two factors, i.e. sound level and degree of coherence influenced evaluations. The first factor is rather associated with volume, while the second one — with the width of an apparent sound source. Geometric dimensions of the actual sound source did not influence evaluations.

A dependence between evaluations and width of noise band was not stated. This conclusion can not be considered as final, because the construction of the psychoacoustic experiment makes it impossible to compare directly sounds with different bands. As it can be seen from an analogic situation concerning investigations on the influence of sound level, experiments including spaciousness evaluations are very sensitive to possibilities of direct comparison between examined factors. This results from a lack of a constant standard relating the value of the estimation and parameters of the signal.

The problem of a relation between auditory spaciousness and localization blurring still remains among questions without satisfactory answers. Data from literature indicate that an increase of localization blurring accompanies an increase of the impression of spaciousness [14]. However, this is far from complete knowledge. In the conditions of our experiment applying a symmetric source we could not achieve data concerning localization.

Also the cause for a discrepancy between listeners' evaluations and the maximum of interaural correlation function for longest sources remains unexplained. Further research should be aimed at the determination whether it is the effect of a not identified physical factor, or maybe this discrepancy could be reduced by applying a different technique of measuring the correlation function.

References

- [1] M. BARRON, *The subjective effects of first reflections in concert halls — the need for lateral reflection*, J. Sound Vib. **15**, 475–494 (1971).
- [2] M. BARRON, H. A. MARSHALL, *Spatial impression due early lateral reflections in concert halls*, J. Sound Vib. **77**, 211–232 (1981).
- [3] G. v. BEKESY, *Experiments in hearing*, McGraw-Hill, New York 1960.
- [4] G. v. BEKESY, *Hearing theories and complex sounds*, J. Acoust. Soc. Am. **35**, 588–601 (1963).
- [5] J. BLAUERT, *Raumliches Hören*, S. Hirzel, Stuttgart 1974.
- [6] J. BLAUERT, W. LINDEMANN, *Auditory spaciousness: Some further psychoacoustic analyses*, J. Acoust. Soc. Am. **80**, 533–541 (1986).
- [7] J. BLAUERT, W. LINDEMANN, *Spatial mapping of intracranial auditory events for various degrees of interaural coherence*, J. Acoust. Soc. Am. **79**, 806–813 (1986).
- [8] J. BRZEZIŃSKI, R. STACHOWSKI, *Application of analysis of variance in experimental psychological tests* (in Polish), PWN, Warsaw 1984.

- [9] M. B. GARDNER, *Image fusion, broadening and displacement in sound location*, J. Acoust. Soc. Am. **46**, 339-349 (1969).
- [10] B. GRANICKI, J. RENOWSKI, K. RUDNO-RUDZIŃSKI, *Error of spaciousness estimation of a linear sound source* (in Polish), Sci. Proc. Inst. Telecomm. and Acoust. Technical University of Wrocław, Series: Conferences, XXXIV Open Seminar on Acoustics, Wrocław 1987, pp. 93-97.
- [11] B. GRANICKI, J. RENOWSKI, K. RUDNO-RUDZIŃSKI, *Effect of experiment organization on results of spaciousness of an apparent sound source* (in Polish), Proc. of the XXXV Open Seminar on Acoustics, Białowieża 1988, pp. 319-324.
- [12] D. GRIESINGER, *Spaciousness and localization in listening rooms and their effects on the recording technique*, J. Audio Eng. Soc. **34**, 255-268 (1986).
- [13] W. L. GULICK, *Hearing, physiology and psychophysics*, Oxford Univ Press, New York-London 1971.
- [14] L. A. JEFFRESS, H. C. BLODGET, B. H. DEATHERAGE, *Effect of interaural correlation on the precision of centering a noise*, J. Acoust. Soc. Am. **34**, 1122-1123 1962.
- [15] W. de V. KEET, *The influence of early reflections on the spatial impression*, 6th International Congress on Acoustics, Tokyo, E-2-4 - 1968.
- [16] W. KUHL, *Raumlichkeit als Komponente des Raumeindrucks*, Acoustica **40**, 167-181 (1978).
- [17] W. LINDEMANN, *Extension of a binaural cross-correlation model by contralateral inhibitions*, J. Acoust. Soc. Am. **80**, 1608-1622 (1986).
- [18] L. E. MARKS, *Sensory processes, The new psychophysics*, Academic Press, New York 1974.
- [19] D. R. PERROT, *Discrimination of the spatial distribution of concurrently active sound sources: Some experiments with stereophonic arrays*, J. Acoust. Soc. Am. **76**, 1704-1712 (1984).
- [20] D. R. PERROT, T. N. BUELL, *Judgements of sound volume: Effects of signal duration, level and interaural characteristics on the perceived extensity of broadband noise*, J. Acoust. Soc. Am. **72**, 1413-1417 (1982).
- [21] M. R. SCHROEDER, D. GOTTLÖB, K. F. SIEBRASSE, *Comparative study of European concert halls: correlation of subjective preference with geometric and acoustic parameters*, J. Acoust. Soc. Am. **56**, 1195-1201 (1974).
- [22] S. S. STEVENS, H. DAVIS, *Hearing, its psychology and physiology*, Wiley, New York 1938.
- [23] G. J. THOMAS, *Equal-volume judgements of tones*, Amer. J. Psychol. **62**, 182-201 (1949).
- [24] G. J. THOMAS, *Volume and loudness of noise*, Amer. J. Psychol. **65**, 588-593 (1952).
- [25] Z. ŻYSZKOWSKI, B. KULESZA, Z. WĄSOWICZ, *Audio monitoring room for subjective examinations of sound transmission quality* (in Polish), Zeszyty Naukowe Politechniki Wrocławskiej, Wrocław 1967, Łączność z. 13 pp. 103-123.

Received on June 11, 1989

LOW-CYCLE FATIGUE INVESTIGATION BY ACOUSTIC EMISSION METHOD

J. SIEDLACZEK **, S. PILECKI *, F. DUŠEK ***

* Institute of Fundamental Technological Research, Polish Academy of Sciences
(00-049 Warsaw, Świętokrzyska 21)

** High Pressure Research Center, Polish Academy of Sciences
(01-142 Warsaw, Sokołowska 21)

*** Institute of Physical Metallurgy, Czechoslovak Academy of Sciences
(616-62 Brno, Žižkova 22)

The results of the measurements of acoustic emission (AE) count rate are presented during low-cycle fatigue of the variously heat treated 45HNMFA structural steel, which can be used for the production of high-pressure chambers. The experimental technique is described briefly. The most important result of this investigation is the occurrence of three stages of the AE activity during the low-cycle fatigue. These dependencies can be applied in monitoring of the service life (safe exploitation period) of high-pressure chambers and/or other studied objects.

W artykule omówione są wyniki pomiarów gęstości zliczeń emisji akustycznej występującej podczas nisko cyklowego zmęczenia stali konstrukcyjnej 45HNMFA, używanej do wytwarzania komór wysokociśnieniowych. Krótko naświetlono przebieg prac doświadczalnych. Najważniejszym wynikiem badań jest stwierdzenie występowania trzech stadiów nasilenia emisji akustycznej w procesie niskocyklowego zmęczenia. Zależności te mogą być wykorzystane podczas monitorowania rozwoju uszkodzeń (oceny bezpiecznego czasu użytkowania) komór ciśnieniowych oraz/lub innych obiektów technicznych.

1. Introduction

When investigating the properties of materials in the region of low-cycle (high loading amplitudes) fatigue, they are supported by the records of hysteresis loops arisen due to elastic-plastic deformations during particular loading cycles. The area delimited by the loop is proportional to the energy dissipated by the material during this loading cycle [1]. From the practical point of view, the purpose of the investigation at low-cycle loading is as follows:

a) determining the service life of a specimen or a machine part at the given loading level;

b) estimating the allowable load for the given number of cycles to failure.

The problems in question are the accuracy we are able to apply in defining this and the certainly how we can put the obtained results into practice. It is difficult to answer these questions in an exhaustive way. It is a very serious problem, for when dimensioning (the calculation) of constructions working at the low number of cycles to failure we can reach either by the influence of necessary scattering or by an inaccurate estimation of the limiting deformation (or stress) value, the close neighborhood of the fracture curve, so that a possible failure of the structure can appear.

Such a case occurs in high-pressure chamber [2] working in conditions of low-cycle loading. The fatigue computations [7] based on the presumptions of Lamé do not give satisfactory results, because the problem is being solved in the region of elastic deformations (strains) and the calculated allowed loading is then (at the security coefficient $n = 1$) up to 4 times lower than that used for dimensioning the high-pressure chamber for laboratory practice. In this situation, a complicated system of protections from possible consequences of a breakdown of the high-pressure chamber must be used. These systems, however, do not protect the materials and equipments inside the chamber or in its close neighborhood. This practice does not enable to make full use of the material for high-pressure chamber rationally, either.

That is why an attempt has been made to include the acoustic emission (AE) method in the research of low-cycle fatigue of the 45HNMFA steel used for the production of high pressure chambers. It was expected that the AE activity, as well as the area of hysteresis loop, would be proportional to the energy dissipated by the material during one loading cycle. Besides, it was supposed that the AE activity in samples would be similar to that in working pressure chambers made of the same material. This would give a possibility to use the AE as a crack detection method for parts serving in the region of low-cycle fatigue — in our case, a possibility of the estimation of safe service life of the high-pressure chambers.

In the present paper, the results of AE measurements on the samples of variously heat treated 45HNMFA steel during low-cycle fatigue transient tensile loading are brought up.

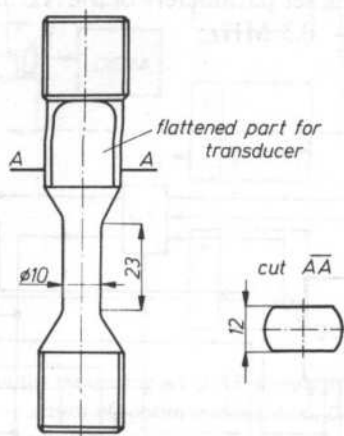
2. Experimental details

The experimental study of AE during the low-cycle fatigue was carried out on the samples of the 45HNMFA steel produced by Polish industry. Its chemical composition is given in Table 1.

From this material, 12 test specimens were made according to Fig. 1. Then they were divided into three groups, heat treated (quenched and tempered) to three

Table 1. Chemical composition of 45HNMFA steel (in weight %)

C	Mn	Si	Cr	Ni	Mo	V	S	P	Fe
0.45	0.50	0.30	1.00	1.70	0.25	0.15	0.027	0.026	Rest

**FIG. 1.** Dimensions and form of test specimens

different Rockwell hardnesses — 30, 40 and 50 HRC and marked: 0, 1 and 2, respectively. Thus, each specimen has double number: the first figure is the number of the group, and the second — is the number of the specimen inside this group, e.g. 03, 21 etc. Conventional mechanical properties after the heat treatment are presented in Table 2.

Table 2. Mechanical properties of 45HNMFA steel

Rockwell Hardness	σ_{ys}	σ_u	A_5	Necking
HRC	MPa	MPa	%	%
30	975	1050	17	44
40	1375	1585	12	34
50	1500	1875	10	32

The loading of specimens in the low-cycle fatigue region was performed with the testing machine Zwick 20T. The specimens were loaded by variable force with triangle-waveform from zero up to the constant maximum amplitude, determined according to the value of total plastic deformation, chosen before. The crossbar shift rate of the testing machine was chosen to 2 mm/min.

The AE was measured by the analyzer AE 10—UFM CSAV (Fig. 2), developed in the Institute of Physical Metallurgy of the Czechoslovak Academy of Sciences in Brno [3]. This analyzer has been constructed as a ten-channel device with amplitude levels firmly set up. The frequency range of linear circuits is 30 kHz ... 2 MHz. The dynamic range of this amplitude analyzer is 40 dB, and therefore the separation of individual channel is 4 dB. The set parameters of the AE analyzer were: amplification 70 dB and band pass 0.1 — 0.3 MHz.

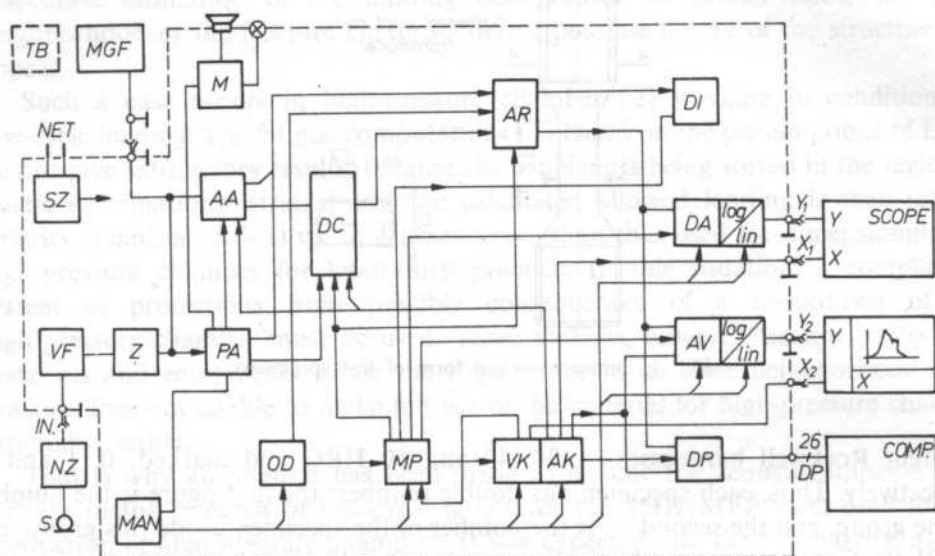


FIG. 2. Block diagram of the AE 10 Analyzer: NZ — low-noise input amplifier, VF — electronic filters, Z — linear amplifier, PA — threshold analyzer, AA — ten-channels amplitude analyzer, DC — counter, OD — control and pilot circuits, MP — multiplexer control, VK — channel choice modulus, DA — D/A converter, M — acoustic and optical monitor, SZ — power supply unit

Besides, AE signals caused by oscillations of the testing machine Zwick were checked, when arranging the measuring set according to Fig. 3, by the AE analyzer DEMA-10 RMS, developed in the Experimental Department TECHPAN attached to the Institute of Fundamental Technological Research of the Polish Academy of Sciences, Warsaw. It was found that no foreign interfering AE signals input into the specimen test result.

To measure AE signals, a suitable probe was chosen from the set products of the Polish firm UNIPAN, Warsaw. The estimation of frequency characteristics by means of a spark calibrator were carried out in the Institute of Physical Metallurgy, Czechoslovak Academy of Sciences [4]. The frequency characteristic is given in Fig. 4.

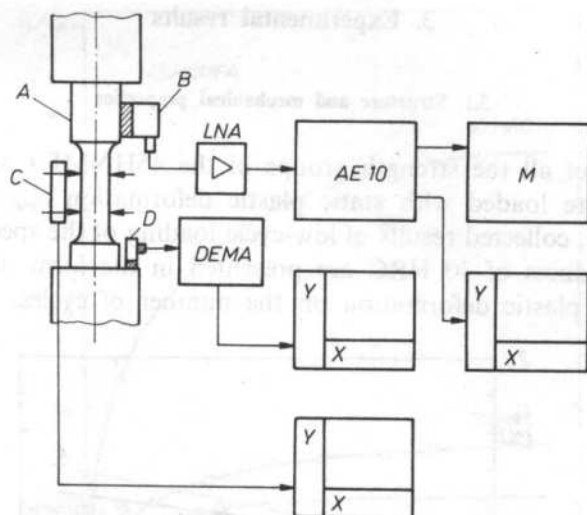


FIG. 3. Diagram of arrangement of the measuring set of AE signals during low-cycle fatigue tests. *A* — test specimen, *B* — AE transducer, *C* — sensor of specimen elongation, *D* — acoustic transducer pickup of test machine vibration, *LNA* — low-noise input amplifier 40 dB, *AE 10* — a Czechoslovak AE analyzer, *M* — monitor, *DEMA* — a Polish AE analyzer, *XY* — coordinate recorder

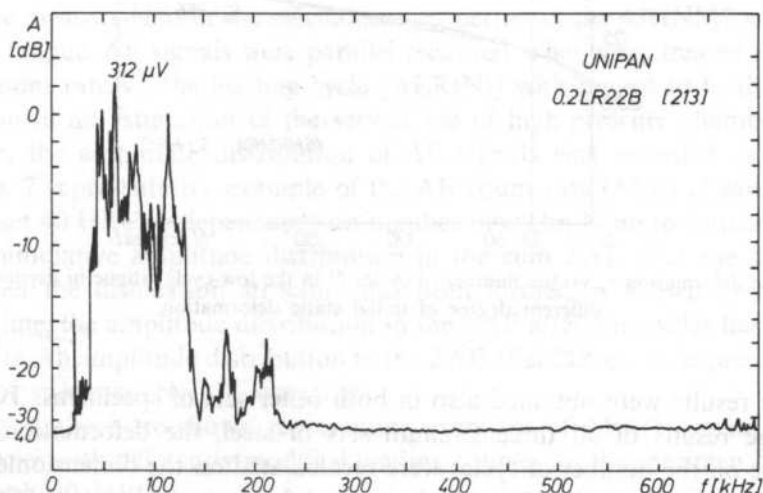


FIG. 4. Frequency characteristic of the acoustic emission transducer UNIPAN — 02LR22B, No. 213

3. Experimental results

3.1. Structure and mechanical properties

The samples of all the strength groups of the 45HNMFA steel — see Table 2 — initially were loaded with static plastic deformation $\varepsilon_{pin} = 0.310$; 0.800 or 1.345%. In Fig. 5, collected results of low-cycle loading of the specimens No. 01, 02 and 03 with hardness of 30 HRC are presented in the form of dependencies of cumulative total plastic deformation on the number of cycles.

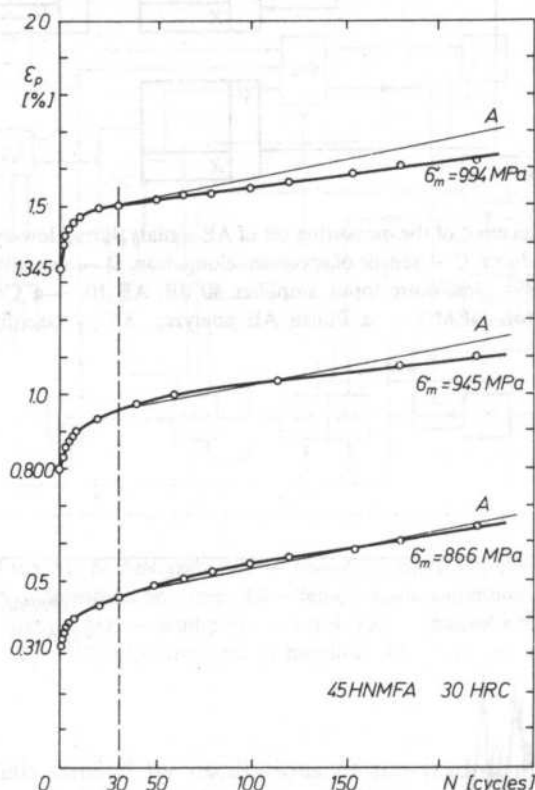


FIG. 5. Plastic deformation ε_p vs. the number of cycles N in the low-cycle fatigue in dependence on the different degree of initial static deformation

Similar results were obtained also in both other sets of specimens. To compare the average results of all three strength sets of steel, the deformation values in dependence on the number of cycles were recalculated on the dimensionless relative quantity given by the ratio of the final plastic deformation ε_p to the initial one ε_{pin} . That made it possible to show all the curves of deformation vs. number of cycles from the beginning of rectangular coordinate system — see Fig. 6.

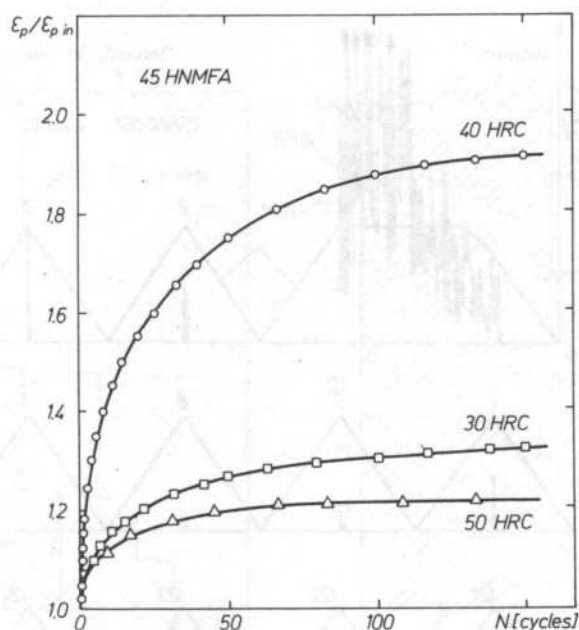


FIG. 6. Normalized courses of plastic deformation $\varepsilon_p/\varepsilon_{pin}$ for all three strength sets of the 45HNMFA material during low-cycle fatigue

3.2. Acoustic emission

During measurement of the mechanical properties of the 45HNMFA steel in the low-cycle fatigue, AE signals were parallel recorded. They were treated in a form of the AE count rate vs. the loading cycle [AER(N)] with regard to further practical application in an estimation of the service life of high-pressure chambers. At this procedure, the amplitude distribution of AE signals was recorded as well.

In Fig. 7 representative example of the AE count rate (AER) of sample No. 11 from the set 40 HRC in dependence on number of cycles N up to fracture is shown.

The cumulative amplitude distribution in the sum ΣAE after the first loading cycle, when the dislocation structure has been formed, is shown in Fig. 8a. By a dashed line, the amplitude distribution in the ΣAE after 136 cycles has been given here. In Fig. 8b amplitude distribution in the ΣAE after 206 cycles is presented, when fracture of specimen No. 11 occurred.

In Fig. 9, there are shown representing examples of AER(N) measurements in several cycles with differently modified loading courses on the specimen No. 03 from the set with 30 HRC.

The results with the same character, even though quantitatively different, were obtained, too, on all other samples in all the hardness sets.

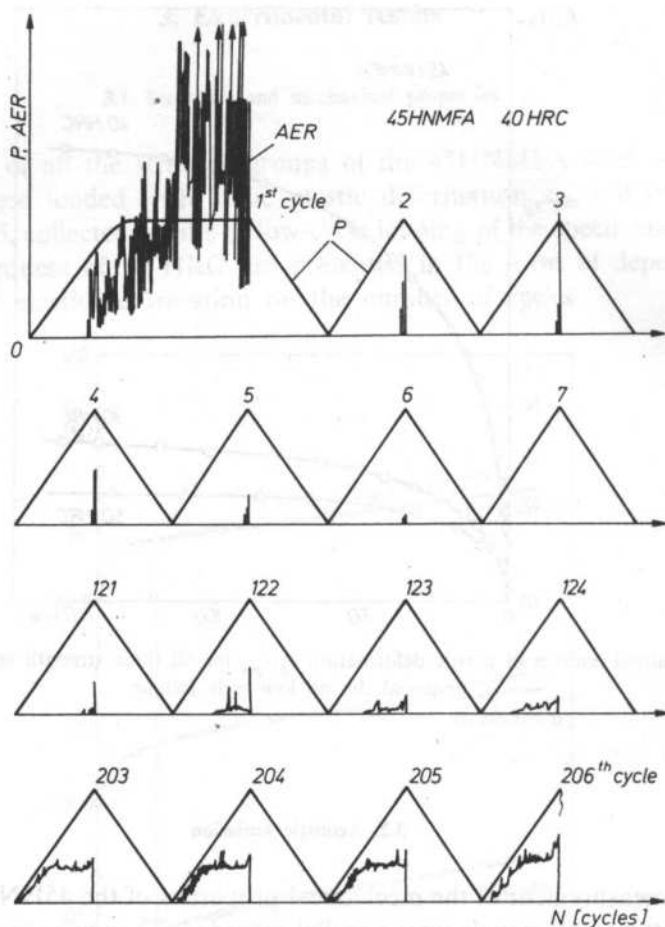


FIG. 7. Activity of the AE signals in the low-cycle fatigue process of the 45HNMFA material, hardness of 40 HRC

By means of the dependencies found this experimental way, three AE activity regions can be marked during low-cycle fatigue:

a) high AE activity in the first cycle (with aftereffects by slight "showers" of AE signals in some few following cycles) bound with forming of a dislocation structure during plastic deformation, i.e. new dislocation generation and displacement;

b) extinguishment of AE signals from several initial cycles up to ca a half of the number of cycles to the failure of the specimen;

c) rise of a new AE activity starting from about half of the number of cycles to the failure. Now the first AE signals occur by maximum loading only (see Fig. 7), then they take place by lower and lower one, and up to the failure. The amplitudes of AE signals increase step-by-step as well.

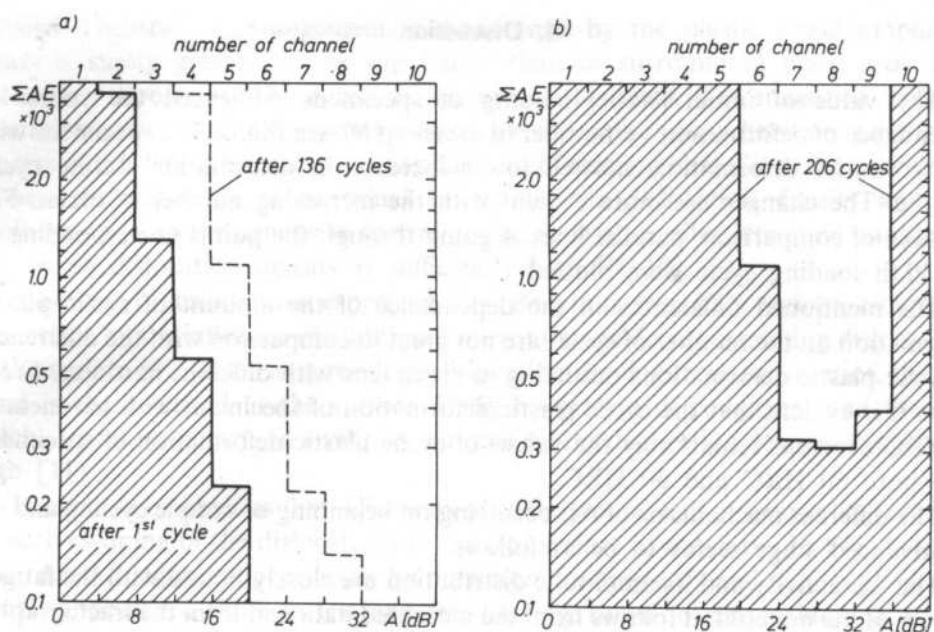


FIG. 8. Amplitude distribution of the AE signals during cyclic loading of the specimen with hardness of 40 HRC

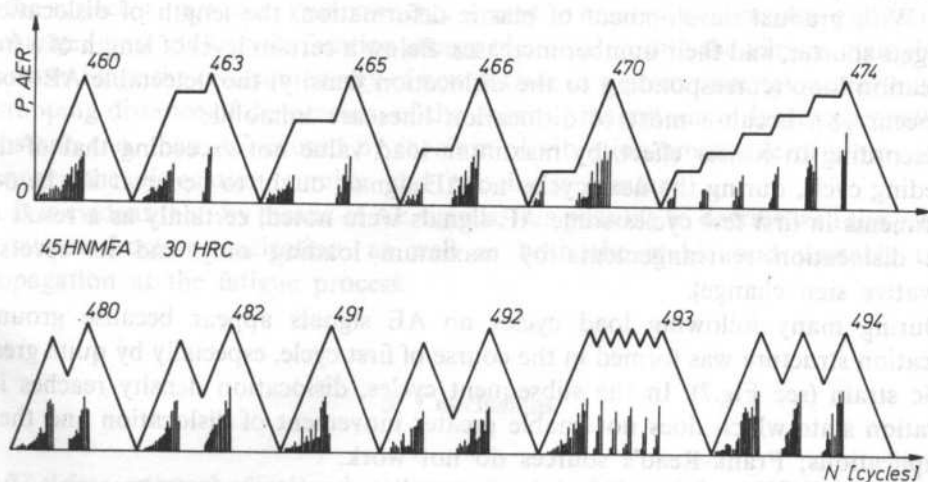


FIG. 9. AE activity in dependence on various modifications of loading courses in the specimen with hardness of 30 HRC

4. Discussion

The value of initial (static) loading of specimens influenced the course of dependence of deformation vs. number of cycles $\varepsilon_p(N)$, see Fig. 5. The specimens with greater initial deformation showed lower increase in deformation during cyclic loading. The changes are more evident with the increasing number of cycles. For the sake of comparison, parallel lines *A* going through the points corresponding to the 30 th loading cycle were plotted.

The mentioned differences in the dependence of the amount of cyclic plastic deformation on the number of cycles are not great in comparison with the differences of cyclic plastic deformations occurring in specimens with different hardness. From Fig. 6 it is evident that the cyclic plastic deformation of specimens with hardness of 40 HRC overtops remarkably the values of cyclic plastic deformation of specimens with both 50 HRC and 30 HRC.

The different mechanisms of AE occurring on beginning of sample cycling and on its advanced stage seems to be as follows.

The AE activity and its amplitude distribution are closely bound with the fatigue process of the material; it follows from the measured data and from the fractographic analysis. In the first loading cycle, a complete dislocation structure forms at the high deformation level [5]. The high AE activity corresponds to this phenomenon – see Fig. 7. The fundamental cause of AE is the dynamical effect of spontaneous dislocation movement, multiplication on sources, and annihilation of parallel segments of loops. Very high quantities of dislocations and Frank-Read's sources take part in these processes in whole volume of the sample and AE results are high, too. They are especially high near $P(N) = \max = \text{const}$, i.e. by very strong plastic flow of the specimen. The AE amplitude is proportional to the length of dislocation loop. With gradual development of plastic deformation, the length of dislocation loop gets shorter, and their number increases. Below a certain level of length of a free dislocation loop (corresponding to the dislocation density) the detectable AE does not occur [8], because most of dislocation lines are immobile.

According to Kaiser effect, by maximum load value not exceeding that of the preceding cycle, during the next cycles no AE signals ought to occur at all. In our experiments in first few cycles some AE signals were noted, certainly as a result of some dislocation rearrangements by maximum loading only and its reversal (derivative sign change).

During many following load cycles no AE signals appear because ground dislocation structure was formed in the course of first cycle, especially by quite great plastic strain (see Fig.7). In the subsequent cycles, dislocation density reaches its saturation state which does not enable greater movement of dislocation and their multiplications; Frank-Read's sources do not work.

After saturation stage reaching (what is usually complete for most materials after 20 to 50% of their life to failure), inhomogeneous plastic strains in the form of slip bands occur. These bands do not begin their development until after saturation is

reached. Dislocation arrangement is determined by the plastic strain amplitude which is surely greater in the slip bands than in surrounding matrix. Because dislocation dipoles are the dominant feature of this state, it is suggested that the saturation state could be accommodated by the equilibrium between generation process of the dislocations and the annihilation of existing ones. Since the generation of new dislocation is proportional to the mobile dislocation density and the annihilation — to the density in square power, such an equilibrium state establishes only when dislocation density is sufficiently high [9, 10].

A portion of dislocations, especially this being in near-surface regions, escapes to the surface by the influence of additional mirror (image) forces attracting dislocations to the surface [9]. Thus, as a result of dislocation moving from the interior, the slip band is characterized at the surface, firstly by growth of roughness and then by notch — peak geometry. In a vicinity of notch tip the dislocation density is especially high [11].

It seems to be obvious that AE observed in the second half of fatigue life is caused by such escaping of the dislocations to the free surface in notch tip. In Fig. 7 we see that such AE signals appear firstly by maximum loading only and then beginning of signals appearance shifts to less and less loading, down to zero value, just before fracture. It means that crack growth makes the escape of dislocations more and more plentiful and thus essential acceleration of crack growth must take place. When number of applied cycles is sufficiently high, it is visible (Fig. 9) that each, even small growth of loading, causes a generation of new AE signals.

Another very important result of this study is that during crack growth the AE amplitude drifts from small value to the high one. It means that fatigue cracking exhausts AE signals of much higher energy than plastic deformation does. This fact throws some light on a cracking mechanism itself. When a mobile dislocation comes to the surface, a part of its kinetic energy is used to create a new surface, and rest of it is changed into additional vibration energy of atoms, i.e. into the vibration amplitude increase. Since the creation energy of new surface in a given material is constant and a stopping distance of dislocation, of the order of magnitude of lattice parameter is constant, too, then AE caused by increase of vibration amplitude of atoms is the stronger the dislocation number and velocity is greater.

It is evident that, by means of AE signals, it is possible to describe well the process of fatigue fracture nucleation, as well as both the stable and unstable crack propagation at the fatigue process.

5. Conclusions

The data on mechanical and structure characteristics of the 45HNMFA steel in the low-cycle fatigue region will be applied in the construction of service-safe high pressure chambers.

The most important results of these experiments is a repeated occurrence of increasing AE activity in the second half of life period of the material, see Figs. 7, 9, with increasing amplitude value of AE signals, see Figs. 8a, b. This information allows to use the AE method to estimate the safe service life of devices working in the fatigue conditions. What concerns the AE signals, it is evidently possible to describe the dependence of exploiting use [6] of a monitored object which consists of three stages:

- I. hardening connected with the high AE activity;
- II. dislocation density saturation characterized by extinguishment of AE activity;
- III. development of crack which corresponds to the increasing AE activity with increasing amplitude of the AE signals up to failure.

References

- [1] W. SZCZEPIŃSKI et al, *Experimental methods in solid state mechanics*, (in Polish) PWN, Warsaw (1984).
- [2] UNIPRESS. *Prospect of the LC liquid cells*. Information Leaflet of High Pressure Research Center, Warsaw (1986).
- [3] F. DUŠEK et al., *The acoustic emission analyzer AE 10*. Patent. Author's Certificate No. 231236, Prague, 1984.
- [4] F. DUŠEK, and C. SEIDL, *Acoustic emission transducers calibration*. Proc. of Summer School of Defectoscopy, (in Czech) Stary Smokovec, 1987, pp. 92-97.
- [5] F. DUŠEK, M. KOTOUK, and C. SEIDL, *Acoustic emission*. Research Report of the Czechoslovak Academy of Sciences, (in Czech) Brno (1987).
- [6] M. HOUSSENY-EMAN and M. N. BASSIM, *Study of the effect of heat treatment on low-cycle fatigue in AISI 4340 steel by acoustic emission*, Mater. Sci. Eng. **64**, No. 1, pp. 79-83 (1983).
- [7] J. SIEDLACZEK, *Acoustic emission in the high pressure vessel testing* (in Polish), XII KKBN (NDT-Conference) Rydzyna (1983).
- [8] J. SIEDLACZEK, *Acoustic emission of metals and alloys in plastic deformation and fatigue* (in Polish), Ph. D. Thesis, IFTR PAS, Warsaw (1987).
- [9] S. PILECKI, *Dislocation — diffusion mechanism of fatigue crack formation*, Fourth International Conference on Fracture, Waterloo, Canada, 2, pp. 687-692 (1977).
- [10] S. PILECKI, *Proliferation, diffusion and vanishing of dislocations in the course of process of metal fatigue*, Bull. L'Acad. Polon. des Sci., Ser. Sci. Techn. **17**, pp. 489-496 (1969).
- [11] T. YOKOBORI, K. SATO, and Y. YAMAGUCHI, *X-ray micro beam studies on plastic zone at the tip of fatigue crack*. Rep. Res. Inst. Strength and Fracture of Materials, Tokohu Univer., Vol. **6**, No. 2, pp. 49-67 (1970).

Received on March 3, 1989

EFFECT OF ELECTRIC FIELD ON THE ULTRASONIC WAVE PROPAGATION VELOCITY IN OILS

A. SKUMIEL, M. LABOWSKI

Institute of Acoustics, Adam Mickiewicz University
(60-769 Poznań, ul. Matejki 48/49)

A dielectric liquid in an external electric field exhibits variations in its physical properties as a result of deformational polarisation and orientational polarisation. Moreover, it undergoes volume deformation due to electrostriction.

The present work represents an attempt at a quantitative description of ultrasonic wave propagation in a dielectric liquid acted on by a transversal electric field. Our search for a functional dependence between the propagation velocity c_E and the external field strength E was based on the change in free energy of the medium under the action of the field.

We derive general expressions valid with regard to polar as well as non-polar dielectrics for the square of the propagation velocity and compare them with our experimental results, obtained by the phase method for some selected oils.

Moreover, we determine the electrostrictional change in density of the medium in the external field for field strengths applied in experiments as well as for their maximal values close to breakdown.

Finally, we perform an analysis of our experimental results in face of the theoretical predictions and propose a new mechanism as responsible for the behaviour of the dielectric in the electric field.

W pracy podjęto próbę ilościowego opisu zjawiska propagacji fali ultradźwiękowej w cieczy dielektrycznej w obecności zewnętrznego poprzecznego pola elektrycznego. Poszukiwania funkcyjnej zależności między prędkością rozchodzenia się fali ultradźwiękowej w ciekłym dielektryku c_E a natężeniem przyłożonego pola E oparto na fakcie zmiany energii swobodnej badanego ośrodka pod wpływem zewnętrznego pola elektrycznego.

Wyprowadzono ogólne wyrażenia — słuszne dla dielektryków polarnych jak i niepolarnych — na kwadrat prędkości oraz porównano je z wynikami eksperymentalnymi otrzymanymi w wybranych olejach przy wykorzystaniu metody fazowej.

Ponadto wyznaczono elektrostrykcyjną zmianę gęstości ośrodka pod wpływem zewnętrznego pola elektrycznego, zarówno dla wartości natężeń stosowanych w doświadczeniach, jak i dla wartości maksymalnych równych wytrzymałości materiałowej.

W końcowej części pracy przeprowadzono analizę uzyskanych wyników doświadczalnych na tle przewidywań teoretycznych oraz przedstawiono inny możliwy mechanizm odpowiedzialny za obserwowane zachowanie się dielektryka w polu elektrycznym.

Theoretical

1. Relation between the propagation velocity of an ultrasonic wave in a liquid dielectric and the externally applied electric field strength

An external electric field applied to a liquid dielectric modifies the physical properties of the latter as a result of deformational polarisation and orientational polarisation. The ultrasonic propagation velocity also undergoes a modification due to its dependence on the field-sensitive properties. Our present considerations bear, in principle, on pure dielectric liquids free of impurities, random charge carriers (ions, free electrons), or gas bubbles. In order to find the relationship between the propagation velocity and the external field strength we made use of the following equation, well known in molecular acoustics [1, 11]:

$$c^2 = \frac{\gamma \cdot V^2}{M} \left[\frac{\partial^2 F}{\partial V^2} \right]_T, \quad (1)$$

with: c — the propagation velocity of the ultrasonic wave, $\gamma = c_p/c_v$ — the ratio of the specific heats at constant pressure and at constant volume, V — the molar volume, M — molecular mass, and F — molar Helmholtz free energy.

When the electric field E is applied to the liquid dielectric the free energy F increases according to the following equation:

$$F = \Delta F + V \cdot \frac{\epsilon_r \cdot \epsilon_0}{2} \cdot E^2, \quad (2)$$

where ΔF is the thermodynamical part of the free energy per one mole, ϵ_r — the relative electric permittivity of the liquid, and ϵ_0 — that of vacuum.

From Eq. (2) the general formulation (1) for the propagation velocity in the presence of an electric field takes the form:

$$c_E^2 = \frac{\gamma \cdot V^2}{M} \left[\frac{\partial^2 \left(\Delta F + V \cdot \frac{\epsilon_r \cdot \epsilon_0}{2} \cdot E^2 \right)}{\partial V^2} \right]_T \quad (3)$$

or:

$$c_E^2 = \frac{\gamma \cdot V^2}{M} \left[\frac{\partial^2 \Delta F}{\partial V^2} \right]_T + \frac{\gamma \cdot V^2 \cdot \epsilon_0}{2 \cdot M} \left[\frac{\partial^2 (V \cdot \epsilon_r \cdot E^2)}{\partial V^2} \right]_T. \quad (4)$$

The second derivative $\left[\frac{\partial^2 (\epsilon_r \cdot V \cdot E^2)}{\partial V^2} \right]_T$ in (4) can be expressed in terms of the specific volume ϑ ; after some transformations, we get:

$$\left[\frac{\partial^2 (M \cdot \vartheta \cdot \epsilon_r \cdot E^2)}{\partial (M \cdot \vartheta)^2} \right]_T = \frac{1}{M} \left[\frac{\partial (\epsilon_r \cdot E^2)}{\partial \vartheta} \right]_T. \quad (5)$$

Eq. (5) inserted into (4) gives:

$$c_E^2 = \frac{\gamma \cdot V^2}{M} \cdot \left[\frac{\partial^2 \Delta F}{\partial V^2} \right]_T + \frac{\gamma \cdot \varepsilon_0 \cdot V^2}{2 \cdot M^2} \left[\frac{\partial(\varepsilon_r \cdot E^2)}{\partial \vartheta} \right]_T. \quad (6)$$

Since $\vartheta = \varrho^{-1}$, Eq. (6) goes over into the general expression:

$$c_E^2 = \frac{\gamma \cdot V^2}{M} \cdot \left[\frac{\partial^2 \Delta F}{\partial V^2} \right]_T - \frac{\gamma \cdot \varepsilon_0}{2} \cdot \left[\varepsilon_r \cdot \frac{\partial E^2}{\partial \varrho} + E^2 \frac{\partial \varepsilon_r}{\partial \varrho} \right]_T, \quad (7)$$

where ϱ is the density of the liquid dielectric.

The derivatives $\left[\frac{\partial \varepsilon_r}{\partial \varrho} \right]_T$ and $\left[\frac{\partial E^2}{\partial \varrho} \right]_T$ occurring in (7) are accessible to determination from expressions that result from the theory of dielectrics and from equations describing electrostriction.

The latter [2], which consists in a deformation under the action of an electric field, obeys the equation:

$$\frac{\Delta V}{V} = K \cdot E^2, \quad (8)$$

where $\Delta V/V$ is the relative deformation in volume and K the electrostriction constant, as well as the equation [3]:

$$p = \frac{\varepsilon_0 \cdot E^2}{2} \cdot \left(\frac{\partial \varepsilon_r}{\partial \varrho} \right)_T \cdot \varrho, \quad (9)$$

describing the pressure caused by the effect.

The last equation, on determination of the first derivative of the pressure with respect to the density, gives:

$$\left(\frac{dp}{d\varrho} \right)_T = \frac{\varepsilon_0 \cdot \varrho}{2} \cdot \frac{\partial \varepsilon_r}{\partial \varrho} \cdot \frac{\partial E^2}{\partial \varrho} + \frac{\varepsilon_0 \cdot E^2}{2} \cdot \frac{\partial \varepsilon_r}{\partial \varrho} + \frac{\varepsilon_0 \cdot E^2}{2} \cdot \varrho \cdot \frac{\partial^2 \varepsilon_r}{\partial \varrho^2}. \quad (10)$$

Taking into account the well known thermodynamical formula $\left(\frac{dp}{d\varrho} \right)_T = \frac{1}{\beta_T \cdot \varrho}$, where β_T denotes the isothermal compressibility of a fluid medium, we obtain:

$$\left(\frac{dE^2}{d\varrho} \right)_T = \left[\frac{2}{\beta_T \cdot \varrho^2 \cdot \frac{\partial \varepsilon_r}{\partial \varrho} \cdot \varepsilon_0} - \frac{E^2}{\varrho} - E^2 \cdot \frac{\frac{\partial^2 \varepsilon_r}{\partial \varrho^2}}{\frac{\partial \varepsilon_r}{\partial \varrho}} \right]_T \quad (11)$$

for the change in density of the dielectric under the action of the field.

Equations (11) involves moreover the first and second derivatives $\left(\frac{\partial \varepsilon_r}{\partial \varrho} \right)_T$ and $\left(\frac{\partial^2 \varepsilon_r}{\partial \varrho^2} \right)_T$, given by the theory of liquid dielectrics [4].

To determine the dependence of ε_r on the temperature T and density ϱ we have recourse to the theory appropriate for the given type of dielectric.

1.1. Liquids obeying the Debye law (non dipolar)

Thus, for non-dipolar liquids and dipolar ones obeying the Debye law one has:

$$\frac{\varepsilon_r - 1}{\varepsilon_r + 2} = A \cdot \varrho, \quad (12)$$

where

$$A = \frac{N_A}{3 \cdot \varepsilon_0 \cdot M} \cdot \left(\alpha + \frac{\mu_0^2}{3 \cdot k \cdot T} \right) \equiv \frac{1}{\varrho} \cdot \frac{\varepsilon_r - 1}{\varepsilon_r + 1}. \quad (13)$$

The above relations lead to:

$$\varepsilon_r = \frac{1 + 2 \cdot A \cdot \varrho}{1 - A \cdot \varrho}. \quad (14)$$

On calculating the first and second one obtains

$$\frac{\partial \varepsilon_r}{\partial \varrho} = \frac{3 \cdot A}{(1 - A \cdot \varrho)^2} \equiv \frac{(\varepsilon_r - 1) \cdot (\varepsilon_r + 2)}{3 \cdot \varrho} \quad (15)$$

and

$$\frac{\partial^2 \varepsilon_r}{\partial \varrho^2} = \frac{2 \cdot A}{1 - A \cdot \varrho} \cdot \frac{\partial \varepsilon_r}{\partial \varrho} \equiv \frac{2 \cdot (\varepsilon_r - 1)^2 \cdot (\varepsilon_r + 2)}{9 \cdot \varrho^2}. \quad (16)$$

On insertion of (15) and (16) into Eq. (11) and with regard to $c_0^2 = \gamma / (\beta_T \cdot \varrho)$ we obtain the following expression for the change in density of a non-dipolar liquid dielectric in an external electric field:

$$\left(\frac{\partial E^2}{\partial \varrho} \right)_T = \frac{6 \cdot c_0^2}{\gamma \cdot \varepsilon_0 (\varepsilon_r - 1) (\varepsilon_r + 2)} - (2\varepsilon_r + 1) \cdot \frac{E^2}{3 \cdot \varrho} \quad (17)$$

or

$$\left(\frac{\partial E^2}{\partial \varrho} \right)_T = \frac{2 \cdot c_0^2 \cdot (1 - A \cdot \varrho)^2}{3 \cdot A \cdot \gamma \cdot \varrho \cdot \varepsilon_0} - \frac{1 + A \cdot \varrho}{\varrho \cdot (1 - A \cdot \varrho)} \cdot E^2. \quad (18)$$

For the case of a non-dipolar liquid dielectric in an electric field we are now able to evaluate the change in density due to electrostriction. For the field strengths applied in our measurements and for a typical non-dipolar liquid dielectric:

$$\begin{aligned} c_0 &= 1400 \text{ [m/s]} & \gamma &= 1.4 & \varrho &= 900 \text{ [kg/m}^3\text{]} \\ E &= 3 \cdot 10^5 \text{ [V/m]} & \varepsilon_r &= 2.2 & \varepsilon_0 &= 8.85 \cdot 10^{-12} \text{ [F/m]} \end{aligned}$$

on insertion into (17) we obtained:

$$\left| \frac{\partial E^2}{\partial \varrho} \right|_T = 1.88 \cdot 10^{17} - 5.5 \cdot 10^7 \cong 1.88 \cdot 10^{17} [\text{V}^2 \cdot \text{m/kg}],$$

meaning that at the above field strength the change in density amounts to:

$$\Delta \varrho = \frac{\Delta(E^2)}{\left(\frac{\partial E^2}{\partial \varrho} \right)_T} = 4.779 \cdot 10^{-7} [\text{kg/m}^3].$$

Thus, the relative change in density is:

$$\Delta \varrho / \varrho = 5.31 \cdot 10^{-10},$$

in good agreement with the literature [2,5].

Admitting a field of $E_{\max} = 3 \cdot 10^7 [\text{V/m}]$ as the pre-breakdown limit, we find

$$\left| \frac{\partial(E^2)}{\partial \varrho} \right|_T = 1.88 \cdot 10^{17} - 1.8 \cdot 10^{12} \cong 1.88 \cdot 10^{17} [\text{V}^2 \cdot \text{m/kg}],$$

and the value of $\Delta \varrho$ corresponding to it as:

$$\Delta \varrho = \frac{\Delta(E^2)}{\left| \frac{\partial(E^2)}{\partial \varrho} \right|_T} = \frac{(3 \cdot 10^7)^2}{1.88 \cdot 10^{17}} = 4.78 \cdot 10^{-3} [\text{kg/m}^3].$$

The relative change in density of the non-dipolar dielectric due to electrostriction thus amounts to

$$\Delta \varrho / \varrho = 5.3 \cdot 10^{-6}.$$

Inserting in the general formula (7) the expressions for $(\partial \varepsilon_r / \partial \varrho)_T$, $(\partial^2 \varepsilon_r / \partial \varrho^2)_T$ and $(\partial E^2 / \partial \varrho)_T$ determined for non-dipolar dielectrics, we finally arrive at the following formula expressing the phase velocity of ultrasonic waves in liquid non-dipolar media in the presence of an external constant electric field:

$$c_E^2 = \frac{\gamma \cdot V^2}{M} \cdot \left(\frac{\partial^2(\Delta F)}{\partial V^2} \right)_T - \frac{3 \cdot \gamma \cdot \varepsilon_r}{\beta_T \cdot \varrho \cdot (\varepsilon_r - 1)(\varepsilon_r + 2)} + \frac{\gamma \cdot \varepsilon_0 \cdot E^2}{6 \cdot \varrho} \cdot (\varepsilon_r^2 + 2) \equiv \quad (19)$$

$$\equiv \frac{\gamma \cdot V^2}{M} \cdot \left(\frac{\partial^2(\Delta F)}{\partial V^2} \right)_T - \frac{\gamma \cdot (1 + 2A\varrho)(1 - A\varrho)}{3 \cdot A \cdot \beta_T \cdot \varrho^2} + \frac{\gamma \cdot \varepsilon_0 \cdot E^2(2A^2\varrho^2 + 1)}{2\varrho \cdot (1 - A\varrho)^2}. \quad (20)$$

Obviously, by Eq. (20), if conditions are such that $A = \varrho^{-1}$, then $c_E \Rightarrow \infty$ and the situation comes to resemble what is referred to as "the Mossotti catastrophe" in the theory of dielectrics.

1.2. Liquids obeying Onsager's equation (dipolar)

In dealing with dipolar liquids fulfilling Onsager's equation we have to use an equation from which it results that the density of the dielectric is described by the following relation:

$$\rho = \frac{9 \cdot \epsilon_0 \cdot M \cdot k \cdot T}{N_A \cdot \mu_0^2} \cdot \frac{(2\epsilon_r^2 - \epsilon_r \cdot \epsilon_\infty - \epsilon_\infty^2)}{\epsilon_r \cdot (\epsilon_\infty + 2)^2}. \quad (21)$$

On calculating $(\partial \rho / \partial \epsilon_r)_T$ from (21) we get:

$$\left(\frac{\partial \rho}{\partial \epsilon_r} \right)_T = \frac{2 \cdot \epsilon_r^2 + \epsilon_\infty^2}{\epsilon_r^2} \cdot \frac{9 \cdot \epsilon_0 \cdot M \cdot k \cdot T}{(\epsilon_\infty + 2)^2 \cdot N_A \cdot \mu_0^2} \equiv \frac{\rho \cdot (2\epsilon_r^2 + \epsilon_\infty^2)}{\epsilon_r \cdot (2\epsilon_r^2 - \epsilon_\infty \cdot \epsilon_r - \epsilon_\infty^2)}, \quad (22)$$

whence

$$\left(\frac{\partial \epsilon_r}{\partial \rho} \right)_T = \frac{\epsilon_r^2 (\epsilon_\infty + 2)^2}{(2\epsilon_r^2 + \epsilon_\infty^2)} \cdot \frac{N_A \cdot \mu_0^2}{9 \cdot \epsilon_0 \cdot M \cdot k \cdot T} \equiv \frac{\epsilon_r (2\epsilon_r^2 - \epsilon_\infty \cdot \epsilon_r - \epsilon_\infty^2)}{\rho (2\epsilon_r^2 + \epsilon_\infty^2)} \quad (23)$$

and

$$\begin{aligned} \left(\frac{\partial^2 \epsilon_r}{\partial \rho^2} \right)_T &= \frac{2 \cdot \epsilon_r^3 \cdot \epsilon_\infty^2}{(2 \cdot \epsilon_r^2 + \epsilon_\infty^2)^3} \left[\frac{(\epsilon_\infty + 2)^2 N_A \cdot \mu_0^2}{9 \cdot \epsilon_0 \cdot M \cdot k \cdot T} \right]^2 \equiv \\ &\equiv \frac{2 \cdot \epsilon_r \cdot \epsilon_\infty^2 (2 \cdot \epsilon_r^2 - \epsilon_\infty \cdot \epsilon_r - \epsilon_\infty^2)^2}{\rho^2 \cdot (2 \cdot \epsilon_r^2 + \epsilon_\infty^2)^3}. \end{aligned} \quad (24)$$

On insertion of the preceding expressions into (11) we obtain the following equation for the change in density of a dipolar liquid dielectric in an electric field:

$$\begin{aligned} \left(\frac{\partial E^2}{\partial \rho} \right)_T &= \frac{2 \cdot \epsilon_r^2 + \epsilon_\infty^2}{\beta_T \cdot \rho \cdot \epsilon_0 \cdot \epsilon_r (2\epsilon_r^2 - \epsilon_\infty \epsilon_r - \epsilon_\infty^2)} - \frac{E^2}{\rho} \cdot \frac{4\epsilon_r^4 + 8\epsilon_r^2 \epsilon_\infty^2 - 2\epsilon_\infty^3 \epsilon_r - \epsilon_\infty^4}{(2\epsilon_r^2 + \epsilon_\infty^2)^2} \equiv \\ &\equiv \frac{18(2\epsilon_r^2 + \epsilon_\infty^2) M \cdot k \cdot T}{\beta_T \rho^2 \epsilon_r^2 (\epsilon_\infty + 2) N_A \mu_0^2} - \frac{E^2}{\rho} \cdot \left[1 + \frac{2\rho \epsilon_r \epsilon_\infty^2 (\epsilon_\infty + 2)^2 N_A \mu_0^2}{9 \epsilon_0 (2\epsilon_r^2 + \epsilon_\infty^2)^2 M \cdot k \cdot T} \right]. \end{aligned} \quad (25)$$

To determine the change in density for the field strengths applied in our measurements we assumed the following values for the synthetic oil FDO (bis-2-ethylohexylic phthalene):

$$c_0 = 1468.8 \text{ [m/s]}, \quad \text{at } T = 273 \text{ [K]},$$

$$\rho = 945 \text{ [kg/m}^3\text{]}, \quad \gamma = 1.3,$$

$$\epsilon_r = 5.2 \quad \epsilon_\infty = 2.24 \quad E = 3 \cdot 10^5 \text{ [V/m]}.$$

which, inserted into Eq. (25), gave

$$\left(\frac{\partial E^2}{\partial \rho} \right)_T = 5.7 \cdot 10^{16} - 1.08 \cdot 10^8 \cong 5.7 \cdot 10^{16} \text{ [V}^2 \cdot \text{m/kg]}.$$

Hence, the relative change in density due to electrostriction amounts to

$$\frac{\Delta \rho}{\rho} = \frac{1}{\rho} \cdot \frac{\Delta E^2}{\left(\frac{\partial E^2}{\partial \rho}\right)_T} = \frac{1}{945} \cdot \frac{(3 \cdot 10^5)^2}{5.7 \cdot 10^{16}} = 1.67 \cdot 10^{-9}.$$

On the assumption that the maximum pre-breakdown field strength for oil is $E = 3 \cdot 10^7$ [V/m], Eq. (25) leads to

$$\left| \frac{\partial(E^2)}{\partial \rho} \right|_T = 5.7 \cdot 10^{16} - 1.08 \cdot 10^{12} \cong 5.7 \cdot 10^{16} \text{ [V}^2 \cdot \text{m/kg]},$$

and the electrostrictional change in density $\Delta \rho$ of the dipolar dielectric under consideration amounts to

$$\Delta \rho = \frac{\Delta(E^2)}{\left| \frac{\partial E^2}{\partial \rho} \right|_T} = \frac{(3 \cdot 10^7)^2}{5.7 \cdot 10^{16}} = 15.78 \cdot 10^{-3} \text{ [kg/m}^3\text{]}$$

and the respective relative change in density to

$$\Delta \rho / \rho = 15.78 \cdot 10^{-3} / 945 = 16.7 \cdot 10^{-6}.$$

On insertion of the quantities given by Eqs (23), (24) and (25) into (7) we obtain a general formula describing the propagation velocity of an ultrasonic wave in a dipolar liquid dielectric in the presence of an external static electric field:

$$\begin{aligned} c_E^2 &= \frac{\gamma \cdot V^2}{M} \cdot \left[\frac{\partial^2(\Delta F)}{\partial V^2} \right]_T - \frac{\gamma \cdot (2 \cdot \varepsilon_r^2 + \varepsilon_\infty^2)}{2 \cdot \beta_T \cdot \rho \cdot (2\varepsilon_r^2 - \varepsilon_r \cdot \varepsilon_\infty - \varepsilon_\infty^2)} + \\ &+ \frac{\gamma \cdot \varepsilon_0 \cdot \varepsilon_r^2 \cdot E^2}{2 \cdot \rho \cdot (2\varepsilon_r^2 + \varepsilon_\infty^2)} \cdot (8 \cdot \varepsilon_\infty \cdot \varepsilon_r - \varepsilon_\infty^2 + 2\varepsilon_r^2) \equiv \\ &\equiv \frac{\gamma \cdot V^2}{M} \cdot \left[\frac{\partial^2(\Delta F)}{\partial V^2} \right]_T - \frac{9 \cdot \gamma \cdot \varepsilon_0 (2 \cdot \varepsilon_r^2 + \varepsilon_\infty^2) \cdot M \cdot k \cdot T}{\beta_T \cdot \rho^2 \cdot \varepsilon_r \cdot (\varepsilon_\infty + 2)^2 \cdot N_A \cdot \mu_0^2} + \\ &+ E^2 \cdot \left\{ \frac{\gamma \cdot \varepsilon_0 \cdot \varepsilon_r}{\rho} + \frac{N_A \cdot \mu_0^2}{9 \cdot M \cdot k \cdot T} \cdot \frac{\varepsilon_r \cdot (\varepsilon_\infty^2 + 2)}{(2 \cdot \varepsilon_r^2 + \varepsilon_\infty^2)} \cdot \left[1 + \frac{\gamma \cdot \varepsilon_r \cdot \varepsilon_\infty^2}{2 \cdot \varepsilon_r^2 + \varepsilon_\infty^2} \right] \right\}. \end{aligned} \quad (26)$$

The two forms of (26) determine the change in phase velocity of the wave in the macroscopic as well as the molecular approach.

1.3. Relation to experiments

In our measurements, we determined the absolute propagation velocity c_0 as well as the change in velocity Δc_E induced by the field E . The Eq. (19), which holds for

non-dipolar liquids, leads to the following relation:

$$c_E^2 - c_0^2 = \frac{\gamma \cdot \epsilon_0 \cdot (\epsilon_r^2 + 2)}{6 \cdot \varrho} \cdot E^2 \cong 2 \cdot c_0 \cdot \Delta c_E, \quad (27)$$

permitting the determination of Δc_E . The latter amounts to

$$\Delta c_E = \frac{\gamma \cdot \epsilon_0 \cdot (\epsilon_r^2 + 2)}{12 \cdot \varrho \cdot c_0} \cdot E^2. \quad (28)$$

Evaluations of Δc_E were carried out for the following values for non-dipolar mineral oil:

$$c_0 = 1508.67 \text{ [m/s]} \quad \varrho = 863 \text{ [kg/m}^3\text{]} \quad \gamma = 1.4$$

$$\epsilon_r = 2.2 \quad E = 3 \cdot 10^5 \text{ [V/m]} \quad \epsilon_0 = 8.85 \cdot 10^{-12} \text{ [F/m]},$$

which led to a change in velocity of

$$\Delta c_E = 4.88 \cdot 10^{-7} \text{ [m/s]}.$$

Assuming for mineral oil a maximal admissible field strength of $E_{\max} = 3 \cdot 10^7 \text{ [V/m]}$ we obtained from (28) Δc_E as

$$\Delta c_E = \frac{1.4 \cdot 8.85 \cdot 10^{-12} \cdot (2.2^2 + 2)}{12 \cdot 863 \cdot 1508.67} \cdot (3 \cdot 10^7)^2 = 4.88 \cdot 10^{-3} \text{ [m/s]}.$$

For the case of dipolar dielectrics we had recourse to Eq. (26). Here, the change in velocity Δc_E is expressed by

$$\Delta c_E = \frac{\gamma \cdot \epsilon_0 \cdot \epsilon_r^2 \cdot (8 \cdot \epsilon_\infty \cdot \epsilon_r - \epsilon_\infty^2 + 2 \cdot \epsilon_r^2)}{4 \cdot c_0 \cdot \varrho \cdot (2 \cdot \epsilon_r^2 + \epsilon_\infty^2)^2} \cdot E^2. \quad (29)$$

We assumed the following values for the synthetic oil FDO — a dipolar liquid:

$$c_0 = 1468.8 \text{ [m/s]} \quad \text{at } T = 273 \text{ [K]}$$

$$\varrho = 945 \text{ [kg/m}^3\text{]} \quad \epsilon_r = 5.2 \quad \gamma = 1.3$$

$$\epsilon_\infty = 2.24 \quad E = 3 \cdot 10^5 \text{ [V/m]}.$$

In this case, the theory predicts a field-induced change in velocity Δc_E equal to

$$\Delta c_E = 2.05 \cdot 10^{-7} \text{ [m/s]}.$$

On assuming as the highest admissible field strength $E_{\max} = 3 \cdot 10^7 \text{ [V/m]}$, we obtained from Eq. (29) the following change in velocity Δc_E due to the increase in free energy:

$$\Delta c_E = \frac{1.3 \cdot 8.85 \cdot 10^{-12} \cdot 5.2^2 \cdot (8 \cdot 2.24 \cdot 5.2 - 2.24^2 + 2 \cdot 5.2^2)}{4 \cdot 1468.8 \cdot 945 \cdot (2 \cdot 5.2^2 + 2.24^2)^2} \cdot (3 \cdot 10^7)^2,$$

$$\Delta c_E = 2.05 \cdot 10^{-3} \text{ [m/s]}.$$

Experimental

2. Phase method for measurements of the ultrasonic wave propagation velocity and its variations in liquid dielectrics

Theoretical studies [6, 7] on the influence of a static electric field on the velocity of ultrasonic waves in liquid dielectrics predict but insignificant changes in velocity.

We accordingly had recourse to the phase method, which is one of the most sensitive experimental methods available. Owing to the use of a digital phase detector with very good parameters and computer technique of data processing we achieved a very high degree of accuracy in our measurements.

With (30), we determined the error on the measurement of the absolute value of the ultrasonic propagation velocity as given by:

$$\Delta(c_0) = \frac{f}{n} \cdot \Delta l + \frac{l \cdot f}{n^2} \cdot \Delta n + \frac{l}{n} \cdot \Delta f. \quad (29a)$$

On insertion of the following experimental data:

$$\begin{aligned} f &= 1.6 \cdot 10^6 \text{ Hz} & \Delta f &= 1 \text{ Hz}, \\ l &= 0.248 \text{ m} & \Delta l &= 10^{-4} \text{ m}, \\ n_0 &= 257 & \Delta n &= \Delta\Phi/2\pi = 5.57 \cdot 10^{-4}, \\ \Delta\Phi_{\min} &= 3.35 \cdot 10^{-3} \text{ rad} & c_0 &= 1544 \text{ m/s} \end{aligned}$$

into (29a), we obtained:

$$\Delta(c_0) = 0.65 + 0.00335 + 0.00097 = 0.63442 \text{ m/s}.$$

The accuracy of our phase measurements amounted to

$$\Delta\Phi_{\min} = 3.5 \cdot 10^{-3} \text{ rad},$$

permitting the recording of the change in propagation velocity, in conformity with Eq. (31), as amounting to $3.35 \cdot 10^{-3} \text{ m/s}$.

On the other hand, the relative change in propagation velocity of the ultrasonic wave is determined from Eq. (29b):

$$\frac{\Delta c}{c_0} = \frac{-\Delta\Phi \cdot l \cdot f \cdot n_0}{2 \cdot \pi \cdot n_0^2 \cdot l \cdot f} = \frac{-\Delta\Phi}{2 \cdot \pi \cdot n_0} = -\frac{\Delta\Phi}{\Phi_0} = 2.17 \cdot 10^{-6}. \quad (29b)$$

By (29b), the relative change in propagation velocity is independent of the length of the measuring vessel and frequency, and is dependent on the phase alone.

The block diagram of our device is shown in Fig. 1. The measuring vessel exhibits two paths along which beams of continuous ultrasonic waves propagate: the one is the reference path and the other the measuring path.

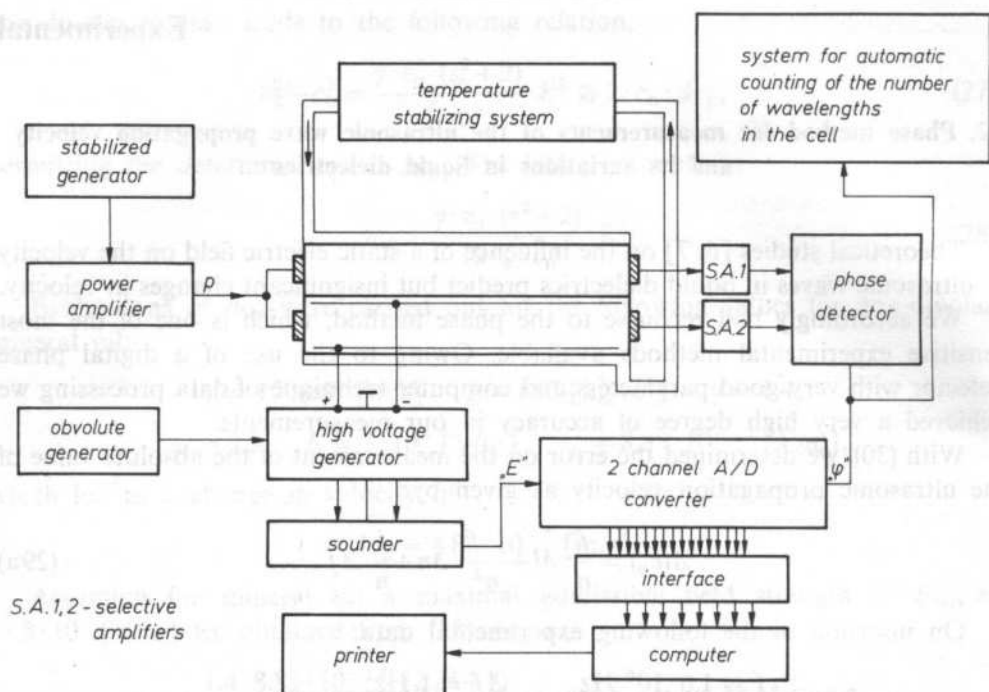


FIG. 1. Block diagram of the measuring setup for measurements of the influence of an electric field on the propagation velocity of an ultrasonic wave in a liquid dielectric

This construction of the vessel was dictated by the need for thermal compensation of the system in order to exclude effects other than that of the external electric field. The vessel holding the liquid was thermostated by means of a cryostat. The emitter and receiver transducers were distant by $l = 0.248$ [m], whereas the distance between the field electrodes amounted to $l_1 = 26$ [mm].

The temperature stability achieved after several hours of operation of the cryostat amounted to 0.05 K, whereas the absolute values of the ultrasonic propagation velocities were determined for different temperatures (Tables 1 and 2) stabilized to within 0.2 K.

When checking for an effect of the external electric field on the temperature of the oil we used a high accuracy quartz thermometer, permitting measurements of the momentary temperature to within 0.001 K. For the duration of this test (Fig. 3), the cryostat was switched off.

To provide for zero potential (necessary for the safety of the experimenter and to ensure proper cooperation with the electronic appliances) the two electrodes introducing the external electric field were connected to a supply of bipolar symmetric voltage. The one electrode was at positive and the other at negative voltage with respect to the housing. In this way we achieved an enhancement of the electric field homogeneity throughout the liquid dielectric.

Our device permitted the measurement of the absolute propagation velocity of ultrasonic waves in liquids as well as its small variations; the relevant formulae are these [7]:

$$c_0 = \frac{l \cdot f}{n}, \quad (30)$$

and

$$\Delta c = -\frac{\Delta \Phi \cdot l \cdot f}{2 \cdot \Pi \cdot n_0^2}, \quad (31)$$

with: l — the distance between the transducers ($l = 0.248$ m), f — the frequency of the ultrasonic wave ($f = 1.6$ MHz), n_0 — the number of wavelengths in the measuring vessel ($n_0 = l/\lambda_0$), $\Delta \Phi$ — the change in phase, measured in radians.

In principle, the formulae (30) and (31) are valid for running waves only. If reflections of the continuous sine wave between the transducers are insignificant, (30) and (31) can be used to determine the phase velocity of the ultrasonic wave and its variations.

In the case of multiple reflections, the shift in phase Φ of a continuous sine wave at the end of a segment of length l is given by Eq. (32) [8]:

$$\Phi = \beta \cdot l + \operatorname{arctg} \left[\frac{k_1 \cdot k_2 \cdot \exp(-2 \cdot \alpha \cdot l) \cdot \sin(2 \cdot \beta \cdot l)}{1 - k_1 \cdot k_2 \cdot \exp(-2 \cdot \alpha \cdot l) \cdot \cos(2 \cdot \beta \cdot l)} \right], \quad (32)$$

where $\beta = 2 \cdot \Pi \cdot f/c = 2 \cdot \Pi/\lambda$ — is the wave number, k_1, k_2 — amplitude reflection coefficients at the two ends of l , and α — amplitude damping coefficient per unit length.

The first term of (32) represents the shift in phase on a single traversal of the path l whereas the second term is related with the phase shift due to multiple reflections. One notes that as $\alpha \cdot l$ increases the effect of multiple reflections decreases. Since the vessel was relatively long and the oils studied were characterized by high damping coefficients for ultrasonic waves, we assumed $\Phi \cong 2 \cdot \Pi \cdot l/\lambda$.

In order to check our assumption we performed an evaluation of the second term of (32) for paraffin oil. The shape of $f(l)$ thus obtained is shown in Fig. 2, where

$$f(l) = \Phi - \beta \cdot l = \operatorname{arctg} \left[\frac{k_1 \cdot k_2 \cdot \exp(-2 \cdot \alpha \cdot l) \cdot \sin(2 \cdot \beta \cdot l)}{1 - k_1 \cdot k_2 \cdot \exp(-2 \cdot \alpha \cdot l) \cdot \cos(2 \cdot \beta \cdot l)} \right].$$

The quantity plotted in Fig. 2 determines the shift in phase due to multiple reflections of the wave as a function of the length of the measuring vessel.

The first term of (32) is a linearly growing function with the following slope coefficient:

$$\beta = 2\Pi/\lambda = 2\Pi f/c = 6.7 \cdot 10^3 \text{ rad/m} = 67 \text{ rad/cm}.$$

For the whole vessel $l = 0.248$ m,

$$\frac{2\pi}{\lambda} \cdot l = 1660 \text{ rad},$$

whence

$$\frac{2\pi}{\lambda} \cdot l \gg f(l).$$

A comparison of the two phase terms for the oil under investigation and paraffin oil (Fig. 2) leads to similar results with regard to the great similarity of the acoustic properties of the two oils.

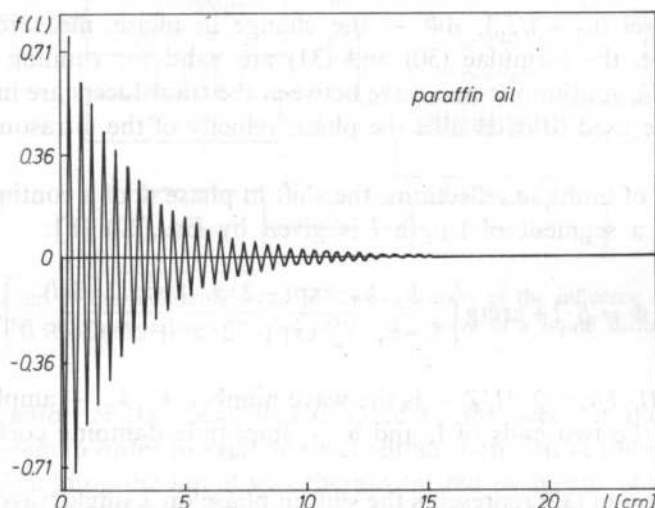


FIG. 2. The phase shift $\Phi(x)$ of the continuous wave arising in multiple reflections as a function of the length of the measuring vessel, for paraffin oil

3. Experimental results for selected liquid dielectrics

Our measurements were carried out in the following oils: mineral condenser oil, and the synthetic aromatic hydrocarbon *AKB* and *FDO*, at field strengths from 0 to 308 [kV/m] and temperatures from 253 to 303 [K]. The oils were carefully purified by various physicochemical methods [9]. Moreover, to check whether the external electric field caused a perceptible rise in temperature of the dielectric (Joule heat), we carried out tests in which, among others, we took accurate recordings of the temperature prior to and after switching the field on.

The time-evolution of temperature in the mineral oil, as shown in Fig. 3, points to

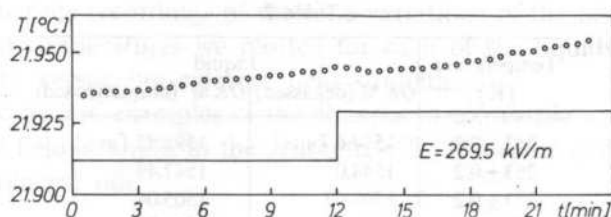


FIG. 3. Time evolution of the changes in temperature in mineral oil (condenser degassed oil) prior to and after application of the electric field

a very high grade of purity, since except for an insignificant creep in temperature (thermostat switched off), the characteristic exhibited no upward trend typical for conducting liquids on application of an electric field.

In the phase method used by us, we first determined (at a given temperature) the absolute value c_0 of the ultrasonic propagation velocity by measuring the delay in phase originating in the liquid between the emitter and receiver transducers.

Next, voltage was applied to the electrodes thus producing an electric field of strength E in the liquid dielectric. Simultaneously, we recorded in the memory of the computer the change in the phase from the moment the field was switched on until $\Delta\Phi$ attained a constant value. It was then possible to re-switch on a field of different strength. In this way we obtained recording of the change in phase with time on switching on the field, for 10 different field strengths, at a well determined temperature.

Table 1 shows the absolute values of c_0 for the synthetic condenser oils at the frequency $f = 1.6$ MHz and different temperatures.

Table 1

Temperature [K]	Liquid		
	FDO	AKB (degassed)	AKBn (non-degassed)
253 ± 0.2	1550 [m/s]	1600 [m/s]	1596.42 [m/s]
262 ± 0.2	1503.1	1562.2	1555.27
273 ± 0.2	1468.8	1520.3	1514.12
283 ± 0.2	1437.7	1486.1	1477.04
293 ± 0.2	1397.2	1448.2	1439.97
303 ± 0.2	1322.7	—	—

Table 2 shows the ultrasonic propagation velocities in the mineral condenser oils determined experimentally under the same conditions and frequency.

As examples, we give in Figs. 4a and 4b the time-evolutions of the change in phase, and thus the changes in propagation velocity, for different field strengths and constant temperature.

Table 2

Temperature [K]	Liquid	
	OKM (degassed)	OKM (non-degassed)
253 ± 0.2	1574.6 [m/s]	1591.35 [m/s]
263 ± 0.2	1544.0	1547.49
273 ± 0.2	1508.67	1505.04
283 ± 0.2	1470.1	1466.05
293 ± 0.2	1432.56	1430.05
303 ± 0.2	1397.2	—

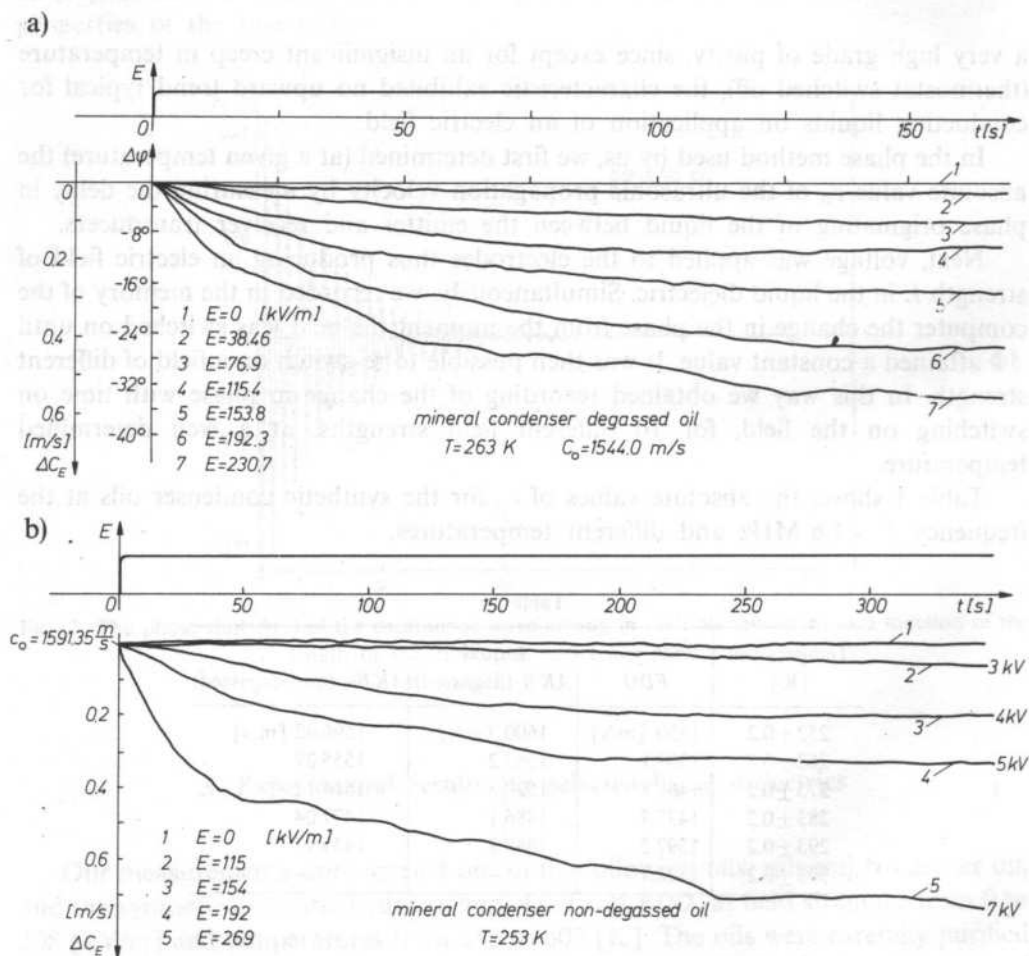


FIG. 4. Time evolution of the changes in phase $\Delta\Phi$ and ultrasonic wave propagation Δc on application of an electric field at constant temperature ($T = 263\text{ K}$): a — in mineral (condenser) oil, b — in synthetic (aromatic hydrocarbon) oil

From our numerous recordings of the time-variations of the phase for different field strengths and temperatures we plotted for each of the liquids, graphs of the changes in velocity versus the external field strength.

Figures 5a and 5b are examples of the changes in ultrasonic wave propagation velocity *versus* the field strength in the synthetic oils. The same is done in Figs. 6a and 6b for the mineral oils.

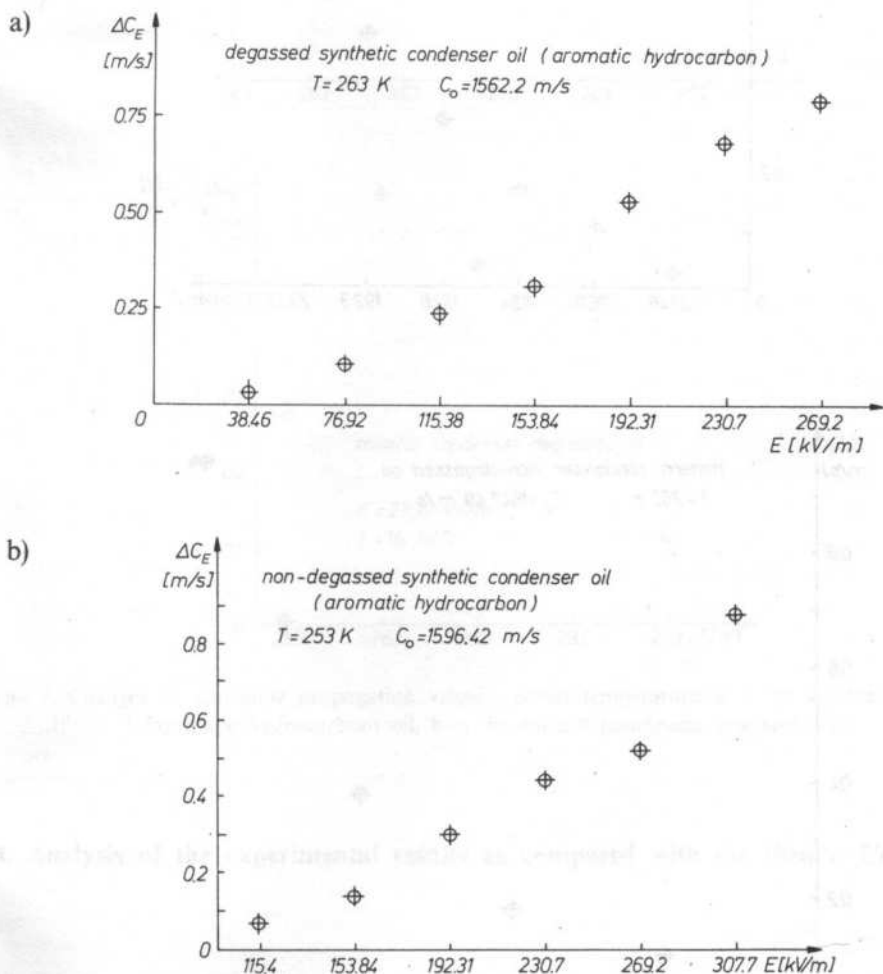


FIG. 5. Changes in propagation velocity *versus* electric field strength, at constant temperature: a — in degassed synthetic oil, b — in non-degassed synthetic oil

On the other hand, in Figs. 7a and 7b we give the changes in velocity *versus* temperature, for a well determined strength of the static electric field.

The electric fields strength $E = U/l_1$ was measured with an accuracy of about 1.4%.

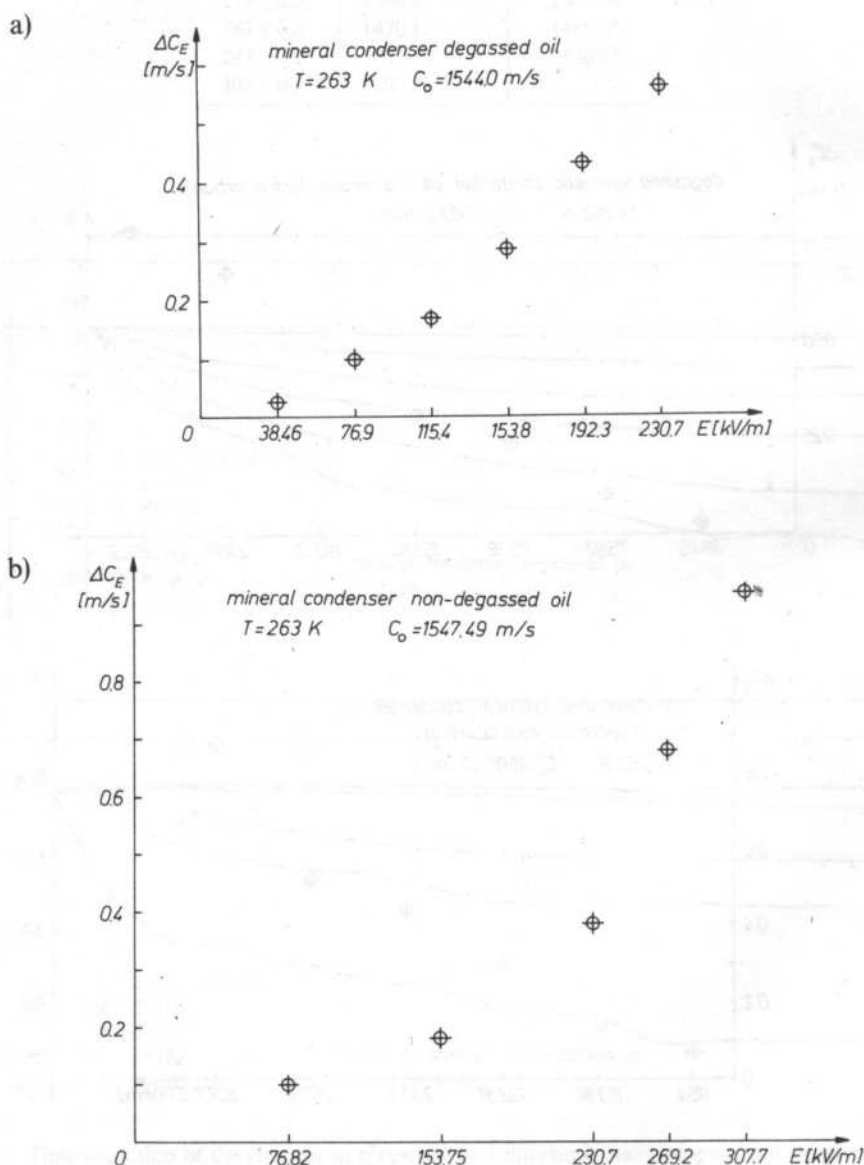


FIG. 6. Changes in propagation velocity *versus* electric field strength, at constant temperature: a — in degassed condenser oil, b — in non-degassed condenser oil

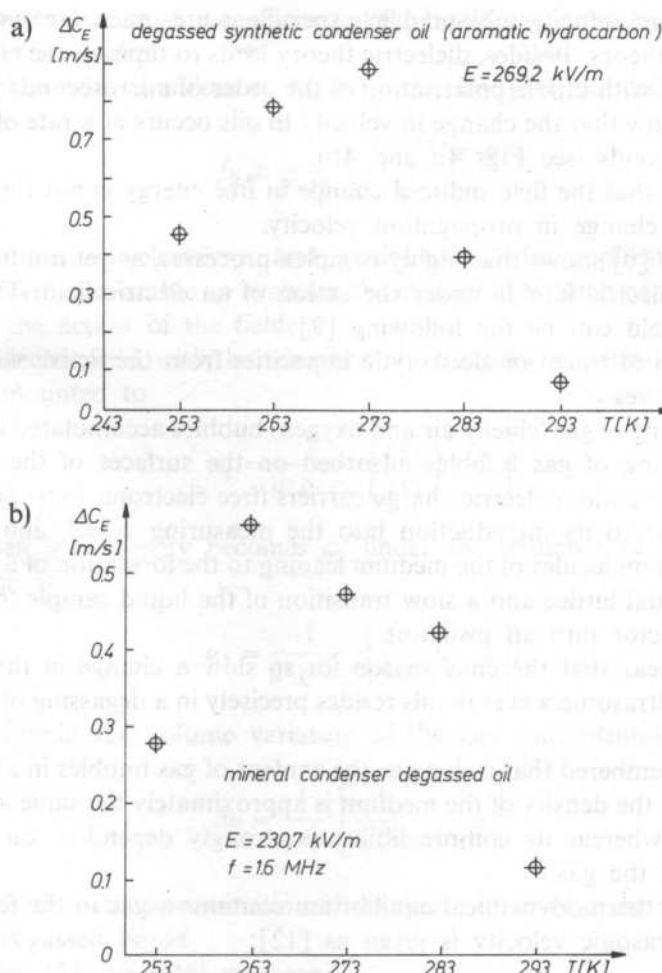


FIG. 7. Changes in ultrasonic propagation velocity *versus* temperature: a — in synthetic condenser (aromatic hydrocarbon) oil, b — in mineral (condenser degassed) oil

4. Analysis of the experimental results as compared with the theory. Conclusions

Our experiments show that an increase in strength of the externally applied electric field causes a well measurable rise in propagation velocity of the ultrasonic wave. However, a comparison of our experimental values for the field-induced changes in velocity of the wave and the values predicted by our theoretical considerations (of the formulae (28) and (29)) reveals important discrepancies.

The changes in velocity measured in experiment are much greater than those predicted by the theory. Besides, dielectric theory leads to times of the change in free energy connected with dipole polarisation of the order of microseconds whereas our measurements show that the change in velocity in oils occurs at a rate of as much as some tens of seconds (see Figs 4a and 4b).

This suggests that the field-induced change in free energy is not the only factor determining the change in propagation velocity.

The literature [9] shows that highly complex processes, as yet not fully clarified, take place in dielectric liquids under the action of an electric field. The processes caused by the field can be the following [9]:

1. elimination of traces of electrolytic impurities from the active volume of the measuring vessel,
2. the vanishing of gas (chiefly air and oxygen) bubbles accumulated in the liquid,
3. the vanishing of gas bubbles adsorbed on the surfaces of the electrodes,
4. removal of random electric charge carriers (free electrons, ions) present in the liquid prior to its introduction into the measuring vessel, and
5. ordering of molecules of the medium leading to the formation of a pseudocrystalline spatial lattice and a slow transition of the liquid sample from a donor semiconductor into an insulator.

It would appear that the chief reason for so slow a change in the velocity of propagation of ultrasonic waves in oils resides precisely in a degassing of the medium by the field.

It will be remembered that as long as the content of gas bubbles in a liquid is not excessively great, the density of the medium is approximately the same as that of the degassed liquid whereas its compressibility is strongly dependent on the volume concentration of the gas.

If a liquid at thermodynamical equilibrium contains a gas in the form of small bubbles, the ultrasonic velocity is given as [12]:

$$c_A = \frac{c_0}{\sqrt{1 + g \cdot u \cdot \varrho \cdot c_0^2}}, \quad (33)$$

with: c_A — the ultrasonic propagation velocity in the liquid with gas bubbles, c_0 — that in the liquid with no bubbles, ϱ — the density of the liquid, u — the volume concentration of the gas in the liquid, and

$$g = \frac{3}{4 \cdot \pi^2 \cdot \varrho \cdot R_0^2 \cdot f_0^2}. \quad (34)$$

In (34), f_0 is the resonance frequency of bubbles of radius R_0 given by

$$f_0 = \frac{1}{2 \cdot \pi \cdot R_0} \cdot \sqrt{\frac{3 \cdot \kappa}{\varrho} \cdot \left(p + \frac{2 \cdot \sigma}{R_0} \right)}, \quad (35)$$

where σ is the surface tension coefficient at the liquid/gas interface, q the hydrostatic pressure, and $\kappa = c_p/c_v$.

For bubbles with a radius of $R_0 > 15 \mu\text{m}$, Eq. (35) reduces to

$$f_0 \cong \frac{1}{2 \cdot \pi \cdot R_0} \cdot \sqrt{\frac{3 \cdot \kappa \cdot p}{q}}. \quad (36)$$

If the propagation velocities c_1 and c_2 prior to and after application of the electric field are known, one is able to evaluate the change in volume concentration of the gas due to the action of the field.

At zero electric field, with the velocity at c_1 , the gas concentration u_1 determined from (33) amounted to

$$u_1 = \frac{1}{g \cdot q \cdot c_0} \cdot \left[\left(\frac{c_0}{c_1} \right)^2 - 1 \right], \quad (37)$$

whereas when the velocity becomes c_2 under the influence of the field the gas concentration is

$$u_2 = \frac{1}{g \cdot q \cdot c_0} \cdot \left[\left(\frac{c_0}{c_2} \right)^2 - 1 \right], \quad (38)$$

whence we obtain the volume variation of the gas concentration $\Delta u = u_1 - u_2$

$$\Delta u = \frac{1}{g \cdot q} \cdot \left[\frac{1}{(c_1)^2} - \frac{1}{(c_2)^2} \right]. \quad (39)$$

One notes that the determination of Δu does not involve the velocity c_0 in the completely degassed liquid.

Since from (34) and (36) we have

$$g = \frac{1}{\kappa \cdot p}, \quad (40)$$

Δu finally takes the form

$$\Delta u = \frac{\kappa \cdot p}{q} \cdot \frac{(c_2 + c_1) \cdot (c_2 - c_1)}{c_1^2 \cdot c_2^2}. \quad (41)$$

For the mineral oil with $q = 900 \text{ [kg/m}^3\text{]}$, for which our measurements gave $c_1 = 1544 \text{ [m/s]}$, $c_2 = 1544.55 \text{ [m/s]}$ and $\kappa = 1.43$, $p = 9.81 \cdot 10^4 \text{ [N/m}^2\text{]}$, the change in volume concentration Δu evaluated from Eq. (41) amounts to

$$\Delta u = 4.655 \cdot 10^{-8}.$$

The mobility of the gas bubbles in the electric field is also accessible to determination from the experimental data. This quantity is defined as the ratio of the velocity of displacement of gas bubbles u_0 and the electric field strength E :

$$\frac{u_0}{E} = \frac{\Delta l}{\tau \cdot E}, \quad (42)$$

with Δl — the distance between the electrodes in the measuring vessel, and τ — the time constant of the change in propagation velocity of the wave.

On the assumption of values currently applied in such studies, we evaluated the mobility of the gas bubbles as

$$\frac{\Delta l}{\tau \cdot E} = \frac{2.6 \cdot 10^{-2} \text{ [m]}}{100 \text{ [s]} \cdot 2.7 \cdot 10^5 \text{ [V/m]}} = 9.6 \cdot 10^{-10} \left[\frac{\text{m}^2}{\text{V} \cdot \text{s}} \right],$$

a value in good agreement with the literature [9].

When, however, comparing the changes in propagation velocity measured for the same field strength but different temperatures, we found a maximum to appear at a well defined value of the temperature (see Figs 7a and 7b). Now, the dynamic viscosity of a liquid is known to vary strongly with temperature — the lower the temperature the greater is the viscosity. Obviously, at decreasing temperature, the dynamic viscosity coefficient of the liquid increases making the displacement of the gas bubbles more and more difficult.

For a given field strength we thus observe smaller and smaller changes of the ultrasonic propagation velocity. Along these lines one would expect the latter to grow monotonically with growing temperature. However, this is by no means the case.

As the temperature increases (and notwithstanding the fact that the viscosity then decreases) the thermal vibrations of the molecules increase thus preventing the displacement of the bubbles in the oil. Presumably, both these effects are responsible for the maximum of Δc_E versus temperature.

It is also noteworthy that the change in propagation velocity occurs much more rapidly in CCl_4 [10] than in oils. This, too, may hinge on the viscosity. It will be remembered that the two kinds of liquid differ very considerably as to their coefficients of dynamic viscosity (by a factor of about 100).

We are further confirmed in our conviction that the change in ultrasonic propagation velocity is due essentially to degassing by the fact that preliminary studies carried out by us in AC fields failed to detect any perceptible, measurable changes in c_E in liquid dielectrics.

Moreover, the theoretical expressions show that in the field strength range $(0 \div E_{\max})$ the magnitude of $(\partial E^2 / \partial \rho)_T$ is practically field-independent, i.e., that the electrostrictive change in density of the medium is proportional to the square of the electric field strength.

Conclusions

1. With growing field strength, the ultrasonic propagation velocity increases; however, the interpretation of the process is still incomplete.
2. The theoretical magnitudes of the electric field-induced variations in ultrasonic velocity are much smaller than those recorded in experiment.
3. Dielectrics theory leads to times of the change in free energy connected with dipole polarisation of the order of microseconds whereas our measurements for oils show the propagation velocity to vary with times of as much as some tens of seconds. This suggests that the electric field modifies the ultrasonic velocity both by affecting the free energy and by way of some other mechanism. The reason for these slow variations in Δc_E in oils is presumed to reside in degassing of the medium by the electric field.
4. The experimentally determined changes in ultrasonic velocity due to the electric field acting on the viscous medium permit the evaluation of the change in volume gas concentration in the liquid dielectric.
5. The change in ultrasonic propagation velocity measured as a function of temperature at constant field strength is found to exhibit a maximum.
6. Tests with an AC electric field failed to detect any measurable change in ultrasonic velocity.
7. The theoretical formulae lead to $(\partial E^2/\partial \rho)_T$ — values practically independent of the electric field strength in the range $(0 \div E_{\max})$, i.e., the electrostrictive change in density is directly proportional to $(E)^2$.

Work carried out within the framework of Project CPBP 02.03.

References

- [1] W. VAN DAEL, *Thermodynamic properties and the velocity of sound*, 11th ed. Butterworths, London 1975.
- [2] И. П. ГОЛУАМИНА [ед], *Ультразвук*, Изд. Советская Энциклопедия, Москва 1979.
- [3] I. E. TAMM, *Fundamentals of the theory of electricity* (in Polish) WNT, Warszawa 1967.
- [4] A. CHELKOWSKI, *The physics of dielectrics* (in Polish) PWN, Warszawa 1979.
- [5] B. HILCZER, J. MAŁECKI, *Elektrety* (in Polish) PWN, Warszawa 1980.
- [6] A. SKUMIEL, M. ŁABOWSKI, *The effect of an external electric field on the propagation velocity of ultrasonic waves in liquid dielectrics* (in Polish). Arch. Akustyki **22**, 1, 81–92 (1987).
- [7] A. SKUMIEL, M. ŁABOWSKI, *Influence of external dc electric fields on the propagation velocity of ultrasonic waves in liquid dielectrics*, Acustica, **63**, 146–150 (1987).
- [8] J. WEHR, *Measurements of the velocity and damping of ultrasonic waves* (in Polish) IPPT-PAN 1972.
- [9] J. ADAMCZEWSKI, *Ionitaton and conductivity of liquid dielectrics* (in Polish) PWN, Warszawa 1965.
- [10] M. ŁABOWSKI, E. SKRODZKA, *Theoretical and experimental evaluations of the electric field effect on the ultrasonic wave velocity in carbon tetrachloride*, Acustica, **68**, 1, 26–32 (1989).

- [11] *Физическая акустика*, В. П. Масон [ед.] т. 1, 2. Изд. Мир, Москва 1968.
- [12] Л. П. ГАВРИЛОВ, *Содержание свободного газа в жидкостях и методы его измерения*, в: *Физические основы ультразвуковой технологии*, Л. Д. Розенберг [ед.], Изд. Советская Энциклопедия Москва 1979.

Received on Mai 8, 1989

PSEUDORANDOM ULTRASONIC DOPPLER METER OF LIQUID FLOW AND PROFILE WITH DIGITAL SERIAL SIGNAL PROCESSING

Z. TRAWIŃSKI, D. J. CATHIGNOL⁽¹⁾

Department of Ultrasonic Institute of Fundamental Technological Research Polish Academy of Sciences
(00-049 Warszawa, Świętokrzyska 21)

⁽¹⁾ Institut Nationale de la Santé et de la Recherche Medicale, Unite 281
(151 Cours Albert Thomas, 69003 Lyon, France)

This paper presents a new method and new ultrasonic device for "real-time" measuring velocity profiles of liquid flow in vessel. Previously a flowmeter with pseudorandom coding of the transmitted signal made it possible to measuring point on a precisely determined depth with respect to the position of the ultrasonic probe. In order to obtain data for the entire penetration depth of the ultrasonic beam with that method, a system consisting of so many delay-receiving systems as there is measuring points, in which we need data for, would have to be built. While the presented original method applies only one transmitting-receiving system, enabling a measurement in all measuring points independently and at the same time.

W pracy zaprezentowano nową metodę i nowe urządzenie ultradźwiękowe do pomiaru profili prędkości przepływu cieczy w czasie rzeczywistym. Dotychczas przepływomierz z kodowaniem pseudolosowym sygnału nadawanego umożliwiał pomiar prędkości przepływu krwi tylko w jednym wybranym punkcie pomiarowym, na ściśle określonej głębokości względem położenia głowicy ultradźwiękowej. Chcąc uzyskać dane na całej głębokości penetracji wiązki ultradźwiękowej używając tej metody, należałoby zbudować system złożony z tylu układów opóźniająco-odbiorczych w ilu punktach pomiarowych pożądaný jest wynik. Prezentowana oryginalna nowa metoda pozwala na stosowanie tylko jednego układu nadawczo-odbiorczego umożliwiającego pomiar we wszystkich punktach pomiarowych niezależnie i jednocześnie.

1. Introduction

Non-invasive ultrasonic Doppler methods of blood flow velocity measurements have become very useful for examination diseases of the circulatory system during the last 20 years. Methods of flow velocity visualisation of blood in a vessel are those worth noticing among them. The method of blood flow velocity visualization

elaborated by NOWICKI and REID in 1978 [12] was based on the principle of "real-time" analog serial signal processing. In the Department of Ultrasonics of the Institute of Fundamental Technological Research of the Polish Academy of Sciences in Warsaw a UDP 30-TES ultrasonic Doppler flow and profile meter of liquid [13] was constructed according to this method. Next constructions of meters with "real-time" digital serial signal processing BRANDESTINI in 1978 [1], HOEKS in 1982 [3], MEISTER in 1983 [10] were complicated realizations, but they visualized blood profiles in a wide measuring range (in the analog method this range was limited by the delay time of applied television delay lines — 64 μ s). Produced now most modern devices visualize a blood vessel and measure blood flow velocity in a chosen vessel at the same time. However, they do not have simultaneous visualization of the flow velocity profile in a vessel in "real-time".

The newly developed method of pseudorandom coding of transmitted signals, may become a basis for the widespread of blood flow profile visualization. This new method will be described in this paper.

2. Physical foundations and principle of operation of a pseudorandom flowmeter

For the first time the Doppler correlation technique was applied 30 years ago in radar systems [5, 14], and then it was transferred to ultrasonic engineering: WAAG in 1972 [16], NEWHOUSE in 1973 [11] and JETHWA in 1975 [9]. Gaussian noise with limited spectrum, white noise and signal with linear frequency modulation were used as the modulating signals at first. Yet, these systems had small dynamics. This seriously limited the application of this technique in cases with strong echoes from quasi-stationary object. In 1980 CATHIGNOL [3] proposed an original solution which avoids mentioned above problems by using a sinusoidal wave modulated by the two pseudorandom codes as the transmitted signal. The block diagram of such a pseudorandom Doppler flowmeter is shown in Fig. 1. The emitted signal, $X(t)$ is a result of phase modulation of a sinusoidal signal with frequency f_0 by a pseudorandom rectangular signal

$$X(t) = A(t)\cos[\omega_0 t], \quad (1)$$

where: $A(t)$ — envelope of emitted signal.

The pseudorandom signal can be generated by the system presented in Fig. 2. The pseudorandom code generation system is based on a synchronous bistable logic element. Its chosen outputs were connected with an exclusive-or adder. The adder's output is connected with the input of the system. A signal with $f_0/4$ frequency is sent to the clock's input. The pseudorandom sequence consists of N states following each other in a series. Fig. 10a presents an example of an output sequence of a pseudorandom code.

An acoustic signal with frequency f_0 , emitted by a sending ultrasonic transducer, is subject to dissipation on mobile morphologic blood elements. A part of this signal

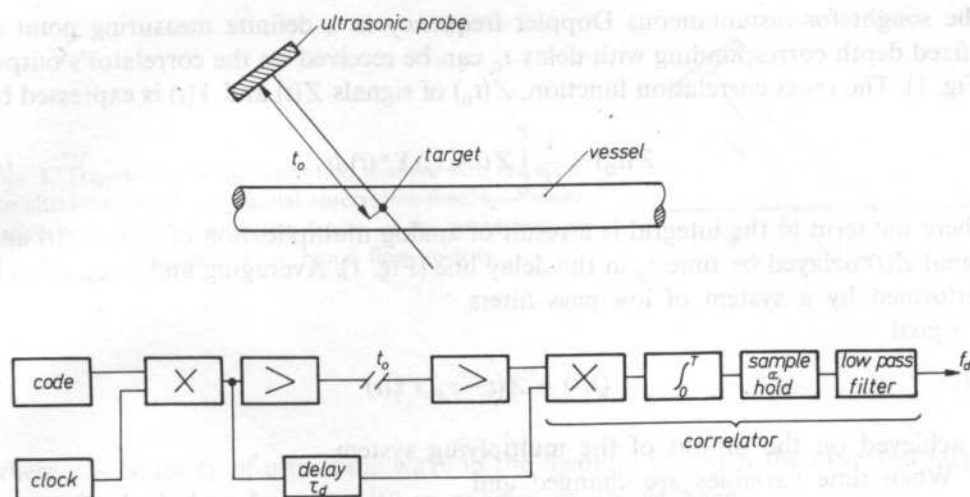


FIG. 1. Block diagram of pseudorandom flowmeter, t_0 — time of flight, τ_d — delay time of delay line, \times — multiplier, $>$ — amplifier, \int — integrating system

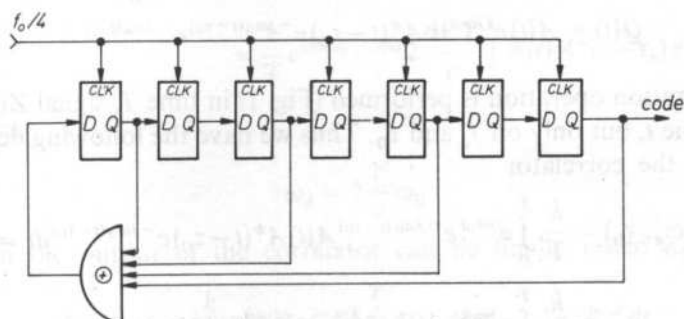


FIG. 2. Principle of generation of the pseudorandom code sequence, L — synchronous M-bite bistable logic element with initial state 1111111

returns to the receiving transducer with changed instantaneous frequency in accordance with the Doppler effect taking place in the blood vessel. If we present the transmitted signal in analytical form

$$Z(t) = A(t) \exp(j\omega_0 t), \quad (2)$$

where: $\omega_0 = 2\pi f_0$, $A(t)$ — complex envelope of transmitted signal,

then the signal received by the receiving transducer of the ultrasonic probe can be noted as

$$Y(t) = kA(t - t_0) \exp[j\omega_d(t - t_0)], \quad (3)$$

where: (t) — analytical form of received signal, k — transmission coefficient (influence of the attenuation effect of the medium on the amplitude of the ultrasonic wave propagating in it), $\omega_d = 2\pi f_d$ — Doppler pulsation, f_d — Doppler frequency.

The sought for instantaneous Doppler frequency in a definite measuring point at a fixed depth corresponding with delay t_0 can be received on the correlator's output (Fig. 1). The cross correlation function, $Z(t_0)$ of signals $Z(t)$ and $Y(t)$ is expressed by

$$Z(t_0) = \frac{1}{T} \int_0^T Z(t - \tau_d) Y^*(t) dt, \quad (4)$$

where the term in the integral is a result of analog multiplication of signal $Y(t)$ and signal $Z(t)$ delayed by time τ_d in the delay line (Fig. 1). Averaging and integration is performed by a system of low-pass filters.

A signal

$$Q(t) = Z(t - \tau_d) Y^*(t) \quad (5)$$

is achieved on the output of the multiplying system.

When time variables are changed and

$$\tau_0 = t_0 - \tau_d \quad (6)$$

is included, we have

$$Q(t) = A(t) e^{j\omega_0 t} k A^*(t - \tau_0) e^{-j\omega_0(t - \tau_0)} e^{-j\omega_d(t - \tau_0)}. \quad (7)$$

After the integration operation is performed (Fig. 1) in time T , signal $Z(t_0)$ no longer depends on time t , but only on f_d and τ_0 . Thus we have the following dependence on the output of the correlator

$$\begin{aligned} Z(\omega_d, \tau_0) &= \frac{k}{T} \int_0^T e^{j\omega_0 t} e^{-j\omega_0(t - \tau_0)} A(t) A^*(t - \tau_0) e^{-j\omega_d(t - \tau_0)} dt = \\ &= \frac{k}{T} \int_0^T e^{j\omega_0 \tau_0} A(t) A^*(t - \tau_0) e^{-j\omega_d(t - \tau_0)} dt = \\ &= \frac{k}{T} e^{j2\pi(f_0 + f_d)\tau_0} \int_0^T A(t) A^*(t - \tau_0) e^{-j\omega_d t} dt. \end{aligned} \quad (8)$$

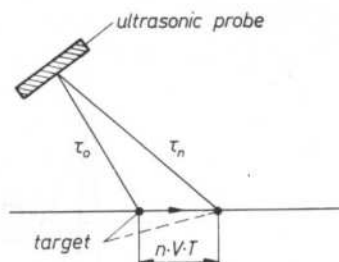
Assuming $f_d \ll f_0$, we have $f_0 + f_d \cong f_0$, so

$$Z(\omega_d, \tau_0) = \frac{k}{T} e^{j\omega_0 \tau_0} \int_0^T A(t) A^*(t - \tau_0) e^{-j\omega_d t} dt. \quad (9)$$

This operation is performed for every repetition period T of signal $X(t)$.

From the set of natural numbers a number corresponding to succeeding repetitions of the sequence of the pseudorandom code can be noted as n . Assuming that the target moves with velocity V , as it is shown in Fig. 3, then the target after the n repetition cycle of the pseudorandom code sequence will travel a path with length equal to nVT . The time τ_n , measured from the beginning of ultrasonic wave emission to the current moment is in direct relationship with velocity V of the observed target, according to the following relation

FIG. 3. Trajectory of target's position changes with respect to the ultrasonic probe, τ_0 — initial observation time, τ_n — observation time after "n" repetition cycles of the pseudorandom code sequence, V — blood flow velocity



$$\tau_n = \tau_0 + 2 \frac{nVT}{c}, \quad (10)$$

where c — velocity of ultrasonic wave in the medium in which the observed target moves in. Including formula (10) in expression (9) we have

$$\begin{aligned} Z(\omega_d, \tau_n) &= \frac{k}{T} e^{j\omega_0 \tau_n} \int_0^T A(t) A^*(t - \tau_n) e^{-j\omega_d t} dt = \\ &= \frac{k}{T} e^{j\omega_0 \tau_0} e^{j\omega_0 2 \frac{nVT}{c}} \int_0^T A(t) A^*(t - \tau_n) e^{-j\omega_d t} dt. \end{aligned} \quad (11)$$

Knowing that

$$\omega_d = 2 \frac{V}{c} \omega_0 \quad (12)$$

the signal on the output of the correlator can be finally noted as

$$Z(\omega_d, \tau_n) = \frac{k}{T} e^{j\omega_0 \tau_0} e^{j\omega_d nT} \int_0^T A(t) A^*(t - \tau_n) e^{-j\omega_d t} dt. \quad (13)$$

Three terms can be distinguished in expression (13):

- $\frac{k}{T} \exp(j\omega_0 \tau_0)$ — constant component, related with constant echoes,
- $\exp(j\omega_d nT)$ — component of Doppler frequency f_d sampled and held with frequency $1/T$,
- integral expression which is the value of the signal's envelope on the output of the correlator for τ_n in plane $\omega = \omega_d$.

The form of dependence (13) indicates that there is a three-dimensional ambiguity function of the following form on the correlator's output

$$\chi(\vartheta, \tau) = \int_{-\infty}^{+\infty} A(t) A^*(t - \tau) e^{-j\omega_d t} dt = \int_{-\infty}^{+\infty} \mathcal{A}(f) \mathcal{A}^*(f - \vartheta) e^{j\omega_d t} df, \quad (14)$$

where $\mathcal{A}(f) = \mathcal{F}[A(t)]$ is a Fourier transform [6], (Fig. 4).

The function of ambiguity (14) becomes an autocorrelation function of the complex function $A(t)$ when the observed target is motionless, i.e. $\vartheta = 0$

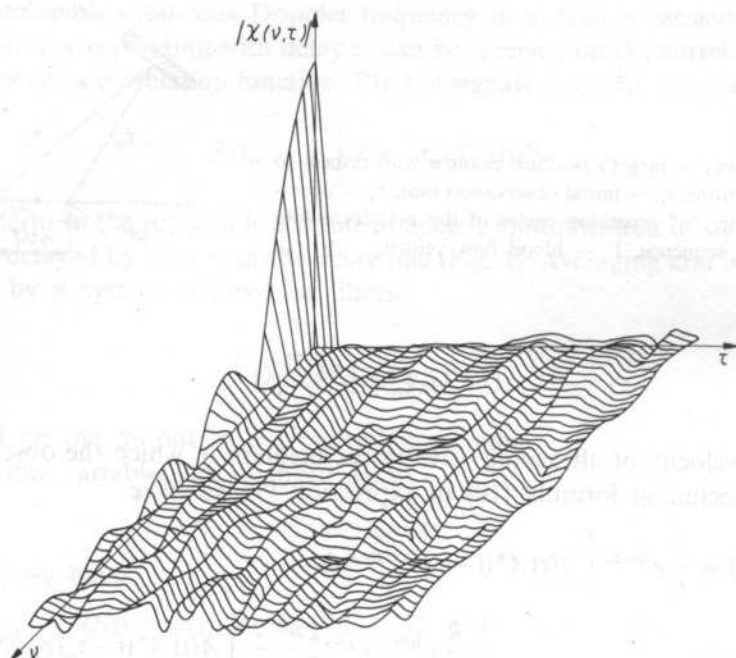


FIG. 4. Spatial distribution of the ambiguity function $\chi(\vartheta, \tau)$ of the pseudorandom code, with $N = 127$ states (according to G. GARAMPON, 1968 [6]). τ — relative time shift, ϑ — relative change of Doppler frequency

$$\chi(0, \tau) = \int_0^T A(t) A^*(t - \tau) dt. \quad (15)$$

In order to achieve high longitudinal resolution, this function should possibly closely resemble the Dirac distribution. Similarly, we have the following function for delay $\tau = 0$

$$\chi(\vartheta, 0) = \int_{-\infty}^{+\infty} \mathcal{A}(f) \mathcal{A}^*(f - \vartheta) df. \quad (16)$$

Expression (16) is an autocorrelation function in the frequency domain. Also expression (16) should be maximally close to the Dirac distribution in order to achieve high resolution during velocity measurements of the moving target. It is worth mentioning here that longitudinal resolution, as well as resolution during velocity measurements in the domain of frequency depends only on the ambiguity function of the transmitted signal. Studies on the choice of an adequate emitted signal have resulted in the choice of a pseudorandom binary signal which meets mentioned above criteria [7].

Fig. 5 presents the signal achieved on the output of the correlator in terms of time for a case of one target moving with constant velocity V . This corresponds to only one Doppler frequency f_d .

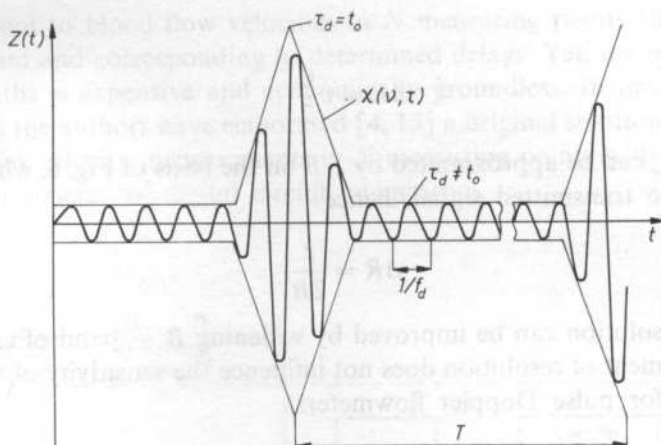


FIG. 5. Time function $Z(t)$ on the output of the correlator for one target moving with constant blood velocity V , T — repetition period of pseudorandom code sequence, t — time

3. Basic parameters of a pseudorandom flowmeter

3.1. Longitudinal resolution

For a motionless target, $\chi(\theta = 0, \tau)$, the ambiguity function for a pseudorandom binary code is a triangle with base equal to $2t_e$ (t_e is the shortest duration time of the pseudorandom code — see Fig. 6). In such a case, longitudinal resolution ΔR is

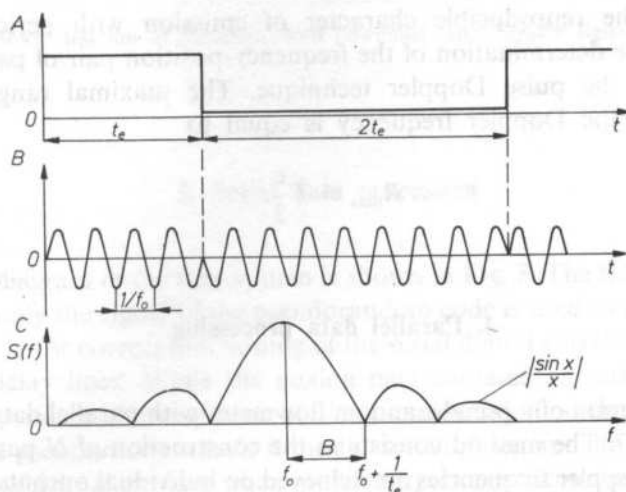


FIG. 6. Modulation effect of carrier wave f_0 by pseudorandom code sequence, a) fragment of pseudorandom code, b) phase modulated carrier wave, c) spectrum of power density of emitted signal

noted as

$$\Delta R = c \frac{t_e}{2}. \quad (17)$$

Dependence $1/t_e$ can be approximated by $1/B$ on the basis of Fig. 6, where B denotes the band of the transmitted signal, hence

$$\Delta R = \frac{c}{2B}. \quad (18)$$

Longitudinal resolution can be improved by widening B — band of emitted signal. So, the improvement of resolution does not influence the sensitivity of the apparatus (as it happens for pulse Doppler flowmeters).

3.2. Maximal measured Doppler frequency

Samples of the Doppler signal f_d appear on the output of the correlator every period of repetition of the pseudorandom code sequence T . The output voltage in the integrating circuit becomes steady during this period. This corresponds to a time interval between two succeeding samples of the Doppler signal on the output of the correlator. Therefore, the measurement of the maximal Doppler frequency depends directly on time T in accordance with Shanon's theorem concerning sampling f_d

$$f_d \max = \frac{1}{2T}. \quad (19)$$

3.3. Maximal range

Because of the reproducible character of emission with period T there is a ambiguity in the determination of the frequency-position pair of parameters, as it also happens in the pulse Doppler technique. The maximal range of univocal determination of the Doppler frequency is equal to

$$R_{\max} = T \frac{c}{2}. \quad (20)$$

4. Parallel data processing

The block diagram of a pseudorandom flowmeter with parallel data processing is presented in Fig. 7. The method consists in the construction of N parallel receiving lines. Values of Doppler frequencies are achieved on individual outputs of correlators for suitably chosen delays of the transmitted signal in delay lines. These frequencies

are proportional to blood flow velocities in N measuring points chosen along the ultrasonic beam and corresponding to determined delays. Yet, the multiplication of measuring paths is expensive and economically groundless. In order to overcome this drawback the authors have elaborated [4, 15] a original solution to the problem of simultaneous velocity measurements in N measuring points with the application of latest achievements of digital circuit engineering.

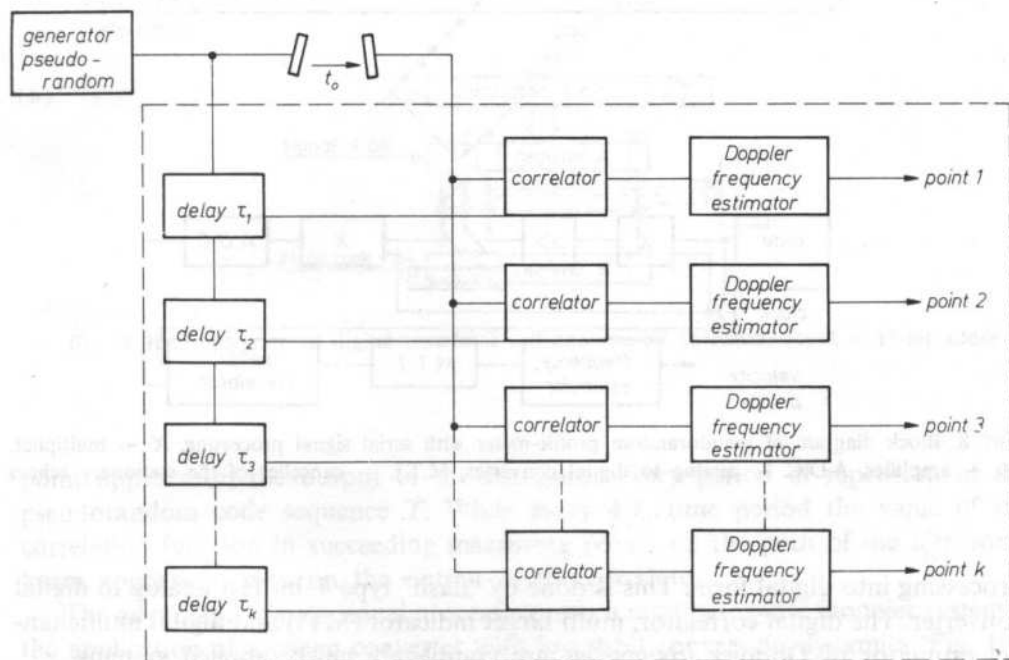


FIG. 7. Block diagram of pseudorandom flowmeter with parallel signal processing

5. Serial data processing

The block diagram of the new system is shown in Fig. 8. The transmitting system is as in Fig. 1, only the signal of the pseudorandom code is used as a reference signal, what is necessary for correct functioning of the serial digital correlator. The receiving system lacks delay lines. While the analog part contains an analog multiplier to demodulate-reproduce the sequence of the pseudorandom code. The reproduced sequence of the pseudorandom code is modulated in phase and amplitude due to the Doppler effect which takes place when mobile targets are encountered on the path of the ultrasonic beam. The signal on the output of the multiplier is subject to

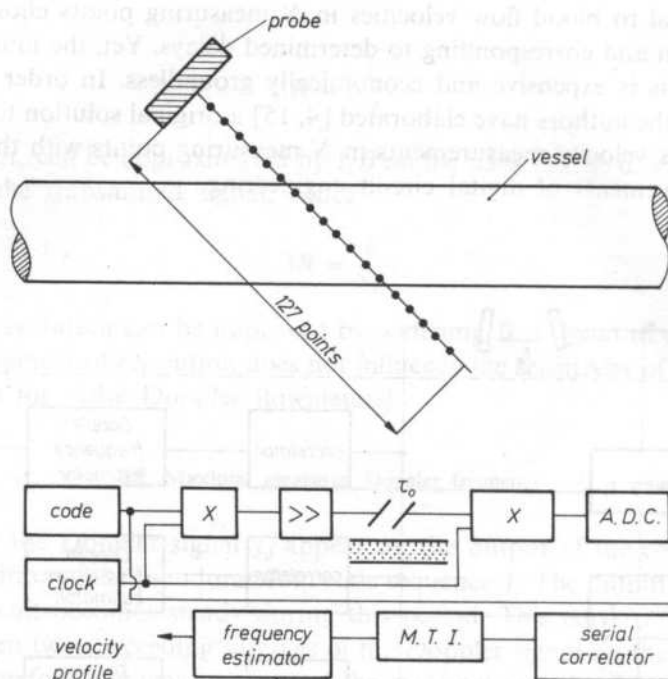


FIG. 8. Block diagram of pseudorandom profile-meter with serial signal processing, X — multiplier, \gg — amplifier, A.D.C. — analog to digital converter, M.T.I. — canceller of the stationary echoes

processing into digital form. This is done by "flash" type 4-bit fast analog to digital converter. The digital correlator, multi target indicator (MTI) and digital multichannel estimator of Doppler frequencies are completely newly applied systems.

5.1. Digital correlator

This new digital correlator (Fig. 9) contains integrated one-bit correlators connected with succeeding outputs of the A/D converter. Every one-bit correlator consists of two serial registers — measuring and reference, multipliers and adders. The reference register has a sequence of pure pseudorandom code, while a weighted sequence of the pseudorandom code after demodulation is passed through the measuring register. The length of both registers corresponds to the length of the used pseudorandom code and unequivocally determines the number of measuring points N in the full measuring range R_{\max} . The same reference signal is sent to all one-bit integrated correlators which determine weights of individual bits in the process of adding. A 11-bit information about the value of the crosscorrelation function of the reference signal and signal received after demodulation is achieved on the output of the correlator. The new value of the correlation function for a definite measuring

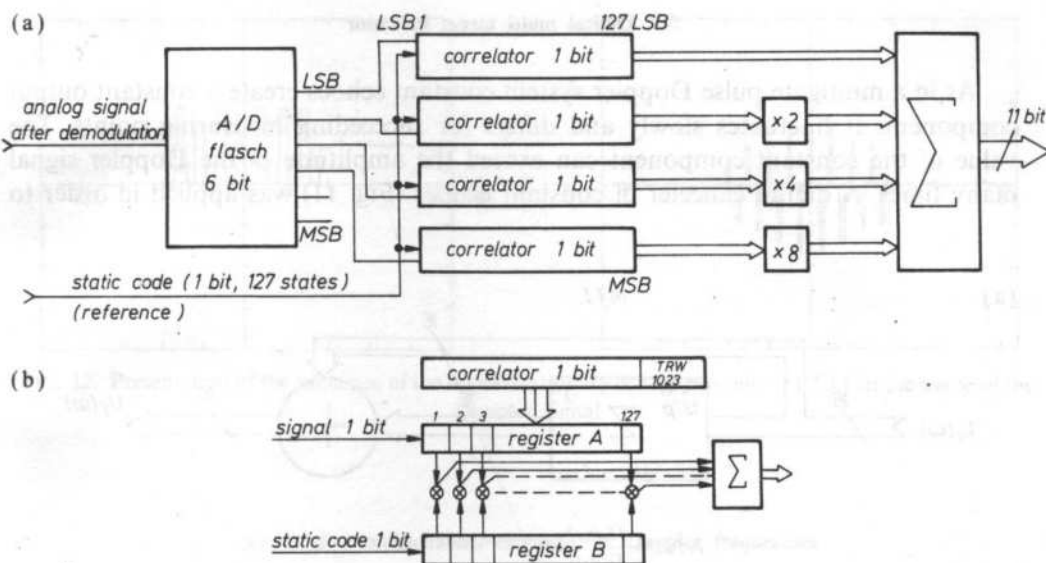


FIG. 9. Block diagram of digital correlator (a/) and one-bit correlator (b). Σ — 11-bit adder

point appears on the output of the correlator every period of repetition of the pseudorandom code sequence T . While every $4/f_0$ time period the value of the correlation function in succeeding measuring points on the path of the ultrasonic beam appears in turn on the output of the correlator.

The advantage of such signal processing over a multigate pulse Doppler system is the application of a cheap converter with low 4-bit conversion dynamics. Fig. 10b presents the autocorrelation function of the signal of pseudorandom code achieved on the output of the described correlator.

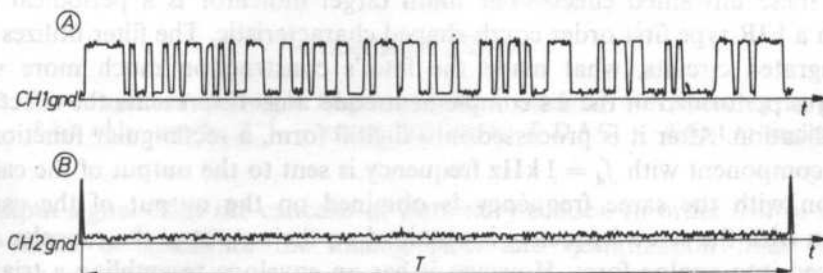


FIG. 10. Autocorrelation function (b/) of the pseudorandom code (a/) on the output of the digital correlator

5.2. Digital multi target indicator

As in a multigate pulse Doppler system constant echoes create a constant output component. It fluctuates slowly and differs for succeeding measuring points. The value of the constant component can exceed the amplitude of the Doppler signal many times. A digital canceler of constant echoes (Fig. 11) was applied in order to

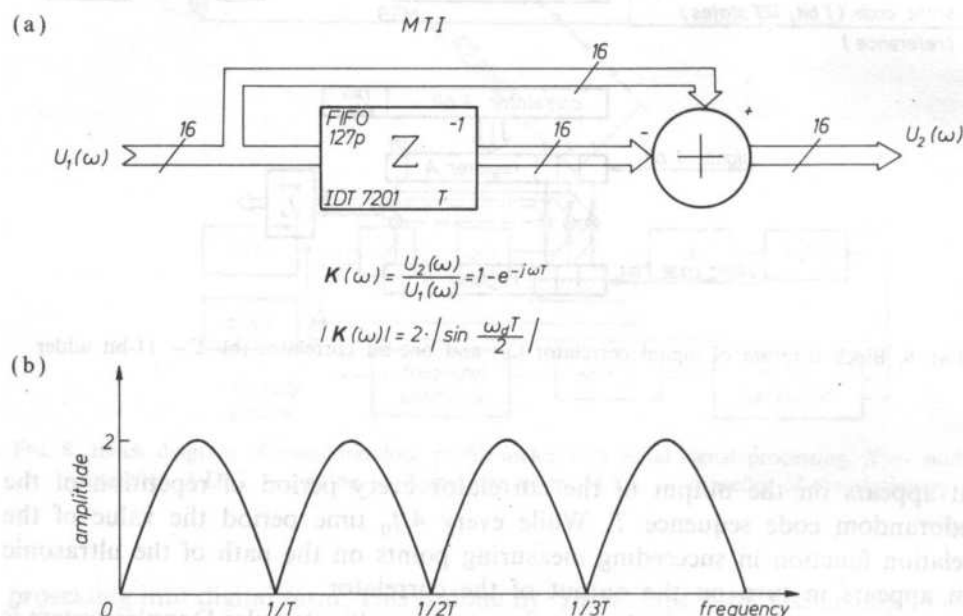


FIG. 11. Block diagram of the system of multi target indicator (a/) with transient characteristics (b/). Z^{-1} — system delaying by T , "+" — 16-bit adder

suppress these unwanted effects. The multi target indicator is a periodical digital filter with a FIR type first order comb-shaped characteristic. The filter utilizes FIFO type integrated circuits, what made the filter's construction much more simple. Summing is performed in the 2's complement code. Fig. 12 presents the effect of the MTI application. After it is processed into digital form, a rectangular function with constant component with $f_d = 1$ kHz frequency is sent to the output of the canceler. A function with the same frequency is obtained on the output of the canceler. A function with the same frequency is obtained on the output of the canceler after it is processed into analog form. However it has an envelope resembling a triangular function but without the constant component. A change of the envelope's shape is a typical effect of comb-shaped transient characteristic of the digital filter.

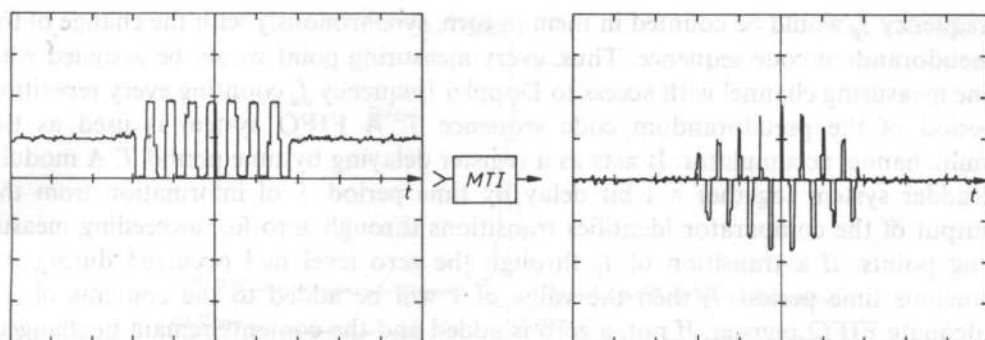


FIG. 12. Presentation of the influence of the digital stationary echoes canceller (M.T.I.) on the shape of the Doppler signal

5.3. Digital multichannel estimator of Doppler frequencies

Fig. 13 presents the block diagram of the system which estimates Doppler frequencies in N channels at the same time. The design utilizes the "zero-crossing" conception in measurements of the number of transitions through the zero level of

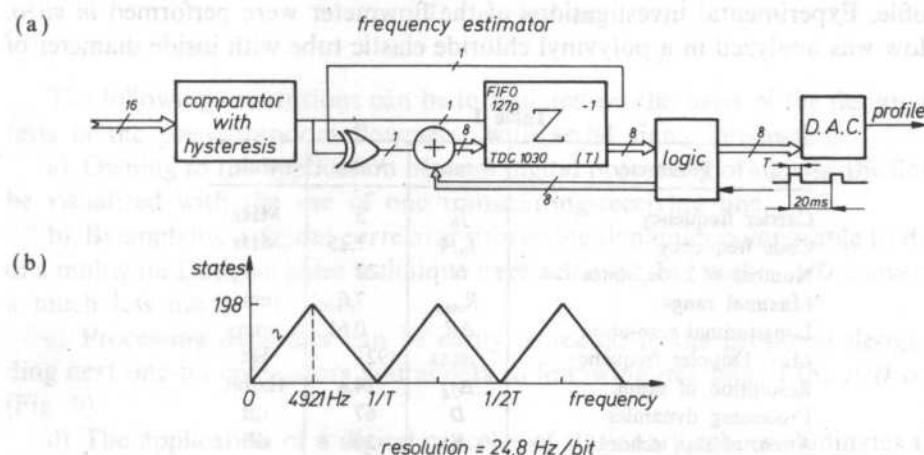


FIG. 13. Block diagram of the Doppler frequency estimator system (a/) with processing characteristic (b/), "+" — 8-bit adder system, Z^{-1} — system delaying by T , D.A.C. — digital to analog converter

the output signal from the canceler of stationary echoes. In order to free the system from effects of noises of the analog path and quantization noise a multibit comparator system with a hysteresis, with comparison threshold setting was introduced. The idea of a multichannel frequency counter lies in the creation of N serial channels. The number of transitions through the zero level of Doppler

frequency f_d would be counted in them in turn, synchronously with the change of the pseudorandom code sequence. Thus, every measuring point would be assigned with one measuring channel with access to Doppler frequency f_d counting every repetition period of the pseudorandom code sequence T . A FIFO system is used as the multichannel accumulator. It acts as a register delaying by time period T . A modulo 2 adder system together a 1-bit delay by time period T of information from the output of the comparator identifies transitions through zero for succeeding measuring points. If a transition of f_d through the zero level had occurred during the previous time period T , then the value of 1 will be added to the contents of the adequate FIFO register. If not, a zero is added and the contents remain unchanged. Owing to the logic system the number of transitions through zero of Doppler frequency f_d is counted during about 20 ms. After this period the contents of N registers from the FIFO system are written out to the digital to analog converter. Values, written out one after the other, are registered on a X - Y plotter giving the image of one of the instantaneous flow velocity profiles of blood encountered by the transmitted ultrasonic beam.

6. Results

Table 1 contains technical data of the designed pseudorandom meter of blood flow profile. Experimental investigations of the flowmeter were performed *in vitro*. Blood flow was analyzed in a polyvinyl chloride elastic tube with inside diameter of

Table 1

Parameter	Symbol	Value	Unit
Carrier frequency	f_0	5	MHz
Code frequency	$f_0/4$	1.25	MHz
Number of code states	N	127	—
Maximal range	R_{\max}	7.6	cm
Longitudinal resolution	ΔR	0.61	mm
Max. Doppler frequency	$f_{d,\max}$	4921	Hz
Resolution of estim.	Δf_d	24.8	Hz/bit
Processing dynamics	D	67	dB
Atten. of stat. echoes	K	20	dB
Profiles	P	50	1/s

6 mm. The angle between the axis of the ultrasonic probe and the tube's axis was equal to 60° . The transmitter and receiver were connected with the ultrasonic probe — separately to two piezoelectric transducers with dimensions 2×3 mm. A specially prepared blood simulating liquid was used in measurements. It was set in cyclic motion with a pump. An example of a flow profile achieved in these conditions is shown in Fig. 14. The maximal Doppler frequency occurred in the centre of the tube and was equal to about 1.7 kHz. Fluctuation visible outside the tube are result of the ambiguity function $\chi(\vartheta, \tau)$ (14).

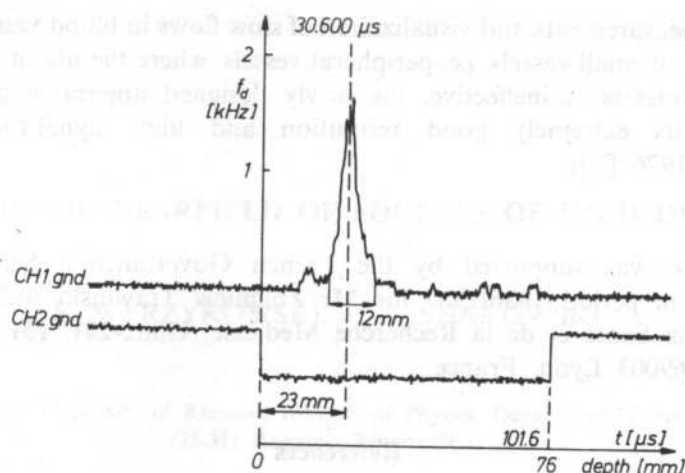


FIG. 14. Visualization of an exemplary flow profile in a light-wall tube, obtained with the designed pseudorandom flowmeter with digital serial signal processing. f_d — measured Doppler frequency

7. Conclusions

The following conclusions can be formulated on the basis of the design and first tests of the pseudorandom flowmeter with serial signal processing:

a) Owing to the application of serial digital processing of signals, the flow could be visualized with the use of one transmitting-receiving line.

b) By applying a digital correlator processing dynamics comparable to dynamics of a multigate Doppler pulse technique were achieved, but with a A/D converter with a much less number of bits.

c) Processing dynamics can be easily increased in the proposed design by adding next one-bit correlators and adders to following free bits of the A/D converter (Fig. 9).

d) The application of a digital canceler of stationary echoes eliminates the slow fluctuating constant component appearing on the output of the correlator. Yet, the used first order FIR type filter attenuates low frequencies. It would be desirable to use a higher order recursive canceler in order to obtain a more flat characteristic in the filter's transmission band.

e) The design of the 127-channel system of Doppler frequency estimation is more integrated owing to the introduction of serial digital signal processing.

f) Using FIFO registers, recording and read-off control in elements delaying by time period T (denoted by Z^{-1} in block diagrams) was considerably simplified.

g) Presented parameters and results of investigations of the pseudorandom flowmeter with serial signal processing indicate practical possibilities of its ap-

plication in measurements and visualization of slow flows in blood vessels Especially in diagnostics of small vessels, i.e. peripheral vessels, where the use of classical pulse Doppler flowmeters is ineffective, the newly designed apparatus can find wide application, its extremely good resolution and high signal-to-clutter ratio (CATHIGNOL 1976 [2]).

This work was supported by the French Governmental Scholarship and I.N.S.E.R.M. in period 1986/1987 for Mr Zbigniew Trawiński M.Sc. in Institut National de la Santé et de la Recherche Medicale, Unite-281, 151 Cours Albert Thomas 151,69003 Lyon, France.

References

- [1] M. BRANDESTINI, *Topoflow — a digital full range Doppler velocity meter*, IEEE Trans. Sonics and Ultrasonics SU-25, 287 (1978).
- [2] D. J. CATHIGNOL, *Signal-to-clutter ratio in pseudo random Doppler flowmeter*, Ultrasonic Imaging, 8, 272-284 (1986).
- [3] D. CATHIGNOL, C. FOURCADE, J. Y. CHAPELON, *Transcutaneous blood flow measurements using pseudorandom noise Doppler system*, IEEE Trans. on Biol. Engineer, BME-27, 1, 1980.
- [4] D. CATHIGNOL, Z. TRAWIŃSKI, J. Y. CHAPELON, *Pseudo-random Doppler flowmeter using serial processing*. Proceedings of 1987 IEEE Ultrasonic Symposium, Denver, pp. 889-892.
- [5] C. E. COOK, M. BERNFELD and C. A. PALMIERI, *Radars*, vol. 3: *Pulse compression*, [Ed.] D. K. Barton, Dedham, MA: Artech House, 1975, pp. 127-129.
- [6] G. J. GARAMPON, G. BONNET, *Extension de la notion de fonction d'ambiguité à des signaux aléatoires*. Ann. Télécom. T-23 Juin 1968.
- [7] G. J. GARAMPON, *Considerations sur la fonction d'ambiguité dans le cas de signaux aléatoires — Etude et génération de certains signaux*. Thèse de Docteur Ingénieur, Grenoble, mai 1970.
- [8] A. P. G. HOEKS, *On the development of a multigate pulsed Doppler system with serial data processing*, Dissertation, University of Limburg, Maastricht 1982.
- [9] C. P. JETHWA, M. KAREN, G. R. COOPER, *Saggiof, Blood flow measurements using ultrasonic pulsed random signal Doppler systems*, IEEE Trans. Sonics and Ultrasonics, 22, 1 pp. 1-10 (1975).
- [10] J. J. MEISTER, *Mesure par échographie Doppler et modélisation théorique de l'effet de troubles cardiaques sur la pression et le débit artériels*. Thèse Lausanne EPFL 1983.
- [11] V. L. NEWHOUSE, G. R. COOPER, H. FEIGENBAUM, *Ultrasonic blood velocity measurement using random signal, correlation techniques*. Digest of the Xth ICMBE, Dresden 1973.
- [12] A. NOWICKI, J. M. REID, *An infinite gate pulse Doppler*, Proc. of 23 rd. AIUM, 139, Oct. 20-23, San Diego (1978).
- [13] A. NOWICKI, *Ultrasonic methods of visualization of blood vessels and blood flows* (in Polish), Qualifying thesis, IFTR Reports, Warsaw, Poland, 65 (1979).
- [14] H. O. RAMP and E. R. WINGROVE, *Radars*, Vol. 3, *Pulse Compression*, [Ed.] D. K. Barton, Dedham, MA: Artech House. 1975, p. 75.
- [15] Z. TRAWIŃSKI, D. CATHIGNOL, *Pseudorandom ultrasonic Doppler meter of blood flow profile with serial data processing* (in Polish), Proc. of XXXV Open Seminar on Acoustics, Białowieża, Poland, 1988 r.
- [16] R. C. WAAG, J. B. MYKLEBUST, W. L. and R. GRAMIAK, *Instrumentation for noninvasive cardiac chamber flow rate measurements*. in 1972 IEEE Ultrasonic Symposium Proceedings; pp. 74-77, IEEE Cat N° 72CH0708-8SU.

Received on February 24, 1989

THE ACOUSTIC NEARFIELD OF SOURCES OF HIGH DENSITY

R. WYRZYKOWSKI, J. K. SNAKOWSKI

Pedagogical University of Rzeszów, Institute of Physics, Department of Acoustics
(35-311 Rzeszów, Rejtana 16a)

Introduction

In the present paper we compute the acoustic potential in the nearfield of a circular source placed in an infinite rigid baffle. Two cases of distribution of velocity amplitude of harmonic vibrations are considered for which high directivity of emitted acoustic field is obtained. As it has been proved in paper [6] such directivity is obtained if one of the following two distributions of velocity amplitude is applied: distribution according to the Gaussian curve and distribution defined by the Bessel function of first order divided by its argument. The first distribution gives, in the farfield, the directivity coefficient also according to the Gaussian curve, while the second produces radiation only in a defined cone. In view of practical applications it is important to investigate also the nearfield in these cases.

Theoretical basis of calculation of the nearfield of radially symmetric sources has been presented in paper [8] and here we limit ourselves only to presentation of general formulae.

We choose the cylindrical system of coordinates such that the polar axis r lies in the plane of the baffle (thus also in the plane of source being at rest) with the origin of the system at the centre of the source. We assume that distribution of velocity amplitude, and therefore the produced acoustic field, is independent on the polar angle φ . The z axis crosses the origin of the system perpendicularly to the baffle plan.

We denote by $u(r)$ the considered distribution of velocity amplitude on the source. The acoustic potential of resultant field can be expressed by the following integral formula [8]:

$$\Phi(r, z) = - \int_0^{\infty} \frac{J_0(qr)}{\sqrt{q^2 - k^2}} H_0[u(r)] e^{-z\sqrt{q^2 - k^2}} q dq. \quad (1)$$

$J_0()$ denotes the Bessel function of zero order.

In Eq. (1) k denotes the wavenumber of the emitted harmonic wave, and $H_0[u(r)] = H_0(q)$ is the Hankel transform of zero order of the considered distribution of velocity amplitude of vibrations. As the baffle is at rest by assumption, thus denoting by a the source radius we have [8]

$$H_0[u(r)] = \int_0^a ru(r) J_0(qr) dr. \quad (2)$$

Considering $H_0[u(r)]$ in the above form we cut the $u(r)$ distribution curve at $r = a$. This is a realistic assumption, but it leads to serious mathematical difficulties. Calculations can be simplified by the following approximation: we choose the $u(r)$ distribution curve such that its ordinates for $r > a$ are negligible so that one can assume that $u(r)$ is stretched to infinity. Obviously the crucial criterion of validity of such approximation is the condition that with increasing r the product $ru(r)$ under integral must tend to zero. This condition is obviously satisfied for both distributions of velocity amplitude considered in this paper. The form of expression (1) for the potential remains the same, but the transform (2) is now given by

$$H_0[u(r)] = \int_0^\infty ru(r) J_0(qr) dr. \quad (3)$$

As we will see below, in both cases considered here integral (3) can be calculated analytically while the exact formula (2) can be integrated only numerically. In this paper we present results of both methods, the exact ("strict") and the approximate.

The references are quoted here in two different manners. Everywhere we refer to the whole item or to its greater part, we give only the number of its position on the reference list. On the other hand, quoting specific formulae from tables, we add also the appropriate page number.

1. Distribution of velocity amplitude of vibrations given by the Gaussian curve

We assume the following distribution of velocity amplitude of vibrations:

$$u(r) = \begin{cases} u_0 e^{-(nr/a)^2}, & 0 \leq r \leq a \\ 0, & r > a. \end{cases} \quad (4)$$

The coefficient n appearing in the exponent is called the coefficient of contraction. We choose the value of this coefficient such that the value of the velocity amplitude is sufficiently small on the edge of the source, what is specially important in approximate cases. We will perform numerical calculations for $n = 2$ and $n = 3$. In the first case we have for $r = a$

$$u(a)/u_0 = e^{-4} = 0.018316, \quad (5)$$

and in the second

$$u(a)/u_0 = e^{-9} = 0.000123. \quad (6)$$

On the other hand, considering the approximate case we have the amplitude distribution in the form

$$u(r) = u_0 e^{-(nr/a)^2}, \quad 0 \leq r \leq \infty. \quad (7)$$

In the first case (4) the Hankel transform reads

$$H_0[u(r)] = u_0 \int_0^a r e^{-(nr/a)^2} J_0(qr) dr \quad (8)$$

and must be computed numerically. Instead, in the second case we obtain

$$H_0[u(r)] = u_0 \int_0^\infty r e^{-(nr/a)^2} J_0(qr) dr. \quad (9)$$

We find this integral in tables of integrals [1, p. 731] and we get

$$H_0[u(r)] = \frac{u_0 a^2}{2n^2} e^{-(qa/2n)^2}. \quad (10)$$

This result is consistent with the well known fact that the Hankel transform of the Gaussian function of argument r is also the Gaussian function of argument q .

In the first case considered (Eq. (8)), we will not write *explicite* the formula for the potential (1) as it can be computed only numerically. On the other hand, in the approximate case (10) we get the acoustic potential in the nearfield in the form

$$\Phi(r, z) = -\frac{u_0 a^2}{2n^2} \int_0^\infty \frac{J_0(qr)}{\sqrt{q^2 - k^2}} e^{-\frac{q^2 a^2}{4n^2}} e^{-z\sqrt{q^2 - k^2}} q dq. \quad (11)$$

When integrating over variable q we have to distinguish between two cases. For $0 \leq q \leq k$ the square root has imaginary value, and for $q > k$ it is real. Taking this into account and separating real and imaginary parts we write Eq. (11) in the form

$$\begin{aligned} \Phi(r, z) = & \frac{u_0 a^2}{2n^2} \left[\int_0^k \frac{J_0(qr)}{\sqrt{k^2 - q^2}} e^{-\frac{q^2 a^2}{4n^2}} \sin(z\sqrt{k^2 - q^2}) q dq + \right. \\ & \left. - \int_k^\infty \frac{J_0(qr)}{\sqrt{q^2 - k^2}} e^{-\frac{q^2 a^2}{4n^2}} \exp(-z\sqrt{q^2 - k^2}) q dq \right] + \\ & + i \int_0^k \frac{J_0(qr)}{\sqrt{k^2 - q^2}} e^{-\frac{q^2 a^2}{4n^2}} \cos(z\sqrt{k^2 - q^2}) q dq. \end{aligned} \quad (12)$$

The integrals in the above formula must also be calculated numerically.

On the axis, i.e. for $r = 0$, we obtain the potential in the nearfield as

$$\begin{aligned}\Phi(0, z) = & \frac{u_0 a^2}{2n^2} \left[\int_0^k \frac{e^{-\frac{q^2 a^2}{4n^2}}}{\sqrt{k^2 - q^2}} \sin(z\sqrt{k^2 - q^2}) q dq + \right. \\ & \left. - \int_k^\infty \frac{e^{-\frac{q^2 a^2}{4n^2}}}{\sqrt{q^2 - k^2}} \exp(-z\sqrt{q^2 - k^2}) q dq \right] + \\ & + i \int_0^k \frac{e^{-\frac{q^2 a^2}{4n^2}}}{\sqrt{k^2 - q^2}} \cos(z\sqrt{k^2 - q^2}) q dq.\end{aligned}\quad (13)$$

One can simplify the integrals in the above formula removing at the same time singularities of the integrand, by means of substitution in the first and in the third integral

$$k^2 - q^2 = t^2; \quad -q dq = t dt, \quad (14)$$

and in the second integral,

$$q^2 - k^2 = t^2; \quad q dq = t dt, \quad (15)$$

Fixing limits of integration and arranging terms we get finally

$$\begin{aligned}\Phi(0, z) = & -\frac{u_0 a^2}{2n^2} e^{-\frac{k^2 a^2}{4n^2}} \left[\int_0^k \frac{t^2 a^2}{e^{4n^2}} \sin(tz) dt + \int_0^\infty e^{-\frac{t^2 a^2}{4n^2}} e^{-tz} dt + \right. \\ & \left. + i \int_0^k \frac{t^2 a^2}{e^{4n^2}} \cos(tz) dt \right].\end{aligned}\quad (16)$$

These integrals are much simpler and more convenient for numerical calculations. Let us note that the second of them can be expressed by means of the probability function. It should be mentioned here that the formula for the nearfield on axis of the source with Gaussian velocity amplitude distribution have been given in paper [7] in the form of a series.

2. The distribution of velocity amplitude of vibrations given by the first order Bessel function divided by the argument

As we have mentioned in Introduction and as it was proved in paper [6], distribution of velocity amplitude of vibrations in the form of the first order Bessel function divided by the argument gives so called absolute directivity in the farfield which means radiation exclusively in a definite cone without sidelobes. Presently we will consider the nearfield of such a source. Similarly as in the case of Gaussian

distribution we will consider here the "strict" case with velocity distribution limited to the source surface, and the approximate one when the distribution curve is stretched to infinity under obvious assumption that for r greater than the source radius, ordinates of the distribution curve are negligible.

Assuming distribution limited to the disk surface we write

$$u(r) = \begin{cases} u_0 \frac{J_1(nr/a)}{nr/a}, & 0 \leq r \leq a, \\ 0, & r > a, \end{cases} \quad (17)$$

where a , as previously, is the source radius. Coefficient n plays here analogous role as for the Gaussian distribution but now we apply an additional condition that the velocity amplitude of vibrations on the source edge $u(a)$ should be equal to zero. This reasonable assumption implies

$$J_1(n) = 0, \quad (18)$$

which gives a discrete series of admissible values of n .

We will perform numerical calculations for n equal to the three first zeros of the first order Bessel function, namely [2]

$$\begin{aligned} n_1 &= 3.8317, \\ n_2 &= 7.0156, \\ n_3 &= 10.1735. \end{aligned} \quad (19)$$

Of course, in the approximate case we apply the same values of n and we will consider the distribution of the form

$$u(r) = u_0 \frac{J_1(nr/a)}{(nr/a)}, \quad 0 \leq r \leq \infty. \quad (20)$$

We pass on to the calculation of the Hankel transform of zero order for both exact and approximate cases. In the first one we have

$$H_0[u(r)] = \frac{u_0 a}{n} \int_0^a J_1(nr/a) J_0(qr) dr. \quad (21)$$

Formally the above integral can be expressed in analytical form [3, p. 259]:

$$H_0[u(r)] = \frac{u_0 a^2}{\Gamma(1)\Gamma(2)} \sum_{p=1}^{\infty} \frac{(-1)^p (n/2)^2 p_2 F_1(-p, -1-p, 1, q^2 a^2/n^2)}{2p(p+1)!}. \quad (22)$$

Anyhow, in either case the Hankel transform must be computed numerically and there is no need to present here the formula (1) for the potential in explicit form.

In the approximate case (Eq. (20)) the appropriate Hankel transform is

$$H_0[u(r)] = \frac{u_0 a}{n} \int_0^{\infty} J_1(nr/a) J_0(qr) dr. \quad (23)$$

This integral can be found in literature [4, p. 100]:

$$\int_0^{\infty} J_1(nr/a) J_0(qr) dr = \begin{cases} a/n, & 0 < q < n/a, \\ 1/2q, & q = n/a, \\ 0, & q > n/a. \end{cases} \quad (24)$$

Substituting this into Eq. (23) we obtain the Hankel transform of interest in the form

$$H_0[u(r)] = \begin{cases} \frac{u_0 a^2}{n^2}, & 0 < q < n/a, \\ \frac{u_0 a}{2nq}, & q = n/a, \\ 0 & q > n/a. \end{cases} \quad (25)$$

Substituting this into Eq. (1) representing the acoustic potential note that integration is now extended only to $q = n/a$. For greater values of q the integrand becomes zero. Therefore we get

$$\Phi(r, z) = -\frac{u_0 a^2}{n^2} \int_0^{n/a} \frac{J_0(qr)}{\sqrt{q^2 - k^2}} e^{-z\sqrt{q^2 - k^2}} q dq. \quad (26)$$

This integral will have two different forms depending on value of k compared to the limiting value

$$k_{\text{lim}} = n/a. \quad (27)$$

If $k > k_{\text{lim}}$ than integrating over q from 0 to n/a we have everywhere $q^2 < k^2$ and formula for the acoustic potential takes form

$$\begin{aligned} \Phi(r, z) = \frac{u_0 a^2}{n^2} & \left[\int_0^{n/a} \frac{J_0(qr)}{\sqrt{k^2 - q^2}} \sin(z\sqrt{k^2 - q^2}) q dq + \right. \\ & \left. + i \int_0^{n/a} \frac{J_0(qr)}{\sqrt{k^2 - q^2}} \cos(z\sqrt{k^2 - q^2}) q dq \right]. \end{aligned} \quad (28)$$

Instead, when $k < k_{\text{lim}}$, the interval of integration must be divided into two parts: for $0 < q < k$ the integrands will be the same as in Eq. (28), while for $k < q < n/a$ we have $q^2 > k^2$. Thus in this case we have

$$\begin{aligned} \Phi(r, z) = \frac{u_0 a^2}{n^2} & \left[\int_0^k \frac{J_0(qr)}{\sqrt{k^2 - q^2}} \sin(z\sqrt{k^2 - q^2}) q dq + \right. \\ & - \int_k^{n/a} \frac{J_0(qr)}{\sqrt{q^2 - k^2}} \exp(-z\sqrt{q^2 - k^2}) q dq + \\ & \left. + i \int_0^k \frac{J_0(qr)}{\sqrt{k^2 - q^2}} \cos(z\sqrt{k^2 - q^2}) q dq \right]. \end{aligned} \quad (29)$$

Integrals in the above equations will be computed numerically. However, the field on z axis can be given analytically. Namely, when $k > k_{\text{lim}}$ we have from Eq. (28) for $r = 0$

$$\Phi(0, z) = \frac{u_0 a^2}{n^2} \left[\int_0^{n/a} \frac{\sin(z\sqrt{k^2 - q^2})}{\sqrt{k^2 - q^2}} q dq + i \int_0^{n/a} \frac{\cos(z\sqrt{k^2 - q^2})}{\sqrt{k^2 - q^2}} q dq \right], \quad (30)$$

and when $k < k_{\text{lim}}$ from Eq. (29) we get

$$\Phi(0, z) = \frac{u_0 a^2}{n^2} \left[\int_0^k \frac{\sin(z\sqrt{k^2 - q^2})}{\sqrt{k^2 - q^2}} q dq - \int_k^{n/a} \frac{e^{-(z\sqrt{q^2 - k^2})}}{\sqrt{q^2 - k^2}} q dq + \right. \\ \left. + i \int_0^k \frac{\cos(z\sqrt{k^2 - q^2})}{\sqrt{k^2 - q^2}} q dq \right]. \quad (31)$$

The integrals in Eqs. (30) and (31) can be reduced easily to elementary ones. For this purpose one has to apply substitution (14) in Eq. (30) and in the first and the third integral of Eq. (31), and substitution (15) in the second one. Thus for $k > k_{\text{lim}}$ we have from Eq. (30)

$$\Phi(0, z) = \frac{u_0 a^2}{n^2} \left[\int_{\sqrt{k^2 - (n/a)^2}}^k \frac{\sin(tz) dt}{t} + i \int_{\sqrt{k^2 - (n/a)^2}}^k \frac{\cos(tz) dt}{t} \right]. \quad (32)$$

Performing integration we can rewrite this in more convenient exponential form:

$$\Phi(0, z) = \frac{u_0 a^2}{zn^2} (e^{-iz\sqrt{k^2 - (n/a)^2}} - e^{-ikz}). \quad (33)$$

Applying formula given in [5, p. 291] to the above expression one can separate the amplitude and the phase:

$$\Phi(0, z) = \frac{2u_0 a^2}{zn^2} \sin\left(\frac{z}{2}(\sqrt{k^2 - (n/a)^2} - k)\right) e^{-i\left(\frac{\pi}{2} + \frac{z}{2}(\sqrt{k^2 - (n/a)^2} + k)\right)}. \quad (34)$$

As we can see, the amplitude of the acoustic potential is greatest for $z = 0$,

$$\Phi(0, 0) = \frac{u_0 a^2}{n^2} (\sqrt{k^2 - (n/a)^2} - k), \quad (35)$$

and then oscillates with increasing z with local extrema decreasing as $1/z$.

Let us now consider the case of Eq. (31), $k < k_{\text{lim}}$. Using substitutions given in Eqs. (14) and (15) we get

$$\Phi(0, z) = \frac{u_0 a^2}{n^2} \left[\int_0^k \sin(tz) dt - \int_0^{\sqrt{(n/a)^2 - k^2}} e^{-zt} dt + i \int_0^k \cos(tz) dt \right]. \quad (36)$$

After performing elementary integration we turn back to convenient exponential notation and get

$$\Phi(0, z) = \frac{u_0 a^2}{n^2 z} [2 - e^{-ikz} - e^{-z \sqrt{(n/a)^2 - k^2}}]. \quad (37)$$

Calculating $\Phi(0, 0)$ we have to find the limiting value of Eq. (37) for $z = 0$, similarly as in case of Eq. (34). Applying the l'Hopital's rule we obtain

$$\Phi(0, 0) = \frac{u_0 a^2}{n^2} (\sqrt{(n/a)^2 - k^2} + ik). \quad (38)$$

It is easy to prove that in the limit $k \Rightarrow k_{\text{lim}}$ the absolute values of $\Phi(0, 0)$ from Eqs. (35) and (38) are equal to each other.

3. Normalization of the output

Performing numerical calculations we assume that the two considered types of sources have the same volume output. In general, if the distribution of velocity amplitude of vibrations on the source of radius a is given by function $u(r)$, the output Q is expressed by

$$Q = 2\pi \int_0^a u(r) r dr. \quad (39)$$

In order to distinguish between the two distributions considered in this paper, we will add indices G and B to respective quantities representing the Gaussian distribution and the Bessel distribution. The source radius will be taken the same in both cases. For "rigorous" Gaussian distribution Eq. (4) we have from Eq. (39)

$$Q_G = 2\pi u_{OG} \int_0^a e^{-(n_G r/a)^2} r dr. \quad (40)$$

This integral is elementary and we get

$$Q_G = \pi u_{OG} (a/n_G)^2 (1 - e^{-n_G^2}). \quad (41)$$

For the Bessel distribution (Eq. (17)) we obtain from Eq. (39)

$$Q_B = 2\pi u_{OB} \int_0^a \frac{J_1(n_B r/a)}{(n_B r/a)} r dr. \quad (42)$$

This integral is also elementary [2] and we obtain

$$Q_B = 2\pi u_{OB} (a/n_B)^2 [1 - J_0(n_B)]. \quad (43)$$

Imposing the condition that both outputs are equal, i.e. $Q_G = Q_B$, we obtain a relation between respective maximal amplitudes of velocity which can be written as

$$u_{OB} = \frac{1}{2} u_{OG} (n_B/n_G)^2 \frac{1 - e^{-n_G^2}}{1 - J_0(n_B)}. \quad (44)$$

For distributions called above the "approximate" ones, i.e. stretched to infinity calculations are even easier. For the Gaussian distribution (Eq. (7)) we have

$$Q_G = 2\pi u_{OG} \int_0^\infty e^{-(n_G r/a)^2} r dr. \quad (45)$$

Elementary integration gives

$$Q_G = \pi u_{OG} (a/n_G)^2. \quad (46)$$

For the Bessel distribution (Eq.(20)) we get,

$$Q_B = 2\pi u_{OB} \int_0^\infty \frac{J_1(n_B r/a)}{(n_B r/a)} r dr. \quad (47)$$

Using the well-known property of definite integral of the Bessel function of any order [1, p. 679],

$$\int_0^\infty J_r(x) dx = 1, \quad (48)$$

we obtain from Eq. (47)

$$Q_B = 2\pi u_{OB} (a/n_B)^2. \quad (49)$$

Comparing both outputs also in this case we obtain the relation between maximal amplitudes of velocity:

$$u_{OB} = \frac{1}{2} u_{OG} (n_B/n_G)^2. \quad (50)$$

As we have noted above, coefficient n_B can be chosen as a zero of the Bessel function of first order, while coefficient n_G can be arbitrary in principle. Then, if we put $u_G = u_B$ in Eq. (50), maximal amplitudes of the velocity will satisfy the relation

$$u_{OB} = \frac{1}{2} u_{OG}. \quad (51)$$

This means that with the same values of maximal amplitudes of the velocity, the Bessel distribution gives twice as great output as the Gaussian distribution.

4. Results and conclusions

Using the formulae derived in previous paragraphs we have performed numerical calculations of the acoustic nearfield for the two types of considered distributions of velocity on the source. In both cases we have compared the results obtained in the

"strict" case, i.e. for the distribution function limited to the finite source surface, and in the "approximate" one, when the distribution is stretched to infinity. To represent the acoustic nearfield, we have plot diagrams of the normalized pressure modulus *versus* normalized coordinates in the neighbourhood of the source. Given the acoustic potential $\Phi(r, z)$, one can calculate the acoustic pressure p as

$$p = ik\rho_D c \Phi(r, z), \quad (52)$$

where ρ_D — rest density of the medium, c — speed of sound. To generalize results, we introduce the normalized pressure defined as

$$P = \frac{p}{\rho_D c \langle v \rangle}, \quad (53)$$

where $\langle v \rangle$ is the average velocity amplitude over the source surface S and

$$\langle v \rangle = \frac{1}{\pi a^2} \int_S u(r) dS = \frac{Q}{\pi a^2}. \quad (54)$$

Preparing formulae for numerical calculations, it is convenient also to introduce everywhere: the normalized wavenumber $\kappa = ka$, the normalized radial coordinate $\mathcal{R} = r/a$ and the normalized orthogonal coordinate $\mathcal{Z} = z/a$ (the procedure is explained in details in paper [8]).

Numerical calculations show that in the case of the Gaussian distribution, for both considered values of the contraction parameter, $n_G = 2$ and $n_G = 3$, the "approximate" and "strict" formulae give practically the same values of pressure amplitude in the nearfield. As the differences are of no importance and even difficult to represent on graphs, we present results for Gaussian source on Fig. 1 and Fig. 2 without specifying the type of approximation. It can be seen from the figures that the pressure amplitude decreases monotonically with respect to both coordinates \mathcal{R} and \mathcal{Z} and for both values of the contraction parameter n_G the pressure amplitude on axis decreases the same way, which is the effect of adequate normalization of outputs.

Instead, for the Bessel distribution the differences between the "strict" and "approximate" cases become important. They are less visible in vicinity of the source, presented on Fig. 3 ($\mathcal{R} < 1$ and $0 < \mathcal{Z} < 1$ for the "approximate" case). For greatest distances, in the "strict" case when the distribution of velocity is nonzero only on the limited circular source surface, the field on axis exhibits characteristic minima (Fig. 4) similar to these observed in the case of rigid piston [5]. The minima become less significant when the contraction parameter n_B becomes greater then the normalized wavenumber (Fig. 4, dotted line). In the "approximate" case, when the distribution is assumed to be stretched to infinity, no minima are observed for all values of n_B (Fig. 5).

Recapitulating approximation consisting in extending the velocity distribution function from finite circular source surface to infinite plane is plausible in the case of

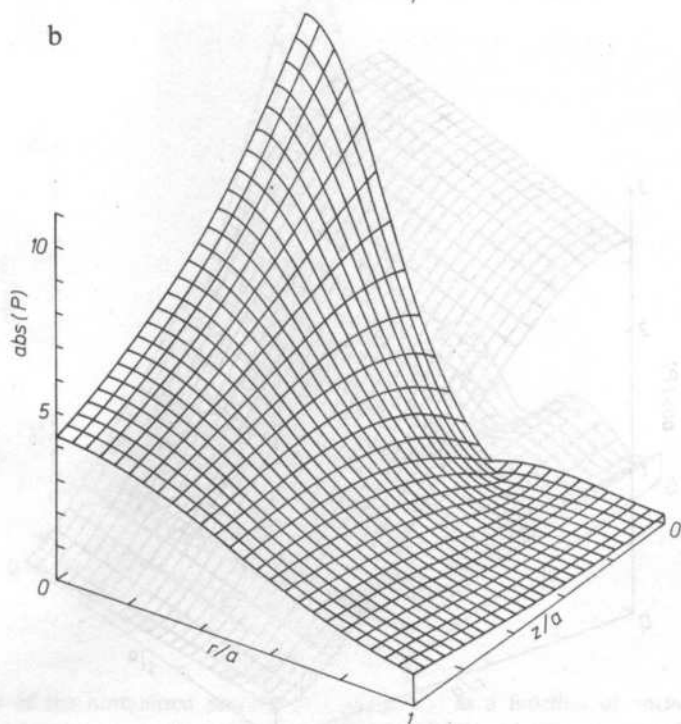
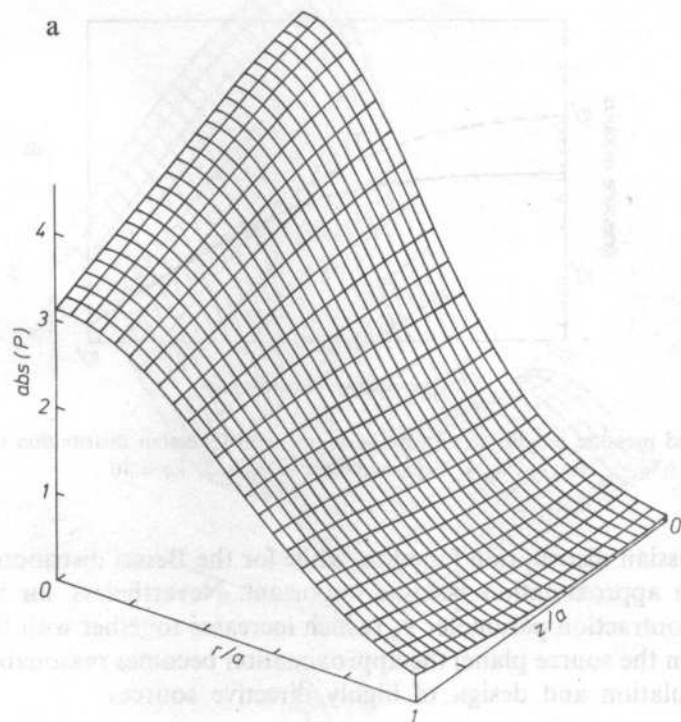


FIG. 1. Modulus of the normalized pressure $P = p/(\rho_D c \langle v \rangle)$ as a function of normalized cylindrical coordinates z/a and r/a near the source of Gaussian velocity distribution for $ka = 10$ and: a) $n_G = 2$, b) $n_G = 3$

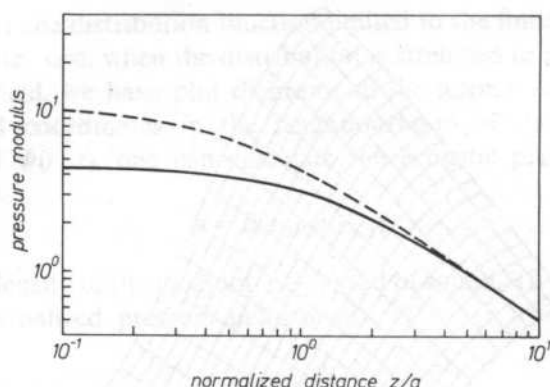
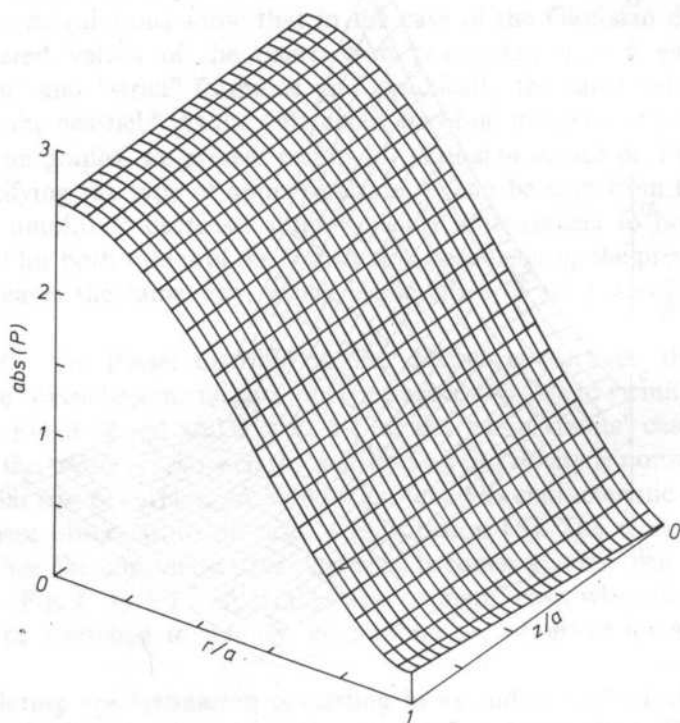


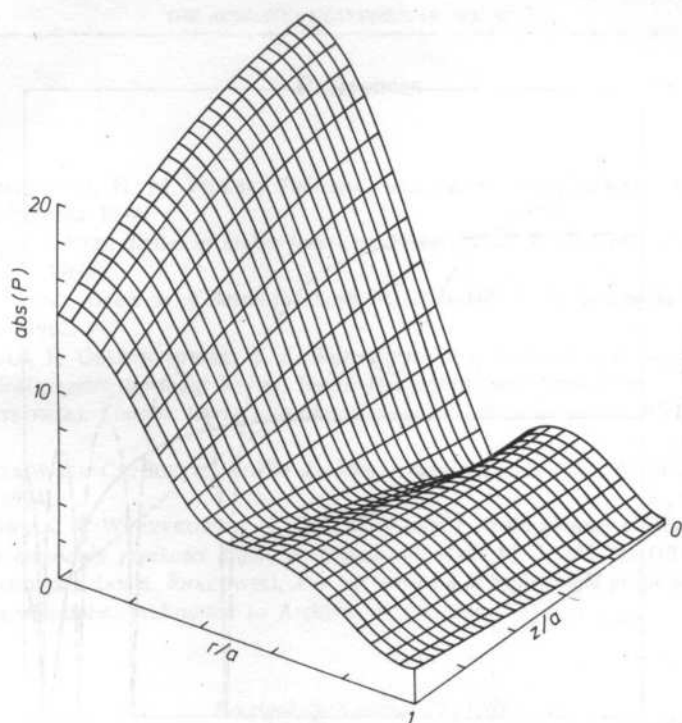
FIG. 2. Normalized pressure amplitude on axis of source with Gaussian distribution of velocity; solid line — $n_G = 2$, dashed line — $n_G = 3$; $ka = 10$

$n > 2$ the Gaussian distribution function, while for the Bessel distribution the errors following such approximation become important. Nevertheless, for wavenumbers less than the contraction parameter n_B (which increases together with the number of nodal circles on the source plane) the approximation becomes reasonable and can be useful in calculation and design of highly directive sources.

a)



b)



c)

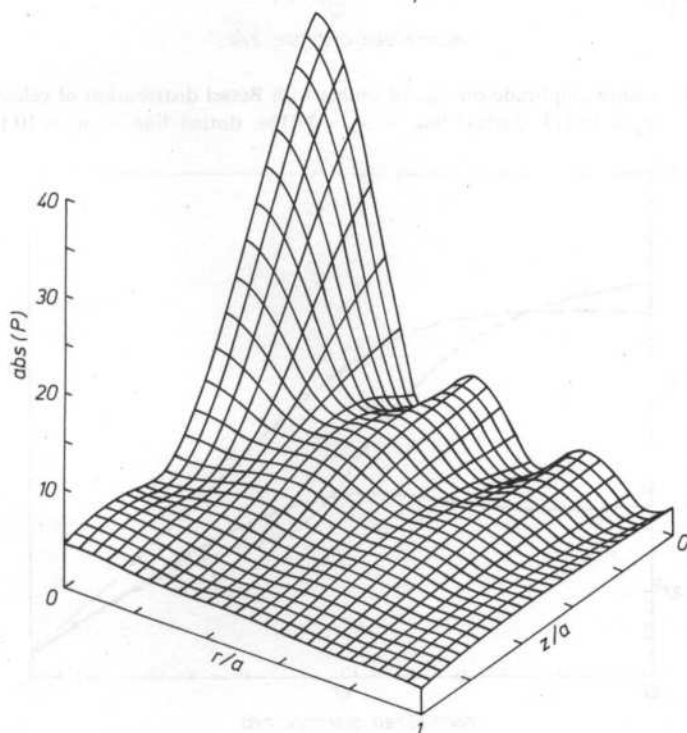


FIG. 3. Modulus of the normalized pressure $P = p/(Q_D c \langle v \rangle)$ as a function of normalized cylindrical coordinates z/a and r/a near the source of Bessel velocity distribution (the "approximate" case) for $ka = 10$ and: a) $n_B = 3.8317$, b) $n_B = 7.0156$, c) $n_B = 10.1735$

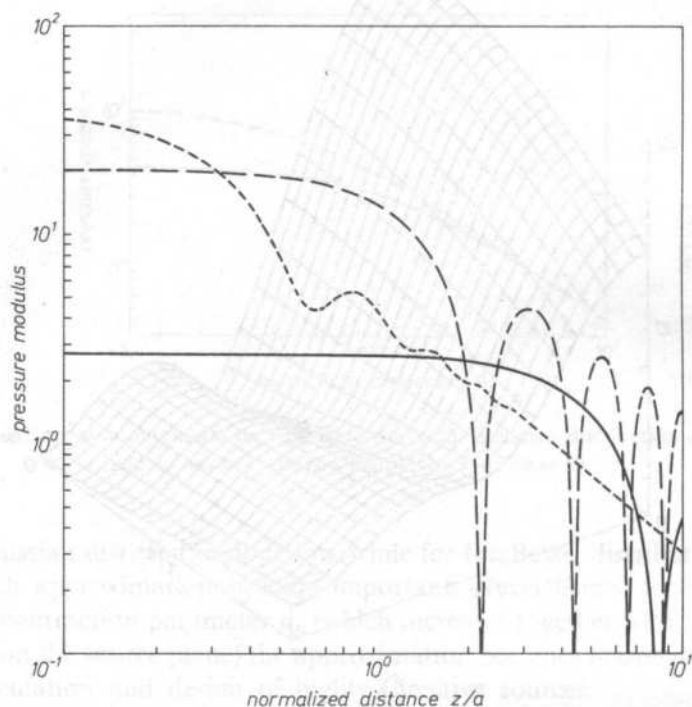


FIG. 4. Normalized pressure amplitude on axis of source with Bessel distribution of velocity (the "strict" case); solid line — $n_B = 3.8317$, dashed line — $n_B = 7.0156$, dotted line — $n_B = 10.1735$; $ka = 10$

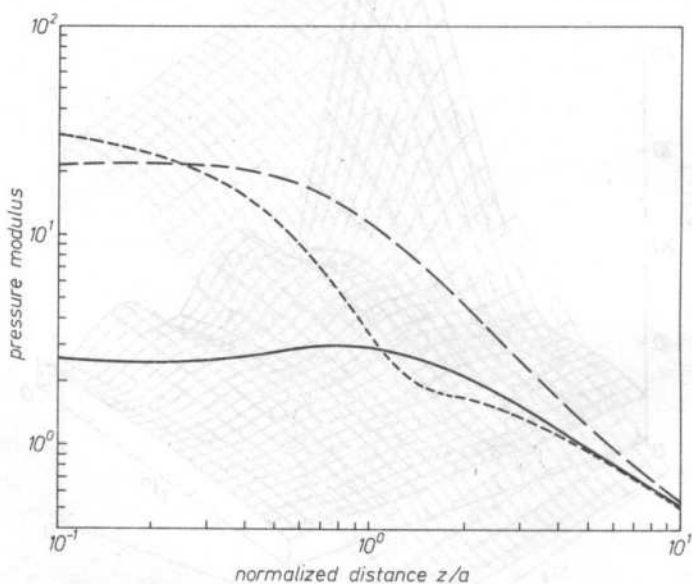


FIG. 5. Normalized pressure amplitude on axis of source with Bessel distribution of velocity (the "approximate" case); solid line — $n_B = 3.8317$, dashed line — $n_B = 7.0156$, dotted line — $n_B = 10.1735$; $ka = 10$

References

- [1] И. С. ГРАДШТЕИН, И. М. РИЖИК, *Таблицы интегралов, сумм, рядов, и произведений*, Изд. „Наука“, Москва 1974.
- [2] JAHNKE-EMDE-LÖSCH, *Tables of higher functions*, McGraw-Hill Book Company, New York-London-Toronto 1960.
- [3] YUDELL L. LUKE, *Integrals of Bessel functions*, McGraw-Hill Book Company, New York-Toronto-London 1962.
- [4] W. MAGNUS, F. OBERHETTINGER, R. P. SONI, *Formulas and theorems for the special functions of mathematical physics*, Springer Verlag, Berlin-Heidelberg-New York 1966.
- [5] R. WYRZYKOWSKI, *Liniowa teoria pola akustycznego ośrodków gazowych*, RTPN, WSP Rzeszów 1972.
- [6] R. WYRZYKOWSKI, CZ. SOLTYS, *Źródła dźwięku o dużej kierunkowości*, *Archiwum Akustyki* **9**, 3, 313-319 (1974).
- [7] A. SNAKOWSKA, R. WYRZYKOWSKI, K. ZIMA, *Pole bliskie na osi głównej membrany o gaussowskim rozkładzie amplitudy prędkości drgań*, *Archiwum Akustyki* **10**, 3, 285-295 (1975).
- [8] R. WYRZYKOWSKI, JAN K. SNAKOWSKI, *Acoustic nearfield of baffled rigid piston and membrane — an integral representation*, submitted to Archives of Acoustics.

Received on October 20, 1989

WAVES WITH FINITE AMPLITUDE IN BESSEL HORNS

T. ZAMORSKI

Institute of Physics, Pedagogical University in Rzeszów Department of Acoustics
(35-310 Rzeszów, ul. Rejtana 16 a)

The equation of the propagation a one-dimensional wave with finite amplitude in Bessel horns filled with nondissipative fluid is formulated in this paper. The solution to the equation of the propagation is analysed with the small parameter method. It was proved that a sinusoidal wave with finite amplitude, generated on the entry of the waveguide, is deformed when it moves along the horn. This manifests itself with the generation of higher harmonics with amplitudes dependent on position and frequency. The case of a conical waveguide filled with air is considered on the basis of general formulae achieved for the family of Bessel horns. Particularly the second harmonic was taken into account.

W pracy sformułowano równanie propagacji jednowymiarowej fali o skończonej amplitudzie w tubach Bessela wypełnionych bezstratnym ośrodkiem płynnym. Przeanalizowano rozwiązanie równania propagacji stosując metodę małego parametru. Wykazano, że fala sinusoidalna o skończonej amplitudzie generowana na wlocie falowodu ulega zniekształceniu przy przesuwaniu się w głąb tuby, co objawia się powstawaniem wyższych harmonicznych o amplitudzie zależnej od położenia i od częstości. Na podstawie ogólnych wzorów uzyskanych dla rodziny tub Bessela rozważono przypadek falowodu stożkowego wypełnionego powietrzem, ze szczególnym uwzględnieniem drugiej harmonicznej.

1. Introduction

The problem of propagation of elastic waves with finite amplitude in waveguides with regularity changing cross-sections (horns) has been relatively rarely considered in acoustic literature, as opposed to the linear theory of horns. This paper is based on the equation of propagation of a wave with finite amplitude in a horn with arbitrary shape. This equation has been formulated in papers [5, 6, 8] in Lagrange's coordinates on the assumption that the wave is one dimensional and that the gas medium in the horn is nondissipative.

Figure 1 presents a layer of the medium in the waveguide. Before the transition of the wave disturbance this layer is contained between surfaces $S_{(a)}$ and $S_{(a+ds)}$, where

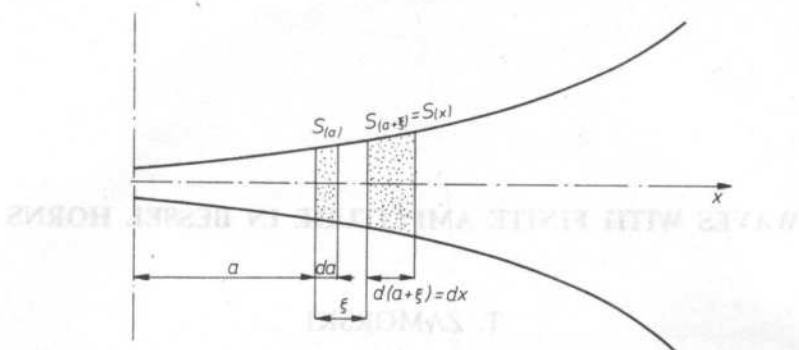


Fig. 1. Displacement of a layer of the medium under the influence of an acoustic wave

a is the Lagrange coordinate. In the wave's presence the layer moves to the position $a + \xi$ and it has thickness equal to $d(a + \xi) = dx = \left(1 + \frac{\partial \xi}{\partial a}\right) da$. In such a case variable a determines the particle's position in the medium at rest and is independent of time t ; while ξ is the displacement of the particle and depends on both, a and t . Variable $x = a + \xi$ is an Euler's coordinate. In Euler's coordinates ξ is the displacement of an arbitrary particle in point x ; ξ depends on x and t here. After several transformations of the equation of continuity, equation of motion and the adiabate equation for considered layer, we can reach the equation of propagation for a wave with finite amplitude for displacement ξ [5, 6, 8]

$$\frac{1}{\left[\frac{S(a+\xi)}{S(a)}\right]^{\gamma-1} (1+\xi')^{\gamma}} \left\{ \frac{\frac{\partial}{\partial a} \left[\frac{S(a+\xi)}{S(a)} \right]}{\frac{S(a+\xi)}{S(a)}} + \frac{\frac{\partial^2 \xi}{\partial a^2}}{1+\xi'} \right\} = \frac{1}{c^2} \frac{\partial^2 \xi}{\partial t^2}, \quad (1)$$

where $\xi' = \frac{\partial \xi}{\partial a}$ is the so-called deformation of the medium, and $\gamma = \frac{C_p}{C_v}$ is the adiabatic

exponent. The quantity $c^2 = \frac{\gamma P_0}{\varrho_0}$ is the square of sound velocity for small amplitudes while $\varrho_0 = \varrho(a) = \text{const}$ is the static density, and $P_0 = P(a) = \text{const}$ is the static pressure in the layer of the medium.

Equation (1) was derivated on the assumption that the horn is filled with gas. It can be also applied for liquid media, if the liquid satisfies empirical equation [11]:

$$P = \bar{P}_0 \left(\frac{\varrho}{\varrho_0} \right)^{\Gamma}, \quad (2)$$

where \bar{P}_0 and Γ are constants determined for a given liquid from experiment [11], with adequate approximation. Equation (1) greatly simplifies itself for exponential

horns and such a case has been discussed in literature [2, 5, 8]. This paper tries to consider the transmission of waves with finite amplitudes in Bessel horns, with special interest in the conical waveguide which is rather frequently applied, because of its simple construction.

2. Discussion of the propagation equation of waves with finite amplitudes in Bessel horns

The following dependence between the cross-sectional area and position of the horn's axis determines the family of Bessel horns [7]:

$$S = B_0(x_0 + \bar{x})^\mu \quad (3)$$

where x_0 is the distance between the throat of a horn and fictitious vertex (Fig. 2), B_0 is a so chosen constant that the area at the throat is equal to $S_0 = B_0 x_0^\mu$, while μ is the coefficient of flare of the waveguide and is a positive real number.

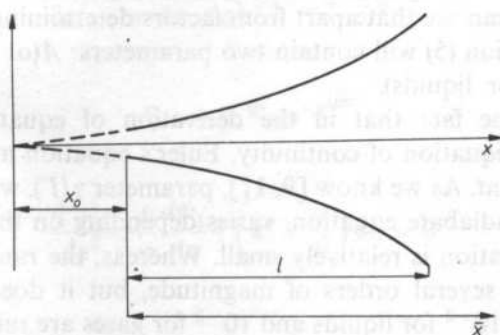


FIG. 2. A schematic presentation of the longitudinal section of a Bessel horn

From (3) it results that

$$\frac{S_{(a+\xi)}}{S_{(a)}} = \left(1 + \frac{\xi}{a}\right)^\mu \quad (4)$$

Including (4) in (1) we achieve the propagation equation of a wave with finite amplitude in a Bessel horn

$$\frac{1}{c^2} \frac{\partial^2 \xi}{\partial t^2} \left[\left(1 + \frac{\xi}{a}\right)^{\mu(\gamma-1)} + (1 + \xi')^\gamma \right] = \mu \frac{a\xi' - \xi}{a^2 + a\xi} + \frac{\partial^2 \xi}{\partial a^2} \frac{1}{1 + \xi'} \quad (5)$$

Let us assume that there are no reflections at the mouth of a horn and that a hypothetical piston vibrating with harmonical motion is the source of waves at the throat. Lagrange's coordinate of the piston, a_0 , is a constant. The piston displacement is time-dependent and is equal to

$$\xi_{(a_0,t)} = \bar{A} \cdot e^{i\omega t}, \quad (6)$$

where ω is the pulsation.

The amplitude of vibration in formula (6) can be expressed in dimensionless notation by relating it to the inverse of the wave number $k = \omega/c = 2\pi/\lambda$:

$$A = \frac{\bar{A}}{k^{-1}} = 2\pi \frac{\bar{A}}{\lambda} = 2\pi M, \quad (7)$$

where M is the ratio of piston's deflection amplitude and wave length λ .

Including (7) expression (6), which defines the boundary condition for a wave in a horn, has the following form

$$\xi_{(a_0,t)} = \frac{c}{\omega} A \cdot e^{i\omega t}. \quad (8)$$

From (5) and (8) we can see that apart from factors determining the horn's geometry the solution of equation (5) will contain two parameters: A (or M) and the adiabatic exponent γ (Γ — for liquids).

This results from the fact that in the derivation of equations (1) and (5) the non-linearity of the equation of continuity, Euler's equation and adiabat equation was taken into account. As we know [9, 11], parameter γ (Γ), which characterizes the non-linearity of the adiabat equation, varies depending on the type of gas (liquid). But its range of variation is relatively small. Whereas, the range of variation of the M number includes several orders of magnitude, but it does not exceed one. In practice M values of 10^{-3} for liquids and 10^{-2} for gases are rarely exceeded even for great intensities. Therefore (see (7)) the dimensionless amplitude A in formula (8) does not exceed one. In this case the small parameter method [11] can be applied in the solution of equation (5). The solution is accepted in the form of a power series for amplitude A :

$$\xi_{(a,t)} = \frac{c}{\omega} [A\varphi_{1(a,t)} + A^2\varphi_{2(a,t)} + A^3\varphi_{3(a,t)} + \dots], \quad (9)$$

where functions $\varphi_1, \varphi_2, \varphi_3$ have to fulfil the boundary condition (8) at the throat of a horn:

$$\varphi_{1(a_0,t)} = e^{i\omega t}; \quad \varphi_{2(a_0,t)} = \varphi_{3(a_0,t)} \dots = 0. \quad (10)$$

Further considerations will be performed in the second approximation, i.e. with the designed of terms with higher order than A^2 . Including (9) in (5) so that the equation

of propagation contains only terms with A and A^2 , we have

$$\begin{aligned} \frac{1}{\omega c}(A\ddot{\varphi}_1 + A^2\ddot{\varphi}_2) + \frac{\gamma A^2}{\omega^2}\varphi_1'\ddot{\varphi}_1 + \frac{\mu(\gamma-1)A^2}{a\omega^2}\ddot{\varphi}_1\varphi_1 = \frac{Ac}{\omega}\varphi_1'' + \frac{A^2c}{\omega}\varphi_2'' + \\ + \mu \frac{a\left(\frac{Ac}{\omega}\varphi_1' + \frac{A^2c}{\omega}\varphi_2'\right) - \left(\frac{Ac}{\omega}\varphi_1 + \frac{A^2c}{\omega}\varphi_2\right)}{a^2 + a\left(\frac{Ac}{\omega}\varphi_1 + \frac{A^2c}{\omega}\varphi_2\right)} - \frac{A^2c^2}{\omega^2}\varphi_1'\varphi_1'', \quad (11) \end{aligned}$$

where dots mark differentiation in terms of time, commas in terms of coordinate a . Expression (11) can be noted in the form of a sum of two equations — one includes factor A , the second A^2

$$A \cdot F_{1(a,t)} + A^2 \cdot F_{2(a,t)} = 0. \quad (12)$$

This equation is fulfilled for an arbitrary $A \neq 0$, it equalities $F_{1(a,t)} = 0$ and $F_{2(a,t)} = 0$ occur independently. It results from (11) that only function $\varphi_{1(a,t)}$ occurs in equation $F_{1(a,t)} = 0$:

$$\frac{\partial^2 \varphi_1}{\partial a^2} + \frac{\mu}{a} \frac{\partial \varphi_1}{\partial a} - \frac{\mu}{a^2} \varphi_1 - \frac{1}{c^2} \frac{\partial^2 \varphi_1}{\partial t^2} = 0. \quad (13)$$

Accepting

$$\varphi_{1(a,t)} = \Phi_{1(a)} \cdot e^{i\omega t} \quad (14)$$

we have

$$\frac{d^2 \Phi_1}{da^2} + \frac{\mu}{a} \frac{d\Phi_1}{da} + \left(k^2 - \frac{\mu}{a^2}\right) \Phi_1 = 0. \quad (15)$$

Substituting then

$$\Phi_1 = y \cdot a^{1-\nu}, \quad (16)$$

where

$$\nu = \frac{\mu+1}{2} \quad (17)$$

we obtain Bessel equation for y [4, 7]

$$\frac{d^2 y}{da^2} + \frac{1}{a} \frac{dy}{da} + \left(k^2 - \frac{\nu^2}{a^2}\right) y = 0. \quad (18)$$

Equation (15) describes wave motion in a Bessel horn in the first approximation. Selecting the solution to equation (18) in the form of a Hankel function [7] and including (16) we have

$$\Phi_{1(a)} = a^{1-\nu} [C \cdot H_{\nu(ka)}^{(1)} + B \cdot H_{\nu(ka)}^{(2)}]. \quad (19)$$

$H_{\nu(ka)}^{(1)}$ and $H_{\nu(ka)}^{(2)}$ are ν - order Hankel functions [7]. It results from the definition of these functions that $H_{\nu(ka)}^{(2)}$ describes a wave propagating in the direction of increasing "a" values, while $H_{\nu(ka)}^{(1)}$ - a wave propagating in the opposite direction. Because we previously assumed that there are no reflections at the mouth of the horn, only a progressive wave occurs and we should accept $C = 0$. Finally, including (14), we have

$$\varphi_1 = a^{1-\nu} \cdot B \cdot H_{\nu(ka)}^{(2)} \cdot e^{i\omega t}. \quad (20)$$

Constant B can be determined from boundary condition (10)

$$B = \frac{a_0^{\nu-1}}{H_{\nu(ka_0)}^{(2)}}. \quad (21)$$

Eventually, the first approximation:

$$\varphi_1 = \left(\frac{a}{a_0}\right)^{1-\nu} \cdot \frac{H_{\nu(ka)}^{(2)}}{H_{\nu(ka_0)}^{(2)}} \cdot e^{i\omega t}. \quad (22)$$

A more detailed discussion of equation (22) is not necessary, because the linear theory of Bessel horns is well known [1, 6, 7]. Equation $F_{2(a,t)} = 0$ with terms containing factor A^2 has the following form (see (11));

$$\frac{\partial^2 \varphi_2}{\partial a^2} + \frac{\mu}{a} \frac{\partial \varphi_2}{\partial a} - \frac{\mu}{a^2} \varphi_2 - \frac{1}{c^2} \frac{\partial^2 \varphi_2}{\partial t^2} = \varepsilon_{(a,t)}, \quad (23)$$

where

$$\varepsilon_{(a,t)} = \frac{c}{\omega} \varphi_1' \varphi_2'' + \frac{1}{\omega c a} (\mu\gamma - \mu + 1) \varphi_1 \ddot{\varphi}_1 + \frac{\gamma}{\omega c} \varphi_1' \ddot{\varphi}_1 - \frac{c}{\omega a} \varphi_1'' \varphi_1. \quad (24)$$

Equation (23) is similar to equation (13), but on the right side it has term $\varepsilon_{(a,t)}$ defined by the solution achieved in the first approximation, $\varphi_{1(a,t)}$. We can see from expression (22) that φ_1 is a periodical function with pulsation ω . Also derivatives of φ_1 in terms of time and position are periodical functions with pulsation ω . Because products of these derivatives occur in (24), ε has to be a periodical function with pulsation 2ω . Expression $\varepsilon_{(a,t)}$ determines the form of the solution of the heterogeneous equation (23), so [4] that the solution can be a function with pulsation 2ω

$$\varphi_{2(a,t)} = \Phi_{2(a)} \cdot e^{2i\omega t}. \quad (25)$$

Hence, function $\Phi_{2(a)}$ which defines the second harmonic, has to satisfy equation

$$\frac{d^2 \Phi_2}{da^2} + \frac{\mu}{a} \frac{d\Phi_2}{da} - \frac{\mu}{a^2} \Phi_2 + k_1^2 \Phi_2 = \Psi_{(a)}, \quad (26)$$

where

$$\Psi_{(a)} = k^{-1} \Phi_1' \Phi_1'' - ka^{-1} (\mu\gamma - \mu + 1) \Phi_1^2 - \gamma k \Phi_1' \Phi_1 - (ka)^{-1} \Phi_1'' \Phi_1, \quad (27)$$

$$k_1 = 2k. \quad (28)$$

The fact that function $\Psi_{(a)}$ in equation (26) is determined by the first approximation of the solution can be explained by the wave's second harmonic being excited due to a disturbance of the medium in the horn by the first harmonic. The solution to equation (26) can be presented in the following form [4]:

$$\Phi_2 = f_2 \int \frac{f_1 \Psi_{(a)}}{W} da - f_1 \int \frac{f_2 \Psi_{(a)}}{W} da + B_1 f_1 + B_2 f_2, \quad (29)$$

where

$$W = \frac{2}{\pi a^2} \quad (30)$$

$$f_1 = a^{1-\nu} \cdot I_{\nu(k_1 a)}, \quad (31)$$

$$f_2 = a^{1-\nu} \cdot Y_{\nu(k_1 a)}. \quad (32)$$

and $I_{\nu(k_1 a)}$, $Y_{\nu(k_1 a)}$ are ν -order Bessel functions of the first and second type respectively [7]. In accordance with condition (10) and expression (25) has to be equal to 0 for a particle at the throat of the horn ($a = a_0$). This condition can be fulfilled for adequately selected constants B_1 , B_2 in expression (29).

Further approximations can be calculated in an analogous manner by including terms with higher powers of A from expression (9) in the equation of propagation (5) and formulating linear differential equations for functions φ_n , corresponding with successive harmonics. Condition (10), i.e. $\varphi_{n(a_0, t)} = 0$ in every time moment t for $n > 1$ is valid for higher harmonics on the entry of the waveguide. Higher harmonics for $a > a_0$ are formed, because of non-linear properties of the medium in the horn. They are a sign of a deformation of the wave front as the wave disturbance moves along the horn. The total power on the entry of the waveguide is the power of the first harmonic. Because the total power remains constant in a nondissipative medium, the formation of higher harmonics is related with a decrease of the acoustic power of a wave with fundamental frequency. In practice most information for a waveguide with definite geometry should be contributed by the analysis of the second harmonic. Higher harmonics are of less significance, because $A < 1$ (see (9)). We will now analyse the second harmonic in a waveguide with conical shape.

3. Conical horn

A conical horn has worse transmission properties than Bessel horns of higher order [1, 7] exponential [6] of catenoidal [10] waveguides, but it is often applied for the simplicity of its shape. In this case the coefficient of flare is equal $\mu = 2$. Therefore, $\nu = 3/2$ (see (17)) and the solution of the equation of propagation for the first harmonic (20) has the following form

$$\varphi_1 = a^{-\frac{1}{2}} B \cdot H_{\frac{3}{2}(ka)}^{(2)} \cdot e^{i\omega t}, \quad (33)$$

where constant B , defined by expression (21), is equal to:

$$B = \frac{\sqrt{a_0}}{H_{\frac{3}{2}}^{(2)}(ka_0)}. \quad (34)$$

In order to determine the second harmonic, equation (26) has to be solved for function Φ_2 . The integral of this equation for $\mu = 2$ can be determined from (29) with the utilization of relationships between Bessel functions $I_{\frac{3}{2}}(k_1 a)$, $Y_{\frac{3}{2}}(k_1 a)$ and trigonometric functions [7]

$$I_{\frac{3}{2}}(k_1 a) = \sqrt{\frac{2}{\pi k_1 a}} \left[\frac{\sin(k_1 a)}{k_1 a} - \cos(k_1 a) \right], \quad (35)$$

$$Y_{\frac{3}{2}}(k_1 a) = -\sqrt{\frac{2}{\pi k_1 a}} \left[\sin(k_1 a) + \frac{\cos(k_1 a)}{k_1 a} \right]. \quad (36)$$

Calculations result in:

$$\begin{aligned} \operatorname{Re}[\Phi_2] = \frac{a_0}{a} \left[D_1(\Sigma - \chi) + D_2(\Theta + \Lambda) + \frac{L_1}{k_1 a} - N_2 \right] \sin(k_1 a) \\ + \frac{a_0}{a} \left[D_1(\Theta - \Lambda) - D_2(\Sigma + \chi) - L_1 - \frac{N_2}{k_1 a} \right] \cos(k_1 a), \end{aligned} \quad (37a)$$

$$\begin{aligned} \operatorname{Im}[\Phi_2] = \frac{a_0}{a} \left[D_2(\Sigma - \chi) - D_1(\Theta + \Lambda) + \frac{L_2}{k_1 a} - N_1 \right] \sin(k_1 a) \\ + \frac{a_0}{a} \left[D_2(\Theta - \Lambda) + D_1(\Sigma + \chi) - L_2 - \frac{N_1}{ka} \right] \cos(k_1 a), \end{aligned} \quad (37b)$$

where D_1 , D_2 , L_1 , L_2 , N_1 , N_2 are constants, while Σ , χ , Θ , Λ are functions with following forms:

$$\Theta = 2 \left(\frac{2}{k_1 a} \right)^4 - 5 \left(\frac{2}{k_1 a} \right)^2 - \frac{\gamma+1}{2} \ln(k_1 a), \quad (38)$$

$$\Lambda = \frac{\gamma+1}{2k_1 a} \operatorname{Si}(2k_1 a) + \frac{\gamma+1}{2} [Ci(2k_1 a) - C], \quad (39)$$

$$\Sigma = 4 \left(\frac{2}{k_1 a} \right)^3 - 3 \frac{2}{k_1 a} + \frac{\gamma+1}{2k_1 a} \ln(k_1 a). \quad (40)$$

$$\chi = \frac{\gamma+1}{2} \operatorname{Si}(2k_1 a) + \frac{\gamma+1}{2k_1 a} [Ci(2k_1 a) - C]. \quad (41)$$

Symbols $\operatorname{Si}(2k_1 a)$, $\operatorname{Ci}(2k_1 a)$ in expressions (39), (41) denote tabularized integral sine and cosine functions, while C is Euler's constant [3].

We can calculate constants D_1 and D_2 from (34)

$$D_1 = (\pi a_0)^{-1} \cdot \operatorname{Re}[B^2]; \quad D_2 = (\pi a_0)^{-1} \cdot \operatorname{Im}[B^2]. \quad (42)$$

Other constants were derived from the boundary condition (10) and have the following form:

$$L_1 = \frac{k_1 a_0}{1 + (k_1 a_0)^2} \{k_1 a_0 [D_1(\Theta_0 - \Lambda_0) - D_2(\Sigma_0 + \chi_0)] - D_1(\Sigma_0 - \chi_0) + D_2(\Theta_0 + \Lambda_0)\} \quad (43)$$

$$L_2 = \frac{k_1 a_0}{1 + (k_1 a_0)^2} \{k_1 a_0 [D_2(\Theta_0 - \Lambda_0) + D_1(\Sigma_0 + \chi_0)] + D_1(\Theta_0 + \Lambda_0) + D_2(\Sigma_0 - \chi_0)\}, \quad (44)$$

$$N_1 = \frac{k_1 a_0}{1 + (k_1 a_0)^2} \{k_1 a_0 [D_1(\Theta_0 + \Lambda_0) - D_2(\Sigma_0 + \chi_0)] - D_2(\Theta - \Lambda_0) + D_1(\Sigma_0 - \chi_0)\}, \quad (45)$$

$$N_2 = \frac{k_1 a_0}{1 + (k_1 a_0)^2} \{k_1 a_0 [D_1(\Sigma_0 - \chi_0) + D_2(\Theta_0 + \Lambda_0)] + D_1(\Theta_0 - \Lambda_0) + D_2(\Sigma_0 + \chi_0)\}, \quad (46)$$

where $\Theta_0, \Lambda_0, \Sigma_0, \chi_0$ are values of functions defined by formulae (38–41) for $a = a_0$. Having calculated Φ_2 we can now determine φ_2 from (25). Then, knowing φ_1 and φ_2 we can find the vibration velocity of a particle from (9)

$$v_{(a,t)} = iAc\Phi_{1(a)} \cdot e^{i\omega t} + i2A^2 c\Phi_{2(a)} \cdot e^{2i\omega t}. \quad (47)$$

Formula (47) determines the vibration velocity in Lagrange's coordinates. If we want to know the vibration velocity in a point with abscissa x (see Fig. 1), then we have to apply the relationship between Lagrange's and Euler's coordinates [11]

$$v_{(x,t)} = v_{(a,t)} - \frac{\partial v}{\partial a} \cdot \xi_{(a,t)} + \dots \quad (48)$$

Applying formulae (9) and (47) we obtain the second approximation

$$v_{(x,t)} = iAc\Phi_{1(a)} \cdot e^{i\omega t} + iCA^2 \left[2\Phi_{2(a)} - \frac{1}{k} \frac{\partial \Phi_1}{\partial a} \cdot \Phi_{1(a)} \right] \cdot e^{2i\omega t}. \quad (49)$$

To end the case of a conical horn ($\mu = 2$) we will present a numerical example. Amplitudes of vibration velocity of the first and second harmonic of a wave in a waveguide with the following dimensions:

distance between the throat of the horn and fictitious of the cone $x_0 = 10^{-1}$ m,
 horn throat diameter $d_0 = 2 \cdot 10^{-2}$ m,
 horn mouth diameter $d_w = 2 \cdot 10^{-1}$ m,
 length $l = 9 \cdot 10^{-1}$ m,

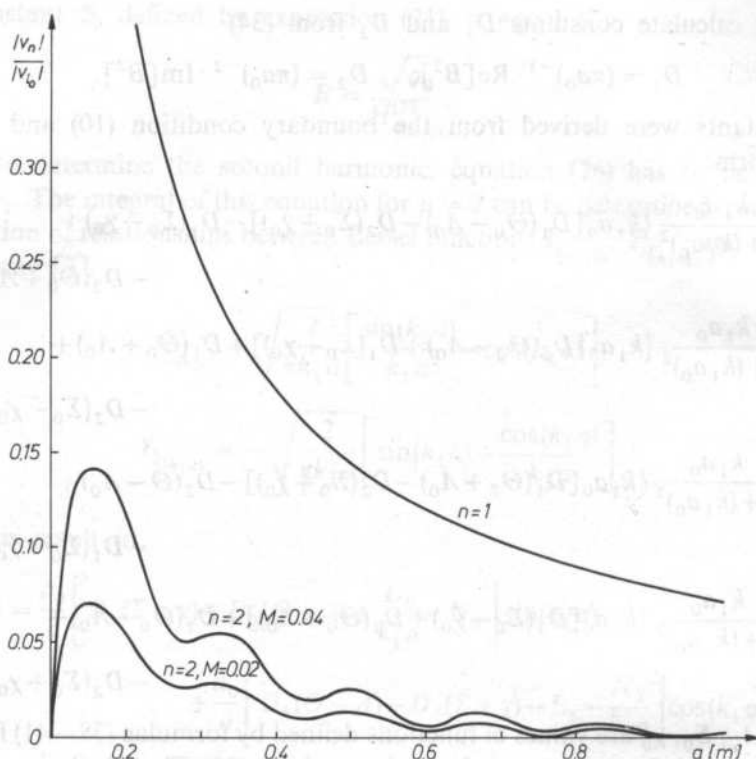


FIG. 3. Amplitudes of vibration velocities of particles of the medium in a horn for the first and second harmonic. Frequency of sine wave at the throat of a horn $f = 540$ Hz ($k = 10 \text{ m}^{-1}$)

were numerically calculated on the basis of expressions (7), (33), (34) and (37–47).

Figure 3 presents the relationship between amplitudes of vibration velocities of the first and second harmonic, and position in the horn of particles of the medium for a definite vibration frequency of the piston at the throat $f = 540$ Hz ($k = 10 \frac{1}{\text{m}}$).

Amplitudes of vibration velocities of both harmonics were related to the amplitude of vibration velocity of the first harmonic on the horn's throat $|v_{10}|$. We can see that the amplitude of vibration velocity of the first harmonic is a monotone function which decreases as it moves away from the throat of the horn. The second harmonic initially rapidly increases near the throat, but then it begins to decrease also, with characteristic oscillations. The amplitude decrease of the vibration velocity of the second harmonic, accompanying the growth of the distance from the throat, means that the flare of the waveguide's walls has a restraining effect on the development of distortions of the wave front during the propagation of a wave with high amplitude. This results from the fact that with the increase of the cross section of the horn, the

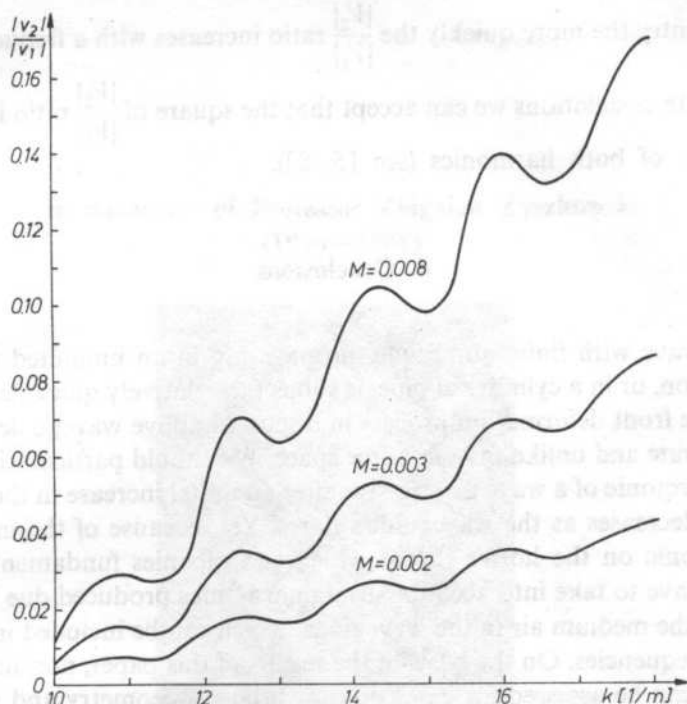


FIG. 4. Ratio of a particle velocities for the second harmonic and the fundamental at the horn mouth

acoustic energy per cross-section area unit decreases and the amplitude of the wave disturbance decreases.

As we know, pulsation of wave's higher harmonics in space (or in time) is caused by dispersion [9, 11]. Therefore, oscillations of the second harmonic, shown in Fig. 3, should prove that in terms of the non-linear theory, a nondissipative fluid contained in the horn is a dispersion medium. As it should have been expected the amplitude of vibration velocity of the second harmonic increases with the increase of the amplitude of the source's vibrations. This is shown in Fig. 3, where calculation

results of $\frac{|v_2|}{|v_1|}$ for two values of the number M (see [7]) on the horn's throat $M = 0.02$ and $M = 0.04$, are taken into account.

The amplitude of vibration velocity of the second harmonic for a given particle of the medium in the horn increases in relation to the amplitude of vibration velocity of the first harmonic when frequency is increased. This relationship is shown in Fig. 4 where results of calculations of the ratio of amplitudes of vibration velocities of both harmonics are presented in terms of wave number k for particles on the horn's mouth. We can see that the higher the amplitude of vibrations of the piston on the

waveguide's entry the more quickly the $\frac{|V_2|}{|V_1|}$ ratio increases with a frequency increase.

In approximate calculations we can accept that the square of $\frac{|V_2|}{|V_1|}$ ratio is equal to the intensity ratio of both harmonics (see [5, 8]).

4. Conclusions

A plane wave with finite amplitude, propagating in an unlimited medium with small dispersion, or in a cylindrical pipe, is subject to relatively quick deformation [9, 11]. The wave front deformation process in discussed above waveguides takes place, at a different rate and unlike than in a free space. We should particularly notice that the second harmonic of a wave progressive after an initial increase in the narrow part of the horn, decreases as the waveguide's flares. Yet, because of the increase of the second harmonic on the horn's throat which accompanies fundamental frequency increase, we have to take into account strong harmonics produced due to non-linear properties of the medium air in the waveguide, which can be included in the range of transmitted frequencies. On the basis of the results of this paper, non-linear effects in Bessel horns can be assessed for cases of known horn's geometry and amplitude on the throat of the waveguide.

References

- [1] S. BALLANTINE, *On the propagation of sound in the general Bessel horn of finite length*, J. Franklin Inst. **203**, 85-102, 852-853 (1927).
- [2] Р. Г. ГАЛЮЛИН, Л. В. КОРКИШКО, *Стоячие волны конечной амплитуды в экспоненциальном канале*, Акуст. Журн. **31**, 4., 520-522 (1985).
- [3] Е. ЯНКЕ, Ф. ЕМДЕ, Ф. ЛЮШ, *Специальные функции*, Изд. „Наука”, Москва 1968.
- [4] Е. КАМКЕ, *Справочник по обыкновенным дифференциальным уравнениям*, Изд. Иностранной Литературы, Москва 1951.
- [5] M. KWIEK, *Laboratory acoustics*, Part 1 (in Polish) PWN, Poznań-Warszawa 1968.
- [6] N. W. McLACHLAN, *Loud speakers*, Oxford University Press, London 1934.
- [7] N. W. McLACHLAN, *Bessel functions for engineers* (in Polish) PWN, Warszawa 1964.
- [8] Y. ROCARD, *General dynamics of vibrations*, Ungar, New York 1960 p. 467-479.
- [9] О. В. РУДЕНКО, С. И. СОЛУЯН, *Теоретические основы нелинейной акустики*, Изд. „Наука”, Москва 1975.
- [10] R. WYRZYKOWSKI, *Linear theory of acoustic field of gas media* (in Polish) RTPN, WSP Rzeszów 1972.
- [11] Л. К. ЗАРЕМБО, В. А. КРАСИЛЬНИКОВ, *Введение в нелинейную акустику*, Изд. „Наука”, Москва 1966.

**In memorize of Professor Zbigniew Żyszkowski
(1910–1988)**



On September 28, 1988, Professor Zbigniew Żyszkowski — one the pioneers of Polish acoustics and electro-acoustics, a founder of Wrocław Acoustic Center died in Wrocław. He was born in Wrocław in 1910. He was graduated in Faculty of Electricity at Warsaw Technical University. In 1933 he started work in the State Tele- and Radiotechnical Works in Warsaw. Here, he was involved first time in electro-acoustic problems to design the telephone receiver. At this time, the scientific foundations of electro-acoustics found to be at the preliminary state of development. Moreover, this scientific domain was not taking into account within the Polish high-school education programme. Therefore, the study on design of microphones, receivers and loudspeaker had to be developed at the beginning. In 1938, Zbigniew Żyszkowski headed the electro-acoustic division in the State Tele and Radiotechnical Works. After the World War II outbreak he stayed in Great Britain as a soldier of Polish Forces. In 1942 he moved to work in Military Communication Institute to involve in the radar equipment design and to study acoustics based on the English and American professional literature. Analysis analogy for acoustic and electrical circuits to be studied and mastered by him was very helpful in his later activity.

He came back to Poland in 1946 and he started work at the Wrocław Technical University, firstly as an adiunkt (1947) then he appointed Associate Professor (1950) and Extraordinary Professor (1954). The years between 1947 and 1954 are very fruitful in his professional activity. However, from the scientific and economic point of view, acoustics and electro-acoustics were still underestimated. Therefore, Professor Zbigniew Żyszkowski was involved in telecommunication but at the same time he was fighting for setting up acoustics and electro-acoustics to education programme. Already, in 1948, the lecture of electro-acoustics was introduced for two hours weekly in Telecommunication Section, moreover the lecture of electro-acoustic devices for students entered the fifth semester in Section of Teletransmission was introduced too. Importance of electro-acoustics as the student education programme was gradually

extended. The new created Departments technical universities introduced following lectures "Theory of electro-acoustic", "Electro-acoustic transducers" and "Design of electro-acoustic devices". In 1954, a speciality of electro-acoustics was appointed after decision which has been undertaken during the conference on students education programmes, attended by Professor Zbigniew Żyszkowski and organized by Technical Section of Main Board at High Education Ministry. A period now to be discussed should be indicated as the most important for Professor's Zbigniew Żyszkowski publication and organization activity. In 1950, Professor headed the Chair of the Cable Transmission Technics, since 1953 the Chair of Teletransmission Technics, at the beginning consisted of three persons staff. The work-shop at the Chair was also established to produce the scientific equipment needed for research and student laboratories. In 1952, Faculty of Communication was appointed, Professor Zbigniew Żyszkowski became its dean. He held this post with some interruptions until 1968. In 1953 he published the first edition of book entitled "Foundations of electro-acoustics" to be most creative in his life. At this time, this book presented the most extensive monography, comparing with this kind of literature published all over the world. Three editions, the each one more improved, were published. There are thirty generations of students who studied using his book, a few fragments of which are still current. His kind of the telecommunication lecture should be also emphasized, in particular, series of lectures concerned about Foundations of Cable Teletransmission, General Teletransmission and Foundation of Telecommunication. During this period of time, he published following textbooks

"Details of teletechnical devices" — Warsaw 1950, "Outline of transmission circuits" — Warsaw 1950, "Foundations of telecommunication — magnetic circuits" — Wrocław 1951, "Foundations of telecommunication — passive circuits" — Wrocław 1954, "Principles of telecommunication" — Warsaw 1952 coauthor Władysław Majewski.

At this moment the following impressions related to this extremely passive political period should be pointed out. The first of them concerns his activity conditions to be passed throughout the period of Stalinism. Professor, as a soldier of Polish Forces in the West and reemigrant from Great Britain could expect for different difficulties and shickaneries but it didn't cause his discouragement and it didn't influence on his efficacious activity in spite of his continuous conflict with dicidents. The second impression concerns the high school didactic problems. As he described in his diary, a didactic process consumed about 60% of his work time, the rest of which was spent on learning and organization activity. At this time he was appointed Extra-ordinary Professor, he also was a head of the Chair and a dean. It proves that the didactic activity was really high estimated and it had an influence on promotion of academic teachers. Moreover, a little time consumption to be spent on organisation activity proves that the academic relationships which came into existance at this time were not formalistic and bureaucratic.

The next period of this professional activity should be emphasized during the years 1954–1968. At this time, the main domain of his activity is devoted to the organisation and scientific problems. As it was above mentioned, apart his posts as a head and dean, he was Pro-Rector of Wrocław Technical University during the years 1958–1959. To discuss his scientific activity, it should be also mentioned his initiative to undertake research which later created independent research directions conducted by his former assistants. A research on a process of linear and non-linear disturbances of fonic tracks to be undertaken and developed by Professor Zbigniew Żyszkowski and his teams should be pointed out a success of which can be presented by the objective measure of stochastic signal as well as by the measurement method of the disturbances and by design of the appropriate measurement equipment. The interesting results were also obtained for research on transmission conditions of the stochastic signal within a high-frequently track for radio receiver, the practical using of which were applied to research on acoustic conditions of radio receivers to be produced in Dzierżoniów Radio Receivers Works. This research programme, stimulated at Wrocław Technical University, caused development of the signal theory.

Professor Żyszkowski assumed that the objective disturbance measurement should be completed by the subjective quality estimation of electro-acoustic circuits, methodology of which, particular for the sound transmission circuits, electro-acoustic transducers as well as the speech and music sounds reproduction, was elaborated by his team. Results were applied for industrial production of electro-acoustic equipment, for instance, in the Loudspeakers Work "Tonsil" in Września, collaboration with which was conducted personally by Professor during a long period of time. These research directions, carried out in Wrocław acoustic center, stimulated the development of psychoacoustics Professor's

interest in telephonometry to be practised in Wrocław Technical University, caused the development of the cybernetic acoustic, the new domain of science, very important for human being and machine relationships.

Professor initiated also the ultrasonic research, particularly its industrial application. The ultrasonic method of capacity measurement for the band conveyor, device for stress evaluation in the rock mass and equipment for measurement of ultrasonic wave rate in fluids were elaborated.

At this time, Professor was engaged in the staff education. He is thesis advisor of seventeen terminated Ph.D studies, from which seven were obtained in his Chair by his younger collaborators. In 1968, at the end of now discussed period of time, the Chair in common with the work-shop consisted of eleven didactic and ten technical collaborators of scientific staff as well as forty two collaborators in management, design and work-shop sections.

In 1968, Institute of Telecommunication and Acoustics was established, Professor Zbigniew Żyszkowski became its director and a head of its Electro-acoustic Department. His professional activity was devoted to electro-acoustics, although in 1971 and 1972 he published a textbook entitled "Foundations of cable teletransmission" based on the lecture programme. His care about materials base and acoustic measurement technics caused the foundation of Section for noise and vibration research. His social activity was expressed by the active participation in the Polish Acoustical Society, particular in its Wrocław Section as well as in the Acoustic Committee of the Polish Academy of Sciences. He was a member of the Expert Board for International Collaboration in Telephony and Telegraphy, member of the Telecommunication Section of Electronics and Telecommunication Main Board at the Science and Technics Committee. In 1980 he was retired but he was still active collaborator engaged in research carried out in the Institute. In 1984 he published the third edition of "Foundations of electro-acoustics" and in 1987 a textbook "Electro-acoustic measurement".

For his professional activity Professor Zbigniew Żyszkowski was distinguished Officer and Chevalier Cross of the Polonia Restituta, the Gold Cross of Merit, Medal of the National Education Board and the others numerous state, regional and professional distinctions. In 1986 he was awarded a honorary title for Teacher of Merit. His name was included in the honorary list Man Merit at the Wrocław Technical University.

For us, scholars and collaborators, Professor Zbigniew Żyszkowski will be kept in our minds as a honest Boss who used to be against the unknowledge and carelessness but with countless reserves of sympathy and support for students and younger collaborators, always finding time to help and guide them. He admired precision and brightlight in his lectures. May be it would be worth mentioning his solicitude for the mother tongue. His papers were made up with an aesthetic sence of the elegance avoiding unnecessarily long introductions and conclusions. His carefulness and systematic allowed him to make the acoustic terminology uniform to be useful for the Polish Standard.

We shall uniss a scientist and an educator, a man of strong personality whose kind of work marked permanent trace in the professional activity of his scholars.

*Andrzej Dobrucki
Wojciech Majewski
Janusz Zalewski*

In memorize of Professor Wiktor Jankowski (1905–1988)



On November 30, 1988 Professor Wiktor Jankowski — a prominent researcher of medical sciences, a pioneer of the Polish physiological acoustics, a honorary member of the Polish Acoustical Society died at Wrocław.

Professor Wiktor Jankowski was born at Lwów on February 21, 1905 in the family of doctor. It was graduated in the Faculty of Medicine at the Jan Kazimierz University in Lwów. In 1930 he received a doctor degree of medical sciences. During the period 1930–1946 he worked in the Otolaryngological Clinic at the Jan Kazimierz University. On the basis of the scientific work he has done, he was awarded habilitation in July, 1939.

In 1946 he moved on to Wrocław where he was involved in reconstruction of the Otolaryngological Clinic. In 1953 he appointed an Extraordinary Professor and he headed the Otolaryngological Clinic at the Academy of Medicine in Wrocław. He appointed a Full Professor in 1963.

His scientific results are presented in 176 papers published in Polish and abroad journals. It is important to stress both his pioneer research on the sound — as well as the limen — and the lintel — audiometry and some research on the physiopathology and electrophysiology of the auditionic organ. These directions are basic for the scientific school created by him involving significant contribution to the acoustic development. Most of his papers are devoted to the problems of human protection within the acoustic environment of industry. Professor was scholar and teacher for successive generations of doctors, in their mids can be found a few professors and many doctors of medical sciences.

Professor Wiktor Jankowski was a principal founder of the Polish Acoustical Society — he used to be its effective member till last his days. He was one of the founders of its Wrocław Section and Medical Division. During the period 1965–1968 he was Vice-President of the Society and President of its Wrocław Section. As the first one, he was awarded honorary membership of the Polish Acoustical Society for the acknowledgement to his pioneer contribution to the development of the physiological acoustics.

We missed a scientist, doctor and scholar whose activity will remain the stable trace in our minds.

In memorize of Dr Jerzy Jaroszyński (1923—1989)

On September 19, 1989 Dr Jerzy Jaroszyński — a merit member of the Polish Acoustical Society — one of the Wrocław Section's principal founders, the high respected researcher within the domain of electro-acoustics, died in Wrocław.

Dr Jerzy Jaroszyński was born in Warsaw on July 29, 1923 in a family of an electrical engineer. In 1942 he entered the Electrical Department at the Warsaw Technical University where in 1947 he received a diploma in electrical engineering. Since April 1947 he has begun his work in Polish Radio Broadcasting in Wrocław as a movement engineer. At this time, after the World War II destructions, he designed and supervised the radio broadcasting system. His high efficiently professional activity have been connected with the technical department of the Polish Radio and Television Broadcasting in Wrocław. At the same time, during the period 1950–1962, he lectured in the Communication Department at the Wrocław Technical University. Till the last days, his active participation in the research projects developed in the Telecommunication and Acoustics Institute at the Wrocław Technical University should be emphasized. It is important to stress his research on design and paractical application of stereophonic and quadrophonic systems. In November 1970, his team, as the first one in Poland, introduced the stereophonic broadcasting system in Wrocław. His experimental research on quadrophonic broadcasting system was also successful. The scientific research on phenomena foundations of audio monitoring in stereophony has been summarized in his doctoral thesis entitled "Correlation model of the auditory direction localization" terminated in 1985 at the Electronic Department of the Wrocław Technical University. A few times professional activity was awarded the state prizes. In 1963, together with Professors W. Jankowski and Z. Żyszkowski, he was one of the principal founders of Wrocław Section of the Polish Acoustical Society. His professional authority and honesty let him hold a few posts in the board of Section in Wrocław and let him to become a delegate during the home meetings.

We forever took leave of noble, honest man, our creative colleague.

In memorize of Professor Stanisław Kossowski (1909—1989)

On October 3, 1989, Professor Stanisław Kossowski, a principal founder of the Polish Acoustical Society has died in Wrocław.

Professor Stanisław Kossowski was born at Lwów on August 31, 1909. In 1934 he was graduated in the Faculty of Medicine at the Jan Kazimierz University in Lwów. During the years 1934–1937 he worked as an assistant in the Surgical Clinic, here in 1937, on completing his study, he received a doctor degree of medical sciences and then he started work at the Otolaryngological Clinic.

During the World War II 1939–1944 he stayed at Lwów and worked at Lwów Medical Institute, later the State Medical Institute. In 1946, together with Professors Teofil Zalewski he organized the Otolaryngological Clinic in Wrocław, here he perfected his professional activity. The results are presented in about 90 research papers including works on the physiological acoustics in particular, the original research on low audition human perception caused by the noisy work conditions. His team was awarded the Health Minister First Prize for the carried out on the animals experimental research on the microphonics effects in the inner ear.

Professor Stanisław Kossowski was an active member of many scientific societies and boards, for instance during the period 1957–1963 he took part in Board of Vibration Effects Research on Human

Structure at the Committee of the Polish Academy of Sciences During thirty years period of this professional work he managed successive generations of otolaryngologist, as well he was thesis advisor of five terminated Ph.D. degrees.

All his professional life, Professor Stanisław Kossowski used to be an effective member of the Polish Acoustical Society its principal founder as well as a founder of its Wrocław Section and Medical Division.

We missed an upright doctor, a great scholar and teacher, who will be long remembered by friends, collaborators and colleagues of a noble, hopeful and cheerful man.



nr inw. 84904